



**HAL**  
open science

# Contribution to the mathematical modeling of immune response

Qasim Ali

► **To cite this version:**

Qasim Ali. Contribution to the mathematical modeling of immune response. Other. Ecole Nationale Supérieure des Mines de Saint-Etienne, 2013. English. NNT : 2013EMSE0709 . tel-00905603

**HAL Id: tel-00905603**

**<https://theses.hal.science/tel-00905603>**

Submitted on 18 Nov 2013

**HAL** is a multi-disciplinary open access archive for the deposit and dissemination of scientific research documents, whether they are published or not. The documents may come from teaching and research institutions in France or abroad, or from public or private research centers.

L'archive ouverte pluridisciplinaire **HAL**, est destinée au dépôt et à la diffusion de documents scientifiques de niveau recherche, publiés ou non, émanant des établissements d'enseignement et de recherche français ou étrangers, des laboratoires publics ou privés.



NNT : 2013 EMSE 0709

## **THESIS**

Présenté par

Qasim ALI

pour obtenir le grade de

Docteur de l'Ecole Nationale Supérieure des Mines de Saint Etienne

Spécialité : Génie des procédés

## **CONTRIBUTION TO THE MATHEMATICAL MODELING OF IMMUNE RESPONSE**

Soutenue à Saint-Etienne le 10 October, 2013

### Membres du jury

Président :	Patrice Nortier	Professeur, INP Pagora, Grenoble
Rapporteurs :	Fabienne Espitalier Shamsul Qamar	Professeur, RAPSODEE Ecole des Mines, Albi Professeur, MPI – Magdeburg, Germany
Examineur(s) :	Gregory Panasenکو Fabien Crauste	Professeur, UFR des Sciences – UJM, Saint Etienne Chargé des Recherches, 1 <sup>ère</sup> classe – CNRS, Lyon
Directeur de thèse :	Frédéric Gruy Claude Lambert Eric Touboul	Professeur, CIS – Ecole des mines, Saint-Etienne médecin et HDR, CHU, Saint-Etienne Ingénieur – Fayol, Ecole des mines – Saint-Etienne

**Spécialités doctorales :**  
 SCIENCES ET GENIE DES MATERIAUX  
 MECANIQUE ET INGENIERIE  
 GENIE DES PROCEDES  
 SCIENCES DE LA TERRE  
 SCIENCES ET GENIE DE L'ENVIRONNEMENT  
 MATHEMATIQUES APPLIQUEES  
 INFORMATIQUE  
 IMAGE, VISION, SIGNAL  
 GENIE INDUSTRIEL  
 MICROELECTRONIQUE

**Responsables :**  
 K. Wolski Directeur de recherche  
 S. Drapier, professeur  
 F. Gruy, Maître de recherche  
 B. Guy, Directeur de recherche  
 D. Graillot, Directeur de recherche  
 O. Roustant, Maître-assistant  
 O. Boissier, Professeur  
 J.C. Pinoli, Professeur  
 A. Dolgui, Professeur

**EMSE : Enseignants-chercheurs et chercheurs autorisés à diriger des thèses de doctorat (titulaires d'un doctorat d'État ou d'une HDR)**

AVRIL	Stéphane	PR2	Mécanique et ingénierie	CIS
BATTON-HUBERT	Mireille	PR2	Sciences et génie de l'environnement	FAYOL
BENABEN	Patrick	PR1	Sciences et génie des matériaux	CMP
BERNACHE-ASSOLLANT	Didier	PR0	Génie des Procédés	CIS
BIGOT	Jean Pierre	MR(DR2)	Génie des Procédés	SPIN
BILAL	Essaid	DR	Sciences de la Terre	SPIN
BOISSIER	Olivier	PR1	Informatique	FAYOL
BORBELY	Andras	MR(DR2)	Sciences et génie de l'environnement	SMS
BOUCHER	Xavier	PR2	Génie Industriel	FAYOL
BRODHAG	Christian	DR	Sciences et génie de l'environnement	FAYOL
BURLAT	Patrick	PR2	Génie Industriel	FAYOL
COURNIL	Michel	PR0	Génie des Procédés	DIR
DARRIEULAT	Michel	IGM	Sciences et génie des matériaux	SMS
DAUZERE-PERES	Stéphane	PR1	Génie Industriel	CMP
DEBAYLE	Johan	CR	Image Vision Signal	CIS
DELAFOSSÉ	David	PR1	Sciences et génie des matériaux	SMS
DESRAYAUD	Christophe	PR2	Mécanique et ingénierie	SMS
DOLGUI	Alexandre	PR0	Génie Industriel	FAYOL
DRAPIER	Sylvain	PR1	Mécanique et ingénierie	SMS
FEILLET	Dominique	PR2	Génie Industriel	CMP
FOREST	Bernard	PR1	Sciences et génie des matériaux	CIS
FORMISYN	Pascal	PR0	Sciences et génie de l'environnement	DIR
FRACZKIEWICZ	Anna	DR	Sciences et génie des matériaux	SMS
GARCIA	Daniel	MR(DR2)	Génie des Procédés	SPIN
GERINGER	Jean	MA(MDC)	Sciences et génie des matériaux	CIS
GIRARDOT	Jean-jacques	MR(DR2)	Informatique	FAYOL
GOEURIOT	Dominique	DR	Sciences et génie des matériaux	SMS
GRAILLOT	Didier	DR	Sciences et génie de l'environnement	SPIN
GROSSEAU	Philippe	DR	Génie des Procédés	SPIN
GRUY	Frédéric	PR1	Génie des Procédés	SPIN
GUY	Bernard	DR	Sciences de la Terre	SPIN
GUYONNET	René	DR	Génie des Procédés	SPIN
HAN	Woo-Suck	CR	Mécanique et ingénierie	SMS
HERRI	Jean Michel	PR1	Génie des Procédés	SPIN
INAL	Karim	PR2	Microélectronique	CMP
KERMOUCHE	Guillaume	PR2	Mécanique et Ingénierie	SMS
KLOCKER	Helmut	DR	Sciences et génie des matériaux	SMS
LAFOREST	Valérie	MR(DR2)	Sciences et génie de l'environnement	FAYOL
LERICHE	Rodolphe	CR	Mécanique et ingénierie	FAYOL
LI	Jean Michel		Microélectronique	CMP
MALLIARAS	Georges	PR1	Microélectronique	CMP
MOLIMARD	Jérôme	PR2	Mécanique et ingénierie	CIS
MONTHEILLET	Franck	DR	Sciences et génie des matériaux	SMS
PERIER-CAMBY	Laurent	PR2	Génie des Procédés	DFG
PIJOLAT	Christophe	PR0	Génie des Procédés	SPIN
PIJOLAT	Michèle	PR1	Génie des Procédés	SPIN
PINOLI	Jean Charles	PR0	Image Vision Signal	CIS
POURCHEZ	Jérémy	CR	Génie des Procédés	CIS
ROUSTANT	Olivier	MA(MDC)		FAYOL
STOLARZ	Jacques	CR	Sciences et génie des matériaux	SMS
SZAFNICKI	Konrad	MR(DR2)	Sciences et génie de l'environnement	CMP
TRIA	Assia		Microélectronique	CMP
VALDIVIESO	François	MA(MDC)	Sciences et génie des matériaux	SMS
VIRICELLE	Jean Paul	MR(DR2)	Génie des Procédés	SPIN
WOLSKI	Krzysztof	DR	Sciences et génie des matériaux	SMS
XIE	Xiaolan	PR0	Génie industriel	CIS

**ENISE : Enseignants-chercheurs et chercheurs autorisés à diriger des thèses de doctorat (titulaires d'un doctorat d'État ou d'une HDR)**

BERGHEAU	Jean-Michel	PU	Mécanique et Ingénierie	ENISE
BERTRAND	Philippe	MCF	Génie des procédés	ENISE
DUBUJET	Philippe	PU	Mécanique et Ingénierie	ENISE
FORTUNIER	Roland	PR	Sciences et Génie des matériaux	ENISE
GUSSAROV	Andrey	Enseignant contractuel	Génie des procédés	ENISE
HAMDI	Hédi	MCF	Mécanique et Ingénierie	ENISE
LYONNET	Patrick	PU	Mécanique et Ingénierie	ENISE
RECH	Joël	MCF	Mécanique et Ingénierie	ENISE
SMUROV	Igor	PU	Mécanique et Ingénierie	ENISE
TOSCANO	Rosario	MCF	Mécanique et Ingénierie	ENISE
ZAHOUANI	Hassan	PU	Mécanique et Ingénierie	ENISE

PR 0	Professeur classe exceptionnelle	Ing.	Ingénieur
PR 1	Professeur 1 <sup>ère</sup> classe	MCF	Maître de conférences
PR 2	Professeur 2 <sup>ème</sup> classe	MR (DR2)	Maître de recherche
PU	Professeur des Universités	CR	Chargé de recherche
MA (MDC)	Maître assistant	EC	Enseignant-chercheur
DR	Directeur de recherche	IGM	Ingénieur général des mines

SMS	Sciences des Matériaux et des Structures
SPIN	Sciences des Processus Industriels et Naturels
FAYOL	Institut Henri Fayol
CMP	Centre de Microélectronique de Provence
CIS	Centre Ingénierie et Santé

# École Nationale Supérieure des Mines de Saint-Étienne

NNT : 2013 EMSE 0709

Qasim ALI

CONTRIBUTION TO THE MATHEMATICAL MODELING OF IMMUNE RESPONSE

Speciality: Process Engineering

Keywords: T-cell, activation rate, reaction rate, proliferation, population balance model

## Abstract:

The early steps of activation are crucial in deciding the fate of T-cells leading to the proliferation. These steps strongly depend on the initial conditions, especially the avidity of the T-cell receptor for the specific ligand and the concentration of this ligand. The recognition induces a rapid decrease of membrane TCR-CD3 complexes inside the T-cell, then the up-regulation of CD25 and then CD25–IL2 binding which down-regulates into the T-cell. This process can be monitored by flow cytometry technique. We propose several models based on the level of complexity by using population balance modeling technique to study the dynamics of T cells population density during the activation process. These models provide us a relation between the population of T-cells with their intracellular and extracellular components. Moreover, the hypotheses are proposed for the activation process of daughter T-cells after proliferation. The corresponding population balance equations (PBEs) include reaction term (i.e. assimilated as growth term) and activation term (i.e. assimilated as nucleation term). Further the PBEs are solved by newly developed method that is validated against analytical method wherever possible and various approximate techniques available in the literature.



# Acknowledgement

I would like to give my sincere gratitude to my thesis director Prof. Frederic Gruy and the thesis co-director Prof. Claude Lambert for providing me this opportunity to start my PhD studies under their supervision. I am highly grateful to my thesis co-director Prof. Eric Touboul for his invaluable guidance during my PhD studies. Their consistent encouragements, regular meetings and technical discussions have helped me to enhance my skills and accomplish my PhD thesis in time. I am also thankful to them for giving me chance to present my work at international conferences and workshops where I met several outstanding researchers who appreciated my work and gave me their precious ideas to improve my knowledge in this area of research.

I am very thankful to the reviewers of my thesis and all the jury members which gave me very encouraging remarks during my PhD thesis defense. I thank to specially Prof. Shamsul Qamar for being part of the jury by traveling a long distance. I highly appreciate the administration of Ecole des mines and specially the secretaries of CIS center for being so nice and well-organized. I always found them helping in the trouble.

I express my deep gratitude to my parents and all my family members who always prayed for my success and appreciated my efforts so that I can focus on my studies with more dedication. Their extreme desire and full support during my whole study career highly motivated me to pursue my higher studies and complete it accordingly.

I had a wonderful time with all the professors, friends and colleagues. Their sincere advices and social gatherings let me to work in a comfortable environment. The recreational activities with my friends reduced my stress and relaxed my mind so that I can work on my thesis with full of energy and devotion. I am thankful to all those who helped me and discussed the problems during the difficult time.



# Table of Contents

<b>CHAPTER 1 INTRODUCTION .....</b>	<b>1</b>
<b>1.1 INTRODUCTION .....</b>	<b>2</b>
1.1.1 LITERATURE REVIEW .....	2
<b>1.2 MECHANISM OF IMMUNE RESPONSE .....</b>	<b>5</b>
1.2.1 THE PATHOGENS .....	5
1.2.2 ANTIGEN PRESENTING CELL.....	6
1.2.3 T-CELLS .....	8
I) T-cell Development.....	9
II) Importance and Structure of T-cells.....	11
III) T-Cell Expressions .....	13
IV) Activation Process of T-cells.....	16
V) Proliferation and Differentiation.....	17
1.2.4 FLOW-CYTOMETRY .....	18
<b>1.3 MATHEMATICAL MODELING FOR THE IMMUNE RESPONSE AGAINST VIRAL INFECTION .....</b>	<b>20</b>
1.3.1 INFECTIONS AND MATHEMATICAL MODELS.....	21
1.3.2 MODELING POPULATION DYNAMICS.....	22
I) Stochastic Modeling .....	23
II) Deterministic Modeling .....	23
1.3.3 FORMER CONTRIBUTIONS TO MATHEMATICAL MODELING .....	27
I) Contribution by Sidorenko ([6], [7]) .....	27
II) Michel Stamatakis ([27]) .....	30
III) Kavousanakis Work on Cell Population Balance Model [27].....	33

IV) Shamsul Qamar [47] .....	35
<b>1.4 OUR CONTRIBUTION .....</b>	<b>37</b>
<b>1.5 TERMINOLOGY USED IN THE THESIS .....</b>	<b>38</b>
<b><u>CHAPTER 2 PROTEINS DYNAMICS .....</u></b>	<b><u>41</u></b>
<b>2.1 INTRODUCTION .....</b>	<b>42</b>
<b>2.2 MATHEMATICAL MODELING .....</b>	<b>42</b>
<b>2.3 CASE 1 .....</b>	<b>44</b>
<b>2.4 CASE 2 .....</b>	<b>47</b>
2.4.1 FIRST MODEL .....	47
2.4.2 SECOND MODEL.....	50
<b>2.5 CASE 3 .....</b>	<b>54</b>
<b>2.6 CASE 4 .....</b>	<b>63</b>
<b>2.7 CONCLUSION .....</b>	<b>67</b>
<b><u>CHAPTER 3 POPULATION DYNAMICS OF T-CELLS .....</u></b>	<b><u>69</u></b>
<b>3.1 INTRODUCTION .....</b>	<b>70</b>
3.1.1 BIOLOGICAL ASPECTS .....	70
<b>3.2 MATHEMATICAL MODELING .....</b>	<b>73</b>
3.2.1 CONSERVATION LAWS AND POPULATION BALANCE EQUATION .....	75
3.2.2 OVERVIEW OF MODELS.....	77
<b>3.3 SOLVING TECHNIQUES .....</b>	<b>78</b>

3.3.1 METHOD OF CHARACTERISTICS .....	79
3.3.2 TRANSPORT METHOD .....	81
3.3.3 LAX-WENDROFF FINITE DIFFERENCE SCHEME .....	82
3.3.4 FINITE VOLUME METHOD .....	84
<b>3.4 CASE 1 .....</b>	<b>86</b>
<b>3.5 CASE 2A .....</b>	<b>88</b>
3.5.1 MODEL DERIVATION BY USING CONSERVATION LAWS .....	90
<b>3.6 CASE 2B.....</b>	<b>95</b>
<b>3.7 CASE 3 .....</b>	<b>98</b>
3.7.1 COUPLING OF CD3 INTERNALIZATION AND PRODUCTION OF CD25 AND CD25–IL2 .....	100
3.7.2 SOLUTION OF DENSITY FUNCTIONS.....	101
I) CD3 Protein.....	102
II) CD25 Protein.....	103
III) CD25–IL2 Protein .....	105
<b>3.8 CASE 4 .....</b>	<b>107</b>
3.8.1 MODIFIED TRANSPORT METHOD.....	107
3.8.2 SOLUTION OF DENSITY FUNCTIONS.....	109
<b>3.9 CONCLUSION .....</b>	<b>112</b>
<b><u>CHAPTER 4 T-CELL PROLIFERATION .....</u></b>	<b><u>115</u></b>
<b>4.1 INTRODUCTION .....</b>	<b>116</b>
4.1.1 BIOLOGICAL STRUCTURES .....	116
4.1.2 SIMPLIFIED MODEL .....	118

<b>4.2 MODELING HYPOTHESES .....</b>	<b>119</b>
4.2.1 HYPOTHESIS 1.....	120
4.2.2 HYPOTHESIS 2.....	121
4.2.3 HYPOTHESIS 3.....	123
<b>4.3 RESULTS .....</b>	<b>124</b>
4.3.1 HYPOTHESIS 1.....	127
I) Without Crossing .....	127
II) Crossing.....	132
4.3.2 HYPOTHESIS 2.....	137
I) Without Crossing .....	138
II) Crossing.....	141
4.3.3 RELATION BETWEEN HYPOTHESIS 1 AND HYPOTHESIS 2 .....	145
4.3.4 HYPOTHESIS 3.....	147
I) Without Crossing .....	148
II) Crossing.....	151
<b>4.4 CONCLUSION .....</b>	<b>155</b>
 <b>CONCLUSION .....</b>	 <b>157</b>

## Figures

Figure 1.1: Evolution due to the activation of T-cells after recognition against viral infection.....	4
Figure 1.2: Invasion of pathogen into antigen presenting cell and the presentation of antigen by MHC. ....	7
Figure 1.3: Schematic representation of thymic lobule. thymocyte enters into the thymic lobule from CMJ and goes to the subcapsular region. Double negative get converted to double positive thymocyte that interacts with macrophage in order to differentiate CD4+ and CD8+	

T-cells. The survived cells are mature T-cells and they migrate to blood stream through CMJ.....	9
Figure 1.4: Interaction of DP T-cells with Mature APC that results as an apoptosis or as a mature T-cell survival. T-cells survive with the probability of 0.1.....	10
Figure 1.5: Cell membrane and its components continuously move on the surface to detect the signals and tiny particles. Receptor proteins are of different shapes and can allow a specific type of protein to get attached and enter or leave the cell cytoplasm.....	12
Figure 1.6: Structure and behavior of Phospholipid. Head contains the positive charge while tail contains the negative charge so that interaction of charged particles between inner and outer surfaces are restrained.....	13
Figure 1.7: Structural diagram of CD3 complex in which CD3, CD4+/CD8+ and TCR proteins are shown in contact with each other.....	14
Figure 1.8: Reappearance of CD3 protein as CD3* protein on the surface of T-cell but outside the synapse for CD3 protein.....	14
Figure 1.9: Protein expressions of T-cells.....	15
Figure 1.10: Activation process of T-cells. Table II illustrate the numbers written in this figure. .	17
Figure 1.11: Flow cytometer with one forward-scatter and four side-scatter detectors.....	19
Figure 1.12: CD3+ and CD25+ T-cells population detected by Flow cytometer (FCM) .....	20
Figure 1.13: Ongoing research in viral disease dynamics.....	21
Figure 1.14: Various modeling techniques for population techn.....	22
Figure 1.15: Illustration of balance law. The change in the protein concentration in a set of population increases the density of T-cells for small step size $\Delta c$ while the total population remains conserved throughout the simulation time.....	26
Figure 1.16: Graphical presentation of flow of population from time $t$ to $t+dt$ .....	27
Figure 2.1: Interaction of T-cell with pMHC.....	42
Figure 2.2: CD3 protein degradation and the production of CD3i protein.....	44
Figure 2.3: Concentration decrease in CD3 Protein.....	46
Figure 2.4: Reappearance of CD3 protein .....	48
Figure 2.5: Surface concentration for individual T-cell. Blue lines show the exact solution while red-circles show the RK-4 solution and the green asteriks (*) indicate the solution by Euler method. ....	49

Figure 2.6: CD3 protein dynamics. Sum of Internalization and reappearance of CD3 protein. Blue lines show the exact solution while red-circles show the RK-4 simulation. The green asterisks (*) are the solution found by Euler Method .....	53
Figure 2.7: Protein dynamics of T-cell. CD3 protein internalizes and produces CD25 and IL-2 that again binds together to give signals inside the T-cells.....	55
Figure 2.8: Plane cutting the 2 dimensional manifold (surface) at a point $t=t_0$ .....	61
Figure 2.9: Graphical representation of the solution of above system of ODEs with the parameter values: .....	62
Figure 2.10: Graphical representation of the solution of above system of ODEs with the parameter values: .....	64
Figure 2.11: 3D visualization of CD25 protein concentration cut by two planes. The cutting curves are shown in the 2D plot attached at the top right of the figure. ....	65
Figure 2.12: 3D visualization of CD25-IL2 protein cut by four planes. The topright plot shows the curves made due to the intersections of the surface plot and the planes. ....	66
Figure 3.1: Population of CD3 and CD25 proteins on the surface of CD8+ T-cells .....	71
Figure 3.2: Initial population of activated T-cells at two different concentrations $c_0$ and $c_1$ . ....	73
Figure 3.3: T-cells are activated with different initial concentrations at time $t = t_0$ and distributed over the $c$ -axis. ....	74
Figure 3.4: Activated T-cells flux in and flux out indicated during the variation in concentration $c$ to $c + \Delta c$ at time $t = t_0$ . T-cells are activated with the activation flux in $N(c, t_0)$ .....	76
Figure 3.5: Solution followed by Method of Characteristics.....	80
Figure 3.6: Flux of the protein and the density of T-cells.....	81
Figure 3.7: The effect of flux limiter on 2nd order Lax-Wendroff Method.....	84
Figure 3.8: Finite volume upwind scheme on cartesian mesh.....	85
Figure 3.9: Population density of T-cells according to their protein levels at different time $t$ .....	88
Figure 3.10: Numerical computation of $\tau_1$ and $\tau_2$ .....	90
Figure 3.11: Principle of the numerical scheme .....	93
Figure 3.12: Diffusion in the numerical scheme at the rear and the front side.....	94
Figure 3.13: Results with finite volume scheme (Upwind as dashed line) and Transport Method (TM as line).....	95
Figure 3.14: Results with finite volume scheme (Upwind – dashed line) and Transport Method (CM - line).....	97

Figure 3.15: Dynamical changes in T-cells with respect to proteins and the population dynamics of the activation T-cells .....	98
Figure 3.16: Population density of CD3 protein with respect to concentration at different times in seconds. The kinetic parameter for CD3 protein concentration is $k_1 = 1/5 \times 10^{-4} s^{-1}$ .....	102
Figure 3.17: Population density of CD25 protein with respect to concentration at different times in seconds .....	104
Figure 3.18: Population density of CD25-IL2 protein with respect to concentration at different times in seconds .....	106
Figure 3.19: Population dynamics between of types of T-cells meeting at the crossing point lies in the interval $[t, t+\Delta t]$ .....	108
Figure 3.20: Population density of CD25 protein with respect to concentration at different times in seconds .....	110
Figure 3.21: Population density of CD25-IL2 protein with respect to concentration at different times in seconds .....	111
Figure 4.1: Division of a single parent T-cell after the getting fully activated. ....	117
Figure 4.2: Protein dynamics at a single T-cell level. Part of the daughter T-cells start their activation process after a transition period of division. ....	119
Figure 4.3: Creation of activated T-cells as virgin. Cells are activated according to Eq. (4.2) and distributed at $t = \tilde{\tau} + T$ according to the distribution defined in the Eqs. (4.3) and (4.4). ...	120
Figure 4.4: Distribution of daughter T-cells after proliferation.....	122
Figure 4.5: Distribution of daughter T-cells over the population of activated T-cells at $t \geq \tilde{\tau} + T$ .....	123
Figure 4.6: Population density of activated T-cells with and without proliferation .....	125
Figure 4.7: Results for the activation of T-cells after proliferation.....	126
Figure 4.8: Graphical representation of protein dynamics at single T-cell level that are activating at succeeding activation times. The threshold level at which the division start is $t = \tilde{\tau} + T$ that is almost $t=100,000$ s. The daughter cells start activating after $t=150,000$ s. The kinetic constants are given the following values:.....	128
Figure 4.9: Population density of T-cells with internalized CD25-IL2i protein. The threshold level at which the division starts is $c_6 = 10^{-3} mol.m^{-3}$ and the time is after almost a day ( $t = 100,000$ s). The daughter cells start activating after time $t = 150,000$ s. ....	129

- Figure 4.10: Population density of T-cells for CD3 protein. The threshold level at which the division starts is  $c_6 = 10^{-3} \text{ mol.m}^{-3}$  and the time is after almost a day ( $t = 100,000 \text{ s}$ ). The daughter cells start activating after  $t = 150,000 \text{ s}$ . 'No Prolif' is the 'No Proliferation' curve showing the population density of T-cells without including daughter cells..... 130
- Figure 4.11: Population density of T-cells with surface protein CD25. The threshold level at which the division starts is  $c_6 = 10^{-3} \text{ mol.m}^{-3}$  and the time is after almost a day ( $t = 100,000 \text{ s}$ ). The daughter cells start activating after  $t = 150,000 \text{ s}$ . 'No Prolif' is the 'No Proliferation' curve showing the population density of T-cells without including daughter cells. .... 131
- Figure 4.12: Population density of T-cells with surface binding CD25-IL2. The threshold level at which the division starts is  $c_6 = 10^{-3} \text{ mol.m}^{-3}$  and the time is after almost a day ( $t = 100,000 \text{ s}$ ). The daughter cells start activating after  $t = 150,000 \text{ s}$ . 'No Prolif' is the 'No Proliferation' curve showing the population density of T-cells without including daughter cells. .... 132
- Figure 4.13: Protein dynamics at single T-cell level that are activating at succeeding activation times and crossing each other. The threshold level at which the division start is  $c_6 = 5.6 \times 10^{-4} \text{ mol.m}^{-3}$  that is almost  $t = 100,000 \text{ s}$ . The daughter cells start activating after  $t = 150,000 \text{ s}$ . The kinetic constants are given the following values: ..... 133
- Figure 4.14: Population density of T-cells with CD25-IL2i internalized protein. The threshold level at which the division starts is  $c_6 = 5.6 \times 10^{-4} \text{ mol.m}^{-3}$  and the time is after almost a day ( $t = 100,000 \text{ s}$ ). The daughter cells start activating after  $t = 150,000 \text{ s}$ . .... 134
- Figure 4.15: Population density of T-cells with CD3 surface protein. The threshold level at which the division starts is  $c_6 = 5.6 \times 10^{-4} \text{ mol.m}^{-3}$  and the time is after almost a day ( $t = 100,000 \text{ s}$ ). The daughter cells start activating after  $t = 150,000 \text{ s}$ . 'No Prolif' is the 'No Proliferation' curve showing the population density of T-cells without including daughter cells. .... 135
- Figure 4.16: Population density of T-cells with CD25 surface protein. The threshold level at which the division starts is  $c_6 = 5.6 \times 10^{-4} \text{ mol.m}^{-3}$  and the time is after almost a day ( $t = 100,000 \text{ s}$ ). The daughter cells start activating after  $t = 150,000 \text{ s}$ . 'No Prolif' is the 'No Proliferation' curve showing the population density of T-cells without including daughter cells. .... 136
- Figure 4.17: Population density of T-cells with surface binding CD25-IL2. The threshold level at which the division starts is  $c_6 = 5.6 \times 10^{-4} \text{ mol.m}^{-3}$  and the time is after almost a day ( $t = 100,000 \text{ s}$ ). The daughter cells start activating after  $t = 150,000 \text{ s}$ . 'No Prolif' is the 'No

Proliferation' curve showing the population density of T-cells without including daughter cells. ....	137
Figure 4.18: Population density of T-cells for CD3 protein. The threshold level at which the division starts is $c_6 = 10^{-3} \text{ mol.m}^{-3}$ and the time is almost a day ( $t = 100,000 \text{ s}$ ). The daughter cells start activating after $t = 150,000 \text{ s}$ . ....	139
Figure 4.19: Population density of T-cells for CD25 protein. The threshold level at which the division starts is $c_6 = 10^{-3} \text{ mol.m}^{-3}$ and the time is almost a day ( $t = 100,000 \text{ s}$ ). The daughter cells start activating after $t = 150,000 \text{ s}$ . ....	140
Figure 4.20: Population density of T-cells for CD25-IL2 protein. The threshold level at which the division starts is $c_6 = 10^{-3} \text{ mol.m}^{-3}$ and the time is almost a day ( $t = 100,000 \text{ s}$ ). The daughter cells start activating after $t = 150,000 \text{ s}$ . ....	141
Figure 4.21: Population density of T-cells for CD3 protein. The threshold level at which the division starts is $c_6 = 5.6 \times 10^{-4} \text{ mol.m}^{-3}$ and the time is almost a day ( $t = 100,000 \text{ s}$ ). The daughter cells start activating after $t = 150,000 \text{ s}$ . ....	142
Figure 4.22: Population density of T-cells for CD25 protein. The threshold level at which the division starts is $c_6 = 5.6 \times 10^{-4} \text{ mol.m}^{-3}$ and the time is almost a day ( $t = 100,000 \text{ s}$ ). The daughter cells start activating after $t = 150,000 \text{ s}$ . ....	143
Figure 4.23: Population density of T-cells for CD25-IL2 protein. The threshold level at which the division starts is $c_6 = 5.6 \times 10^{-4} \text{ mol.m}^{-3}$ and the time is almost a day ( $t = 100,000 \text{ s}$ ). The daughter cells start activating after $t = 150,000 \text{ s}$ . ....	144
Figure 4.24: Effect of the variation in the value of $q_2$ on the population density of CD3 T-cells. ....	145
Figure 4.25: For CD3 protein, the population density of T-cells by using hypothesis 2 approaches the population density of T-cells by using hypothesis 1 if the Eq (4.10) holds. ....	147
Figure 4.26: Population density of T-cells for CD3 protein. The threshold level at which the division starts is $c_6 = 10^{-3} \text{ mol.m}^{-3}$ and the time is almost a day ( $t = 100,000 \text{ s}$ ). The daughter cells start activating after $t = 150,000 \text{ s}$ . $\alpha$ is the number of daughter cells undergo in the process of activation. The time $t = 50,000 \text{ s}$ and the time $t = 100,000 \text{ s}$ are before proliferation while the time $t = 175,000 \text{ s}$ and $t = 250,000 \text{ s}$ are after proliferation. ....	149
Figure 4.27: Population density of T-cells for CD25 protein. The threshold level at which the division starts is $c_6 = 10^{-3} \text{ mol.m}^{-3}$ and the time is almost a day ( $t = 100,000 \text{ s}$ ). The daughter cells start activating after $t = 150,000 \text{ s}$ . $\alpha$ is the number of daughter cells undergo in the	

process of activation. The time  $t = 50,000$  s and the time  $t = 100,000$  s are before proliferation while the time  $t = 175,000$  s and  $t = 250,000$  s are after proliferation..... 150

Figure 4.28: Population density of T-cells for CD25-IL2 protein. The threshold level at which the division starts is  $c_6 = 10^{-3} \text{ mol.m}^{-3}$  and the time is almost a day ( $t = 100,000$  s). The daughter cells start activating after  $t = 150,000$ s.  $\alpha$  is the number of daughter cells undergo in the process of activation. The time  $t = 50,000$  s and the time  $t = 100,000$  s are before proliferation while the time  $t = 175,000$  s and  $t = 250,000$  s are after proliferation..... 151

Figure 4.29: Population density of T-cells for CD3 protein. The threshold level at which the division starts is  $c_6 = 5.6 \times 10^{-4} \text{ mol.m}^{-3}$  and the time is almost a day ( $t = 100,000$  s). The daughter cells start activating after  $t = 150,000$  s.  $\alpha$  is the number of daughter cells undergo in the process of activation. The time  $t = 50,000$  s and the time  $t = 100,000$  s are before proliferation while the time  $t = 175,000$  s and  $t = 250,000$  s are after proliferation..... 152

Figure 4.30: Population density of T-cells for CD25 protein. The threshold level at which the division starts is  $c_6 = 5.6 \times 10^{-4} \text{ mol.m}^{-3}$  and the time is almost a day ( $t = 100,000$  s). The daughter cells start activating after  $t = 150,000$  s.  $\alpha$  is the number of daughter cells undergo in the process of activation. The time  $t = 50,000$  s and the time  $t = 100,000$  s are before proliferation while the time  $t = 155,000$  s and  $t = 250,000$  s are after proliferation..... 153

Figure 4.31: Population density of T-cells for CD25-IL2 protein. The threshold level at which the division starts is  $c_6 = 5.6 \times 10^{-4} \text{ mol.m}^{-3}$  and the time is almost a day ( $t = 100,000$  s). The daughter cells start activating after  $t = 150,000$  s.  $\alpha$  is the number of daughter cells undergo in the process of activation. The time  $t = 50,000$  s and the time  $t = 100,000$  s are before proliferation while the time  $t = 155,000$  s and  $t = 250,000$  s are after proliferation..... 154

Figure 4.32: Graphical comparison between Biological and Mathematical results.. ..... 155

## Tables

Table I: Diseases caused by viruses. .... 6

Table II: Six processes involved in this study to describe the T-cell activation dynamics. .... 16

Table III: Terminology used in the thesis ..... 39

Table IV: Step wise description of T-cell activation process..... 43

Table V: Prominent attributes of activated T-cells..... 78

## Table of Abbreviations:

<u>ABB.</u>	<u>DESCRIPTION</u>	<u>ABB.</u>	<u>DESCRIPTION</u>
<b>PBM</b>	Population balance model	$c$	Concentration of protein
<b>T-cell</b>	Cell	$t$	Time
<b>RNA</b>	Ribonucleic acid	$n(c,t)$	Density of T cells with protein concentration $c$ at time $t$
<b>APC</b>	Antigen presenting cell	$G(c)$	Reaction rate with protein concentration $c$
<b>MHC</b>	Major histo-compatibility complex	$N(c,t)$	Initial population density of activated cells with concentration $c$ within the change in time $t$ and $t + \Delta t$
<b>CD</b>	<i>Cluster of differentiation</i> (protein)	$D(c)$	Distribution of initial population
<b>T<sub>H</sub> cell</b>	Helper cell	$B(t)$	Birth rate (production) of activated T-cell
<b>IFN</b>	Interferon	$\delta(c - c_0)$	Dirac-delta function
<b>IL-2</b>	Interleukin 2	$N_{AC}(t)$	Concentration of activated T-cell
<b>IL-2R</b>	IL-2 receptor	$N_{APC}(t)$	Concentration of antigen presenting cell
<b>kDA</b>	Kilo dalton	$N_{NAC}(t)$	Concentration of non-activated T-cell
<b>DNA</b>	Deoxyribonucleic acid	ODE	Ordinary differential equation
<b>TCR</b>	T Cell receptor	PDE	Partial differential equation
<b>GFP</b>	Green fluorescent protein	FCM	Flow cytometer
<b>Cy</b>	Cytokine		



# **Chapter 1**

## **Introduction**

## 1.1 Introduction

---

### 1.1 Introduction

Mathematical modeling (MM) of dispersed systems is well enriched in all fields of sciences. It is sufficiently prevalent in chemical industries and biological sciences where population density of particulate systems is studied as a function of the particle size, age and other physical properties. Crystallization, comminution, fluidized-bed granulation and aerosol-science are the most common applications in the chemical industries [1], [2]. In biological sciences, MM is getting enriched by modeling of continuous variation in the microbial populations [3] and the immunity response against such pathogens [4], [5]. Correspondingly, the applications include the population dynamics of virus replication and vaccine production for their control [6], [7]. The immune response was studied for the activation of T-cells against the influenza virus infection [8], [4]. This study is a continuation of the previous work for the population dynamics that was based on the experimental observations of in-vitro [8], [4]. Here the cell population balance model is applied efficiently as a modeling technique in order to analyze the population density function for the activated T-cells with respect to the surface protein concentration. Several analytical and numerical methods are utilized to find the solution of the modeled problem.

#### 1.1.1 Literature Review

T-cells are responsible for the cognitive immunity response by providing specific protection against infections such as virus. Each T-cell clone is highly specific for one antigenic determinant peptide that is exposed by the self MHC molecule as a peptide – MHC complex. The T-cell has the capacity to recognize the antigenic determinant and starts an activation process that could eventually lead to its proliferation and maturation. The TCR – peptide – MHC complex binding is very fragile but strengthened by co-receptors (proteins) such as CD4 or CD8 and adhesion molecules, forming the immune synapse [9], [10]. As TCR does not have cytoplasmic tail, the signal induced by the recognition is transduced through the CD3 molecular complex that is physically associated to the TCR [11], [12]. The involved CD3-TCR complex is then internalized inducing a significant decrease of the membrane CD3/TCR density [13], [14]. A minimal level of TCR/CD3 engagement in a limited period of time is required to reach an efficient threshold for a full T-cell activation [15], [16].

## 1.1 Introduction

---

The full engagement of T-cells in the activation process leads to the production of several proteins required for the next steps. These proteins can be measured on cell surface (e.g. CD69, CD25, CD71, HLA-DR ...) [17], [18] or as soluble cytokines released in the biological medium such as IL-2 [17]. The CD25, the alpha chain of the IL-2 receptor, is also induced in T-cell activation and join the other ( $\beta$ ,  $\gamma$ ) chains to constitute a complete, functional receptor with high affinity for IL-2 on the cell membrane [17], [18]. Thus, the produced IL-2 binds to its newly produced receptor. The complex is internalized and induces signal transduction that amplifies the subsequent steps of the T-cell activation. The internalized level of IL-2 IL-2R complex (CD25-IL2 binding) makes the decision for the full T-cell activation that ends in the cell proliferation [17].

Thus, the dynamics of T-cell activation directly depends on biophysical parameters such as the respective membrane concentrations of the peptide-MHC and TCR-CD3 and their mutual avidity [19], [20]. It can be quantified according to the classical kinetic rules of association and dissociation. It can then be modeled by using ordinary differential equation systems (ODEs) that have been already used in modeling other biological processes [21], [22], [23]. Previously an ODE model is developed mimicking the dynamics of specific activation of a single T-cell [3].

We achieved experiments where a selected peptide is presented to the relevant specific T-cells *ex-vivo* in perfectly controlled conditions using an animal model and *ex-vivo* cell stimulation, and we measured the early activation induced changes on T-cell by multicolor flow cytometry [4], [8]. On flow cytometry, the membrane amount of proteins can be directly estimated by immune-labeling. The protein concentration is directly proportional to their fluorescence intensity and several markers can be analyzed simultaneously, at high speed, on a large amount of individual cells. However, actual tools available are not adapted for the analysis of the dynamics of each single cell inside a heterogeneous population with continuous variable. This is why we considered using dynamics of cell population concept. This leads us to propose a Population Balance Equation (PBE) with an order depending on the number of internal variables considered (protein concentrations). Higher is the number of internal cell parameters describing the cell state, more difficult is solving the population balance equation.

## 1.1 Introduction

---

Population balance modeling has been successfully applied in chemical engineering including polymerization, crystallization and precipitation processes [2], [24], [25]. PBE is a partial differential equation containing terms for birth and death of individuals such as particles or crystals. In this example, each term of the PBE corresponds to a precipitation status such as particle nucleation, growth or dissolution, settling, collision and agglomeration. Each single particle of the population is individually characterized. PBE has also been used for the mathematical description of the biological processes occurring in microbial or eukaryote cell populations [26], [27]. Cell populations are complex heterogeneous systems in which each cell is characterized by its size, morphological parameters and proteins content. Generally, the PBE cannot be solved analytically. Deterministic numerical schemes or stochastic approach have to be implemented for getting the solution of the given PBE [26].

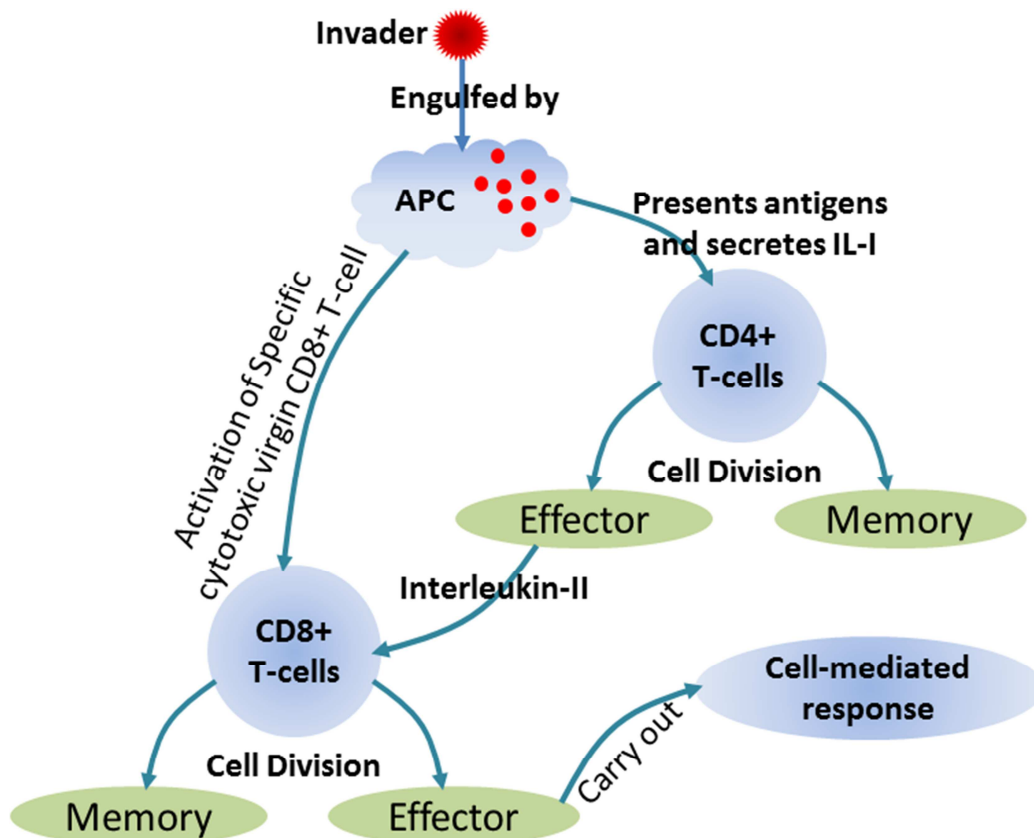


Figure 1.1: Evolution due to the activation of T-cells after recognition against viral infection.

In order to better analyze the precise individual dynamics of T-cell activation FCM (Flow Cytometer Machine) data, we have developed an original mathematical model based on PBE by

## 1.2 Mechanism of Immune response

---

considering theoretical single T-cell fate on the basis of the rules of ligand-receptor interaction which had been developed previously [3]. The cell distribution of the complete heterogeneous population could then be addressed considering the diversity of their initial parameters. Our approach has opened a new area of interest on the very early steps of the activation process and analysis by flow cytometry.

## 1.2 Mechanism of Immune response

T-lymphocytes lie in the category of leucocytes and have a very important role in the antigen specific (cognitive) cellular immunity. T-lymphocytes response is considered as the secondary immune response as it comes into action after the frontline immune system in order to prevent further viral infection. They are antigen specific and need to be educated before optimal activation performances. They can detect virally infected cells and tumor cells. Cytotoxic T-cells gradually exposed to the infected cell and kill them either by means of cell surface interactions between them and infected cell or through intermediates soluble mediators by forming pores in the infected cell and releasing cytotoxins in it.

### 1.2.1 The Pathogens

Pathogens are microscopic organisms that are natural disease producers. Mainly there are three types of pathogens, namely, bacteria, virus and parasites. Bacteria are unicellular micro-organisms that can survive in any hot place with nutriment. It can also live in animal's body and can be helpful in digesting the food (saprophytes). Most of the bacteria are not infectious, some are infectious (invade and harm the body by invasion, proliferation and toxin production) but their treatment is possible by antibiotics that strongly help immune system to perform its role to reduce the burden.

On the other hand the viruses are smaller than bacteria but are biggest threat to human and other animals. They cannot survive without living hosts (organism) and, after invasion, enters inside the cell and holds the cell mechanism to reproduce identical viruses. The virus reproduction ends in the destruction of the host cell and the invasion of nearby new fresh cells. Unfortunately, antibodies failed to help once the virus is inside the cell. Early destruction of the cell is the most

## 1.2 Mechanism of Immune response

---

efficient way to stop the virus reproduction. Alternatively some viruses can alter the behavior of host cells and possibly induce cancer or cell degeneration. Below is a table that describes such viral infections with their invasion targets and transmission mediums.

Virus induced response can induce misrecognition and self-damaging of the host itself. These are called an auto-immune attack that includes insulin-dependent diabetes mellitus, rheumatoid arthritis, multiple sclerosis and Guillain-Barré (GB) syndrome. As an example, the GB syndrome appearance has been related to bacterium *Campylobacter-jejuni* or by influenza viral infection but the main cause for 60% of such cases is still unknown [28].

Disease	Causal Agent	Organs affected	Transmission
Influenza	RNA	Respiratory Track	Droplets
Hepatitis A	RNA	Liver	Food, Water, Contact
Hepatitis B	DNA	Liver	Contact with body Fluids
Dengue Fever	RNA	Blood, Muscles	Mosquito ( <i>Aedes Aegypti</i> <sup>1</sup> )
AIDS	Retrovirus (RNA)	T-lymphocytes	Contact with body Fluids
Polio	RNA	Intestine, Spinal Cord	Food, Water, Contact
Chicken pox	DNA	Skin, Nervous System	Droplets, Contact

Table I: Diseases caused by viruses.

### 1.2.2 Antigen Presenting Cell

Certain cells are antigen presenting cells (APCs). APCs act as the primary response against the virus infection. In the primary infection, the virus needs to invade the body and, after some rest that can be several days or years, the virus starts replicating and inducing cell damages, and thereafter disease. At this stage, viral particles can be trapped by APCs and presented to the specific immune cells. The immune response takes further time (few 10-15 days) to mature and become efficient. The immune response must be strong, fast enough and adapted. Too light response will not be efficient and a too strong response may be harmful for the host itself. In

---

<sup>1</sup> A mosquito that transmits yellow fever and dengue.

## 1.2 Mechanism of Immune response

---

some conditions, some cells can act as antigen presentation (non-professional APCs) with lower performances.

The professional APCs include dendritic cells, macrophages, B-cells and certain activated epithelial cells. They are very efficient to internalize the virus and present it on the surface by a peptide attached with a molecule major histocompatibility complex class 2 (MHC-II). The non-professional APCs include all other body cells. It presents the pathogen (particularly virus) by a peptide attached with different molecule, namely MHC-I. A detailed analysis of the structure and function of APCs can be found in [29].

In the secondary exposure, the specific immune response is already prepared and can act directly and efficiently. Thus in the primary response, the kinetics of both the infection and the immune process are crucial to know which of the invader or the defense will be prominent. The delay, the speed and the intensity of the response depend mainly on the density and avidity of the peptide presented to the T-cells. For one given cause (virus), many peptides are made available and many T-cells can act in different way according to their avidity for their respective peptide and their own individual capacity to respond.

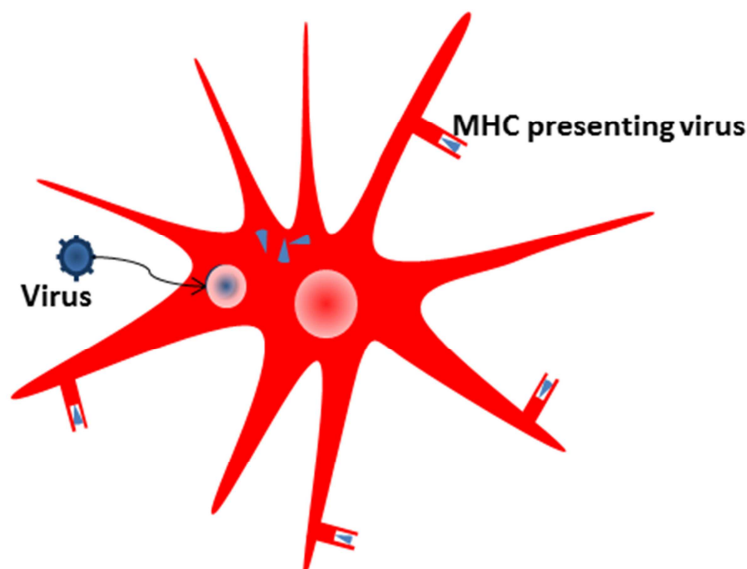


Figure 1.2: Invasion of pathogen into antigen presenting cell and the presentation of antigen by MHC.

## 1.2 Mechanism of Immune response

---

### 1.2.3 T-cells

T-cell is one of the major types of lymphocytes present in the blood as a part of white blood cells. T-cells are early stage matured in the thymus and later matured in lymph nodes. Some proteins are present on the surface of T-cell according to maturation stage while hundreds of more proteins are produced during the process of T-cell activation. They are discriminated from other lymphocytes, mainly B-cells, and natural killer cells (NK-cells) due to the presence of T-cell receptor [30] on their surface. This receptor protein (membrane) allows the T-cells to recognize antigens. After the recognition of T-cells with the antigens, the T-cells activate, proliferate, differentiate and kill those body cells that are considered as harmful for the body homeostasis. At the end, the apoptosis of T-cells takes place that reduce the specific T-cells to a normal amount in the blood stream.

T-cells categorize in two classes due to distinction between their T-cell receptors and they are known as  $\gamma\delta$  and  $\alpha\beta$  T-cells. Majority of peripheral blood T-cells in humans and mice are  $\alpha\beta$  T-cells ( $\approx 98\%$  of total T-cells). In contrast to  $\alpha\beta$  T-cells,  $\gamma\delta$  T-cells have T-cell receptor made up of  $\gamma$  chain and  $\delta$  chain. The  $\gamma\delta$  T-cells do not recognize peptide bound to MHC-I and MHC-II. Moreover, the antigenic molecules that activate  $\gamma\delta$  T-cells are not peptides but glycolipids. Therefore, we focus on  $\alpha\beta$  T-cells that are activated by MHC peptides and well established by the experimental procedures.

The  $\alpha\beta$  T-cells are further classified into two main categories according to the T-cell interaction with MHC: one is the CD4<sup>+</sup> T-cells while the second category is CD8<sup>+</sup> T-cells. CD4<sup>+</sup> T-cells are helper cells that cannot fight against the antigen directly; instead they help CD8<sup>+</sup> T-cells and B-cells to act against the APCs. Also they are used as regulatory cells that coordinate the immune response after their proliferation. The CD8<sup>+</sup> T-cells are cytotoxic and are self-motivated that can act against the APC without any interference of other body cells, e.g. B-cells. We will further talk about these cells consistently. Now a brief description of the T-cell development and differentiation is stated below that explains different stages of T-cells during their life.

## 1.2 Mechanism of Immune response

### 1) T-cell Development

In mammals, lymphocytes (B and T) and professional APCs are mainly brought to full maturation in the primary lymphoid organs. During fetal life they are found in yolk sac that is taken over by the fetal liver and spleen. In adult life, all the blood cells including lymphocytes and professional APCs are generated in Bone-marrow. All the cells including B lymphocytes and Natural Killer (NK) cells diffuse into the blood stream [31]. While T-cells leave early bone-marrow as immature and come to develop in thymus where CD4 and CD8 distinction takes place after passing through different stages.

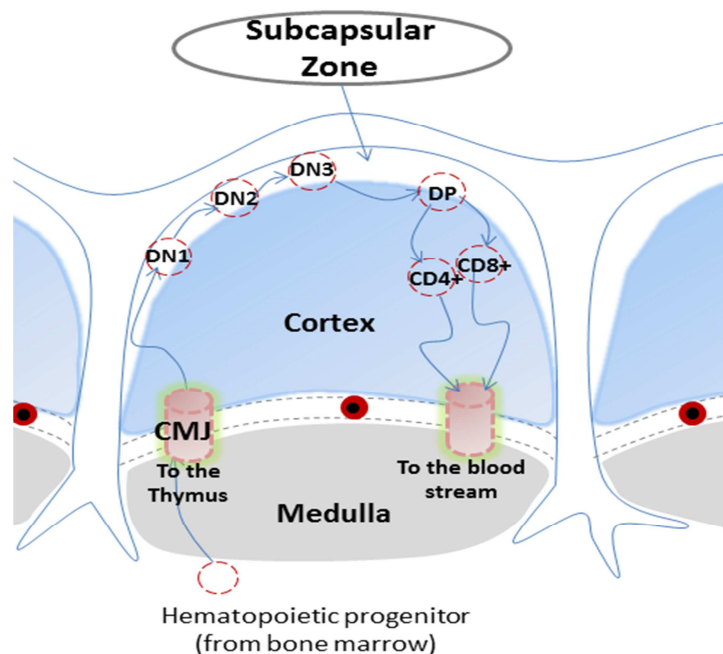


Figure 1.3: Schematic representation of thymic lobule. thymocyte enters into the thymic lobule from CMJ and goes to the subcapsular region. Double negative get converted to double positive thymocyte that interacts with macrophage in order to differentiate CD4+ and CD8+ T-cells. The survived cells are mature T-cells and they migrate to blood stream through CMJ.

The development of T-cells in the thymus involves a strict selection process in which 1% to 3% of thymocytes succeed and export into the blood stream. The selection procedure involves the recognition roots that are produced randomly and useful (not self-dangerous) cells are eliminated. Thymocytes dynamically migrate across different regions of thymic lobule each representing a unique strong environment in order to introduce key elements in the development process of T-cells. The most notable regions are the corticomedullary junctions (CMJ), cortex, subcapsular zone and finally the medulla. T-cells arrive from stem cells and differentiate into lymphoid progenitor cells.

## 1.2 Mechanism of Immune response

T-cell progenitors move into the thymus (and become thymocytes) by means of endothelial venules present on CMJ and crawl to a subcapsular zone. At this time the thymocytes lack TCR, CD4 and CD8 and therefore termed as double negative (DN). These thymocytes pass through different stages of DN (DN1, DN2, DN3, DN4) in which they express pre-TCR  $\alpha\beta$  chains [32]. During cell progress from DN2 to DN4, the thymocyte expresses both CD4 and CD8 expressions as well as TCRs and rearrange the  $\alpha$  and  $\beta$  chains which yield a complete  $\alpha\beta$ -TCR. This leads to extensive cell proliferation during the phase transition from double negative (DN) to double positive (DP). As development proceeds and cell begins to express its specific receptor, these thymocytes migrate further into the thymic cortex where a high density of MHC-I and MHC-II molecules are associated with self-peptides. An interaction between  $\alpha\beta$ -TCR+CD4+CD8+ and MHC – peptide complex takes place that is displayed by the thymic cortical epithelial cells. This process plays an important role in deciding the faith of the thymocyte [33].

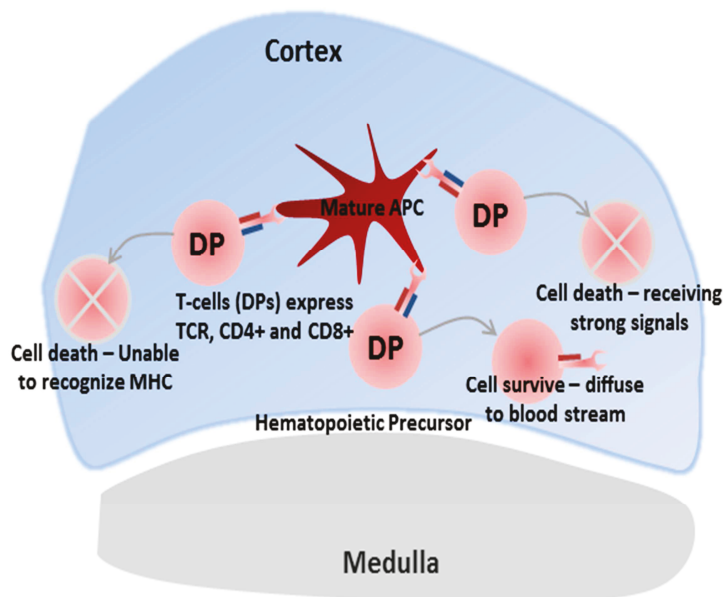


Figure 1.4: Interaction of DP T-cells with Mature APC that results as an apoptosis or as a mature T-cell survival. T-cells survive with the probability of 0.1.

A TCR that is able to recognize the MHC class I molecule receives both a survival signal and a maturation signal. Eventually, the cell stops expressing CD4 and maintains expression of CD8. A thymocyte that obtains a survival signal is set to undergo a positive selection. Similarly, a cell that has receptor able to recognize MHC class II molecules also receives a survival signal and a

## 1.2 Mechanism of Immune response

---

different maturation signal. Finally this cell stops expressing CD8 and maintain the expression of CD4. Those thymocytes that are unable to recognize either MHC-I or MHC-II molecules fails to receive any survival signals and die by programmed cell death or apoptosis [34].

Thymocytes that are able to recognize MHC-I or MHC-II peptide complexes too avidly receives strong signals and it drives them into cell death. In this way thymocytes that are able to respond against self-peptide antigens are eliminated in a process known as negative selection or central tolerance. The surviving T-cells migrate from thymic cortex to medulla. At this stage they remain capable of recognizing self-peptide antigens expressed on other cell types such as dendritic cells or thymic macrophages and receive sufficient signals to cause them to undergo program cell death. The remaining thymocytes are now mature CD4<sup>+</sup> and CD8<sup>+</sup> T-cells and pass out of the thymus. They either return into the blood stream directly by passing through the venules or by the lymphatic system. These cells are fully equipped with the necessary knowledge and tools to mount an immune response [31].

### ***II) Importance and Structure of T-cells***

T-cells are the type of lymphocytes that have a prominent role in specific immune recognition in variety of cell-mediated responses that includes anti-viral immunity, anti-tumor immunity and help in the production of antibody by B-cells. They play an important role in cell-mediated immunity and memory eventually when innate immune response has removed a limited invasion. There are various types of T-cells which have specific functions to fight against the foreign invaders, e.g. CD4<sup>+</sup> T-cells and CD8<sup>+</sup> T-cells. The limitation of T-cells is that they can only recognize the foreign antigen when it is presented on the surface of the body cell that is also known as Antigen Presenting Cell (APC).

The importance of T-cells can be categorized according to their structure and function. Like other body cells, T-cells are also composed of nucleus and cytoplasmic region that are covered by cell membrane. Nucleus is covered up by nuclear membrane that mostly contains genetic information. Tiny pores on the membrane cover whole nucleus by making a complex known as nuclear pore complex (NPC). The cytoplasm of T-cell is mostly composed of water, salt and organic molecules [35]. It includes cell organelles for all cell functions like respiration, digestion, etc.

## 1.2 Mechanism of Immune response

---

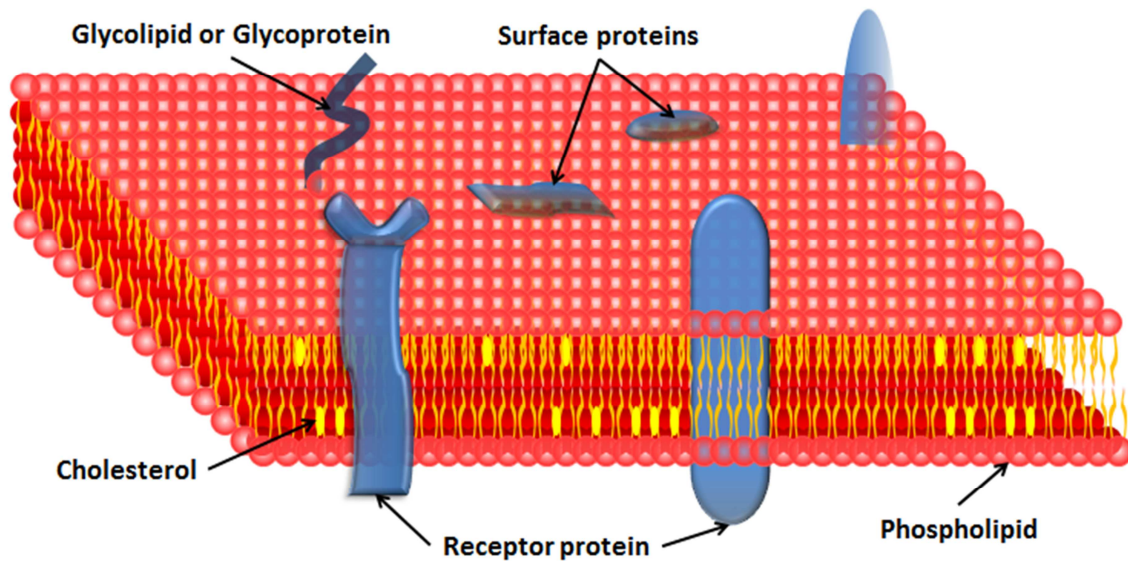


Figure 1.5: Cell membrane and its components continuously move on the surface to detect the signals and tiny particles. Receptor proteins are of different shapes and can allow a specific type of protein to get attached and enter or leave the cell cytoplasm.

In particular to our interest, cell membrane plays a vital role due to its selective permeability property by which it can interact selectively with the foreign components. Cell membranes are mostly composed of fluidic substances and it contains several components. The composition of cell membrane is well defined by fluid mosaic model (FMM) [36]. According to this model, cell membrane can be divided into rafted and non-rafted regions. Part of the cell membrane is composed of glycoprotein, cholesterol and glycolipids that have significant importance. The rest of the portion is based on the phospholipids (i.e. fats, phosphoric acid, and nitrogenous base) that are amphipathic in nature. The glycoproteins like TCR, CD3, CD25 and CD69 etc. are inserted in between phospholipids as shown in Figure 1.5.

The phospholipids have a shape like a head with a long tail as shown in Figure 1.6. The head has a charge that makes it polarized while in contrast, the tail is non-polarized. This stops the diffusion of charged substance like water between the inner and outer portion of T-cell. The cell membrane, phospholipids, is in a continuous motion. The phospholipids are bind with cholesterol molecules so that they stick together at any circumstances. Therefore the uncharged but small elements like oxygen and carbon dioxide are allowed to pass. For the bigger and charged molecules, proteins receptors are usually used. These proteins come in bunch of different shapes and sizes and, therefore, it is not possible for them to accept each kind of molecule. This

## 1.2 Mechanism of Immune response

---

classifies the T-cells into different categories and assigns the job to each of its type. This shows the importance of the proteins receptors and why the transfer of signal needs various protein receptors.

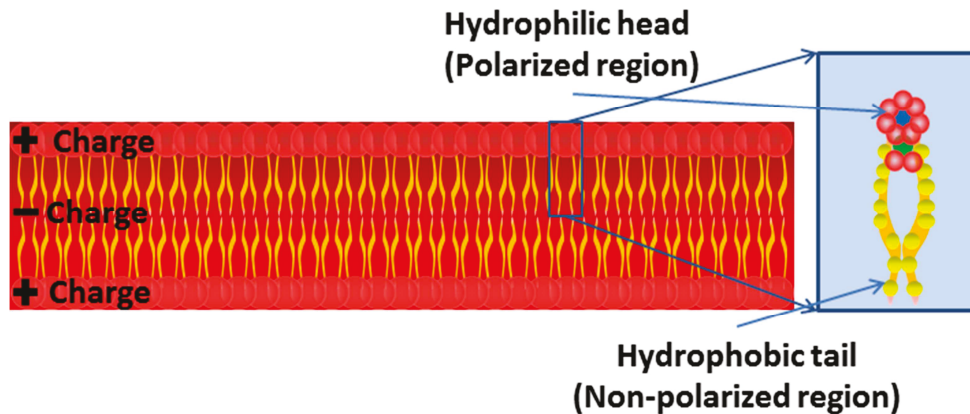


Figure 1.6: Structure and behavior of Phospholipid. Head contains the positive charge while tail contains the negative charge so that interaction of charged particles between inner and outer surfaces are restrained.

### III) *T-Cell Expressions*

T-cells involve several hundreds of protein expressions during the process of activation against the foreign invaders. These membrane receptors are almost the same for all T-cells and comprise of the proteins majorly involved in recognition of antigen (by means of peptide shown by MHC on the surface of APCs) with adhesion and co-activation of T-cells. In  $\alpha\beta$  T-cells, there are helper T-cells ( $T_H$  or  $CD4^+$  T-cells), Cytotoxic T-cells ( $CD8^+$  T-cells), and Regulatory T-cells ( $T_{regs}$ ).  $CD4^+$  and  $CD8^+$  T-cells are the major types that are involved in the activation process before the proliferation.

$CD4^+$  T-cell surface proteins are 60% to 70% of mature T lymphocytes in the blood. The  $CD8^+$  proteins are also present on average 30% to 40% of mature T lymphocytes. They are expressed either as a homo-dimer of two  $\alpha$  chains or most frequently a hetero-dimer of  $\alpha$  and  $\beta$  chain complex [11]. The  $CD4^+$  and  $CD8^+$  proteins are necessary not only for the activation of T-cell but also for the survival of T-cell. The  $CD4^+$  and  $CD8^+$  T-cells have most of the proteins in common. In this study, we follow six T-cell expressions (proteins) that are present on both ( $CD4^+$  and  $CD8^+$ ) types of T-cells. These include  $CD3$ ,  $CD3i$ ,  $CD25$ ,  $IL-2$ ,  $CD25-IL2$  and  $CD25-IL2i$  proteins.

## 1.2 Mechanism of Immune response

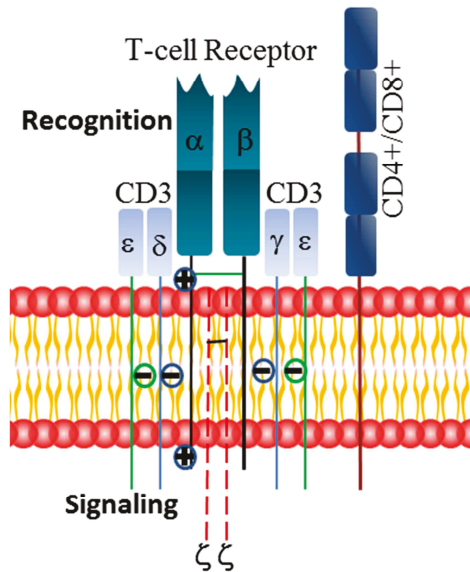


Figure 1.7: Structural diagram of CD3 complex in which CD3, CD4+/CD8+ and TCR proteins are shown in contact with each other.

CD3 protein is one of the first proteins that trigger the activation process of T-cells. It is composed of one  $\gamma$ , one  $\delta$ , two  $\epsilon$  and two  $\zeta$  chains. TCR, CD3 and CD4/CD8 combines to make a complex that deals with recognition of antigens and signal transduction [11]. Each T-cell contains  $10^4 - 10^5$  TCRs that are identical and can recognize specific antigens. T-cell receptors (TCR) are heterodimeric<sup>2</sup> and have antigen specific  $\alpha$  and  $\beta$  chains associated with four types of CD3 protein chains to make a complex called CD3 complex that is always present on T-cells.

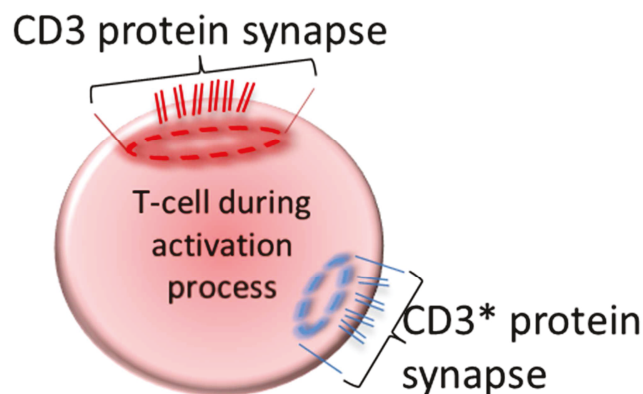


Figure 1.8: Reappearance of CD3 protein as CD3\* protein on the surface of T-cell but outside the synapse for CD3 protein.

<sup>2</sup> A protein composed of two polypeptide chains differing in composition in the order, number, or kind of their amino acid residues (© 2011 Merriam-Webster, Incorporated).

## 1.2 Mechanism of Immune response

During the process of activation, the internalized CD3 protein is known as CD3<sub>i</sub> protein. Due to the CD3 internalization, the concentration of CD3 protein decreases in the synapse (a place on the surface of T-cells where all the concentration of protein gathers). It is observed experimentally that, during the activation process, a protein that behaves like CD3 gathers outside the synapse [37]. This protein is denoted as CD3\* protein. This protein has not been on the surface before activation, therefore it is considered that it is produced after the internalization of CD3 protein. This protein will also remain the part of our study in the next chapters.

TCR has  $\alpha$  and  $\beta$  chains as shown in the Figure 1.7. During the activation process, TCR, attached with MHC peptide, it degrades CD3 protein in order to transduce signals (ITAMs) in the cytoplasmic domain to take first step of the activation process. Its main task is in cell development and transduces signals to activate T-cell after the recognition of antigen.

The engagement of CD3 protein induces production of several proteins like, in particular to our interest, CD25 and IL-2 proteins as shown in Figure 1.9. CD25, also known as IL-2R $\alpha$ , is the  $\alpha$ -chain of IL-2 receptor (IL-2R). It is a type-1 transmembrane glycoprotein that acts like a binding for IL-2 in order to present it on the surface of T-cell with the help of  $\gamma$ -chain. CD25 protein is expressed on all types of activated T-cells. They are also present during the T-cell development and on the regulatory T-cells. It has low affinity to bind itself with IL-2 though the high affinity is produced by heterotrimeric receptor complex when IL-2R $\alpha$  associate itself with IL2-R $\beta$  and IL2-R $\gamma$ .

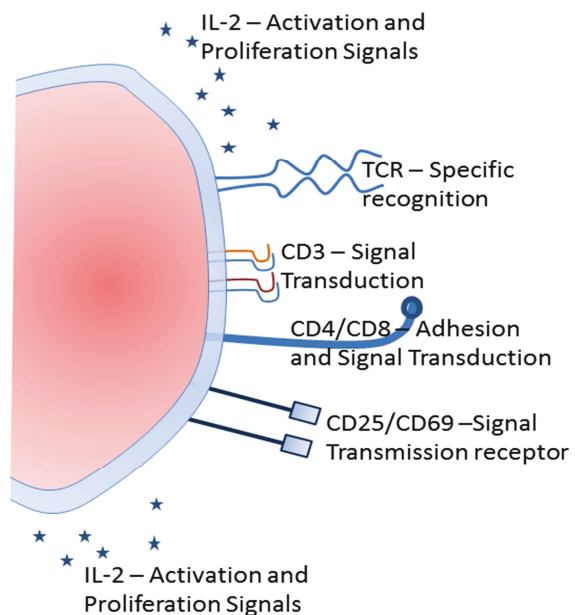


Figure 1.9: Protein expressions of T-cells.

IL-2 is a molecular communicator and growth factor for activated T-cells. Interleukin-2 is a global protein that is shared by all the T-cells. It plays a vital role in the growth of T-cells by

## 1.2 Mechanism of Immune response

---

initiating autocrine and paracrine signaling. This means that T-cell diffuses signals eventually into the blood and transduces signals randomly into any specific CD25+ T-cell [38].

### IV) *Activation Process of T-cells*

The activation of T-cells is physically interpreted by the dynamical changes occurring on the surface of T-cells by means of the degradation or the up regulation of membrane proteins. In particular to our interests, the surface proteins, like CD3 is internalized, CD25 is produced and CD25-IL2 is the binding of CD25 and IL-2 protein, vary their concentrations in order to keep up the process of activation. Each T-cell (specific to the antigen) follows the same procedure according to the kinetics rule, depending upon their avidity towards antigen, during the process of activation and lasts until it becomes fully activated.

The process triggers when the interaction of TCR-pMHC results with the down-regulation of CD3 protein from the surface into the cytoplasm of T-cell. Due to the continuous interaction of TCRs with pMHC, a significant decrease in the CD3 protein (along TCR) is observed on the surface of T-cell. This variation differs from cell to cell depending upon the concentration of pMHC on the surface of the APC and the association and dissociation rate of the TCR-pMHC binding.

1	Binding of CD3 to its receptor TCR and CD3 internalization.....	$L + T \rightarrow LT \rightarrow T^*$
2	Subsequent Production of CD3i (due to internalization of CD3)....	$T^* \rightarrow T^*i$
3	Induction of CD25 protein.....	$T^*i \rightarrow CD25$
4	Production of IL-2 protein.....	$T^*i \rightarrow IL-2$
5	Binding of IL-2 to its receptor CD25 protein.....	$CD25+IL2 \rightarrow CD25-IL2$
6	Full Activation / internalization of IL-2 receptor.....	$CD25-IL2 \rightarrow CD25-IL2i$

Table II: Six processes involved in this study to describe the T-cell activation dynamics.

The population of activated T-cells increases with the passage of time during the process of internalization of CD3 protein. The simulation time starts after the first recognition of antigen by any specific T-cell. From time to time, other T-cells also start recognizing and down regulating CD3/TCR for the partial activation. This process continues throughout the simulation time until

## 1.2 Mechanism of Immune response

the antigen available on APC. Although the activation is partial, yet the CD3 T-cells, that are varying the CD3 protein concentration on the surface, are considered as activated. The internalization of CD3/TCR consequently produces CD25 surface protein. This makes the T-cell activated regarding CD25 protein. The T-cells produce some cytokines like IL-2 that interacts with other T-cells containing the CD25 protein on their surface. The process continues as IL-2 receptor protein combines with its receptor CD25 in order to make a binding complex CD25-IL2. The T-cell population with CD25-IL2 bound protein increases gradually depending upon the concentration of CD25 and IL2 proteins. The internalization of CD25-IL2 leads to the T-cell in a state where T-cell gets ready to proliferate. Some simple steps are written in the Table II and these steps are presented in the Figure 1.10. During the activation time, all the cells shows the similar process regarding the protein dynamics but their concentrations of proteins can be different.

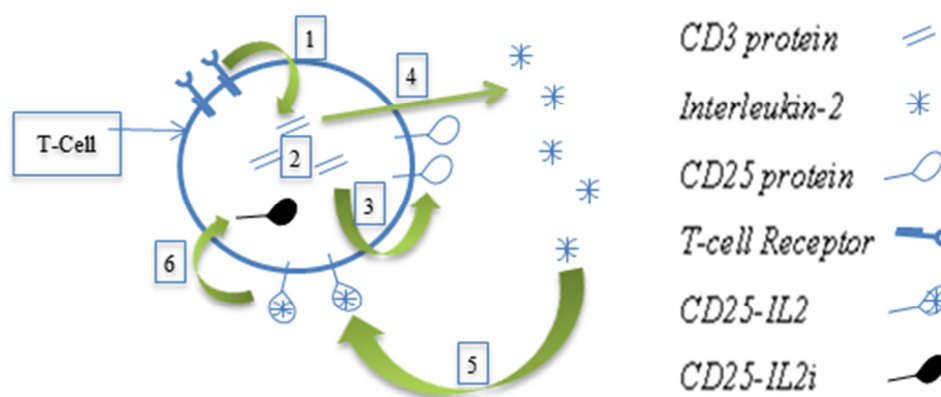


Figure 1.10: Activation process of T-cells. Table II illustrate the numbers written in this figure.

### V) Proliferation and Differentiation

The proliferation of T-cells is a division process which starts when the full activation of T-cells is achieved. This process needs a threshold of the activation measured by internalized protein CD25-IL2i concentration that will build a sufficient force inside the parent T-cell to divide it into two daughter cells. These daughter cells further divides into two and this process goes on for several generations. During this process, the total population increases while the concentration of proteins divides between the new daughter cells.

## 1.2 Mechanism of Immune response

---

After the proliferation of T-cells, another major event takes place that is known as differentiation. The differentiation of T-cells assigns the responsibility either to become effector or a memory T-cell. The effector T-cells act to kill the body cell containing virus while the memory cells remember the infection for a long time for an early and efficient response in case of re-exposure with the same antigen. The effector CD4<sup>+</sup> T-cells help in proliferation of CD8<sup>+</sup> T-cells and B-cells while the effector CD8<sup>+</sup> T-cells directly attacks on the diseased cells.

The population of T-cells starts decreasing after the pathogen is killed and majority of the killer cells abolish after taking some time but the memory cells remains alive for long period of time. The above phenomenon of protein dynamics can be observed by flow cytometry technique (FCM) as it is described in Section 1.2.4.

The variation in the concentrations of different proteins depends upon the stage of activation process. After the activation of T-cell, we observe the response of activated T-cells against such infections. The activation rate (production of new T-cells which undergo the process of activation) and the reaction rate (rate of change in the concentration of proteins) of T-cells are the two major biological processes that reflect the quality and level of immune response against the viral infections.

### 1.2.4 Flow-cytometry

The flow cytometry is a powerful technique to study the dynamical behavior of multiple parameters of microscopic individuals (cells), in heterogeneous population, by mixing in a fluid and passing cells one-by-one from a thin flow. It has wide range of applications in cell characterization such as immunophenotyping, ploidy analysis, cell counting and GFP expression analysis. The cells are at a very small distance from each other and passed with the speed of 10 m/s. The flow cytometer can detect T-cells with different magnitudes from 1  $\mu\text{m}$  to 15 $\mu\text{m}$ , and well adapted for lymphocytes with 8  $\mu\text{m}$  of diameter.

A laser beam focuses with a single wavelength that is followed by an optical focus to make it sufficiently narrow for a single cell. The flow cytometer is efficient enough to pass up to 10 thousands of cells per second and capturing the light from each cell that passes through. The laser

## 1.2 Mechanism of Immune response

---

strikes the cell surface to scatter the fluorescence in different directions. It produces the spectrum of light which further strikes dichroic filter. A deflection process takes place that is divided into two types of scattering. One is 'forward scatter' that send low angle diffraction towards the detector by passing from the lens proportional to cell sign. Another large angle diffraction (after striking the cell) moves towards the side filters known as 'side scatter' that gives information on cell structure (presence of organelles). Cell proteins / compounds labeled by fluorescence of different wavelength are captured by electronic amplifier and that are selected by filter. The filtered light is sent to the respective detector after passing from a lens. All these detectors send signals towards the computer that represents different properties of cells. In the Figure 1.11, there is one forward-scatter and four side-scatters shown but in some laboratories of the world there are cytometers that can recognize up to 18 different colors.

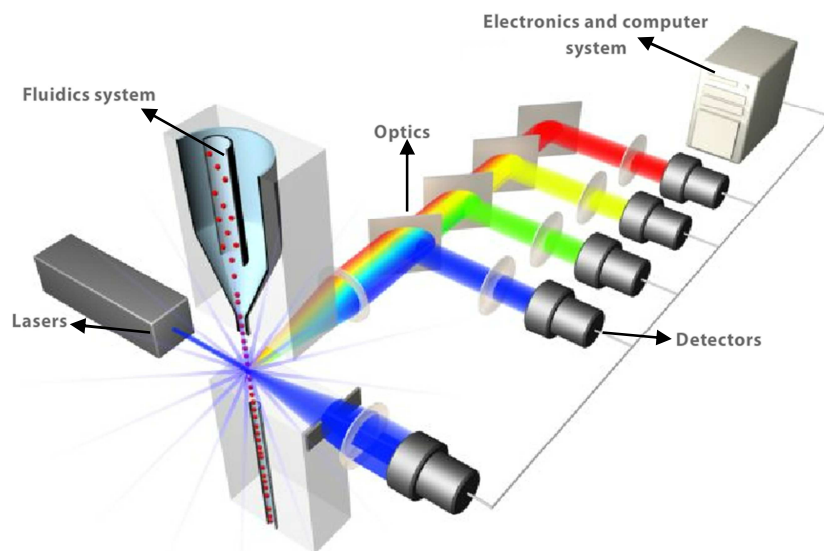


Figure 1.11: Flow cytometer with one forward-scatter and four side-scatter detectors  
[http://probes.invitrogen.com/resources/education/tutorials/4Intro\\_Flow/player.html](http://probes.invitrogen.com/resources/education/tutorials/4Intro_Flow/player.html)

Flow cytometry is a distinctive tool that not only counts the cells but also note down their respective properties by sending signals to the computer device on large number of cells among heterogeneous population. The information gathered by flow cytometry can be analyzed statistically and can be graphically represented in respect to the populations selected with the given properties. This study is concerned to the dynamical changes of the protein concentration on the surface of each cell.

## 1.3 Mathematical Modeling for the Immune Response against Viral Infection

In Figure 1.12, four panels have been shown to illustrate the result found by FCM. Panel-1 shows CD4+ and CD8+ T-cells selected population. Panel-2 shows the up regulation of CD25 protein in the activated CD4+ and CD8+ T-cells. The contour plot shows the concentration of CD25 present in the selected population of CD4+ and CD8+ T-cells. Here we can see the stimulation is not so strong in CD8 CD25+ T-cells while in panel-3 the stimulation is much strong not only in CD8+ CD25+ T-cells but also in CD4+ CD25+ T-cells. The panel-4 shows the selected T-cells from the population of lymphocytes present in the sample that is studied by using FCM.

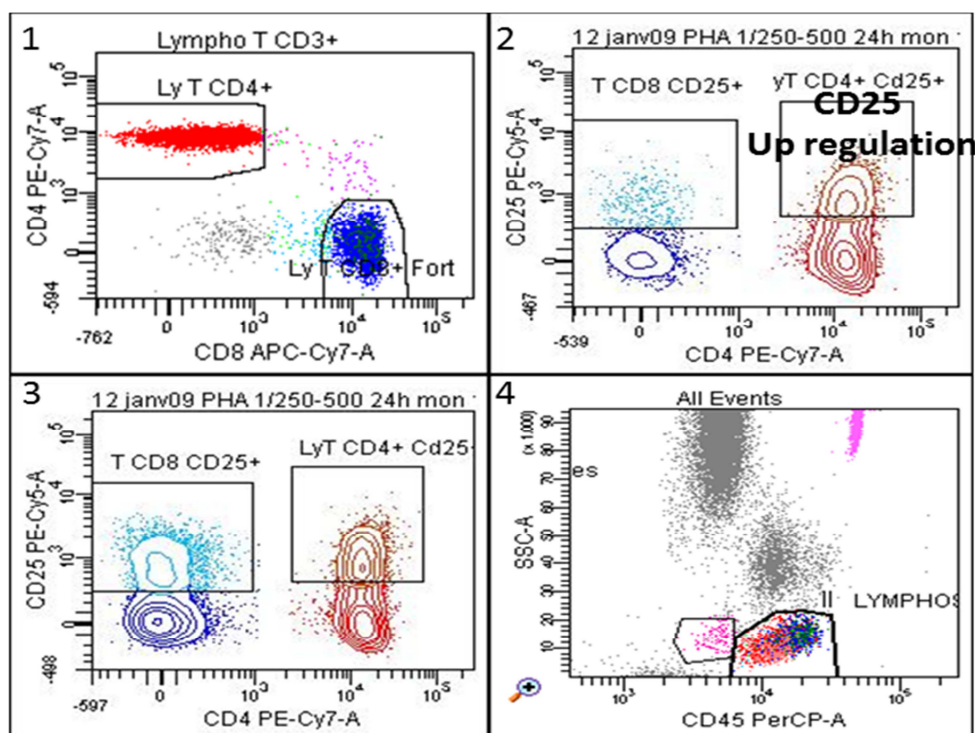


Figure 1.12: CD3+ and CD25+ T-cells population detected by Flow cytometer (FCM)

## 1.3 Mathematical Modeling for the Immune Response against Viral Infection

The mathematical modeling for the dynamical response of immune system turns into a frontrunner against the experimental procedures due to its continuity in time and the availability of vast variety of techniques. Although experimental results are necessary to understand the

## 1.3 Mathematical Modeling for the Immune Response against Viral Infection

phenomenon of any natural process but it is difficult to revise the procedure after small variations especially because of the time consumption. In particular to our interest, several modeling techniques have been developed against the viral infections to understand and try to anticipate the fortune of disease dynamics.

### 1.3.1 Infections and Mathematical Models

Infections caused by viruses have numerous types depending upon the affection of organs in the body. Among all, some viral infections are epidemic that needs continuous efforts to control their transmission to other individuals [39]. Different Stochastic and deterministic models have been studied to represent the susceptibility, transmission and treatment of such epidemic infections [40], [41]. These models mainly deal with the large populations of infected patients which have subgroups known as compartments. Each compartment is abbreviated according to its epidemic stage as M (Maternally-derived immunity), S (Susceptible), E (Exposed), I (Infective) and R (Recovered). The analysis of population dynamics of such models are based on simple ordinary differential equations (ODEs) where each ODE represents a compartment [42]. Public health practitioners and researchers are frequently pointing out the emerging areas in order to make their mathematical models and classify ongoing challenges [43]. These epidemic models mainly work on the outbreaks and spread of diseases in the society.

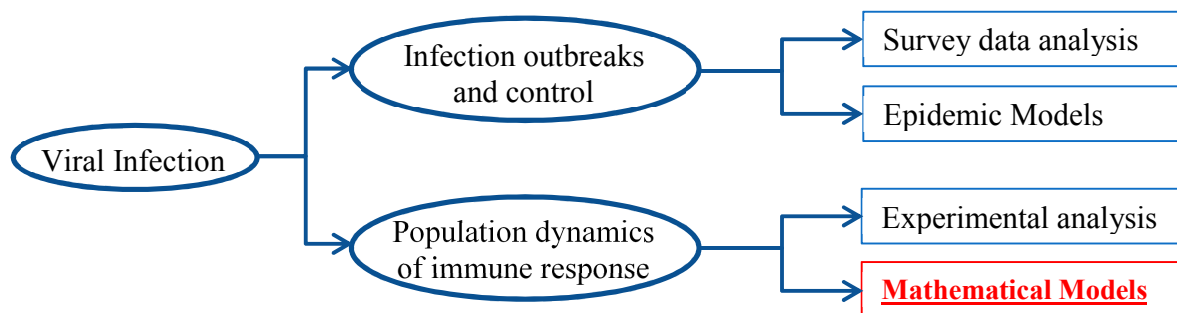


Figure 1.13: Ongoing research in viral disease dynamics

Another category in the modeling techniques is the mathematical modeling of the mechanism involved in virus propagation and immune response during the epidemic infection (in a human body). These models are used to analyze the dynamical changes by following the behavior of their physical parameters. Many researchers have shown their interest to model such evolutions by using numerous modeling techniques. The multi-scale modeling of such infections are used to

## 1.3 Mathematical Modeling for the Immune Response against Viral Infection

---

study the variation in the population of infectious cells due to their age of infections [21] and the population dynamics of specific T-lymphocytes activated after the antigen detection [4], [44].

If we go further deep in the study of specific immune system, we come across the activation and proliferation of T-lymphocytes that are based upon the chemical signals exchange by the help of numerous markers (proteins) associated with T-lymphocytes. These viral infections are mathematically modeled by using variety of modeling techniques that have effectively revealed the implicit mechanism of their pathogenesis. For example, the rate of viral production, the age of infected cells, the treatment for infection caused by Hepatitis B virus (HBV) and Hepatitis C virus (HCV) are modeled to analyze the interferon and ribavirin therapy [21], [45] and the memory of the infections by means of memory T-cells in order to respond more abruptly in future.

### 1.3.2 Modeling Population dynamics

The modeling techniques for discrete particle systems of chemical engineering are assimilated in the biological sciences in order to understand, particularly, the dynamics at a single cell level and at the population level. Each model is based on distinct assumptions and therefore can yield unique information at different computational expense.

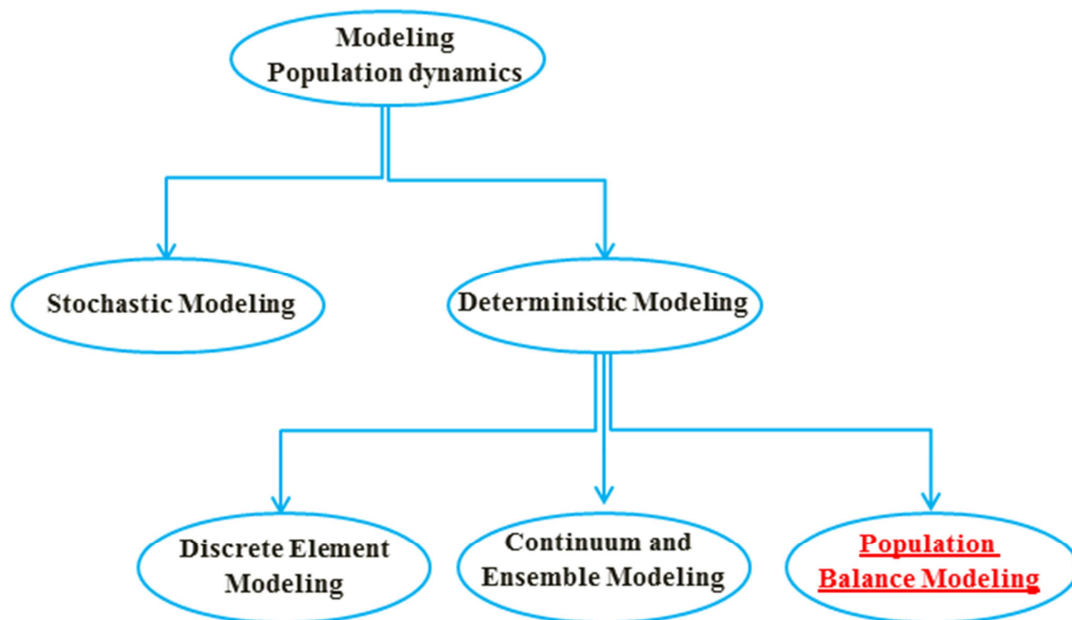


Figure 1.14: Various modeling techniques for population techn

## 1.3 Mathematical Modeling for the Immune Response against Viral Infection

---

### I) *Stochastic Modeling*

Stochastic modeling (SM) technique is based upon the probability of being in a state rather than predictable selection of the state. It has wide variety of applications in chemical engineering as well as in the biological sciences including cell population dynamics.

The dynamical effects at single cell level are defined by a random variable that can vary under the possible range of values. The random variable represents the rate at which the intracellular content changes, for example concentration of proteins etc. The range of values gives an entire space to the stochastic variable to decide the path according to the defined parameters.

The population dynamics involves the physical properties of cell by introducing a probability of virion interaction with uninfected cells to make it infected, the probability of infected cell to become uninfected and the probability of degradation of infected cells [6], [7].

The dynamical behavior is not predictable at any stage and the repetition of the simulations can vary the random variable value according to its defined probability. This makes it less interactive for the analysis of the cell population. Although the physical processes are random yet the random variables lack the tools and techniques to analyze their behavior under the desired circumstances. These arguments compel us to use the deterministic modeling that is more focused to follow the set directions; therefore one can anticipate the succeeding situation.

The stochastic models deal separately with the single cell dynamics and the population dynamics of cells. However, many dynamical systems in cell biology need a relation between the intracellular contents and the cell population due to the influence of cell on each other. Our aim of this study is to deal with such relations in order to develop a better idea about the immune response against viral infections.

### II) *Deterministic Modeling*

Deterministic modeling (DM) involves prediction of dynamical changes under the given data without involving any randomness during the simulation. DM techniques are based up on the differential and integral equations to study the dynamical changes at intracellular and

## 1.3 Mathematical Modeling for the Immune Response against Viral Infection

---

extracellular levels as well as at the population level depending upon their deterministic frameworks. In these frameworks, it is assumed that the system evolves in a continuous and well-prescribed manner by considering that the population of cells is sufficiently large [46]. Following are the modeling techniques that are frequently used to study the natural processes.

### **Discrete Element Modeling**

Discrete element modeling (DEM) is a numerical method for predicting the flow of individuals and moving objects. This technique best fits with the analysis of disaggregation and motion of particles or where the scientific principles are applied to govern each particle interaction possibly including particle-particle interaction, friction, electrostatic, magnetic, and gravitational forces.

A Discrete element modeling starts with the collection of particles along with their current position and velocities. The physical characteristics depend upon the forces applied on the particle and some other effects like cohesion. These forces are then used to determine the position based on the current velocity. Similar steps can be followed to determine the behavior of each particle during the whole simulation time.

This technique is capable of treating simple particle shapes like spheres and ellipsoids that puts a restriction on its usage. However the cell population dynamics can be followed due to their rounded shapes and structures. DEM allows the analysis of particulate systems in more depth as compared to the physical experiments but it is bounded to either the simulation time or the number of particles due to lack of computational resources. Several software have been developed to enhance the computational needs. Until now the number of particles up to  $10^7$  is allowed to study with sufficiently long simulation time. This reason has decisively blocked the DEM technique in the biological sciences, particularly to study the cell population dynamics, because the population of cells is normally treated above its computational bound.

### **Continuum and Ensemble Modeling**

At a single cell level, the intracellular and surface contents (e.g. concentrations) are considered as dispersed in the continuous phase of the cell. Ordinary differential equations are used to represent such models by assuming that all the cells share the same concentrations [27]. Therefore, the

## 1.3 Mathematical Modeling for the Immune Response against Viral Infection

---

variation at a single cell level is reflected as a general behavior of cell dynamics. Such models are denoted as Continuum models. These models are simpler but do not address the distribution of contents among the population of T-cells. Therefore, the heterogeneity of the contents among the cells is neglected.

A more effective modeling technique is the ensemble modeling which treats the heterogeneous nature of the cells by dealing with the concentration of each cell individually. Each ODE represents rate of change at the single cell level with randomly distributing the initial concentration, known as ensemble [27]. This gives efficient analysis of contents at single cell level but in a case of huge population, the simulation of this modeling technique is time consuming. Also, the homogeneity in the cellular contents can make this technique less advantageous as compared to continuum modeling.

### **Population Balance Model**

Deterministic models, like continuum and ensemble models, works at single cell level or at the population level while we need the modeling technique that can work at both ends to provide a relation among them. Population balance models provide such interface that helps us to make a connection between the single T-cell dynamics with the population dynamics of T-cells during their process of activation.

Population balance modeling symbolizes the diversity of features in a given population. These features are measurable intrinsic qualities such as age, size, shape, DNA/RNA contents and concentration belongs to an isolated set of population. Therefore, the population can be distributed according to the strength of such feature. The population undergoes several physical and chemical processes with the passage of time. These processes make the evolutionary changes in the population by varying the measure of the feature. However, the total population remains conserved during the course of action as shown in the Figure 1.15. Such conservation in the population is generally referred as balance law or conservation law for population balances.

The population balance model (PBM) is introduced by Huburt and Katz in the field of chemical engineering that is followed by Fredrickson in 1970s in biological sciences. It has shown

### 1.3 Mathematical Modeling for the Immune Response against Viral Infection

remarkable achievements in the field of chemical industries [24], [47]. In biological science, PBM is creating its place due to a vast application of population dynamics [5], [26]. Our study is roughly the change in the concentration of proteins and their respective population densities of T-lymphocytes after activation in the presence of given cell contents (proteins). For example, after the interaction of TCR with MHC, the CD3 protein, attached with TCR, degrades into the cell which shows a decrease of CD3 protein concentration on the cell surface. The rate of change in the proteins concentration at a single T-cell gives the idea of reaction rate and mimics the dynamical effects on the T-cell population density comprised of the same concentration.

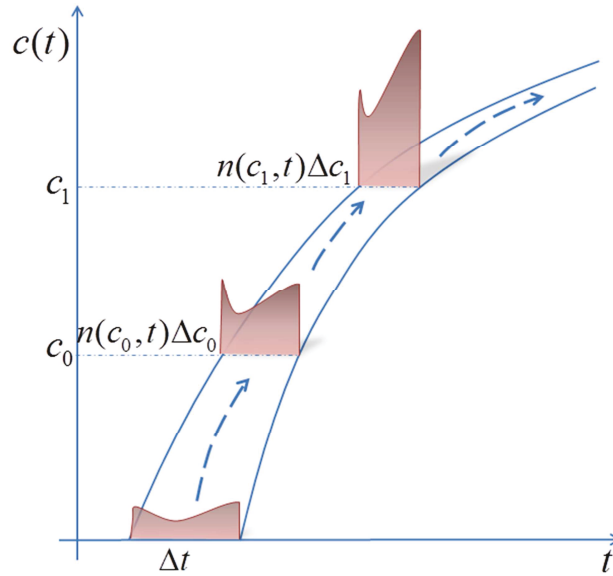


Figure 1.15: Illustration of balance law. The change in the protein concentration in a set of population increases the density of T-cells for small step size  $\Delta c$  while the total population remains conserved throughout the simulation time.

The collision with APC and the initial variation in the concentration of proteins change the status from non-activated to the activated T-cell. This change in the status is called as activation rate. At the initial level of T-cell activation, the above two processes, reaction rate and activation rate, exist which evolve the population of T-cells by variations. By conserving the total population during the whole dynamical process, the conservation law can be stated as “Under the given initial population of T-cells which undergo the process of activation, the rate of change in the population density of T-cells at concentration  $c$  is equal to the flux of the population density varying between the concentration  $c$  to  $c + \Delta c$ ”. If  $n(c, t)$  is the density function with  $c$  as a concentration of protein and  $t$  as time, one can write the mathematical form of the above quoted statement as,

## 1.3 Mathematical Modeling for the Immune Response against Viral Infection

$$\frac{\partial n(c,t)}{\partial t} + \frac{\partial}{\partial c}(G(c)n(c,t)) = N(c,t) \quad (1.1)$$

$$n(c,0) = 0$$

The function  $G(c)$  is considered as the reaction rate while  $N(c,t)$  is the activation rate. The associated initial condition shows that there is no activated T-cell at time  $t = 0$ . According to the conservation law defined above, the flow of the total population remains conserved while the population density varies due to the inflow and outflow of the T-cells at a given concentration  $c$  to  $c + \Delta c$  during the process of activation, Figure 1.16. A detailed analysis of population balance modeling technique is given in section 3.2.

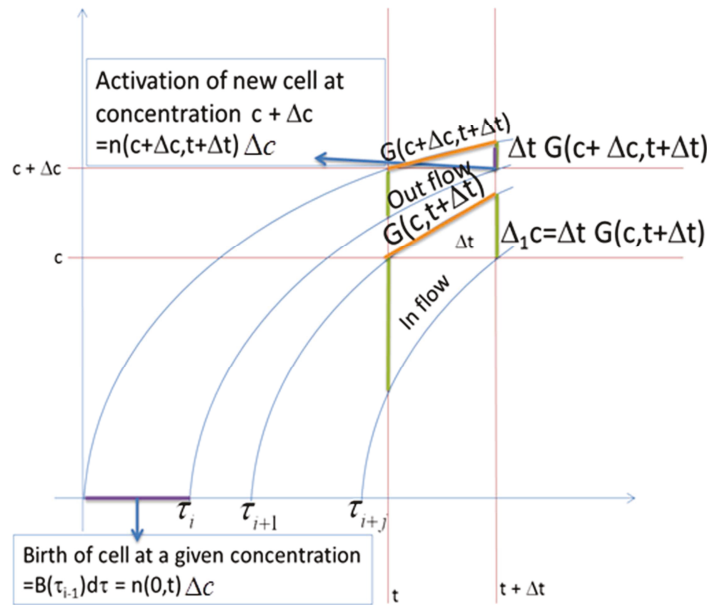


Figure 1.16: Graphical presentation of flow of population from time  $t$  to  $t+dt$ .

There is an overview about the contributions by researchers on the population dynamics of infected cells followed by the flow cytometry analysis and cell population balance model.

### 1.3.3 Former contributions to mathematical modeling

#### 1) Contribution by Sidorenko ([6], [7])

Sidorenko Y. [6], [7] worked on a stochastic population balance model that is described for influenza-A virus replication in MDCK (Madin-Darby Canine Kidney) cells. The model

### 1.3 Mathematical Modeling for the Immune Response against Viral Infection

---

quantitatively reproduced and interpreted flow cytometry data for the intracellular dynamics (proteins and RNA molecules) of the population of infected cells.

In his model, the interaction of virus and host-cells are considered with an explicit population of virions instead of considering the spread of virus from cell to cell. Let  $N_z$  be the initial total concentration of cells. The ratio between the free virions (virions in the blood but outside the cell) concentration and  $N_z$  is denoted by  $V$  (*virions/cell*). Similarly the ratios of uninfected and infected cells with  $N_z$  are denoted by  $Z_{un}$  and  $Z_{in}$ . The sum of the two ratios,  $Z_{un}$  and  $Z_{in}$ , is less than 1, i.e.  $Z_{un} + Z_{in} \leq 1$ . Now, by taking ratios, the model is independent of initial concentration.  $Z_d$  is the ratio of degraded cells (dead cells) in the suspension that is defined as:

$$Z_d = 1 - Z_{in} - Z_{un}. \quad (1.2)$$

The concept of transition probability is introduced for the concentration of cells in the simulation using kinetic Monte Carlo (MC) method. By this concept, the uninfected cells are set in transient state (change to any state) while the degraded cells are taken as in the absorbing state (no change to their state). The infected cells are further differentiated into different classes “ $J$ ” ( $1 < J < J_{\max}$ ) with respect to the internal coordinate  $j$  which corresponds to the intracellular number of viral components stated as the virus equivalents (VEs). In this way,  $j$  virus equivalents lies between the range  $W \times J$  to  $W \times (J + 1)$  where  $W$  is the width (VEs/cell). The cells in each class  $J$  are assumed to have the same behavior. Fluorescence intensity of cells is measured by flow cytometry for intracellular proteins M1 and NP. If  $j$  is the number of intracellular VEs then the fluorescence intensity is defined as:

$$F = F_0 + a_f \times j, \quad (1.3)$$

where  $F_0$  is the low non-specific fluorescence intensity and  $a_f$  is the fluorescence intensity for one VE. The uninfected cell ( $J=0$ ) has the probability  $P_{un-un}$  to remain uninfected,  $P_{un-in}$  to become infected of class 1 and  $P_{un-d}$  to become degraded while the degraded cells will never change their states. Random walk formulation is adopted for the study of infected cells. The infected cell degrades with probability  $P_{in-d}$  or shift to class  $J-1$  (due to virus release),  $J$  (no

### 1.3 Mathematical Modeling for the Immune Response against Viral Infection

---

change of state) or  $J+I$  (due to virus replication) with probabilities  $P_r, P_{in-in}$  or  $P_m$  respectively. All the transition probabilities are defined as constants for simplicity but, in general, they depend upon the class of the cell.

The dynamics of virus release was studied on each simulating step ( $k$ ) using a deterministic approach, rather than a stochastic approach, to reduce complexity. At each  $k^{th}$  step, an infected cell produces  $W$  virions with probability  $p_r$ . The ratio for the number of infection producing cells with  $N_z$ , each releases  $W$  virions, at the given step is  $p_r \times Z_{in}^{(k)}$ . Similarly the fraction of accumulated virions in the cell at simulation step ( $k$ ) is  $a_{ads} \times Z_{un}^{(k)}$ , where  $a_{ads}$  is a constant parameter of virus adsorption. Also a constant degradation  $a_{dgr}$  is assumed at each simulation time step. This all process gives a mathematical equation for calculating the number of virions at extracellular medium for  $(k+1)^{th}$  step, denoted by  $V$  virions/cell,

$$V^{(k+1)} = V^{(k)} + p_r \times W \times Z_{in}^{(k)} - a_{ads} \times Z_{un}^{(k)} \times V^{(k)} - a_{dgr} \times V^{(k)}. \quad (1.4)$$

In simulation, at each time step  $\Delta t$  of MC run, an array of test cells is considered. For each test cell, random numbers are drawn to determine whether the cell changes its state or not. After that the number of free virions  $V$  is calculated by above formula.

Sidorenko extended his work by describing the virus replication and release process with more detail. The concept of transcription, translation and replication of viral genome, synthesis and degradation are held under discussion in the model formulation. The infected cells are detailed under the 14 basic processes occurred during the influenza A virus infection [7].

The model parameters obtained from the optimization strategy (14 processes) are used to predict the general behavior of virus and cell populations. The sharp increase of the number of infected cells in the beginning of infection is due to the absence of a time shift in the present model. Since all the processes are not estimated in the beginning of infection, therefore, a disagreement between the simulation of the present model and the experimental data is appeared.

## 1.3 Mathematical Modeling for the Immune Response against Viral Infection

---

As we discussed above in the section 1.3.2, stochastic population balance modeling analyzed the population of infected cells and virions but there is no information present at the intracellular dynamics. Normally the viral infection affects the intracellular processes that evoke an effect at the population level. Lack of investigation at single T-cell level may affect the drug therapies as drugs usually targets intracellular components.

### II) *Michel Stamatakis ([27])*

Three modelling frameworks are discussed by Michel Stamatakis for the mathematical description of microbial populations, namely cell population balance (CPB), ensemble and continuum modelling [27]. One can get a good idea for choosing the appropriate modelling approach for the particulate application after going through his work.

Apart of the above modeling techniques, cell population balance modeling (CPBM) is also under his discussion. The continuum and ensemble modeling techniques deals with the intracellular contents but give no information about the population density of cells with respect to their concentration. In CPBM, a relation is defined between the dynamical changes in the intracellular components with the population of T-cells. Therefore, this model deals at single cell level as well as the population level. The CPBM is well established in chemical engineering and known as population balance modeling (PBM). The general CPB equation is a balance of expected cell numbers in the state space and it can be written as:

$$\begin{aligned} \frac{\partial N(z,t)}{\partial t} + \nabla_z [r(z,S)N(z,t)] + \Gamma(z,S)N(z,t) \\ = 2 \int_G \Gamma(y,S)p(z|y,S)N(y,t)dy - DN(z,t), \end{aligned} \quad (1.5)$$

subject to the regularity condition

$$r(z,S)N(z,t) = 0, \quad z \in \partial G.$$

In the above equation,  $z$  is a vector which consist of intracellular and morphomoric contents of the cell while  $S$  is also a vector representing the extracellular substrate concentration.  $N(z,t)$  is the number density function,  $r(z,S)$  is the rate at which the cells goes to intracellular reaction

### 1.3 Mathematical Modeling for the Immune Response against Viral Infection

---

and  $\Gamma(z, S)$  is the rate at which the cells goes to intracellular division. Also  $D$  is the dilution rate and  $p(z | y, S)$  is the probability for the division of a cell into two cells having states  $z$  and  $y - z$ .

For single cell models, the ensemble modelling is used that tracks the timecourses and simulate them at different initial conditions. A single cell model for the concentration  $C$  can be written as:

$$\frac{dC}{dt} = f(C, S, k, t), \quad (1.6)$$

where  $k$  is the random parameter and  $f$  is a vector giving the rate of change of the concentrations. Let  $p_0(k)$  be the probability density for  $k$  that deals with the change in the intracellular contents. If  $\rho(C, t)$  is the normalized density of cells in the ensemble volume  $dC$  at time  $t$ , then ensemble model can be formulated as:

$$\frac{\partial \rho(C, t)}{\partial t} + \int_M \nabla \times f(C, S, k, t) \rho(C, t) p_0(k) dk = 0. \quad (1.7)$$

It is interesting to note that the above equation becomes an advection equation if we are perturbing the initial condition having the parameter set fixed to  $k_0$ .

The continuum modelling deals with the evolutionary changes of the intracellular concentrations and it is represented as

$$\frac{dC}{dt} = q(C, S, k, t) - \mu C, \quad (1.8)$$

where  $\mu$  is the average specific growth rate, that remains constant in these models, defined as

$$\mu = \left( \overline{\frac{1}{V} \frac{dV}{dt}} \right) \quad (1.9)$$

where  $V$  is the volume of the cell. Two exact hybrid models are derived under some biological plausible conditions that simplifies the CPB model without any approximation. In these hybrid models the evolution of the species concentrations is captured by an ensemble model and by a continuum model with one-dimensional population balance equation. By these remarks, one can write the equation (1.5) as:

### 1.3 Mathematical Modeling for the Immune Response against Viral Infection

$$\begin{aligned} & \frac{\partial N(x, V, t)}{\partial t} + \nabla_x [r(x, V, S)N(x, V, t)] + \Gamma(x, V, S)N(x, V, t) + \frac{\partial}{\partial V} (g(x, V, S)N(x, V, t)) \\ & = 2 \int \int_{\mathbb{R}_0^+ G} \Gamma(y, W, S)p(x, V | y, W, S)N(y, W, t)dydW - DN(x, V, t), \end{aligned} \quad (1.10)$$

with the regularity condition defined as

$$\begin{aligned} & r(x, V, S)N(x, V, t) = 0, \\ & g(x, V, S)N(x, V, t) = 0 \text{ when } x_i = 0 \text{ for any } i = \overline{1, n} \text{ or } V = 0, \end{aligned} \quad (1.11)$$

where  $x$  is the replacement of  $z$  and it is a vector with molar contents that are extensive quantities.  $r(x, V, S)$  is the reaction rate by which the intracellular contents  $x$  goes into the reactions and  $g(x, V, S)$  is the single cell growth rate. The Eq. (1.11) ensures us the the number density is bounded and does not leave the orthant of  $z \in \mathbb{R}^{n+1}$ . Define a transformation for  $x$  as:  $C = \frac{x}{V}$  and take the total differential of  $x$  and  $C$ . This gives us a relation between these two variables and we can transform the above model by using this relation. Let us define the number density as  $N(x, V, t) = V^{-n} \bar{N}(C, V, t)$  and reaction rate as  $r(x, V, S) = V \star r(C, V, S)$ . Also suppose that the growth and division rates with respect to concentrations are  $g(x, V, S) = G(C, V, S)$  and  $\Gamma(x, V, S) = \mathfrak{S}(C, V, t)$ . The population balance equation can be written as:

$$\begin{aligned} & V^{-n} \frac{\partial \bar{N}(C, V, t)}{\partial t} + \nabla_C [r(C, V, S)V^{-n} \bar{N}(C, V, t)] + \mathfrak{S}(C, V, S)V^{-n} \bar{N}(C, V, t) \\ & + \frac{\partial}{\partial V} (G(C, V, S)V^{-n} \bar{N}(C, V, t)) - \sum_{i=1}^n \frac{C_i}{V} \frac{\partial}{\partial C_i} [G(C, V, S)V^{-n} \bar{N}(C, V, t)] \\ & = 2 \int \int_{\mathbb{R}_0^+ \Theta} \mathfrak{S}(Y, W, S)V^{-n} \bar{N}(Y, W, t)p(C, V | Y, W, S)dYdW - DV^{-n} \bar{N}(C, V, t), \end{aligned} \quad (1.12)$$

with given regularity conditions:

$$\begin{aligned} & r(C, V, S)V^{-n+1} \bar{N}(C, V, t) = 0, \\ & g(C, V, S)V^{-n} \bar{N}(C, V, t) = 0 \text{ when } C_i = 0 \text{ for any } i = \overline{1, n} \text{ or } V \rightarrow 0. \end{aligned} \quad (1.13)$$

Six conditions are imposed to introduce a new set of equations that is simple and exact alternative of population balance model. These conditions are: equal species concentrations in mother and

## 1.3 Mathematical Modeling for the Immune Response against Viral Infection

---

daughter cells, size-dependent intensive reaction rates, size-dependent but concentration-independent growth and division rates and partitioning mechanism. Under these conditions one can derive a hybrid model that consists of 1-D population balance and an ensemble model. If two more conditions are imposed that is the average cell growth rate is constant and the initial cell population is homogeneous, then the ensemble model transforms to structured but unsegregated continuum model with 1-D population balance that is actually the basis of this dissertation. The work can be extended to more realistic model by working on multi-component cell-to-cell interaction.

### III) *Kavousanakis Work on Cell Population Balance Model [27]*

The basic aim of this paper is to study the impact of extrinsic type of heterogeneity (type of heterogeneity originating from unequal division of the intracellular contents of the mother cell) on the behavior of entire cell population. A boundary algorithm for the numerical solution of cell population balance (CPB) problems is developed that is based on a transformation of variables with respect to the average intracellular content of iso-genic populations. The implementation is studied in a software package COMSOL Multiphase. The CPB model is represented by a integro-partial differential equation. If  $F(x,t)dx$  represents the number of cells per unit biovolume (intracellular content between  $x$  and  $dx$ ) at time  $t$  then CPB equation with B.C. is given by:

$$\frac{\partial F(x,t)}{\partial t} + \frac{\partial}{\partial x} [R(x)F(x,t)] + \Gamma(x)F(x,t) = 2 \int_x^{x_{\max}} \Gamma(x')P(x,x')F(x',t)dx', \quad (1.14)$$

$$F(0,t) = F(x_{\max},t) = 0.$$

$R(x)$  is the single cell reaction rate,  $\Gamma(x)$  is the single cell division rate and  $P(x,x')$  is the partition probability density function by which a mother cell of content  $x'$  will produce, by division, a daughter cells of contents  $x'$  and  $x' - x$ . The above model is reformulated by defining number density function,  $n(x,t)$ . which denotes the fraction between number of cells with content  $x$  at time  $t$ ,  $F(x,t)$ , and total number of cells at the same time, i.e.

$$n(x,t) = \frac{F(x,t)}{\int_0^{x_{\max}} F(x,t)dx}.$$

### 1.3 Mathematical Modeling for the Immune Response against Viral Infection

---

The substitution in the Eq. (1.14) yields the following equation with imposed boundary conditions (BCs):

$$\begin{aligned} \frac{\partial n(x,t)}{\partial t} + \frac{\partial}{\partial x} [R(x)n(x,t)] + \Gamma(x)n(x,t) \\ = 2 \int_x^{x_{\max}} \Gamma(x')P(x,x')n(x',t)dx' - n(x',t) \int_0^{x_{\max}} \Gamma(x)n(x,t)dx, \\ n(0,t) = n(x_{\max},t) = 0. \end{aligned} \quad (1.15)$$

A free boundary algorithm is used to find the co-existing solutions of the above mathematical model. The normalized physiological state space, i.e.  $[0, x_{\max}]$ , with respect to the average intracellular content  $\langle x \rangle$ :

$$0 \leq x \leq x_{\max} \Rightarrow 0 \leq \xi \equiv \frac{x}{\langle x \rangle x_{\max}} \leq 1. \quad (1.16)$$

Define a transformation  $n(x,t)dx = g(\xi,t)d\xi$ , where  $g(\xi,t)$  is a transformed density function, and differentiate it with respect to time. After some manipulation of above equations, we get a differential equation that tracks the temporal behavior of  $\langle x \rangle$  in the transformed domain  $\xi$  with similar boundary conditions on  $g(\xi,t)$  as on  $n(x,t)$ :

$$\begin{aligned} \frac{d\langle x \rangle}{dt} = \int_0^1 \tilde{R}(\xi)g(\xi,t)d\xi - \langle x \rangle \int_0^1 \tilde{\Gamma}(\xi)g(\xi,t)d\xi, \\ g(0,t) = g(1,t) = 0. \end{aligned} \quad (1.17)$$

To demonstrate the efficiency of the above algorithm, a lac operon gene regulatory network is used as a model system and perform transient and asymptotic behavior analysis. This gives a complete formulation of CPB problem for an isgenic population, each cell of which carries the lac operon gene network. The analytical solution of the CPB problem is intractable, therefore a numerical approach is necessary for it. Here finite element method is implemented for the solution by using COMSOL software package. Finite element methods are actually computationally expensive and complex methods whereas the Finite volume methods (FVMs) can best fit with CPB equation particularly when the equation obeys conservation law for population balances. FVMs cover the entire domain by defining control volumes that are easy to handle instead of FEM that is more useful in complex geometries and solid mechanics.

## 1.3 Mathematical Modeling for the Immune Response against Viral Infection

---

### IV) *Shamsul Qamar [47]*

Qamar is working on the population balance modeling in chemical engineering as well as biological sciences. His recent article [48] is about the Multivariable cell population balance models (CPBM) in which he studied the single-variate and bivariate cell population balance equations (CPBEs) during the division process in terms of their biomass. The CPBE consist of increase in the amount of cell biomass represented by cell growth and an integro-differential equation demonstrating the substrate consumption. Let  $x$  be the amount of biomass (the protein contents of cell),  $g(x,t)$  be the cell growth and the source term describing the substrate consumption is denoted by  $Q(x,t)$ . The total population with the amount of biomass  $x$  at time  $t$  is represented by  $N(x,t)$  such that  $N(x,t) \times dx$  represents the number of cells per unit volume which at time  $t$  have physiological state representation between  $x$  and  $x + dx$ . The single-variate CPBE for the state distribution function  $N(x,t)$  can be written as:

$$\begin{aligned} \frac{\partial N(x,t)}{\partial t} + \frac{\partial}{\partial x}[g(x,s)N(x,t)] &= Q(x,t), \\ N(x,0) &= N_0(x). \end{aligned} \quad (1.18)$$

The variable  $s$  is the substrate concentration. The first term in the Eq. (1.18) is the accumulation term while the second term gives us the cell growth in which the amount of biomass monotonically increases. The source term  $Q(x,t)$  describes the process of division that is represented by division rate  $\Gamma(x,s)$ , and the birth process is described by the partitioning function  $P(x,y,s)$ . Thus,

$$Q(x,t) = -\Gamma(x,s)N(x,t) - DN(x,t) + 2 \int_x^{x_{\max}} \Gamma(y,s)N(y,t)P(x,y,s)dy. \quad (1.19)$$

The first term denotes the cell loss due to the partitioning of cells; the second term denotes the rate at which the cells leave the bio reactor and the integral term is the division of parent cell into two daughter cells. Each parent cell divides into two daughter cells is the reason of multiplying the integral term by two. The mass of the parent cell is divided equally into two daughter cells which can be described mathematically by assuming partition probability density function  $P(x,y,s)$  as a dirac delta function and can be defined as  $P(x,y,x) = \delta\left(x - \frac{y}{2}\right)$ . Therefore, Eq.

(1.19) reduces to

## 1.3 Mathematical Modeling for the Immune Response against Viral Infection

---

$$Q(x,t) = -\Gamma(x,s)N(x,t) - DN(x,t) + 2^2\Gamma(2x,s)N(2x,t).$$

Substrate consumption obeys the following integrodifferential equation:

$$\frac{ds}{dt} = D(s_f - s) - \int_{x_{d,\min}}^{x_{\max}} N(x,t)q(x,s)dx, \quad (1.20)$$

with initial condition  $s(0)=s_0$ . The parameter  $s_f$  is the inlet concentration while  $s$  is the outlet rate from the reactor.  $D$  is the dilution constant and  $q(x,s)$  is the consumption rate. The integral defines the rate of loss of substrate due to cell growth.

This model is extended afterwards to the bivariate CPBM in which two internal property variables  $x$  and  $y$  are studied with their respective cell growths  $g_1(x,t)$  and  $g_2(x,t)$ . The bivariate CPBE is written as:

$$\begin{aligned} \frac{\partial N(x,y,t)}{\partial t} + \frac{\partial}{\partial x}[g_1(x,s)N(x,y,t)] + \frac{\partial}{\partial y}[g_2(y,s)N(x,y,t)] &= Q(x,y,t), \\ N(x,y,0) &= N_0(x,y) \quad (x,y,t) \in \mathbb{R}^3. \end{aligned} \quad (1.21)$$

The source term for equal partitioning is given by

$$Q(x,t) = -\Gamma(x,y,s)N(x,y,t) - DN(x,y,t) + 2^3\Gamma(2x,2y,s)N(2x,2y,t). \quad (1.22)$$

The mass balance for the substrates is constructed as integro-differential equation

$$\begin{aligned} \frac{ds}{dt} &= D(s_f - s) - \int_{x_{d,\min}}^{x_{\max}} \int_{y_{d,\min}}^{y_{\max}} N(x,t)q(x,s)dx dy, \\ s(0,0) &= s_0. \end{aligned}$$

Three numerical schemes are applied to investigate the solution for both CPBEs. A simple finite volume scheme together with two high resolution schemes, namely the High resolution Flux-Limiting Scheme of Koren [49] and the High resolution Flux-Limiting Scheme of Leveque [50], are studied for single-variate as well as bivariate CPBM. Four test problems are studied for the equal and unequal cell partitions with constant, linear, quadratic and linear combination growth rates. Single-variate CPBM deals with both equal and unequal cell partitions in first three test problems while the bivariate CPBM deals with only equal cell partitions in the last two problems.

## 1.4 Our contribution

---

Qamar has investigated the single-variate and bivariate cell population balance modeling by assuming the internal coordinates as biomass or internal property variables; however the cell biomass contains several contents which vary dynamically depending upon each other throughout the cell life. The biomass always increased in this case which gives a conventional cell growth rate. Also the work of Qamar discusses the process of division and how the biomass is shared between the daughter cells. In our study, the mathematical models are investigated as single-variate CPBM and analyzed according to their cell contents (proteins). These proteins are depending upon each other and therefore sometimes the concentration of cell content follows an increasing as well as decreasing phenomena with the passage of time which makes the problem more interesting. Also, in our study, the process of division is not explicitly studied. We investigated the dynamics of cell before and after cell division (but not during the cell division).

The numerical schemes are highly efficient in the work done by Qamar and have provided efficient results. These methods are validated when the model is based on PDEs while in our case, due to non-monotonic behavior by internal property variable, i.e. concentration of cell contents, the PDE formation is questionable. Therefore, we need such method which can directly find the population density instead of following the population balance equation.

## 1.4 Our contribution

This dissertation describes the mathematical modeling of immune response against influenza virus infection. This work is divided into two main parts: the dynamical behavior of proteins at single T-cell level and the overall population dynamics of activated T-cells. Also, there are some hypothetical models that are validated for the process of evolution in the T-cells after proliferation.

At single T-cell level, continuum models are studied. These models are divided into four categories (Cases 1 – 4) according to their level of complexities as given in Chapter 2. The models are presented by using ordinary differential equations (ODEs) that are solved analytically whenever possible while a simple Euler method and Runge-Kutta order four method are also used to validate the results for Case 3 and Case 4. A graphical analysis of these models made a

## 1.5 Terminology Used in the Thesis

---

thorough investigation of the intracellular dynamics. The kinetic parameters used in this study are defined according to experimental observations presented in [3], [13].

At population level, the population balance models are studied by introducing the reaction and activation rates in order to analyze the population dynamics of T-cells during the process of activation, Chapter 3. The ODEs used in the Chapter 2 are considered as the reaction rates at single T-cell level while the initial population of activated T-cells is defined by an activation rate. Again four cases are studied in the same complexity sequence followed in Chapter 2. Each one has described the population dynamics of T-cells with respect to their surface proteins under the conservation laws for hyperbolic equations. Several methods have been used to find the solution for each model depending upon the complexity of the model. An innovative approach is used to find the solution by the methods existing in the literature. Also a new method ‘Transport Method’ has been introduced by using the differential geometry in order to deal with such conundrums without using the PBMs.

The Chapter 4 is based upon the proliferation of T-cells occurring after the full activation stage. The behavior of T-cells after proliferation is observed based on single T-cell level and also at population level. Three hypotheses are defined for the proliferation process. The results have been obtained by using the Transport Method that are validated by comparing the results found in Chapter 3.

The deduction and critical analysis of the thesis is written at the end of the thesis as a Conclusion.

## 1.5 Terminology Used in the Thesis

In the biological and mathematical literatures, several words exist which have the similar meaning but they can confuse the reader as their second meanings also exists. For the sake of convenience, in Table III, we define a decisive terminology according to the literature that can help to understand the dissertation.

## 1.5 Terminology Used in the Thesis

<b>Decisive Terminology</b>	<b>Variable / Function</b>	<b>Synonyms / Description</b>
Activation rate	$B(t)$	Assimilated as Nucleation rate in Chemical Engineering
Activation time	$\tau$	Triggering (beginning) of the activation process of a certain type of T-cell
Activated cells		Cell that has begun its activation process but not yet fully activated
Activation process		Activated cell; The dynamical change in the T-cell after activation time
Antigen		Pathogen; invader; Virus
Concentration	$c$	Level
Population Density	$n(c,t)$	The number of T-cells per unit volume and per unit protein concentration
Initial population	$N(c,t)$	Number of T-cells change the phase from non-activated to become activated T-cells
Proliferation		Process of division of more than one cell
Protein		Membrane receptor; content; marker; binding
Reaction rate	$G(c)$	Assimilated as Growth rate in Chemical Engineering
T-cell		Cell; T-lymphocyte

Table III: Terminology used in the thesis



# **Chapter 2**

# **Proteins Dynamics**

## 2.1 Introduction

### 2.1 Introduction

The recognition of foreign invasion by T-cells requires several proteins. These proteins play a vital role to trigger the process of T-cell activation by moving inside the T-cell from the cell membrane and compel the nucleus to produce more proteins. Consequently, several proteins, each with different function, come on the surface or go into the blood stream to alarm the other specific T-cells as shown in Figure 2.1. The process of activation needs an immediate and continuous action in order to reach the threshold level that is necessary to ready the T-cell for further actions like proliferation. In this study, four levels of mathematical modeling are studied in order to depict the protein dynamics during the activation process. The evolutionary models are based on the analysis of experimental observations done by [4], [8]. These mathematical models are comprised of the set of ordinary differential equations (ODEs) and cover almost all the circumstances that are possible to study the rate of change in the proteins concentration at the cell scale. The system of ODEs is solved by using analytical methods wherever possible while the Euler method as well as the Runge-Kutta (order 4) method is also used to find their numerical solutions. The kinetic parameters and initial conditions are chosen according to the values given in the literature [3].

### 2.2 Mathematical Modeling

The protein dynamics in the activation process needs to be understood by the help of mathematical modeling that can simulate the behavior by varying the kinetic parameters. After

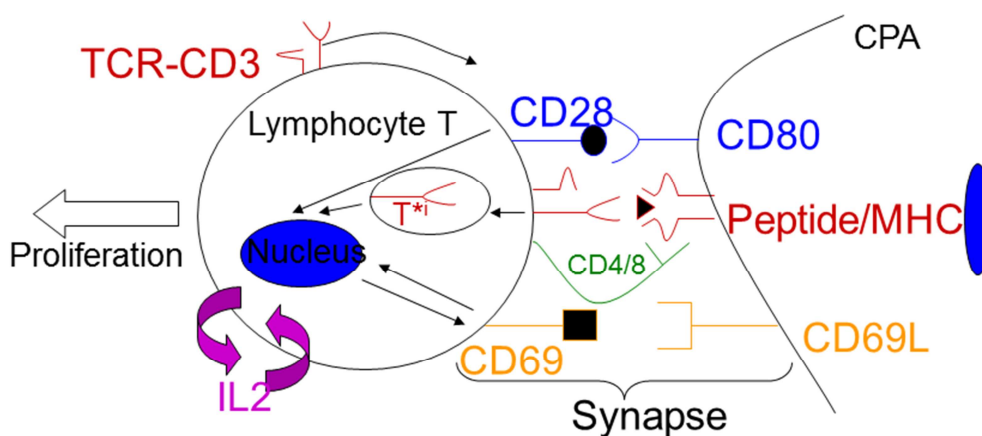


Figure 2.1: Interaction of T-cell with pMHC

## 2.2 Mathematical Modeling

---

reviewing the literature about experimental works and the mathematical models, a conviction has been made to develop a model based on the protein concentration at single T-cell level.

The established concept of T-cell activation is considered [3] that explains us about the binding of peptide-MHC complex and the TCR with the help of accessory molecules present on the surface with their particular ligand(s) under classical thermo-physical rules as shown in Figure 2.1. This initial step induces sequential involvement of the evolution in the proteins including production, binding to its ligand, activation and destruction that are considered all together in the previous work [3]. The mechanism of the activation of T-cell is based on hundreds of proteins that make it pretty complex. The major steps required for T-cell activation can be mathematically represented as in Table IV.

1. TCR (T) recognizes the pMHC complexes from APC (L).....	$L + T \rightarrow LT$
2. First step of the TCR activation.....	$T \rightarrow T^*$
3. Second step of TCR activation ends with an irreversible internalization	$T^* \rightarrow T^*i$
4. Induction of early activation marker CD69.....	$T^*i \rightarrow CD69$
5. Subsequently induction of CD25.....	$T^*i \rightarrow CD25$
6. CD69 meets its ligand and get internalized.....	$CD69 \rightarrow CD69^*i$
7. Stimulation of production of soluble IL-2 protein.....	$CD69^*i \rightarrow IL2$
8. Binding of IL-2 to its receptor.....	$CD25 + IL2 \rightarrow CD25-IL2$
9. Internalization of IL-2 receptor.....	$CD25-IL2 \rightarrow CD25-IL2i$

Table IV: Step wise description of T-cell activation process

The resolution of the above defined steps provides the cell kinetics at different activation levels at time  $t$ . The CD69 and CD25 proteins show a very similar behavior. Therefore, it is permissible to understand the behavior of one of the two proteins in order to understand the other. The mathematical models are presented to analyze the evolution in the above proteins concentrations. To solve such models, they are divided into four cases and are studied and presented in a sequence as given below. Following are the cases that we are going to discuss:

## 2.3 Case 1

---

1. Monotonic variation in the protein concentrations.
2. Non-monotonic variation in the protein concentrations with same behavior in all T-cells.
3. Non-monotonic variation with different behavior of each T-cell.
4. Non-monotonic variation with different behavior of each T-cell while the concentration of proteins present in/on any T-cell can intersect the others concentration at any time  $t$ .

The models are based on the single type of T-cell protein dynamics (also known as single T-cell dynamics) that are defined by the set of ODEs. Each ODE presents the rate of change in the concentration of a particular protein during activation process. Let's start with the first case describing the internalization of CD3 protein:

### 2.3 Case 1

The interaction of T-cells with an antigen presenting cell (APC) is the first and foremost among the other processes. This process is done by the help of CD3 protein which lies on the surface of T-cell attached with T-cell receptor (TCR) and CD8 protein (or CD4 protein that is not physically associated with CD3-TCR) in order to give the primary activation signals to the cytoplasm. The combination of the above three proteins is known as CD3 complex. It is closely associated with the T cell receptor and is internalized when the TCR recognizes the Major Histo-compatibility Complex peptide (pMHC).

During the process of activation, the concentration of CD3 protein decreases on the surface of T-cell after dissociation with pMHC and the CD3-TCR engagement carries on until the cell gets its minimal level of activation [15]. The rate of association and dissociation of CD3-TCR with pMHC motivates T-cells to produce other proteins and amplify the process of activation [51]. On the other hand, several studies have experimentally proved that CD8+ T cell activation is governed by TCR-

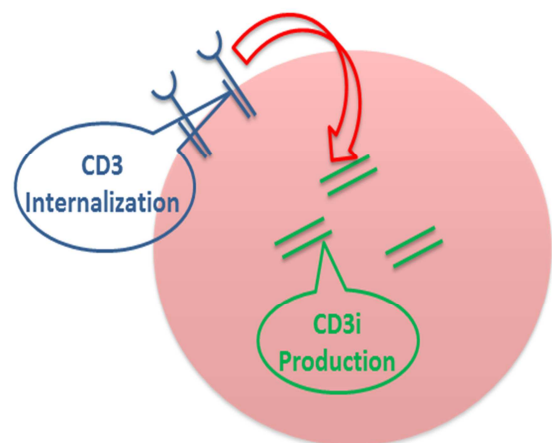


Figure 2.2: CD3 protein degradation and the production of CD3i protein.

## 2.3 Case 1

---

peptide/MHC affinity, more than only the dissociation rate [52]. However, in this study, the rate of dissociation is considered appropriate and the rate of internalization of CD3 protein is focused. El-Hentati [4] has shown this process in a reaction way by analyzing experimentally in-vitro that was helpful to model the equations.

The membrane concentration of CD3 decreases in a kinetic proportion to the strength of linking to the target. This decrease on the surface of T-cells is independent of any other protein and the cell is considered to be activated. Similarly, there are many other T-cells that are in contact with APC (Antigen Presenting Cell) and getting activated with some delay in time  $t$  at different level of initial concentration of CD3 protein. If we want to study all such type of T-cells we need to know about their activation time and their rate of change in concentrations. This can make a little complex function. In order to give a better understanding of our modeling way, we start with a simple case where we assume that we deal with only those T-cells that will have the same amount of protein at the time of activation.

Every T-cell has a different internalization rate according to its initial condition [15] and there can be some T-cells that will not follow the whole process (until the threshold level) of activation. Here we are considering the association and dissociation rate appropriate for the T-cell activation. Also beside the variability of initial condition and possible delay in meeting the pMHC complex, we have considered that the T-cells are activating at each time  $t = \tau$  and the internalization rate is same for all the activated T-cells. If  $c_1$  is the concentration of CD3 on the surface of T-cell at time  $t$  and it is decreasing with the passage of time, one can write the rate of change in the concentration as:

$$G(c_1) = \frac{d}{dt} c_1(t, \tau) = -k_1 \times c_1^m, \quad k_1 \in \mathbb{R}^+, m = 1, 2, \dots \quad (2.1)$$

with the initial condition  $c_1(0, \tau) = c_{10}$ .

where  $k$  is the kinetic constant (i.e. concentration rate constant) and  $m$  shows the order of the polynomial equation i.e. the order of the chemical reaction. The negative sign shows the decrease in protein concentration on the surface due to their internalization. We can clearly see that  $c_1$  is showing the dynamical change in the concentration of CD3 protein that is shown as  $c_1 = c_1(t, \tau)$ .

## 2.3 Case 1

$G$  is the reaction rate which can be assimilated as Growth and dissolution rate by analogy with the dynamics of growing or dissolving crystals. The linear growth rates are frequently considered in particulate processes; the dispersed systems are mathematically modeled in order to analyze their dynamical behavior regarding the time variation in size of particles. Despite the linearity in the concentration rate, in biological sciences, it has significant meaning in the microbial population balances where reaction rates are considered as the time variation in external and internal characteristics (i.e. proteins) [46], [26] or in morphometric characteristics of cells such as volume, membrane area, length e.t.c. [27].

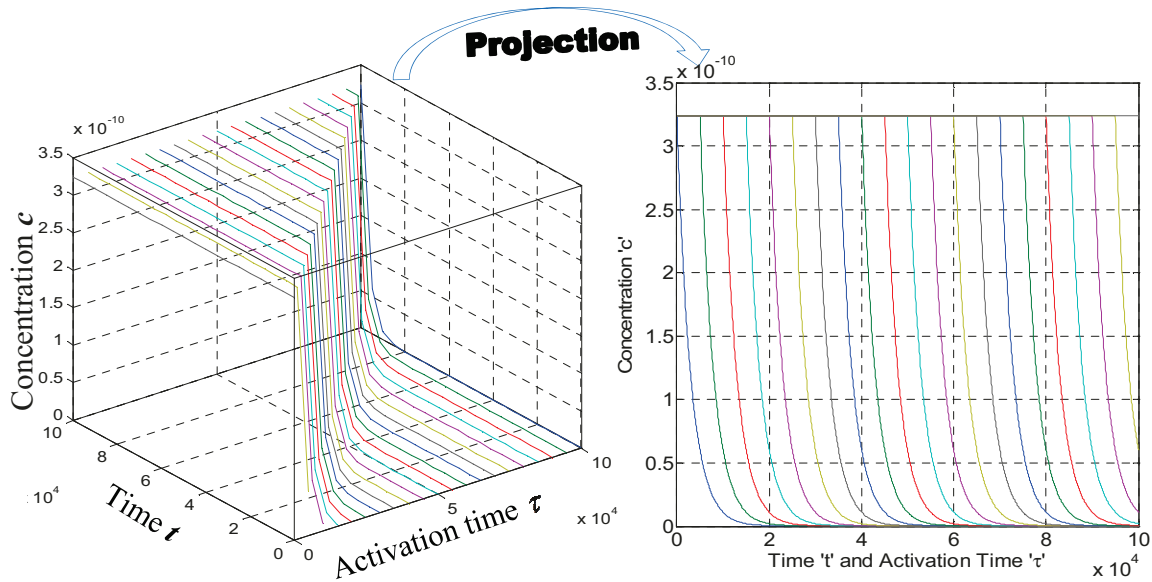


Figure 2.3a: Three dimensional view

Figure 2.3b: Projection to two dimensional view

Figure 2.3: Concentration decrease in CD3 Protein

The solution of Eq. (2.1) is found for the parameter values  $c_{10} = 3.24 \times 10^{-10} \text{ mole} \times \text{m}^{-2}$ ,  $m = 1$  and  $k_1 = 1/3000 \text{ s}^{-1}$ . It can be observed from the equation that the ‘actual time’ starts for the T-cells after their ‘activation time’ and therefore there is no change in the protein concentration before  $t < \tau$ . The cells will start their activation process after each  $t > \tau$  and therefore we have set of ODEs that are independent of activation time and they give simple exponential solutions that are shown as 3D plot in Figure 2.3a. In reality, there is a continuous activation of T-cells that gives a surface instead of discrete lines at different activation times  $\tau$ . As activation time is the starting time of each actual time  $t$ , we can merge both the times on the same axis. In other words, we can

## 2.4 Case 2

---

easily project it into two-dimensional graph that can not only save a dimension but also give us a better understanding of relation between actual time and the activation time as shown in Figure 2.3b. The solution of this equation will be studied for the population dynamics of activated T-cells in the next chapter.

## 2.4 Case 2

In this case, we again focus on the CD3 protein in a broader aspect. The CD3 protein has shown an interesting phenomenon in the T-cell: experimentally, it is observed that the CD3 protein concentration decreases inside the synapse by internalization during the activation process. This makes a significant deficiency of signals on the surface of T-cell. It is experimentally observed that the T-cell receptors (TCRs) move towards the signaling portion rapidly in order to strengthen the induction of T-cell activation [37]. The recruitment of CD3 protein is inevitable to make the TCR complex that is necessary to carry on the signaling process [15], [10]. Therefore, we will be concerned about the non-monotonic case of CD3 internalization as CD3<sub>i</sub> (volume protein) and reappearance as CD3\* (recruited protein). We divide this case into two different models according to the level of complexity. First model is more obvious and the solution is analytically found but for the second case, we studied the RK-4 (Runge Kutta Method of order 4) to find its solution.

### 2.4.1 First Model

For each cell, the surface CD3 and CD3\* concentrations are respectively noted  $c_1(t)$  and  $c'_1(t)$ , while the inner CD3<sub>i</sub> concentration is noted  $c_2(t)$ . The total protein surface concentration, that can be measured by cytometry, is  $c(t) = c_1(t) + c'_1(t)$ . For each cell, this concentration evolves, from the instant the cell get activated, in a way governed by kinetic laws. For each individual T-Cell, the following steps can describe the beginning of the activation process [15], and the evolution of the protein concentration:

1. Recognition of p-MHC and peptide by T-cell receptor after a collision event:  $L + T \rightarrow LT$  (the parameters L and T represent APC and TCR respectively). This step is called

## 2.4 Case 2

“activation”. From this collision, the T-cell becomes active, and kinetic laws describe the evolution of proteins concentration.

2. CD3-TCR internalization:  $T \rightarrow T_i$
3. Re-appearance of the CD3 protein (CD3<sup>\*</sup>) on the surface:  $T_i \rightarrow T^*$

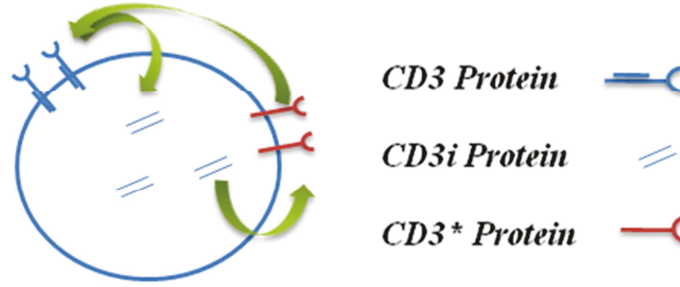


Figure 2.4: Reappearance of CD3 protein

For a given cell, activated at time 0, a linear kinetic law gives the following equations:

$$\frac{dc_1}{dt} = -k_1 c_1, \quad \frac{dc_2}{dt} = \frac{S_c}{V_c} k_1 c_1, \quad \frac{dc'_1}{dt} = \frac{V_c}{S_c} k'_1 c_2, \quad (2.2)$$

with initial conditions,

$$c_1(0) = c_{10}, \quad c_2(0) = c'_1(0) = 0, \quad (2.3)$$

where  $S_c$  and  $V_c$  are the surface and volume of T-cells. The above equations can be solved analytically by using the fact that the total initial concentration is the sum of the CD3 protein concentration present on the synapse and the CD3i protein present inside of the T-cell. Therefore, by integrating the Eq.(2.2), we get,

$$c_1 = c_{10} e^{-k_1 t}, \quad (2.4)$$

This implies that  $c_2 = \frac{S_c}{V_c} (c_{10} - c_1) = \frac{S_c}{V_c} c_{10} (1 - e^{-k_1 t})$ . The third equation follows the solution of  $c_2$

as,

$$\frac{dc'_1}{dt} = k'_1 c_{10} - k'_1 c_{10} e^{-k_1 t}, \quad c'_1 = k'_1 c_{10} t + \frac{k'_1}{k_1} c_{10} e^{-k_1 t} - \frac{k'_1}{k_1} c_{10}. \quad (2.2d)$$

## 2.4 Case 2

Hence the expression of  $c(t)$  is given by,

$$c_1(t) + c_1'(t) = c(t) = \left(1 + \frac{k_1'}{k_1}\right) c_{10} e^{-k_1 t} + k_1' c_{10} t - \frac{k_1'}{k_1} c_{10} = \alpha e^{-k_1 t} + \beta t + \gamma. \quad (2.2e)$$

For a cell activated at time  $\tau < t$ , the expression of  $c$  has to be shifted. We can thus define a family of non-monotonic curves indexed by  $\tau$ , noted  $\tilde{c}(t, \tau)$ , derived by translation from  $c(t)$ ,

$$\begin{cases} c_\tau(t) = c(t - \tau) = \alpha e^{-k_1(t-\tau)} + b(t - \tau) + d & \text{if } t > \tau, \\ c_\tau(t) = c_{10} & \text{if } t < \tau. \end{cases} \quad (2.2f)$$

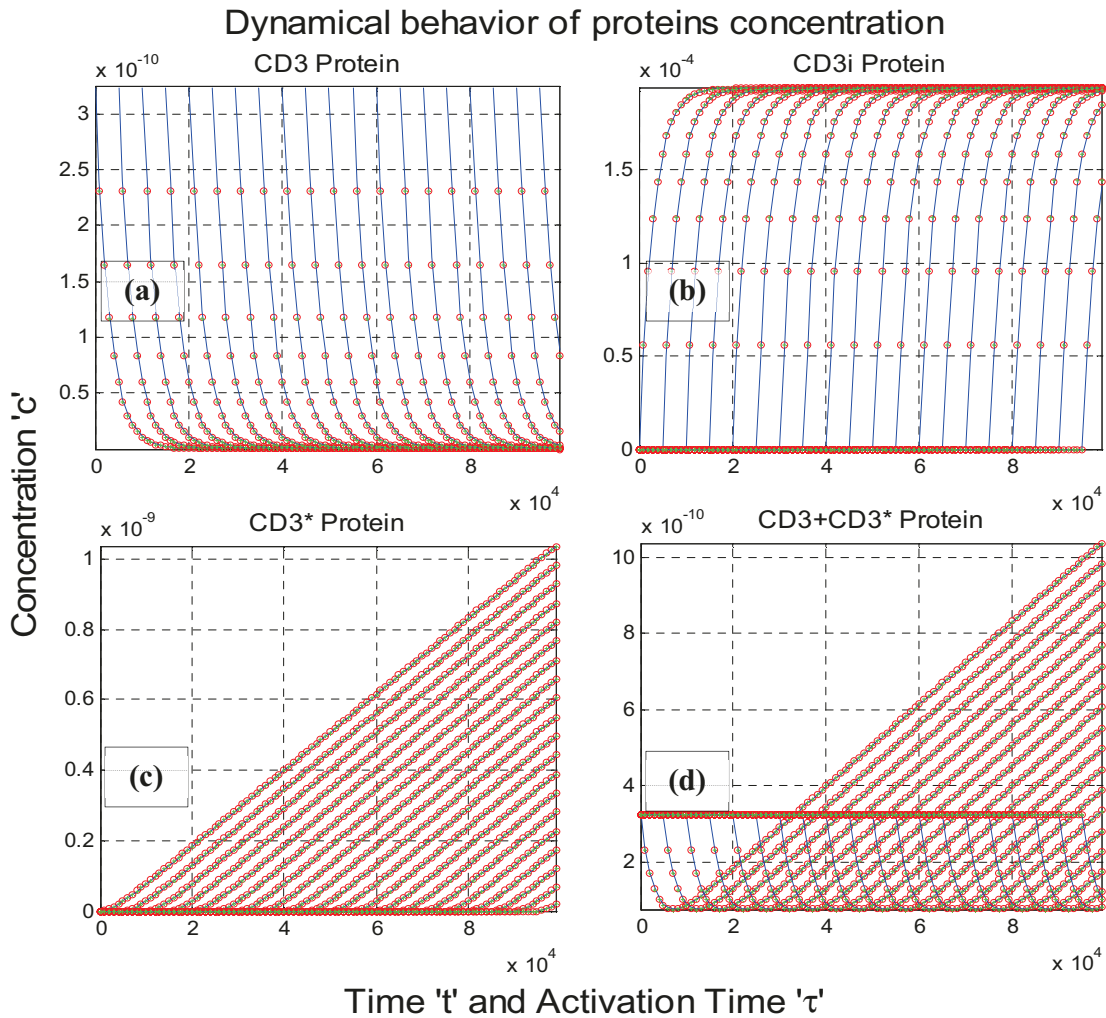


Figure 2.5: Surface concentration for individual T-cell. Blue lines show the exact solution while red-circles show the RK-4 solution and the green asteriks (\*) indicate the solution by Euler method.

## 2.4 Case 2

---

The solution curves are generated for  $k_1 = 1/3000s^{-1}$ ,  $k'_1 = 1/30000s^{-1}$  and  $c_{10} = 3.24 \times 10^{-10} \text{ mole} \times \text{m}^{-2}$  at different activation times as shown in Figure 2.5. The curves are simply shifted because neither the coefficients  $k_i$  nor the initial concentration  $c_{10}$  depend on time. But one could imagine more complex situations. It is also important to mention here that crossing of curves is coming just because of the projection as discussed in Case 1.

The common minimum value for the curves is noted as  $c_{\min}$ . In Figure 2.5d, any two consecutive curves cross each other at  $c > c_{\min}$  and cross several other curves until it reaches the initial concentration level. Also we can observe that the concentration is exceeding the initial level after some time  $t$ . Realistically, the concentration of protein will be steady after some time due to a finite surface area on the cells. Here we are not considering the steady part of the problem otherwise there will be a change in the concentration of  $c(t)$  by considering that the concentration is bounded for large values of time as shown in our Second Model below.

### 2.4.2 Second Model

The concentration of CD3 on the surface, internalization and reappearance is represented by the same notation as in 1<sup>st</sup> model, i.e.  $c_1(t)$ ,  $c_2(t)$  and  $c'_1(t)$ . The total concentration on the surface will be same as  $c(t) = c_1(t) + c'_1(t)$ .

In this model, we deal with this phenomenon more generally. As the activation process starts, the CD3 protein internalizes with the rate  $k_1$  as we discussed in our previous model. The internalized protein increases its concentration with the same kinetic parameter  $k_1$  but this time we include a term that follows the half-life principle with kinetic parameter  $k_2$ . The internalized protein signals in the cytoplasmic domain to produce numerous other proteins. The deficiency of CD3/TCR in the synapse compels the T-cell to recruit more CD3 proteins by membrane transfer, at linear reappearance rate [37]. The location of these new proteins CD3\* is different from the initial protein CD3, therefore the CD3\* protein concentration is denoted by  $c'_1$ . This phenomenon will be followed at each activation time but in a similar way. Therefore, we can write the modeled equations only at activation time  $\tau = 0$  as follows:

## 2.4 Case 2

---

$$\frac{dc_1}{dt} = -k_1c_1, \quad \frac{dc_2}{dt} = \frac{S_c}{V_c} k_1c_1 - k_2c_2, \quad \frac{dc'_1}{dt} = k'_1 \frac{V_c}{S_c} \frac{c_2}{c_{10}} (c'_{1,\max} - c'_1). \quad (2.5)$$

The initial conditions can be followed from the above modeled equations while the parameter  $c'_{1,\max}$  is the bounded value of CD3\* protein concentration (surface concentration of CD3\* may not exceed  $c'_{1,\max}$ ). Here  $S_c$  and  $V_c$  are the surface and volume concentrations. This case is more sophisticated and gives a better idea to analyze the protein dynamics at a single T-cell.

The kinetic parameter responsible for the internalization of CD3 proteins is taken as  $k_1 = \frac{1}{3000} s^{-1}$ , while the parameter value for the rate of half-life of the internalized proteins is chosen to be  $k_2 = 1/30000 s^{-1}$  [8]. The constant for the reappearance rate of CD3\* protein on the surface after the internalization of CD3 protein is defined by  $k'_1 = 6 \times 10^{-5} s^{-1}$ . The values of the surface ( $S_c = 3 \times 10^{-10} m^2$ ) and the volume ( $V_c = 5 \times 10^{-16} m^3$ ) of T-cell are taken from the literature [8] and are also used in the next cases while the other kinetic parameters take different values. For simplicity,  $c'_{1,\max}$  is taken as  $c_{10}$ .

The first equation is dependent of its own concentration showing a simple linear concentration rate phenomenon as it is discussed above with its analytical solution. For the second equation, if we use the solution of  $c_1$  in the second equation we can have a simple ordinary differential equation that only needs an integrating factor ( $e^{k_1 t}$ ) to have an analytical solution in the form of an exponential function. Similarly, we can use the solution of  $c_2$  in the 3<sup>rd</sup> equation to find the solution for third differential equation. The integrating factor for the 3<sup>rd</sup> equation is given by,

$$I.F'_{c'_1} = e^{\left( \frac{k'_1(-k_2 e^{k_2 t} + k_1 e^{k_1 t})}{(k_1 - k_2)k_2 e^{(k_1 + k_2)t}} \right)}. \quad (2.6)$$

By using the above integrating factors of the 2<sup>nd</sup> and 3<sup>rd</sup> equation, following the solution of the above system can be obtained,

## 2.4 Case 2

$$\left. \begin{aligned} c_1(t) &= c_{10}e^{-k_1t}, \\ c_2(t) &= \frac{k_1c_{10}}{k_1-k_i} \left( \frac{S_c}{V_c} \right) \left( 1 - e^{(k_2-k_1)t} \right) e^{-k_1t}, \\ c'_1(t) &= \left( c'_{1,\max} e^{\left( \frac{k'_1}{k_2(k_1-k_2)} (k_2e^{-k_1t} - k_1e^{-k_2t}) \right)} - c'_{1,\max} e^{\left( \frac{k'_1}{k_2} \right)} \right) \left( e^{\left( -\frac{k'_1}{k_2(k_1-k_2)} (k_2e^{-k_1t} - k_1e^{-k_2t}) \right)} \right) \end{aligned} \right\} \quad (2.7)$$

Now we can extract the combined solution of CD3 and CD3\* by adding 1<sup>st</sup> and 3<sup>rd</sup> equation:

$$\begin{aligned} c(t) &= c_1(t) + c'_1(t) \\ &= c_{10}e^{-k_1t} + \left( c'_{1,\max} e^{\left( \frac{k'_1}{k_2(k_1-k_2)} (k_2e^{-k_1t} - k_1e^{-k_2t}) \right)} - c'_{1,\max} e^{\left( \frac{k'_1}{k_2} \right)} \right) \\ &\quad \times \left( e^{\left( -\frac{k'_1}{k_2(k_1-k_2)} (k_2e^{-k_1t} - k_1e^{-k_2t}) \right)} \right). \end{aligned} \quad (2.8)$$

When  $t \rightarrow \infty$ ,  $c \rightarrow c'_{1,\max} \left( 1 - e^{-\frac{k'_1}{k_2}} \right)$  gives the bounded value for  $c(t)$ . The initial concentration of CD3 protein is  $c_{10} = 3.24 \times 10^{-10} \text{ mole} \times \text{m}^{-2}$  while the initial concentration of CD3i is considered 0. It means there is no CD3 protein outside the synapse on the surface of T-cell at the initial time. The solution of the complex systems of ODEs is not always possible as discussed in the next cases. Therefore we validate the results by finding the numerical solution of above system of ODEs by using two different numerical methods, Euler Method and highly accurate RK-4 (Runge-Kutta method of order 4) method. The solution curves are overlapping each other in order to show a good commitment between exact and numerical solutions as shown in the Figure 2.6. This is again a 3-dimensional plot that is presented in 2D for convenience and to save one dimension as we discussed in our first case. The shifting of curves can be observed by replacing  $t$  by  $t - \tau$ .

The numerical methods are applied in a routine manner as the equations are simple ODEs. It is obvious to see that the Figure 2.7(d) is the combination of Figure 2.6(a) and Figure 2.6(c) plots that shows the total concentration of protein evolved during the time  $t = 10^5$  sec. The Figure 2.7(b) is clearly showing that the term reserved for the half-life dominates the other term after

## 2.4 Case 2

some time  $t$ . It means the concentration of internalized protein increases for a passage of time and shows very less half-life effect in the start. But this effect dominates after an interval of time that shows the proteins are diminishing inside due to their half-lives.

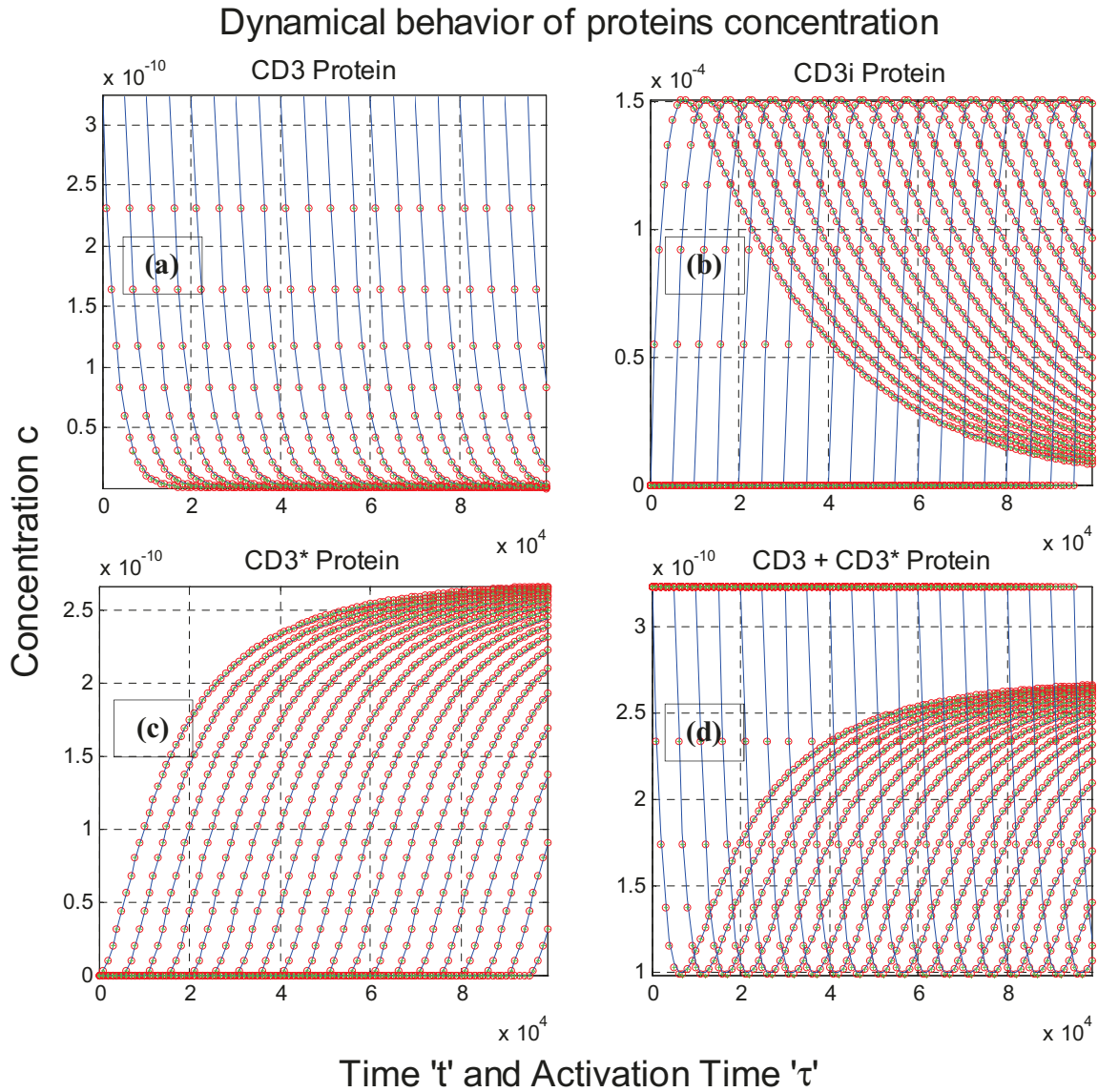


Figure 2.6: CD3 protein dynamics. Sum of Internalization and reappearance of CD3 protein. Blue lines show the exact solution while red-circles show the RK-4 simulation. The green asterisks (\*) are the solution found by Euler Method

The Figure 2.6(c) is very important in the sense that the CD3 protein reappears rapidly on the membrane that is very essential to reinforce the signal strength for the T-cell activation. On the other hand, the stability in the concentration of protein also represents the maximum limit available on the surface of T-cell. This phenomenon can be observed more closely in the Figure

## 2.5 Case 3

---

2.6(d) where the concentration of CD3 and CD3\* are added to show the total concentration of CD3 protein. Recall that the maximum capacity of CD3\* protein is considered equal to the initial CD3 concentration present in the synapse. The increase in the combined concentration of CD3 protein confines itself in the middle as shown in Figure 2.6(d). The reason is the death of the internalized protein CD3<sub>i</sub> due to its half-life and the limited capacity of CD3\*. The kinetic increase on the membrane is balanced with the disappearance of CD3 protein from the synapse due to internalization.

The phenomenon of reappearance of CD3 protein on the surface is more hypothetical while the recruitment of CD3 protein in the synapse is studied in the literature [15], [53]. Since the non-increasing phenomenon studied in the above model for CD3 protein present inside synapse clearly states that the membrane concentration is irreversible. But it is possible to include it so that the protein again works like a reversible protein. Mathematically, there will be no significant change in total CD3 protein concentration but it is possible that it can contribute significantly with any other aspect during the activation process. For example, it can affect the threshold level needed to produce other proteins that are depending on the rate of internalization of CD3 co-receptor proteins.

In the above cases we studied only the CD3 protein concentration. It has given the idea of modeling the dynamical changes at one T-cell level. Now we extend our model to study the evolution of several proteins depending upon each other. The reappearance of CD3 protein is not considered in the cases below.

## 2.5 Case 3

In our case 3, we study about the non-monotonic variation with different behavior of each cell activating with the same concentration of proteins. The study of this case reveals the protein dynamics of some other proteins that are necessary for the proliferation of T-cells. It is assumed that the T-cells with the concentration of these proteins activated at different times are not coinciding at any time even though the proteins are depending upon each other. A mathematical model is presented that analyze the evolution of these proteins concentrations with the passage of

## 2.5 Case 3

time. The model is based on the system of six ODEs that is evolved according to the kinetic parameters and shows their dynamical behavior. Each ODE presents the rate of change in the concentration of the protein that is solved by using the RK method for the system of ODEs.

The process of activation, as shown in Table IV, begins as the CD3 protein gets internalized with a rate that is considered linear with kinetic parameter  $k_1 (s^{-1})$  as discussed in above cases. It is obvious to consider here that the T-cells are beginning their activation process at different initial times. It is therefore assumed that at every time  $t = \tau$ , some T-cells begins internalization process with same concentration and continue their process.

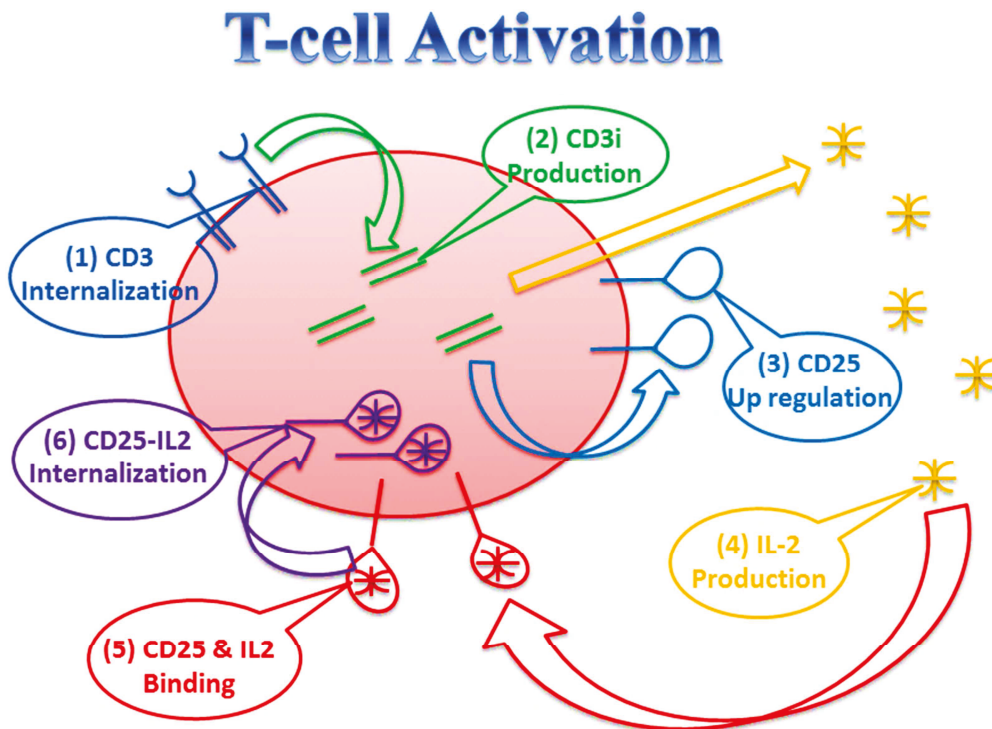


Figure 2.7: Protein dynamics of T-cell. CD3 protein internalizes and produces CD25 and IL-2 that again binds together to give signals inside the T-cells

In this case, the activation time has significant impact on other proteins concentration as the rate of change of the concentration is not depending upon the activation time. The reason for such a distinguishable behavior is that the IL-2 protein is shared by all T-cells and it binds with CD25. This binding decreases the concentration of IL-2 and CD25 as well. The concentration of CD3

## 2.5 Case 3

---

protein is considered independent of any other protein and it is represented by  $c_1$ . The equation is the same discussed in the above cases:

$$\frac{dc_1(t, \tau)}{dt} = -k_1 c_1(t, \tau), \quad \text{where } t > \tau \quad (2.9)$$

where  $c_1(t, \tau) = c_{10}$ , ( $t < \tau$ ) is the total initial concentration of CD3 protein present on the surface.

The concentration of the internalized CD3 protein (i.e. CD3i) is denoted by  $c_2$ . The CD3i increases inside the T-cell due to the internalization of CD3 while the CD3i protein decreases with kinetic parameter  $k_2$  ( $s^{-1}$ ) due to its half-life. Therefore,

$$\frac{dc_2(t, \tau)}{dt} = k_1 \frac{S_c}{V_c} c_1(t, \tau) - k_2 c_2, \quad \text{where } c_2(t < \tau, \tau) = 0. \quad (2.10)$$

The first two equations are similar to Case 2b. Further, we have more proteins to include which show more complex dynamics at a single T-cell level. Since the total concentration of CD3 protein present on the surface of T-cell is denoted by  $c_1$ , therefore, one can write a relation between CD3 and CD3i as,

$$c_1 + \frac{V_c}{S_c} c_2 \leq c_{10}, \quad (2.11)$$

The T-cells activation needs to reach a threshold of the concentration of CD3i protein to further undergo the chemical process that results in the increase of many other proteins like CD25, IL-2. At each time  $t = \tau$ , we assume that some of the T-cells start producing CD25 (concentration  $c_3$ ) on their surfaces with the kinetic parameter  $k_3$  ( $s^{-1}$ ). As there are many T-cells undergoing with the process of activation, they can have distinct rate of increase in the concentration of CD25 protein. At the same time, the production of IL-2 ( $c_4$ : concentration of IL-2 in the biological fluid) begins at the rate  $k_4$  ( $ms^{-1}$ ) that is shared by all the T-cells as a messenger between them. IL-2 uses CD25 protein as a receptor and forms a CD25-IL2 complex. We assume that the interaction of CD25 and IL-2 happens at the rate defined by the kinetic constant  $k_5$  ( $m^3 mole^{-1} s^{-1}$ ). Therefore, the rate of change in the CD25 protein concentration can be written as,

## 2.5 Case 3

---

$$\frac{dc_3(t, \tau)}{dt} = k_3 \frac{V_c}{S_c} c_2 - k_5 c_3 c_4, \quad \text{where } c_3(t < \tau, \tau) = 0. \quad (2.12)$$

While the IL-2 protein concentration can be written as an integro-differential equation,

$$\frac{dc_4(t)}{dt} = k_4 \alpha \times S_c \int_0^t B(\tau) c_2(t, \tau) d\tau - k_5 \alpha \times S_c \times c_4(t) \int_0^t B(\tau) c_3(t, \tau) d\tau. \quad (2.13)$$

The activation rate of the T-cells is denoted by  $B(\tau)$ , i.e. number of cells activated per unit of time and per unit of volume ( $s^{-1}m^{-3}$ ) at  $t = \tau$ .  $\alpha$  is the ratio between the volume of biological suspension and the volume of liquid. Its value is close to 1. It is important to mention here that IL-2 protein is independent of activation time due to its presence outside the T-cells. It is produced by all T-cells that are undergoing in the process of activation, therefore, the integration is defined which sums up all the concentrations of IL-2 in a continuous manner. It is also known as the activation rate of the T-cells due to collision with APC (Antigen Presenting Cell) and it is defined as,

$$B(t) = ae^{-bt}, \quad a, b > \mathbb{R}. \quad (2.14)$$

As IL-2 protein is produced and is shared by all the activated T-cells, therefore, IL-2 has one activation time, i.e. when it is produced for the first time by any T-cell. The change in the IL-2 concentration is examined without taking their activation time into consideration. As the CD25 protein decreases due to the interaction between CD25 and IL-2, therefore, the concentration rate of CD25–IL2 protein can be formulated as,

$$\frac{dc_5(t, \tau)}{dt} = k_5 c_3(t, \tau) c_4(t) - k_6 c_5, \quad c_5(t < \tau, \tau) = 0. \quad (2.15)$$

This binding of CD25-IL2 protein is internalized with kinetic parameter  $k_6 (s^{-1})$  that results in the production of CD25-IL2i and is modeled as,

$$\frac{dc_6(t, \tau)}{dt} = k_6 \frac{S_c}{V_c} c_5, \quad c_6(t < \tau, \tau) = 0. \quad (2.16)$$

## 2.5 Case 3

---

The analytical solution of the above system of six ODEs is not possible due to their dependency on each other. Each concentration curve of CD25 and CD25-IL2 proteins at  $t = \tau$  is different from the curve at  $t = \tau + d\tau$ . On the contrary, activation time always belongs to the actual time from where we follow the change in the concentration of any protein. We solve the above system by fixing the time step  $t$  in order to show the protein dynamics at the next time step  $t + dt$ . The above equations are solved simultaneously by Runge-Kutta Method of order 4 that has given the approximate solution in order to analyze the change in the concentration with respect to time 't' as shown in the Figure 2.8. It is important to mention here that the Eq. (2.13) is not treated in the same way because it is depending only on actual time. An algorithm is written below for the solution of above system of integro-differential equations.

The algorithm to find a solution of above system of differential equations (2.9) – (2.16) is based on the Runge-Kutta Method of order 4 in the given time interval  $0 \leq t \leq 10^5$  sec .

**INPUT:** The values of the parameters and the initial conditions as follows,

$$k_1 = 1/5 \times 10^{-4} s^{-1}, k_2 = 1/5 \times 10^{-5} s^{-1}, k_3 = 10^{-4} s^{-1}, k_4 = 10^{-9} ms^{-1},$$

$$k_5 = 10^3 m^3 mole^{-1} s^{-1}, k_6 = 10^{-3} s^{-1}, Vc = 5 \times 10^{-16} m^3, Sc = 3 \times 10^{-10} m^2$$

$$B(\tau) = 3 \times 10^8 e^{-\frac{\tau}{7200}}$$

$$c_1(t, \tau) = c_{10}, c_4(0) = 0$$

$$c_i(t, \tau) = 0 \quad \forall i = 2, 3, 5, 6 \text{ and } t \leq \tau$$

**OUTPUT:** The approximation of  $C(t, \tau)$  and  $c_4(t)$ , where  $t > \tau$

$$\text{and } C(t, \tau) = \begin{bmatrix} c_1(t, \tau) \\ c_2(t, \tau) \\ c_3(t, \tau) \\ c_5(t, \tau) \\ c_6(t, \tau) \end{bmatrix}.$$

## 2.5 Case 3

---

We write the differential equations in the matrix form as,

$$F(t, \tau) = \begin{bmatrix} \frac{dc_1(t, \tau)}{dt} + k_1 c_1(t, \tau) \\ \frac{dc_2(t, \tau)}{dt} - k_1 \frac{S_c}{V_c} c_1(t, \tau) + k_2 c_2(t, \tau) \\ \frac{dc_3(t, \tau)}{dt} - k_3 \frac{V_c}{S_c} c_2(t, \tau) + k_5 c_3(t, \tau) \times c_4(t, \tau) \\ \frac{dc_5(t, \tau)}{dt} - k_5 c_3(t, \tau) \times c_4(t, \tau) + k_6 c_5(t, \tau) \\ \frac{dc_6(t, \tau)}{dt} - k_6 \frac{S_c}{V_c} c_5(t, \tau) \end{bmatrix} = 0$$

and 
$$\frac{dc_4(t)}{dt} - k_4 \times \alpha \times S_c \times I_1(t) + k_5 \times \alpha \times S_c \times c_4(t) \times I_2(t) = 0,$$

where the integral terms are,

$$I_1(t) = \int_0^t B(\tau) c_2(t, \tau) d\tau,$$

$$I_2(t) = \int_0^t B(\tau) c_3(t, \tau) d\tau.$$

**Step 1:** Define step size  $h = (b-a)/N$ , where  $a \leq t \leq b$  and  $N$  is an integer describing the Number of discrete points at  $t$ -axis .

**Step 2:** For  $i = 1, 2, \dots, N$

Define  $C(t_0, \tau) = C_0$ , for  $t \leq \tau$

$$\text{where } C_0 = \begin{bmatrix} c_{10} \\ 0 \\ 0 \\ 0 \\ 0 \end{bmatrix} \text{ and } c_4(0) = 0.$$

## 2.5 Case 3

---

**Step 3:** For  $j = 1, 2, \dots, i-1$

**Step 4:** Set

$$\begin{aligned} K_1 &= F(C_{i,j}, t_i, \tau_j) \\ K_2 &= F(C_{i,j} + hK_1/2, t_i, \tau_j) \\ K_3 &= F(C_{i,j} + hK_2/2, t_i, \tau_j) \\ K_4 &= F(C_{i,j} + hK_3, t_i, \tau_j) \end{aligned}$$

$$\text{Set } C(t_i, \tau_j) = C(t_i, \tau_{j-1}) + h(K_1 + K_2 + K_3 + K_4)/6$$

END loop  $j$

$$c_4(t_i) = c_4(t_{i-1}) + \alpha \times S_c \times \left( k_4 \times \sum_{k=0}^i c_2(t_i, \tau_k) B(\tau_k) + k_5 \times c_4 \times \sum_{k=0}^i c_3(t_i, \tau_k) B(\tau_k) \right)$$

END loop  $i$

**Step 5:** Output  $(t - \tau, C(t, \tau))$ , STOP.

The matlab coding was used to implement this above algorithm of Runge-Kutta method of order 4. The solutions obtained are shown in the Figure 2.8. The behavior of the considered protein can be better visible in the 3-dimensional space. Here we will describe only the CD25 protein dynamics in the 3D plot that has shown an unconventional variation during the simulation time. Contrary to Figure 2.3(a) where we have drawn a discrete 3D curves plot, we have a surface (2D manifold) plot in Figure 2.8 that shows a smooth curvy region. We need to study the evolution in the concentration of proteins present on the T-cells at different activation times  $\tau$ .

We consider an actual time  $t = t_0$  and observe the concentration on T-cells at all the activation times shown in Figure 2.8. We draw a plane (rectangular surface) that cuts the 2D manifold (surface) into two sections at the considered actual time  $t = t_0$ . This plane is shown as the 2D plot between concentration and activation time at the top-right of the Figure 2.8. We observe that it shows a monotonically decreasing behavior. This can be observed at any actual time  $t$ . It shows that there is a unique concentration present on the T-cells for each activation time. Therefore, we

## 2.5 Case 3

can deduce a statement that if we project the surface plot to a 2D plane, the curves will not cross each other. It can be followed for all other proteins at any time  $t$ .

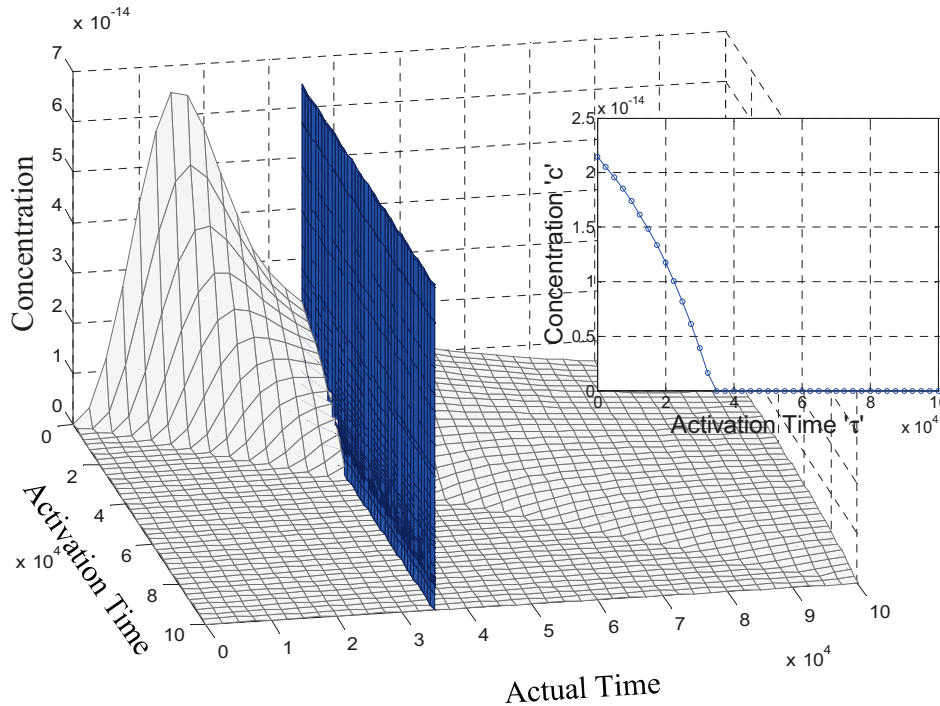


Figure 2.8: Plane cutting the 2 dimensional manifold (surface) at a point  $t=t_0$

In the Figure 2.9, we projected the solution of CD25 protein concentration together with the solutions of all other proteins concentrations that are modeled in this case. One can observe that the proteins have followed the natural phenomena. CD3 protein shows a decreasing behavior that is  $c_1 \rightarrow 0$  as  $t \rightarrow \infty$ . The internalization of CD3 protein generates CD3i while the half-life of CD3i protein can be observed due to its curvy behavior that shows the stability in the concentration after time  $t$ .

Correspondingly, CD25 increases rapidly depending on its kinetic constants  $k_3$  and decrease after taking a maximum value. The IL-2 protein starts increasing in the beginning and shows a continuous increase in the concentration. The reason seems to be behind a rapid decrease of CD25 protein concentration is the high production rate of IL-2 protein and a fast binding rate. As IL-2 is produced and shared by all T-cells simultaneously, it can be clearly deduced that there is

## 2.5 Case 3

no activation time after its first increase. The binding CD25-IL2 shows a vital increase in the start and its slope decreases gradually with the passage of time. The decrease in the binding on the surface of T-cells compels us to study the internalization of CD25-IL2 protein during the activation process. It is the most important action in our model with respect to the splitting of T-cell into its daughter cells. This can lead the problem to study the division process of T-cells that is actually known as the proliferation of T-cells.

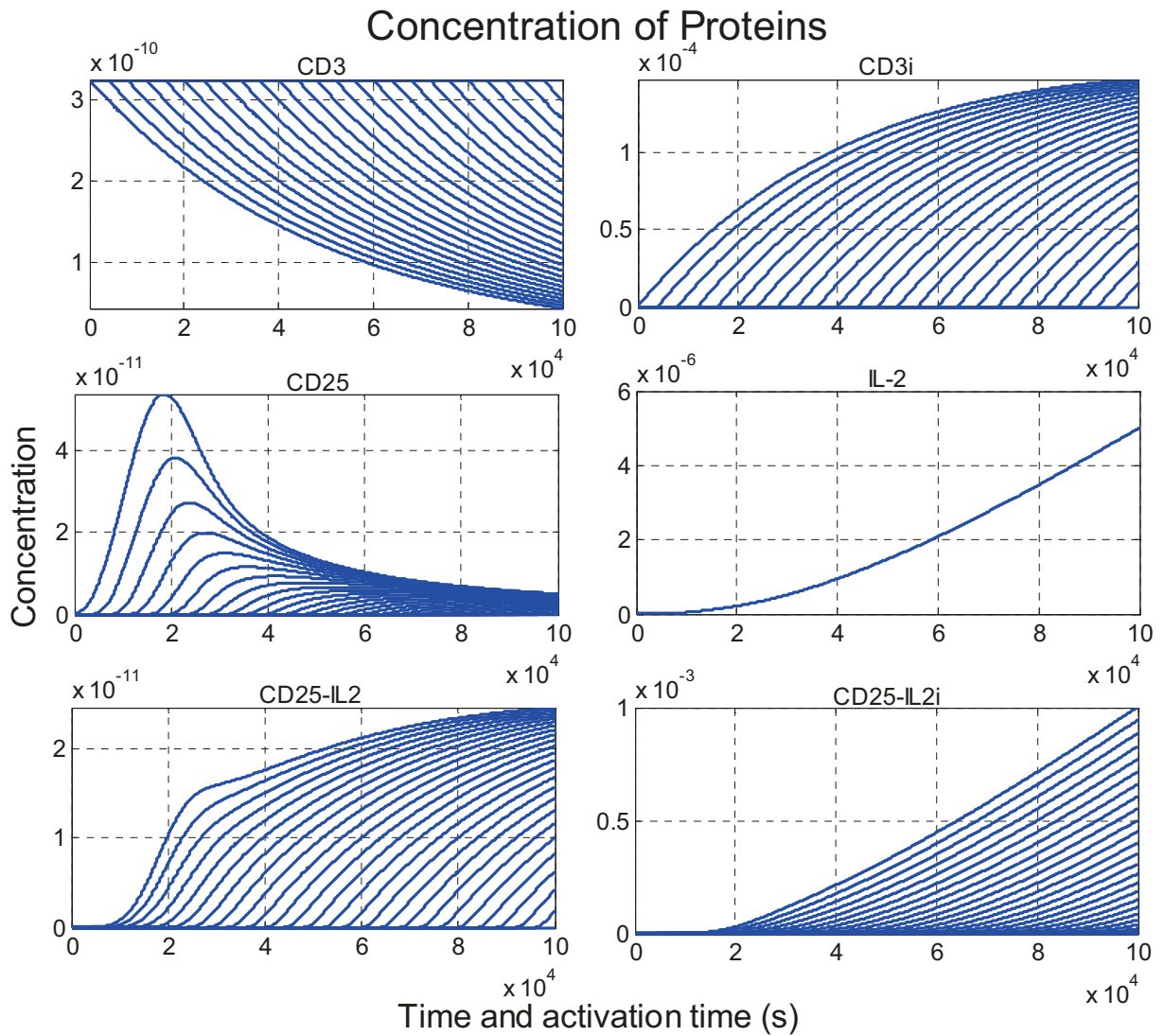


Figure 2.9: Graphical representation of the solution of above system of ODEs with the parameter values:

$$k_1 = 1/5 \times 10^{-4} s^{-1}, k_2 = 1/5 \times 10^{-5} s^{-1}, k_3 = 10^{-4} s^{-1}, k_4 = 10^{-9} ms^{-1}, k_5 = 10^3 m^3 mole^{-1} s^{-1}, k_6 = 10^{-3} s^{-1}$$

## 2.6 Case 4

---

### 2.6 Case 4

This case focus on the same proteins as discussed in the last case with an addition of a phenomenon of intersection of concentration curves as shown in Figure 2.10. The rate of change of the protein concentration for the T-cell varies in such a way that T-cell activated at time  $\tau = \tau_0$  may equate with the T-cell activated at time  $\tau \neq \tau_0$ . Therefore, the concentration of proteins of two or more T-cells can coincide each other at any time  $t$ . This makes a difference with the cases discussed above.

The mathematical model is same as in the last case. There is a change of kinetic parameters in order to study different behavior of curves. This behavior is important to study in order to understand the dynamics of T-cells during concurrence in their concentrations. We applied the same technique of Runge-Kutta method of order 4 in order to find the solution of the system of equations (2.9) – (2.16). The kinetic parameters reserved for CD3 and IL-2 proteins played an important role to find the curve crossing problem. Here we increase the rate of internalization of CD3 protein by defining  $k_1 = 1/3000 s^{-1}$  and increase the rate of IL-2 production by choosing  $k_5 = 10^4 ms^{-1}$ .

The kinetic parameters vary their values from cell to cell in order to decide the fate of T-cell activation. All the other parameters including the surface area and volume of T-cells are same as in the previous cases. The Runge Kutta method of order 4 numerical method is used again to approximate the modeled equations. For this case, we used the same algorithm as defined in case 3. The results are shown in the Figure 2.10. In this figure, three proteins dynamics show the phenomenon of curve crossing. We discuss two of them (CD25 and CD25-IL2) in 3-dimensional space that will be studied in the next chapter.

The CD25 protein kinetics is showing a rapid change in the start and get stable possibly due to less amount of protein left on the surface. The T-cells that are activated at time  $0$  start producing IL-2 protein. Therefore, CD25 suddenly joins with it, results in the drastic decrease of CD25 protein. At the same time when activated T-cells at time  $\tau = \tau_0$  starts decreasing their

## 2.6 Case 4

concentration, some more T-cells start increasing CD25 proteins that are activated at time  $\tau = \tau_1 (> \tau_0)$ . It is possible that the concentration of both types of T-cells cross each other at a certain level of CD25 proteins. This behavior can be observed in the 2D plot shown in the Figure 2.11 where the 3D plot represents the concentration of CD25 versus time and activation time.

### Concentration of Proteins

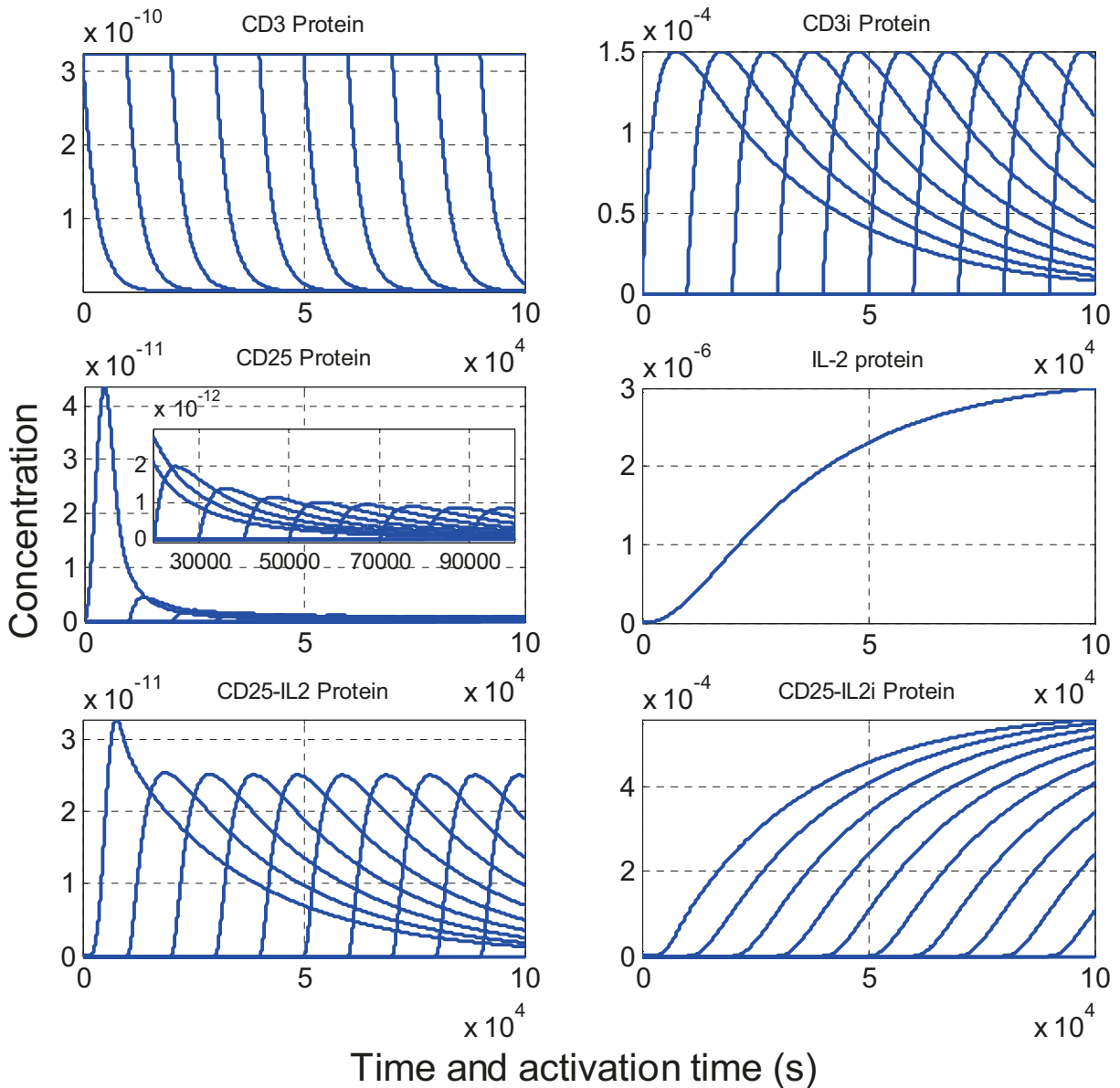


Figure 2.10: Graphical representation of the solution of above system of ODEs with the parameter values:

$$k_1 = 1/3 \times 10^{-3} s^{-1}, k_2 = 1/3 \times 10^{-4} s^{-1}, k_3 = 10^{-4} s^{-1}, k_4 = 10^{-9} ms^{-1}, k_5 = 10^4 m^3 mole^{-1} s^{-1}, k_6 = 10^{-3} s^{-1}$$

## 2.6 Case 4

In Figure 2.11, the surface plot is cut by two planes at different times. To justify the phenomenon of crossing curves, the crossing points are shown on the 2D plot at a particular time  $t$ . We observed that the behavior of concentration of proteins is non-monotonic and therefore it has repeated itself by attaining the same level. The first plane is shown as the blue curve in the 2D plot (i.e. the plane between the actual time  $t = 0$  to  $5 \times 10^4$ ) while the 2<sup>nd</sup> plane cuts at the values displayed as green curve (i.e. the plane between the actual time  $t = 5 \times 10^4$  to  $10^5$ ). One can observe that there is more repetition in the concentration of T-cells when it is low (i.e. the green plane is showing more repetition). This suggests that the CD25 protein increases rapidly in the start but it gets linked with IL-2 and internalized from the surface of T-cell abruptly. The decrease phenomenon in the concentration reveals another fact that, after some time, the concentration of IL-2 protein gets so high that CD25 protein converges to 0.

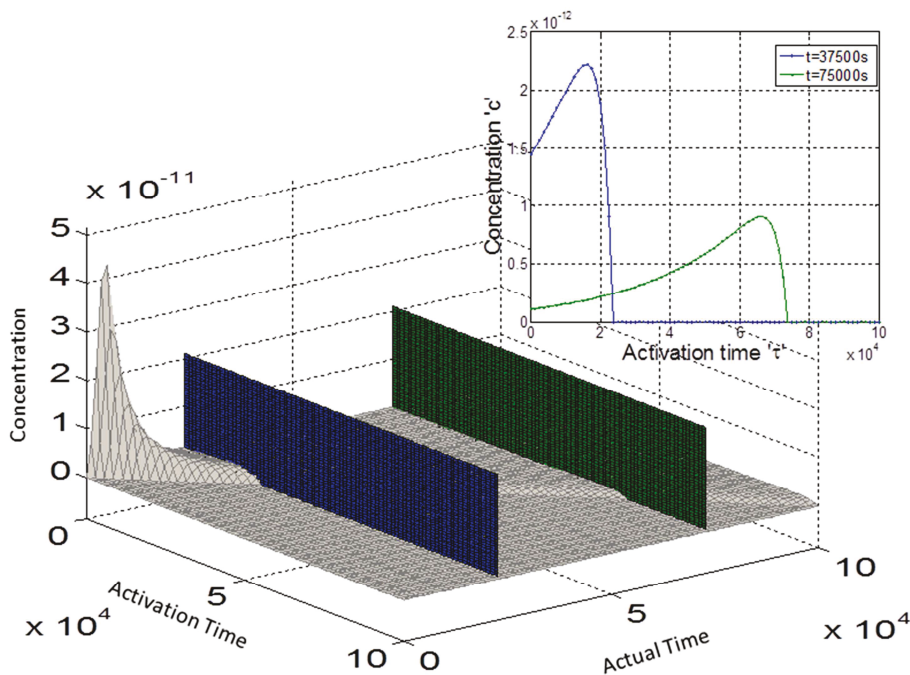


Figure 2.11: 3D visualization of CD25 protein concentration cut by two planes. The cutting curves are shown in the 2D plot attached at the top right of the figure.

In a similar way one can also observe the crossing curves showing the CD25-IL2 complex in the Figure 2.12. In this figure, we plotted several planes cutting the surface of CD25-IL2 protein concentration that are presented in the 2D plot at the top right corner. All the repetitions in the

## 2.6 Case 4

concentration shows the two types of activated cells showing the same amount of concentration at a particular time  $t$  having a different rate of change of the concentration.

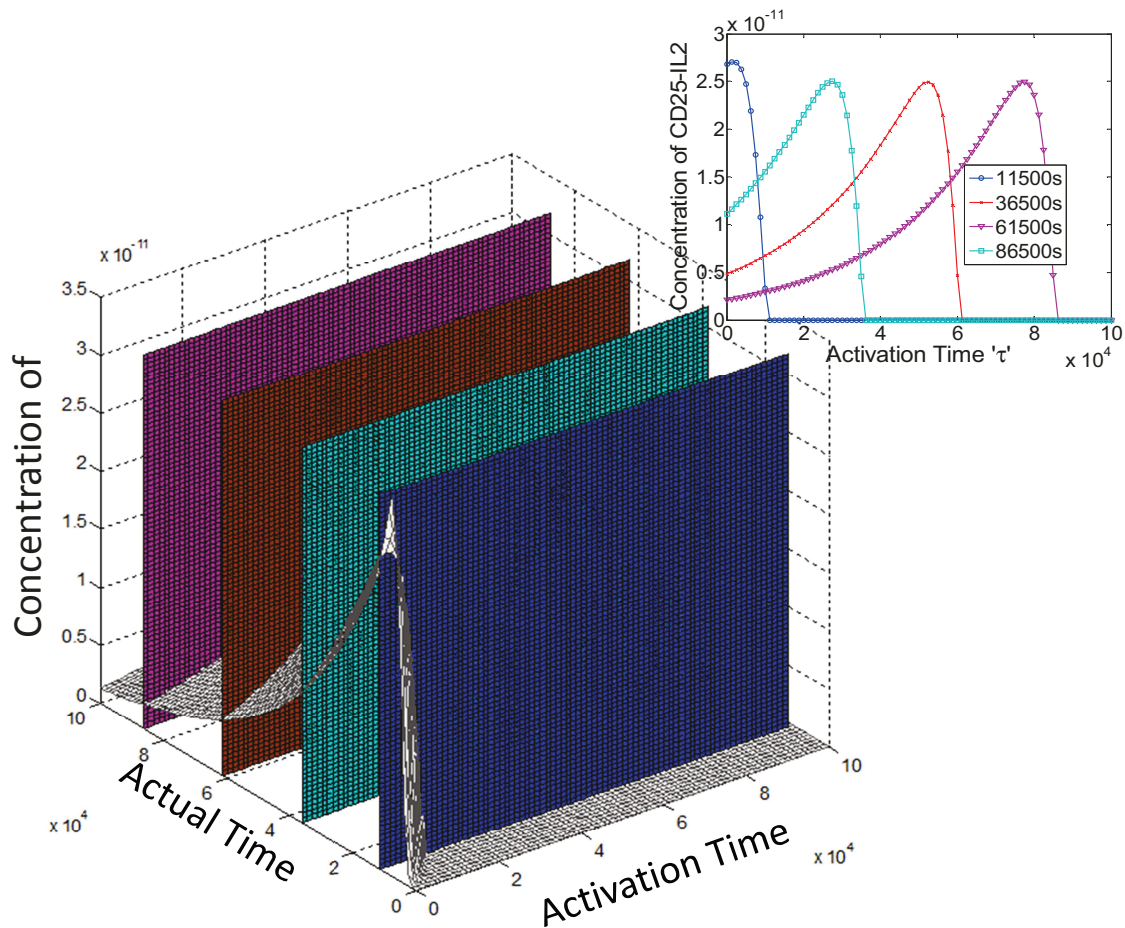


Figure 2.12: 3D visualization of CD25-IL2 protein cut by four planes. The topright plot shows the curves made due to the intersections of the surface plot and the planes.

The concentration is not varying in the same manner as of CD25 protein but still it seems to be converging to  $0$ . It is important to mention here that the first curve is the leading curve and all the other curves cross afterwards. This shows that the crossing is a continuous process that ends with the end of viral infection. If we closely observe the next curves, the peak value is not the same in any curve of the Figure 2.12. There can be two reasons why a curve has peak higher than the peaks of the next curves. Firstly, the CD25 protein concentration increases in the start rapidly and then the process slows down due to the binding of IL2 protein with CD25. Secondly, due to high

## 2.7 Conclusion

---

CD25 protein concentration, it is expected that the rate of internalization of CD25-IL2 protein is less effective in a given curve than the rate of internalization in the next curves.

## 2.7 Conclusion

In this chapter, we developed several dynamical models categorized in four cases to analyze the evolutionary changes that took place in the proteins at a single T-cell level. These models were based on the phenomena observed experimentally in [4]. The models were classified into monotonic and non-monotonic behaviors. The non-monotonic behavior is diversified in three different cases. The solution curves presented in the Case 2 have shown a shifting phenomenon but the slope of each curve remains same. The last two models have shown the solution curves which vary the slope of each curve starting at different activation times. Despite their non-monotonic behaviors, another interesting phenomenon was the crossing of curves that was observed by taking an image of a surface plot on the plane.

We started from a simple problem where only the concentration of CD3 protein decreased. This case was studied to understand the initial immune response. The CD3/TCR engagement with the pMHC exposed a rapid decrease in protein at the start that has been observed experimentally by various researchers concluded it as the partial activation of T-cells [37], [54]. In spite of a rapid decrease observed in the Figure 2.3, the model lacked some information that is necessary to better analyze the physical phenomenon. For example, it is not necessary that a decrease in the CD3 protein concentration could fully engage the T-cell during the activation process to produce other proteins. However, it was possible to adjust the kinetic parameters according to the experimental values where the range of each kinetic parameter has been defined. Despite the simplicity of the model, it has provided the basis to study the information waiting ahead.

The increase of internalized protein CD3<sub>i</sub> inside the T-cell led to the production of several other proteins. Beside other proteins, in Case 2, we studied an interesting phenomenon about the CD3 protein reappearance on the surface of T-cell which has revealed an innovative approach to study the variation in CD3 protein concentration [55]. The major fascination of such problem was the crossing of curves that has given an impression of real problem. This model has shown an

## 2.7 Conclusion

---

unbounded increase in the protein concentration that was the major flaw in the model. The subsection Second Model in Case 2 has taken into account the limitation of CD3i protein by considering its half-life as well as the phenomenon of bounded concentration of CD3 protein on the surface of T-cell. This model has overcome the deficiency of the first model but it has originated more questions about the generalization like the study of Single T-cell dynamics if each type of T-cell, activating at different activation times, has followed the different phenomena (shifting and similar slope). Although the model has used the kinetic parameters that were observed experimentally, yet the model was simple and therefore it was possible to find the analytical solution. Despite of the analytical solution, numerical methods have also been validated in this case in order to apply them in the cases where the analytical solutions were not possible.

The internalization of CD3 protein produced many other proteins which have shown versatile behaviors during the simulation time. The mathematical modeling of the third case included the two major proteins that were depending upon each other, i.e. the CD25 and IL-2 proteins. The rapid binding of both proteins was another interesting phenomenon that has originated the reason of decrease in the concentration of CD25 and IL-2 proteins. We have observed this decrease by studying the change in the slope of each solution curve of CD25 protein concentration which has shown the impact of IL2 protein intervention. Although the model has the deficiency due to a non-intersecting behavior of curves and needs to be modified, yet the integro-differential equation has motivated us to analyze it before moving towards the next step.

In Case 4, the change in the parameters values investigated the fast reaction rate (in comparison to Case 3) and it has shown a wide range of intersection between the curves. This model was generalized for the problem of one point crossing. However, during the activation process, it was possible to have more than two different types of T-cells crossing each other at the same time. For such idea, we may need to follow more complex model by introducing other dynamical behaviors. Probably, e.g., if the CD3 protein concentration shows the non-monotonic behavior that was discussed in our Case 2 we can observe crossing within three types of T-cells during the simulation time.

# **Chapter 3**

## **Population dynamics of T-cells**

## 3.1 Introduction

---

### 3.1 Introduction

The population dynamics of T-cells deal with the evolution process of the population that is affected by the change in the protein concentration. It is considered as one of the most effective ways to understand the immune response against viral infections. The continuum modeling of such dynamical systems is popular among the modern scientific environs. There are variety of models that helps us to understand the evolutionary process by means of age, size and some internal and external characteristics of infected cells ( i.e. concentration of proteins) [3], [7], [46], [27]. In this chapter we study four mathematical models describing the population density  $n(c, t)$  of T-cells with respect to their surface proteins concentration  $c$ . These models are studied in an increasing pattern of complexity. First three cases are represented for each surface protein by a population balance equation (PBE) while the fourth case is validated against a newly developed approximate method based on differential geometry technique called as Transport Method (TM). The work described in the previous chapter is frequently referred here in order to reduce repetition.

The population balance equation has been previously studied by many researchers [47], [2]. Such type of complexity is dealt in the first case where the exact solution was possible by using Method of Characteristics (MOC). In the next cases, the exact solution of the hyperbolic equations was not possible due to dependency of protein concentrations on each other. Therefore, it was inevitable to introduce an approximate technique to find the population density function. The results are compared between the TM and numerical methods like finite difference and finite volume schemes. The exact solution is found whenever possible. At the end of this chapter is the conclusion where we critically overviewed the mathematical models and tried to elaborate the difficulties regarding the future improvements.

#### 3.1.1 Biological aspects

A detailed experimental analysis of Flow-cytometry technique for the discussed proteins and T-cell dynamics has been studied in the literature [3], [4], [15], [56]. The population densities of activated T-cells are studied with respect to the concentration of proteins present on their surfaces. During an experiment of immune response, sampling of the biological fluid is carried

### 3.1 Introduction

out. Then, by using FCM (Flow-Cytometry) technique, individual cells are analyzed and their protein content is measured. From these data, cell densities  $n(c,t)$  for each protein are deduced. The evolution of proteins and the T-cells dynamics are observed at particular times as shown in Figure 3.1. The figure shows various bunches of activated T-cells with CD3 and CD25 markers present on the surfaces of CD4+ T-cells and CD8+ T-cells at different times  $t$ .

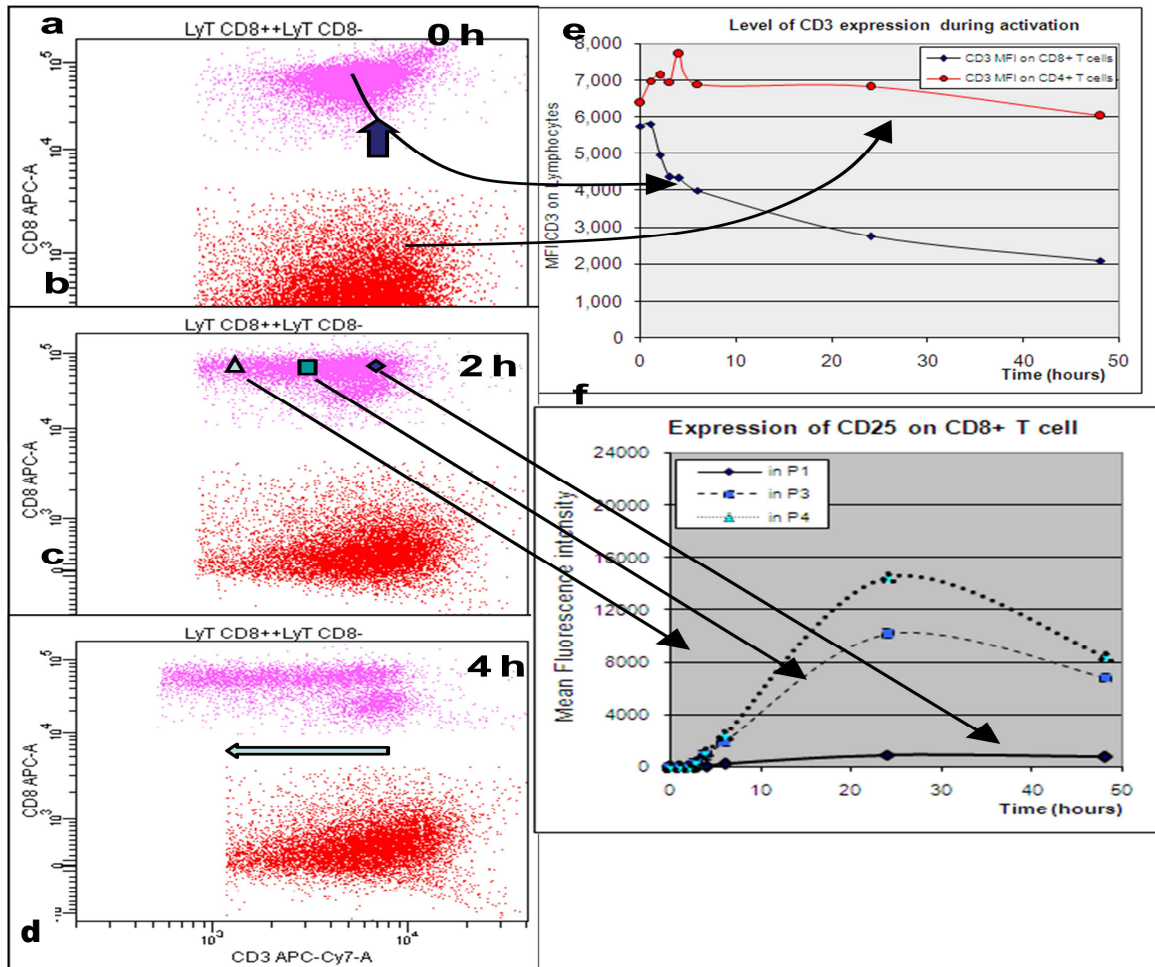


Figure 3.1: Population of CD3 and CD25 proteins on the surface of CD8+ T-cells

Each bunch of dots indicates the level of the protein at different time  $t$ . It is obvious to observe the decrease in the CD3 protein level while an increase followed by a decrease in the CD25 protein level. This phenomenon describes the protein dynamics of CD3 protein present on the surface of activated T-cells. Experimental values are always based on discrete time steps that cannot predict those drastic changes that are possible to happen in the intervening time. But it

## 3.1 Introduction

---

makes an overall scenario that can be further used to analyze by mathematical models. By following the same approach, these observations have given an idea to mathematically model and analyze the FCM by using population balance equations.

It is mandatory to briefly introduce the biological phenomena before defining the main problem. During an experimental study of the immune response against viral infection, it is observed that first of all the T-cell encounters antigen presenting cell (APC). Shortly, T-cell receptors connect with a specific antigen fraction (peptide) that is linked with a self-molecule Major Histocompatibility Complex (MHC) of Antigen Presenting Cell (MHC) and induces the cell activation whose first effect is revealed by changes of protein concentration at their surface or in the close medium. This first step is the source of activated T-cells and it is assimilated as an activation rate of the T-cells. The dynamics of the process depends upon the strength of the binding that involves many components. In this study, we consider the cells with different time of activation but the same level of proteins present at the time of activation. Therefore, the number of activated T-cells at a certain amount of initial protein concentration, produced per unit time, will be known as the activation rate (or rate of activation) of the T-cells. It corresponds to the start of the activation process at the cell scale.

A high concentration of CD3 protein is present on the surface of the T-cells and this concentration varies during the activation process. Due to its variation, the T-cells produce several other proteins in order to react against the infected cells (i.e. APCs). The variation in the protein concentration with time is assimilated as the reaction rate of the activated T-cells. The reaction rate can be an increase or a decrease of the concentration of the considered protein. In chapter 2, we talked in detail about the complexity of reaction rates in four cases.

A mathematical modeling of the above discussed evolutionary process is presented below. The models follow the linear first order hyperbolic conservation laws with a source term representing the birth of activated T-cells after collision between T-cells and APCs.

## 3.2 Mathematical Modeling

### 3.2 Mathematical Modeling

The mathematical modeling for the activation process of T-cells is studied at the initial stage when the division process (proliferation) is not started. Their evolution is divided into two processes, the reaction rate and the activation rate, as we discussed in the Chapter 2. Since the total amount of T-cells remains same during the activation time, it is deduced that the rate of change in the total amount (number concentration) of activated T-cells  $N_{AC}$  ( $m^{-3}$ ) is equal to the rate of change in the non-activated T-cells  $N_{NAC}$  ( $m^{-3}$ ). Mathematically,

$$B(t) = \frac{dN_{AC}}{dt} = -\frac{dN_{NAC}}{dt} = k^* N_{NAC} N_{APC}. \quad (3.1)$$

Here  $k^*$  is the kinetic constant that indicates the probability of connection between non-activated T-cells and antigen presenting cells (APCs).  $N_{APC}$  is the total amount of APCs loaded with the specific virus. The negative sign shows that the population of non-activated T-cells is decreasing. Let us define the initial population of activated T-cells  $N(c, t)$  ( $s^{-1} (mol / m^2)^{-1}$ ) varies between  $c$  to  $c + dc$  within time  $t$  to  $t + \Delta t$  where  $c$  is considered as a surface protein. Due to voluminous amount of activation of specific T-cells with versatile concentration of protein in a the continuous interval of time, we get a continuous distribution describing the initial population of activated T-cells as shown in Figure 3.2.

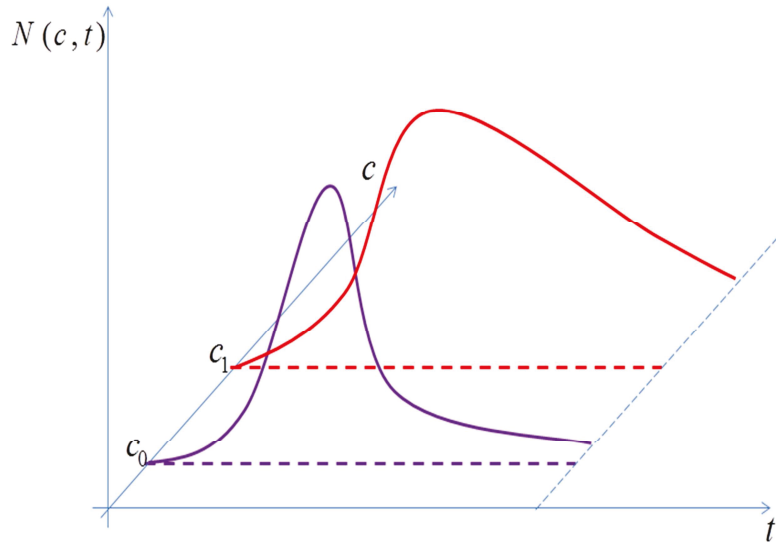


Figure 3.2: Initial population of activated T-cells at two different concentrations  $c_0$  and  $c_1$ .

## 3.2 Mathematical Modeling

One can write for the initial population (birth) of activated T-cells as,

$$N(c,t)\Delta t = \text{Number of T-cells having concentration } c \in [c, c + \Delta c] \text{ and activated within } [t, t + \Delta t]. \quad (3.2)$$

As T-cells activate with an initial concentration, it is possible that at a particular time  $t$ , they activate with different concentrations of proteins as shown in the Figure 3.3. If the distribution for the T-cells activated with an initial stage will be  $D(c)$  then it can be represented for the interval  $[c, c + dc]$  by  $D(c)dc =$  portion of T-cells activated at  $c \in [c, c + dc]$ . At any time  $t$ , the initial amount of activated T-cells can be written as,

$$\int_{\Omega_c} N(c,t)dc = B(t) \int_{\Omega_c} D(c)dc. \quad (3.3)$$

provided that

$$\int_{\Omega_c} D(c)dc = 1.$$

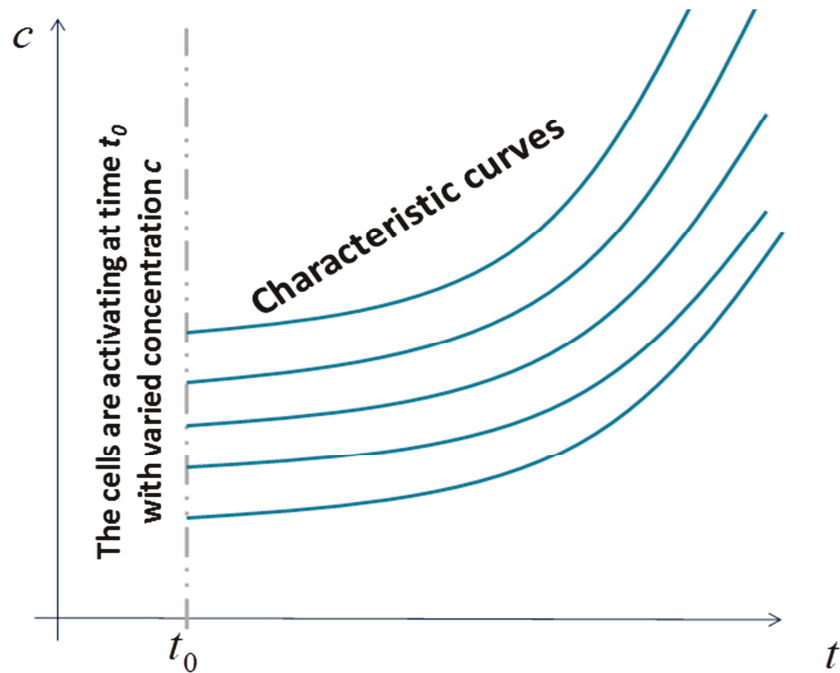


Figure 3.3: T-cells are activated with different initial concentrations at time  $t = t_0$  and distributed over the  $c$ -axis.

## 3.2 Mathematical Modeling

---

Since, in our study, we consider that all the T-cells are activating at the same initial concentration  $c_0$ , therefore, the distribution function  $D(c)$  will become a delta function that has the following property,

$$\int_{\Omega_c} \delta(c - c_0) dc = 1. \quad (3.4)$$

Clearly, all the T-cells activating at  $c = c_0$  give us the following equation,

$$N(c, t) = B(t)\delta(c - c_0). \quad (3.5)$$

The above equation gives the total initial population of activated T-cells at any time  $t$ . In order to understand the phenomenon that how the density functions evolve during the whole simulation time with respect to the reaction rate (variation) of the protein concentration, we used the population balance models.

Since the experimental observations by using FCM are based upon the concentration of proteins involved during the activation time of T-cells, therefore we need the population density function  $n(c, t)$ . This means that the function defined for reaction rate must be the explicit function of concentration of proteins as presented in the previous chapter.

### 3.2.1 Conservation Laws and Population Balance Equation

In this study, the protein concentration based cell population balance model follows the conservation laws that show the total number of activated T-cells at any time  $t$  remains same while the density of T-cells changes with the change in the concentration of proteins present on the surface of T-cells. The conservation laws states that the rate of change of the total activated population of T-cells is equal to the flow of the activated T-cells during the change in the concentration over control volume  $\Omega$ . We elaborate the conservation law in the following way:

$$\begin{aligned} & \text{Rate of change in the total population of activated T-cells in a control volume } \Omega \\ & = \\ & \text{Source of activated T-cells at time } t \\ & + \text{Rate of Flow-in of activated T-cells} - \text{Rate of Flow-out of activated T-cells} \end{aligned}$$

## 3.2 Mathematical Modeling

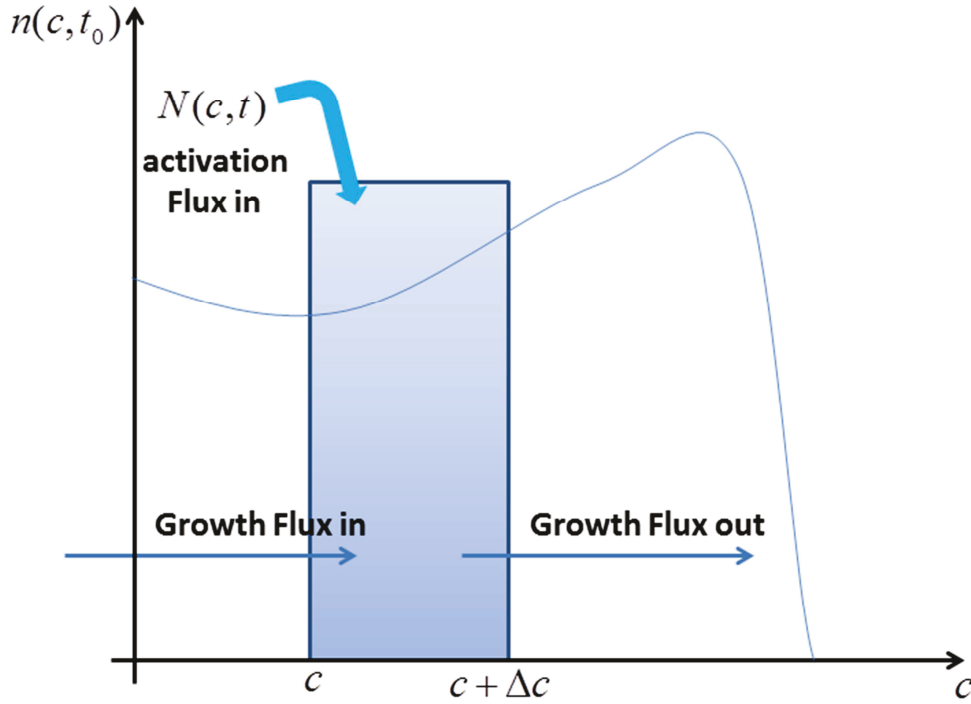


Figure 3.4: Activated T-cells flux in and flux out indicated during the variation in concentration  $c$  to  $c + \Delta c$  at time  $t = t_0$ . T-cells are activated with the activation flux in  $N(c, t_0)$ .

The rate of flow-in and flow-out of activated T-cells give us the flux of the activated T-cells as shown in Figure 3.4. The flow of activated T-cells can be followed on the solution curves that are discussed in the previous chapter. These solution curves satisfy the rate of change in the protein concentrations and that are considered as the reaction rates  $G(c, t)$  of the T-cells. Therefore, in accordance with the proteins behavior, we can write the above phenomena mathematically as,

$$\int_{\Omega} \frac{\partial n(c, t)}{\partial t} = \int_{\Omega} N(c, t) + G(a) \times n(a, t) - G(b) \times n(b, t), \quad \Omega \in [a, b] \quad (3.6)$$

or equivalently, by Newton-Leibniz axiom,

$$\int_{\Omega} \frac{\partial n(c, t)}{\partial t} dc = \int_{\Omega} N(c, t) dc - \int_{\Omega} \frac{\partial}{\partial c} (G(c) \times n(c, t)) dc. \quad (3.7)$$

where,  $N(c, t) = B(t) \delta(c - c_0)$ . Therefore, we can have the following partial differential equation:

## 3.2 Mathematical Modeling

---

$$\frac{\partial n(c,t)}{\partial t} + \frac{\partial}{\partial c}(G(c)n(c,t)) = B(t)\delta(c-c_0). \quad (3.8)$$

Since the population density outside the computational domain is considered zero, therefore, the above equation can be converted to homogeneous PDEs by considering the non-homogeneous part as the boundary condition. Hence the final model for the PBE with initial and boundary conditions can be written as,

$$\left. \begin{aligned} \frac{\partial n(c,t)}{\partial t} + \frac{\partial}{\partial c}(G(c)n(c,t)) &= 0 \\ n(c,0) &= 0 \\ n(c_0,t) &= \frac{B(t)}{|G(c_0)|} \\ \text{where } G(c) &= \frac{d}{dt}c(t,\tau) \\ \text{and } B(t) &= ae^{-bt}, a, b \in \mathbb{R} \end{aligned} \right\} \quad (3.9)$$

The parameters  $a$  and  $b = k^* N_{APC}$  are real positive numbers. It is important to mention here that  $G(c)$  is the implicit function of time  $t$  and activation time  $\tau$  while it is explicitly defined by the activation stage in terms of protein concentration as mentioned in the previous chapter for each case. Now we have used these reaction rates to find the population density functions of T-cells for the surface proteins (CD3, CD25 and CD25-IL2) in order to analyze the evolution in the activated T-cells.

### 3.2.2 Overview of Models

In this chapter, four cases are studied that deals with several models describing the population density functions of T-cells. These cases are constructed according to the cases defined in the Chapter 2. The population densities are found for the surface proteins representing their concentration. The models are defined according to their complexity levels as well as the dependency of proteins on each other. Each of the four cases follows the respective single T-cell dynamics that was studied in the previous chapter. The population density of T-cells is modeled for CD3, CD25 and CD25-IL2 proteins that are lying on the surface. The data is taken from the PhD thesis of El Hentati [4] and Bidot [8] with some adjustments for the sake of better results as

### 3.3 Solving Techniques

described in Chapter 2. The Table V reminds the prominent attributes of activated T-cells and gives a critical overview about the cases according to their limitation and advantages.

Cases – Proteins	Characteristics	Limitation	Advantages
1. CD3 protein	Surface protein. Decreases with the course of time	Do not increase. No analysis about other dynamical processes.	A leading process that trigger the activation process.
2(a). CD3, CD3i and CD3* proteins	Surface & internalized protein.	Not bounded. Follows the population density of CD3+CD3* protein.	Non-monotonic behavior. Discuss the reappearance of CD3.
2(b). CD3, CD3i and CD3* proteins	Surface & internalized protein.	Follows the density of CD3+CD3* protein. Only the CD3 protein.	Bounds CD3+CD3* by limited capacity and half-life phenomena.
3. CD3, CD3i, CD25, IL-2, CD25-IL2 and CD25-IL2i proteins	Surface, internalized & a fluid protein that is shared by all T-cells.	T-cells populations do not coincide. Exact solution not possible.	Follows the overall initial behavior ( 28 hrs approx.) of activated T-cells.
4. CD3, CD3i, CD25, IL-2, CD25-IL2 and CD25-IL2i proteins	Differs from case 3 by the values of the kinetic parameters.	No PBM. T-cells dynamics before proliferation.	More realistic behavior. T-cells are ready for proliferation

Table V: Prominent attributes of activated T-cells

### 3.3 Solving Techniques

In the previous chapter, Runge-Kutta Method of order four is used to find the solution (characteristic) curves. Here several methods are studied in order to validate the above described PBM. As we found the reaction rate for CD3 protein analytically, the Method of Characteristics (MOC) is applied to find the density functions. Also an innovative numerical approach (Transport Method – TM) is used to find the solution for the density functions by the mathematical analysis as described below. For more complex population balance models, when there is non-conservative term, it can be difficult to find the analytical solution and the solution

### 3.3 Solving Techniques

---

by Transport Method. Therefore, we need some efficient numerical methods that can approximate our model gently. A finite volume upwind scheme is used to find the numerical solution and a 2<sup>nd</sup> order Lax-Wendroff technique is used with a “minmod” flux limiter. An attempt has been made to give a general overview of these four solving methods.

#### 3.3.1 Method of Characteristics

The MOC is based on the characteristic curves that satisfy the required ODEs so that the given PDE reduces to the set of ODEs that can be solved analytically or by highly accurate approximate techniques under the given conditions [57], [58]. After manipulation the ODEs solution transform to the solution of PDE. This method deals with every type of hyperbolic (linear/nonlinear) PDEs [59]. In particular to our interest, the method exactly solves the one dimensional first order linear PDEs. Below is some motivation related to our model by describing a general overview of linear PDEs using the MOC. Consider the above system of eq. (3.9) and rewrite the PDE by assuming without any loss of generality that  $y(c_i, t) = G(c_i) \times \mathcal{M}(c_i, t)$ . Similarly, the initial and boundary conditions can be written in terms of  $y(c_i, t)$  in the following form,

$$\left. \begin{aligned} \frac{\partial y(c_i, t)}{\partial t} + G_i(c_1, c_2, \dots, c_m) \times \frac{\partial}{\partial c_i} (y(c_i, t)) &= 0 \\ y(c_{i_0}, t) &= B(t) \\ y(c, t_0) &= 0 \end{aligned} \right\} \quad (3.10)$$

In this study, the coefficient  $G_i$  is an explicit function of  $c = [c_1, c_2, \dots, c_m]$  while the MOC needs  $G_i$  as a function of  $c_i$  that can be found by solving the system. The modulus in the boundary condition shows that the population density is always positive. Now we parameterize the variables  $c_i$  and  $t$  as  $(c_1, c_2, \dots, c_m, t) = (c_1(s), c_2(s), \dots, c_m(s), t(s))$ , such that at  $s = s_0$ , we have  $t = t_0 = 0$  and  $c = c_0$ . Therefore the parameterized variables give the solution curves which satisfy the following ODEs,

$$\frac{dc_i}{ds} = G_i(c_1(s), c_2(s), \dots, c_m(s)), \quad \forall i = \overline{1, m}, \quad \text{where } c_i(0) = c_{i_0} \quad (3.11)$$

### 3.3 Solving Techniques

$$\frac{dt}{ds} = 1 \quad \text{with } t(0) = 0 \quad \text{and} \quad \frac{dy(s)}{ds} = \frac{dt}{ds} \frac{\partial y}{\partial s} + \frac{dc}{ds} \frac{\partial y}{\partial c} = 0 \quad (3.12)$$

The last ODE is followed by taking the total derivative of the above PDE. The ODEs given in the Eq. (3.12) can be solved easily by using their initial conditions while the Eq. (3.11) can be solved by using any higher order method depending upon the complexity. In this study, the Eq. (3.11) gives a system of equations that are depending on each other. Therefore, analytical solution is not possible for whole the system and the method of characteristics cannot be applied in a classical way. For the Eq. (3.10), the initial and boundary condition are used to find the solution of the PDE as shown in the Figure 3.5. The final result can be followed by transforming the problem into  $n(c_i, t)$  by using the above relation with  $y(c_i, t)$ .

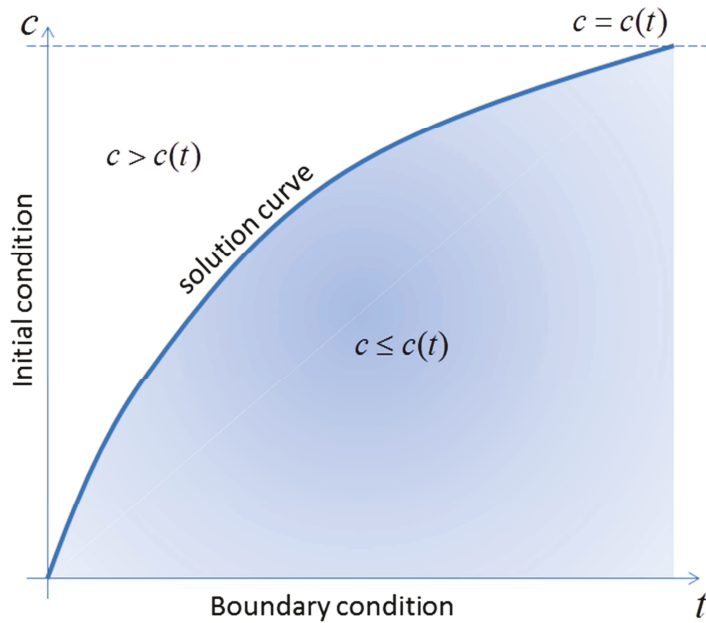


Figure 3.5: Solution followed by Method of Characteristics

A Maple procedure has been defined and implemented to find the analytical solution of the above problem by using Method of Characteristics. The method is not valid for most of our cases when the reaction rate  $G$  is dependent of several proteins. Due to this reason, another method, Transport Method, is developed that is based on the differential geometry. This method directly approaches the solution without using population balance equation as described below.

### 3.3 Solving Techniques

#### 3.3.2 Transport Method

The Transport method obeys the conservation laws and allows us to find the analytical solution by following the behavior on the characteristic curves. In order to explain the method briefly, a general behavior is studied for the characteristic curves increasing with time  $t$ . The method is independent of the complexity of the characteristic curves. It follows an initial population of the activated T-cells to generate the density at required time  $t$ . For any protein, we observe that the T-cells activate continuously during the viral infection as discussed in chapter 2.

Let us consider the T-cells activate during the time  $t \in [\tau_i, \tau_i + \Delta\tau]$  as demonstrated in the Figure 3.6. We have to find the solution for  $t > \tau_i$  by following the curves. The total number of T-cells start their process of activation at  $t \in [\tau_i, \tau_i + \Delta\tau]$  can be written as,

$$\int_{\tau_i}^{\tau_i + \Delta\tau} B(\tau) d\tau \approx B(\tau_{i+\frac{1}{2}}) \Delta\tau \quad \forall i=1,2,\dots \quad (1.13)$$

If we observe the flow of population on the concentration axis ( $c$ -axis), it seems like the population is increasing with the passage of time and the total population within the concentration  $[c_i, c_{i+1}]$  is given by,

$$\int_{c_i}^{c_i + \Delta c} n(c, t_j) dc \approx n(c_i, t_j) \Delta c_i \quad \forall i=1,2,\dots \quad (1.14)$$

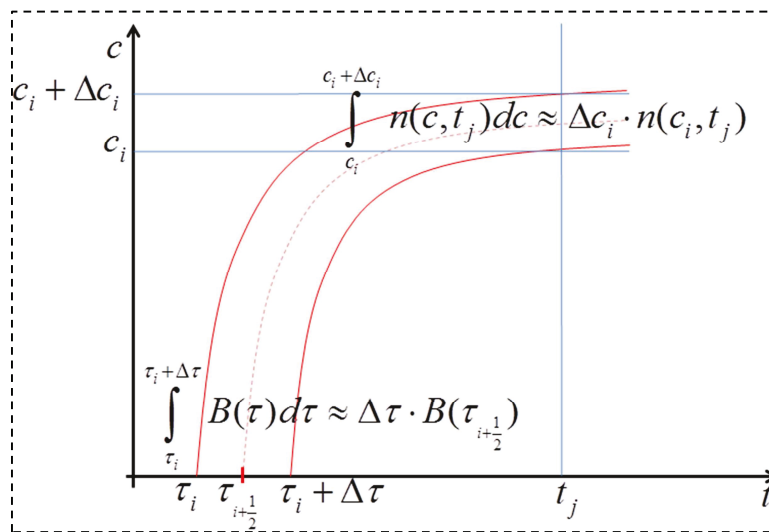


Figure 3.6: Flux of the protein and the density of T-cells

### 3.3 Solving Techniques

---

By conservation laws, the rate of change of the total population of the activated T-cells at any time  $t$  is equal to the flux of that population of activated T-cells for the given number of activated cells at the boundary. Therefore, in simple, the total population of T-cells activated between time  $\tau_i$  to  $\tau_i + \Delta\tau$  is equal to the population density of the activated T-cells at any time  $t$  within the concentration  $c_i$  to  $c_i + \Delta c_i$ , that is,

$$n(c_i, t_j) \times \Delta c_i = B(\tau_{i+\frac{1}{2}}) \times \Delta \tau \quad \forall i = 1, 2, \dots \quad (3.15)$$

The Transport Method is highly efficient and gives a solution overlapping the exact one. In order to validate the method for those cases when exact solution is not possible, we must study the numerical solution of population balance equation that is based upon reaction rate and activation rate as shown in Eq. (3.9). For this, we chose upwind finite volume method and second order Lax-Wendroff method to approximate the population density functions with respect to the surface protein concentrations. The upwind FVM is frequently used in the literature [47], [55]. A brief description is given below about the Lax-Wendroff Finite difference Method that is applied to solve the problems by using Flux limiters.

#### 3.3.3 Lax-Wendroff Finite difference Scheme

Let us consider the linear hyperbolic first order PDE,

$$\frac{\partial n(c, t)}{\partial t} + \frac{\partial F(c, t, n)}{\partial c} = 0 \quad (3.16)$$

where  $F(c, t, n) = G(c)n(c, t)$ . The initial and boundary conditions are defined below,

$$n(c_{10}, t) = \frac{B(t)}{|G(c)|}, \quad n(c, 0) = 0, \quad \text{where } G(c) \neq 0$$

The modulus of  $G(c)$  is used to ignore the negative sign in the reaction rate (decrease in the concentration). Differentiate the above equation with respect to  $t$ , by solving, we get:

$$\begin{aligned} \frac{\partial^2 n(c, t)}{\partial t^2} &= -\frac{\partial^2 F(c, t, n)}{\partial t \partial c} \\ &= -\frac{\partial}{\partial c} \left( \frac{\partial F(c, t, n)}{\partial t} \right) \\ &= \frac{\partial}{\partial c} \left( \frac{\partial F(c, t, n)}{\partial c} \frac{\partial c}{\partial t} \right) \end{aligned} \quad (3.17)$$

### 3.3 Solving Techniques

---

where  $G(c) = \frac{\partial c}{\partial t}$ , the rate of change of concentration. Using Taylor's series for time  $t$ , we can

find the following equation,

$$\begin{aligned} n(c, t + \Delta t) &= n(c, t) + \Delta t \frac{\partial n(c, t)}{\partial t} + \frac{\Delta t^2}{2} \frac{\partial^2 n(c, t)}{\partial t^2} \\ &= n(c, t) - \Delta t \frac{\partial F(c, t, n)}{\partial c} + \frac{\Delta t^2}{2} \frac{\partial}{\partial c} \left( \tilde{G}(c) \frac{\partial F(c, t, n)}{\partial c} \right). \end{aligned} \quad (3.18)$$

We define the discretization for  $c$  as  $c_i$  and for  $t$  as  $t^j$ . In order to approximate the above equation, in terms of  $c$ , we define,

$$F_i^j = G_i n_i^j, \quad \tilde{G}(c_i) = (G(c_{i+1}) + G(c_i)) / 2. \quad (3.19)$$

Writing the Lax-Wendroff scheme in the form of scalar conservation law, we get the final form:

$$n_i^{j+1} = n_i^j - \frac{\Delta t}{2\Delta c} (F_{i+1}^j - F_{i-1}^j) + \frac{\Delta t^2}{2\Delta c^2} (\tilde{G}_i (F_{i+1}^j - F_i^j) - \tilde{G}_{i-1} (F_i^j - F_{i-1}^j)). \quad (3.20)$$

The solution at end points,  $i = 1$  and  $i = N_{\max}$ , are found by using first order upwind scheme. The time step is chosen according to Courant – Friedrichs – Lewy (CFL) condition that is necessary (but not sufficient) for the convergence of this scheme. CFL condition is given by:

$$\max_{1 \leq i \leq N} |G_i| \frac{\Delta t}{\Delta c} \leq \frac{1}{2} \Rightarrow \Delta t \leq \frac{\Delta c}{2 \max_{1 \leq i \leq N} |G_i|}$$

#### Flux Limiter

Flux limiters are used to diminish the spurious oscillations that are observed in high resolution schemes. There is several flux limiters studied in the literature where each one work at some specific solution behaviors. The Lax-Wendroff finite difference scheme (LWF) has second order approximation but it is highly oscillatory in nature at the discontinuities and at the portion where solution is changing drastically. It gives better approximation by using the appropriate flux limiter to make the solution total variation diminishing [50] as shown in Figure 3.7. Rearrange the Eq. (3.20) in order to apply the flux limiter,

$$n_i^{j+1} = n_i^j - \frac{\Delta t}{\Delta c} F_i^j - \frac{\Delta t}{2\Delta c} \left( 1 - \frac{\Delta t}{\Delta c} \tilde{G}_i \right) (F_{i+1}^j - F_i^j) + \frac{\Delta t}{\Delta c} F_{i-1}^j + \frac{\Delta t}{2\Delta c} \left( 1 - \frac{\Delta t}{\Delta c} \tilde{G}_{i-1} \right) (F_i^j - F_{i-1}^j) \quad (3.21)$$

By considering  $F_L(c_i) = F_i^j$ ,  $F_H(c_i) = \frac{1}{2} \left( 1 - \frac{\Delta t}{\Delta c} \tilde{G}_i \right) (F_{i+1}^j - F_i^j)$ , we can write the method as,

### 3.3 Solving Techniques

$$n_i^{j+1} = n_i^j - \frac{\Delta t}{\Delta c} (f(c_i, t_j) - f(c_{i-1}, t_j)), \quad (3.22)$$

where  $f(c_i, t_j) = F_L(c_i) + F_H(c_i)\Phi(r_i)$ . The function  $F_L(c_i)$  is the low resolution flux and  $F_H(c_i)$  is the high resolution flux that makes the solution oscillatory. In this study,  $\Phi(r_i)$  is considered as minmod flux limiter function that remains in the interval  $[0,1]$  and chooses the smaller value between the two slopes by using the following function,

$$\Phi(r_i) = \text{minmod}(1, r_i) = \max(0, \min(1, r_i)),$$

where  $r_i$  is the ratio between the slopes of two functions and it is defined as,

$$r_i = \frac{(n_{k+1} - n_k)}{n_{i+1} - n_i}, k = i - \text{signum}(\tilde{G}(c_i)).$$

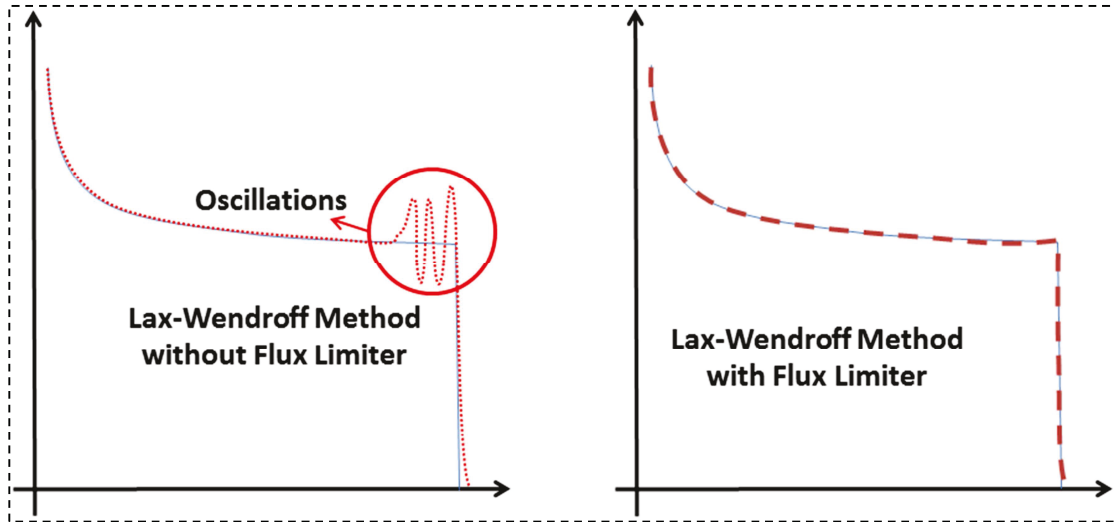


Figure 3.7: The effect of flux limiter on 2nd order Lax-Wendroff Method

#### 3.3.4 Finite Volume Method

Finite Volume Schemes (FVS) divide the entire domain into finite number of subdomains (control volumes). Each control volume is denoted by a grid point which represents the integral of the subdomain. Several finite volume schemes exist in the literature depending upon the location of the grid point [50]. In this study, we used Finite Volume Upwind scheme that uses the center of the control volume as a grid point as shown in the Figure 3.8. Let us consider the

### 3.3 Solving Techniques

concentration variable  $c = \left\{ c_{i+\frac{1}{2}} \right\}_{i=0}^n$  such that  $\Omega_i$  is the control volume over the interval

$\left[ c_{i-\frac{1}{2}}, c_{i+\frac{1}{2}} \right]$  and it is defined as,

$$c_{1/2} = c_N; c_i = \frac{c_{i-\frac{1}{2}} + c_{i+\frac{1}{2}}}{2}; c_{N+1/2} = c_N; i = 1, 2, \dots, N \quad (3.23)$$

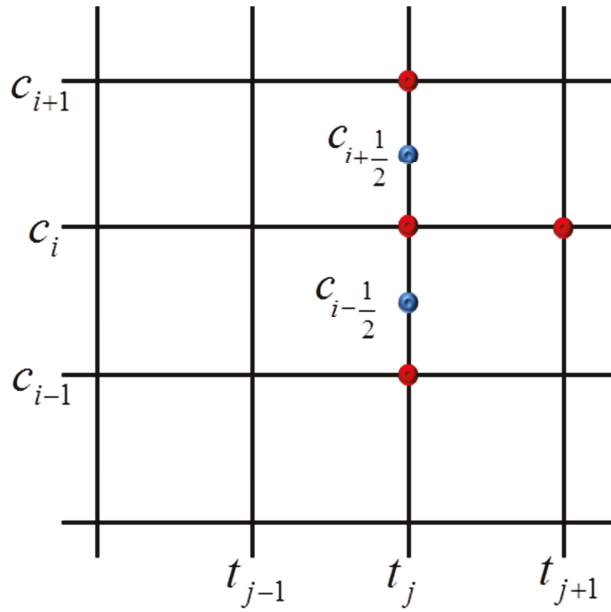


Figure 3.8: Finite volume upwind scheme on cartesian mesh.

with  $\Delta c = c_{i+\frac{1}{2}} - c_{i-\frac{1}{2}}$ . Integrating Eq. (3.16) over the control volume  $\Omega_i = \left[ c_{i-\frac{1}{2}}, c_{i+\frac{1}{2}} \right]$ :

$$\int_{c_{i-\frac{1}{2}}}^{c_{i+\frac{1}{2}}} \frac{\partial n(c,t)}{\partial t} dc + \int_{c_{i-\frac{1}{2}}}^{c_{i+\frac{1}{2}}} \frac{\partial F(c,t,n)}{\partial c} dc = 0 \quad (3.24)$$

where  $F(c,t,n)$  is defined with Eq. (3.16). Suppose that the average population density function for each cell  $\Omega_i$  is  $n_i(t)$  then one can write the integral form of  $n_i(t)$  as,

$$n_i(t) = \frac{1}{\Delta c} \int_{c_{i-\frac{1}{2}}}^{c_{i+\frac{1}{2}}} n(c,t) dc \quad (3.25)$$

### 3.4 Case 1

---

Therefore,

$$\frac{d}{dt} \int_{c_{i-\frac{1}{2}}}^{c_{i+\frac{1}{2}}} n(c,t) dc = \Delta c \frac{d}{dt} n_i(t) \quad (3.26)$$

The second term in Eq. (3.24) can be written as

$$\int_{c_{i-\frac{1}{2}}}^{c_{i+\frac{1}{2}}} \frac{\partial F(c,t,n)}{\partial c} dc \approx F_{i+\frac{1}{2}} - F_{i-\frac{1}{2}} \quad (3.27)$$

By comparing the Eqs. (3.26) and (3.27), we get,

$$\frac{d}{dt} n_i(t) = -\frac{1}{\Delta c} \left( F_{i+\frac{1}{2}} - F_{i-\frac{1}{2}} \right) \quad (3.28)$$

The equation needs some approximation depending upon the direction of the fluxes  $F_{i-\frac{1}{2}}$  and  $F_{i+\frac{1}{2}}$ . When the concentration is increasing, we apply backward difference scheme while for the decreasing phenomenon, we apply the forward difference scheme. Also we can use some other high resolution scheme to find the flux of the Eq. (3.28) [47]. In this study, the flux is defined according to first order upwind scheme as,

$$F_{i-\frac{1}{2}} = G_{i-\frac{1}{2}} n_i^j, \quad F_{i+\frac{1}{2}} = G_{i-\frac{1}{2}} n_{i+1}^j$$

The results obtained from the proposed methods are analyzed by their comparison and their graphical behaviors below. We divide our work again into four cases where each case followed by the one mentioned in the Chapter 2.

### 3.4 Case 1

In this problem we deal with CD3 T-cells activation with a given initial protein concentration that is observed just before their activation. The concentration of CD3 protein is the one present on the surface of T-cells at the time of recognition of the viral infection. After recognition, the concentration decreases exponentially to signal the cytoplasm of T-cell to start the process of activation. The major component involved in this process is the highly variable affinity of the T-cell receptor for the peptide. Also the speed and level of proteins up-regulated is proportional to

### 3.4 Case 1

---

the strength of the binding and the final effect on the T-cells. The rate of internalization (reaction rate) of CD3 protein is followed from Eq. (2.1) while the rate of activation can be found by solving Eq. (3.1) with initial condition:  $N_{NAC}(0) = 1$ . Thus,

$$B(\tau) = a \times e^{-b\tau} \quad (3.29)$$

In this case, the characteristic curves  $c_\tau(t)$  found by solving Eq. (2.1) are monotonic as shown in Figure 2.3. For a given couple  $(c, t)$  with  $c > c_{\min}$ , there is only one curve  $c_\tau(t)$  passing through this point. Thus there is one corresponding  $\tau(c, t)$  and one derivative  $\frac{dc_\tau}{dt}(t) = \frac{dc}{dt}(t - \tau)$ . Note that, the case where the curves are deduced by translation,  $\frac{dc_\tau}{dt}$  can also be considered as a function of  $c$  as  $\frac{dc_\tau}{dt}(c) = \frac{dc}{dt}(c)$ . During a time step  $dt$ , the number of cells activated between  $\tau$  and  $\tau + d\tau$  is travelling along the characteristic curve  $c(t, \tau)$ , and the conservation of cells gives:  $n(c, t)dc = B(\tau(c, t))dt$ . The population density  $n(c, t)$ , is thus simply linked to the slope of this curve and to the activation rate  $B(\tau)$ :

$$n(c, t) = \frac{B(\tau(c, t))}{\left| \frac{dc}{dt}(t - \tau(c, t)) \right|} \quad (3.30)$$

This is almost analytical way to derive  $n$  from  $B$  and the slopes  $\frac{dc}{dt}$ . This concept is described above in detail in the section 3.3.2. The derivation of PBE for such case can be easily derived from the general idea for the derivation of PBE described above in the Mathematical Modeling section 3.2. Therefore, in this case, the hyperbolic conservation law can be written in terms of PBE as defined in Eq. (3.9) with,

$$G(c) = -k c(t, \tau) \quad (3.31)$$

The parameters for the activation rate defined in Eq. (3.29) are chosen as  $b = 1/7200 \text{ s}^{-1}$  and  $a = 3 \times 10^8 \text{ s}^{-1} (\text{mole} \times \text{m}^{-2})^{-1}$ . The method of characteristics is used to find the analytical solution while a frequently used numerical scheme, finite volume scheme for solving homogeneous hyperbolic PDEs, is applied to solve the PBE. The numerical scheme is validated against the analytical solution and the solution found by TM.

### 3.5 Case 2a

In this case, the model is considered as the simplest way to describe the activation process of T-cells. The solution of the above defined problem is sketched in the Figure 3.9 at four different times  $t = 20000s$ ,  $50000s$ ,  $80000s$ ,  $100000s$ . The figure is a log-log plot because the values are at extreme ends. One can observe the validation of both approximate methods that are overlapping the exact solution. This validation will be helpful in dealing with other cases where the exact solution is not possible.

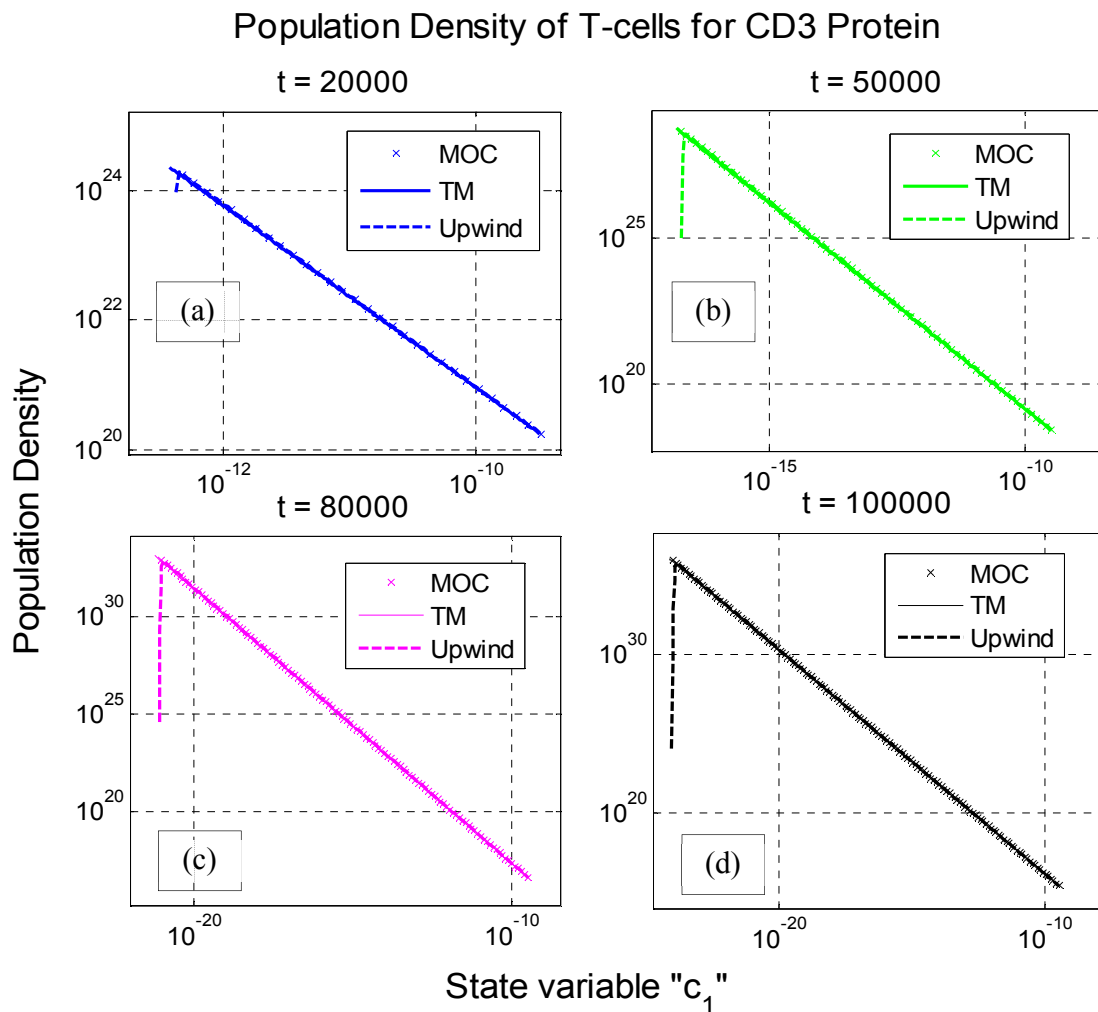


Figure 3.9: Population density of T-cells according to their protein levels at different time  $t$

### 3.5 Case 2a

In case 2a, T-cell activation is studied with respect to their surface protein (CD3) concentration that internalizes and reappear on the surface of T-cell outside of the synapse. The activation is

### 3.5 Case 2a

---

again described by an activation rate function  $B(\tau)$ , number of cells activated per unit of time at activation time  $\tau$ . Classically, the rate of variation of the number of non-activated cells  $N_{NAC}$  is taken proportional to this population:  $\frac{dN_{NAC}}{dt} = -bN_{NAC}$ , where  $N_{NAC} = a \exp(-bt)$  with  $b = k^* N_{APC}$ . Thus usually  $B(\tau)$  is a decreasing exponential function. Here we consider as,

$$B(\tau) = a e^{-bt}. \quad (3.32)$$

In the Case 2a, the curves have shown the decrease as well as increase in the concentration. The instance where  $t < t^*$ , the behavior is very similar to the 1<sup>st</sup> case. For  $t > t^*$ , given couple  $(c, t)$  with  $c > c_{\min}$ , there are two curves passing through the point, i.e.  $\tau_1 < \tau_2$ , with their corresponding derivatives as shown in Figure 3.10. The value of  $\tau$  has been obtained either numerically, with a Newton-Raphson method, or by approximation of  $c(t)$  by a polynomial and then the determination of the roots of this polynomial.  $t_1(c) < t_2(c)$  are obtained from the curve  $c(t)$ , then the  $\tau_i$  values are deduced:  $\tau_i(c, t) = t - t_i(c)$ . The derivatives are computed from the expression of  $c$  versus  $t$ .

The population density is the sum of two terms  $n_1$  and  $n_2$ . The  $n_1$  and  $n_2$  correspond to the two populations activated at  $\tau_1$  and  $\tau_2$ , having a protein concentration  $c$  at time  $t$ . For the first population, the concentration is increasing, while for the second, it is decreasing. The accumulated population density can be given by the following equation:

$$n(c, t) = n_1(c, t) + n_2(c, t) = \frac{B(\tau_1(c, t))}{\left| \frac{dc}{dt}(t - \tau_1(c, t)) \right|} + \frac{B(\tau_2(c, t))}{\left| \frac{dc}{dt}(t - \tau_2(c, t)) \right|}. \quad (3.33)$$

Recall the Case 2a in Chapter 2 where we have described the characteristic curves (solution curves) on which the solution for the density of T-cells is travelling. Each curve took the minimum value where the speed (variation in the concentration) became equal to 0. One can observe that the population density of T-cells  $n(c, t)$  tends to infinity when the concentration approaches its minimum level (i.e.  $n(c, t) \rightarrow \infty$  when  $c \rightarrow c_{\min}$ ), since the derivative

### 3.5 Case 2a

$\frac{dc}{dt}(c = c_{\min}) = 0$ . But the integral of the function  $n(c, t)$  remains finite (by quadrature rules), and

thus the number of cells in any interval  $[c_{\min}, c]$  can be computed. Moreover,

$$\int_{c_{\min}}^c n(c, t) dc < \infty \text{ when } c \rightarrow c_{\min}.$$

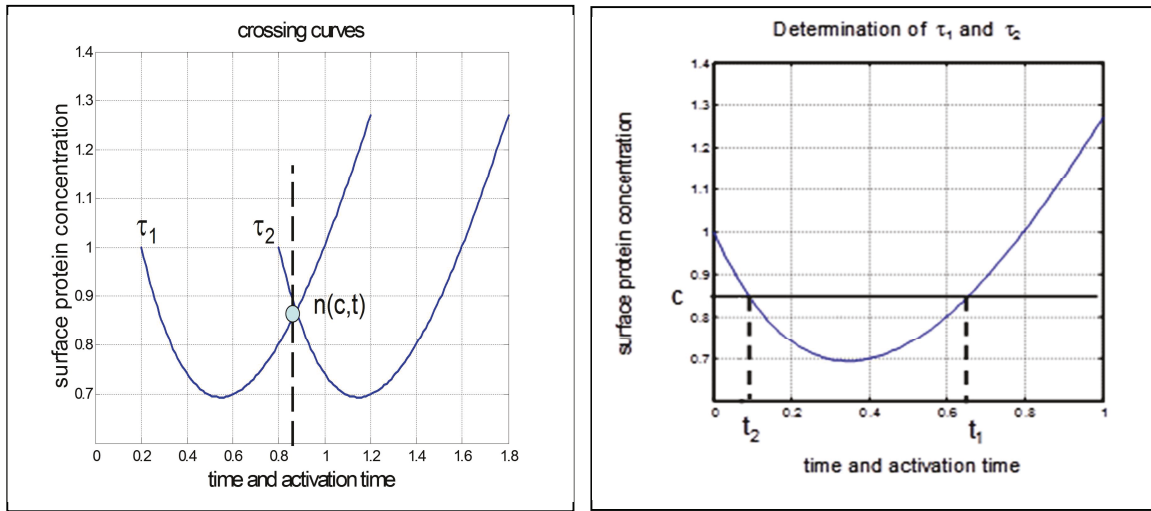


Figure 3.10: Numerical computation of  $\tau_1$  and  $\tau_2$

Numerically, in case of finite volume method, the value of  $n(c, t)$  at a node is the mean value that represents its integral on a cell divided by the size of the cell. Thus the numerical values of  $n(c, t)$  at  $c = c_{\min}$  for a given mesh will be finite. Nevertheless this behavior may affect the numerical accuracy.

#### 3.5.1 Model Derivation by using conservation laws

The validation of the Transport Method presented in the section 3.3.2 is questionable in more complex cases because it directly approaches the solution by geometrical analysis. The geometrical interpretation is quite difficult especially in multi-dynamical systems. Therefore, it is more convenient to adapt the classical conservation law approach (hyperbolic equation) for the non-monotonic variation in  $c(t)$  curve.

### 3.5 Case 2a

---

Let us recall that, in case of monotonic function  $c = c(t)$ , with no crossing, the conservation equation can be written as a scalar transport equation, with the concentration  $c$  as an inner variable (space variable in classical advection equation). For example, in our case, at a time  $t < t^*$ , the population flux at concentration  $c$  is:  $Q = \frac{dc_{\tau(c,t)}}{dt}(c) \times n(c,t)$ . The populations are travelling downward on the  $c$ -axis. Since the curves are deduced by translation in time, the derivative only depends on  $c$ . This derivative, classically called as the growth rate, is noted  $G(c) = \frac{dc}{dt}(c)$ . Thus the conservation equation and the initial and boundary conditions can be written as,

$$\left. \begin{aligned} \frac{\partial n(c,t)}{\partial t} + \frac{\partial}{\partial c}(G(c).n(c,t)) &= 0, \\ n(c,0) &= 0, \\ n(c_{10},t) &= \frac{B(t)}{G(c_{10})}. \end{aligned} \right\} \quad (3.34)$$

where  $c_{10}$  is the initial concentration. We can also write the conservation equation on a non-conservative way:

$$\frac{\partial n(c,t)}{\partial t} + G(c) \frac{\partial n(c,t)}{\partial c} = -G'(c)n(c,t) \quad (3.35)$$

Along a characteristic curve beginning at  $\tau$ , like the equation:  $\begin{cases} \frac{dc_{\tau}}{dt} = G(c) \\ c_{\tau}(0) = c_{10} \end{cases}$ , the variation of

$n(c(t),t)$  is  $\frac{dn(t)}{dt} = -n(t)G'(c)$ , and

$$n(t) = n_0 \exp\left(-\int_0^t \left(\frac{dG(c)}{dc}\right) dt\right) \quad (3.36).$$

But in our case, for  $t > t^*$ , characteristics are crossing each other. At each point  $(c,t)$ , for  $c > c_{\min}$ , two opposite fluxes are present:

### 3.5 Case 2a

---

1. Flux of the cells activated at time  $\tau_1$  whose concentration is increasing, and thus who travel upward on the  $c$  - axis. If the density of population of these cells is noted  $n_1$ , their flux is equal to  $G_1(c).n_1(c,t)$  with  $G_1(c) = \frac{dc_{\tau_1(c,t)}}{dt}(c)$ .
2. Flux of the cells activated at time  $\tau_2 > \tau_1$ , whose concentration is decreasing and travel downward on the  $c$  - axis with a flux  $G_2(c).n_2(c,t)$ ,  $G_2(c) = \frac{dc_{\tau_2(c,t)}}{dt}(c)$ , where  $n_2$  is the population density of these cells.

The resulting total flux can be computed from the equation:  $F_T = \frac{n_1 G_1(c) + n_2 G_2(c)}{n_1 + n_2}$ , with  $G_2 < 0$ .

But it is not possible to compute equivalent reaction rate  $F_T$  as a function of  $c$  only since  $n_1$  and  $n_2$  need to be known. A way of solving this problem is to write one conservation equation for each population, and then to compute the total density  $n(c,t)$  as,  $n = n_1 + n_2$

$$\frac{\partial n_i(c,t)}{\partial t} + \frac{\partial}{\partial c}(G_i(c).n_i(c,t)) = 0, \quad i=1,2 \quad (3.37)$$

The initial and boundary conditions for the first equation ( $i=1$ ) are:  $\begin{cases} n_1(c,0) = 0 \\ n_1(c_{10},t) = n_0 \end{cases}$ . While for the

second equation, the value of  $n$  at  $c = c_{\min}$  (minimum value of  $c$ ) is not finite. A way to overpass this problem is to consider a little fixed interval  $[c_{\min}, c_{\min} + \Delta c]$  on which  $n(c,t)$  is replaced by its mean value. This is naturally the case in the numerical solving, using a finite volume method. On each cell, the unknown will be the mean value of  $n(c,t)$  on the cell.

We use here a simple one order upwind explicit finite volume scheme.  $n_i^k \approx n(c_i, t^k)$  is the approximate average value of  $n(c,t)$  at time  $t^k$  on a block centered on  $c_i$ .  $F_{i-1/2}^k$  and  $F_{i+1/2}^k$  are the fluxes respectively upwind and downwind at the boundary of this block. The scheme is of the following form:

### 3.5 Case 2a

$$(n_i^{k+1} - n_i^k) \Delta c + (F_{i+1/2}^k - F_{i-1/2}^k) \Delta t = 0 \quad (3.38)$$

The fluxes are computed upwind on the following

$$\text{way: } \begin{cases} F_{i-1/2}^k = G(c_{i-1/2}) n_{i-1} \\ F_{i+1/2}^k = G(c_{i+1/2}) n_i \end{cases}$$

The two fluxes are treated in the continuity on one to the other, the first block on the  $c$ -axis ( $c = c_{\min}$ ) making the connection. But each equation is solved on a separate grid, since one have to distinguish  $n_1$  and  $n_2$ . Then, between  $c_{\min}$  and  $c_0$ ,  $n_1$  and  $n_2$  are added to obtain the density  $n(c, t)$ . The principle of the scheme is exposed in Figure 3.11.

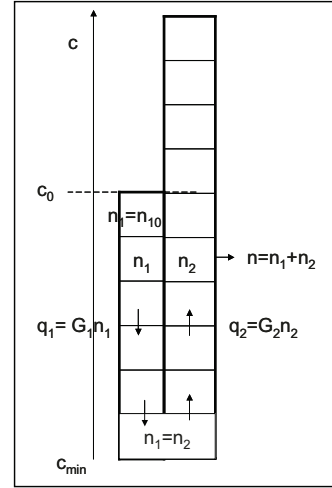


Figure 3.11: Principle of the numerical scheme

This scheme, known to be stable provided that the classical CFL condition is satisfied on the time step, presents the drawback of developing a high numerical diffusion. In order to decrease the numerical diffusion around the discontinuity front, we can use the following idea:

The flux at the discontinuity on the  $c$  - axis can be numerically derived from the computation of the reaction rates  $G(c)$ . The reaction rates are computed at each boundary between blocks in the finite volume scheme. Thus, the time at which the propagating discontinuity reaches a given block can be numerically approximated. In order to avoid numerical diffusion around the propagating discontinuity, the flux on the boundary between two grid blocks can be set to 0 until this boundary is reached by the front computed from  $G(c)$  (diffusion limitation scheme). But this method does not prevent diffusion behind the front. The result derived is then very close to the solution found by Eq. (3.33).

## 3.5 Case 2a

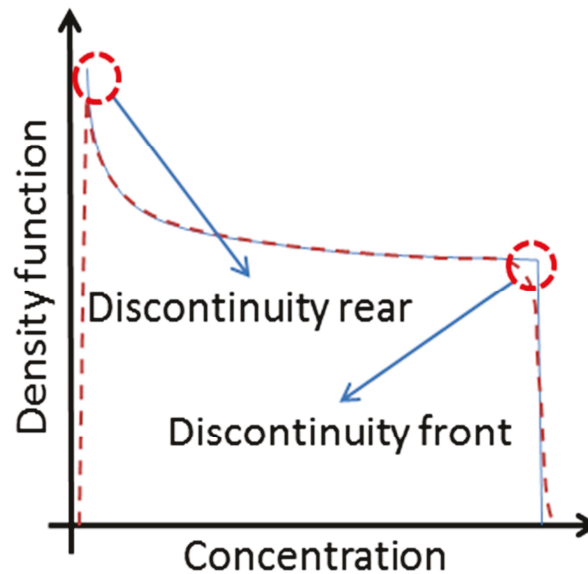


Figure 3.12: Diffusion in the numerical scheme at the rear and the front side

### Comments

The results for density function obtained by TM and Upwind method are displayed in Figure 3.13. For this example, the parameters chosen are  $k_1 = 1/3000s^{-1}$ ,  $k_2 = 1/30000s^{-1}$ ,  $c_{10} = 3.24 \times 10^{-10} \text{ mole} \times \text{m}^{-2}$  and  $B(\tau) = a \exp(-b\tau)$  at four different times (in seconds) are  $t = 10000s$ ,  $20000s$ ,  $50000s$  and  $100000s$ . The solutions found by the methods are very close to each other. The Upwind method shows diffusion in the Figure 3.13(c) because of the interpolation of reaction rate function  $G(c)$ .

There are three discontinuities coming; one discontinuity is at the rear side while the other is in the middle and moving from the middle of the curve to the front to meet the third discontinuity. The rear side discontinuity shows that there is no activated T-cell with the concentration before discontinuous point. The second discontinuity initially lies at the middle of the curve, Figure 3.13(a) and (b). This discontinuity occurs due to the intersection of the concentration curves as shown in Figure 2.5. The discontinuity moves forward and meets the discontinuity at the front as shown in the Figure 3.13(c) and (d). The front discontinuity is actually the maximum concentration of CD3+CD3\* protein present on the surface of T-cell.

### 3.6 Case 2b

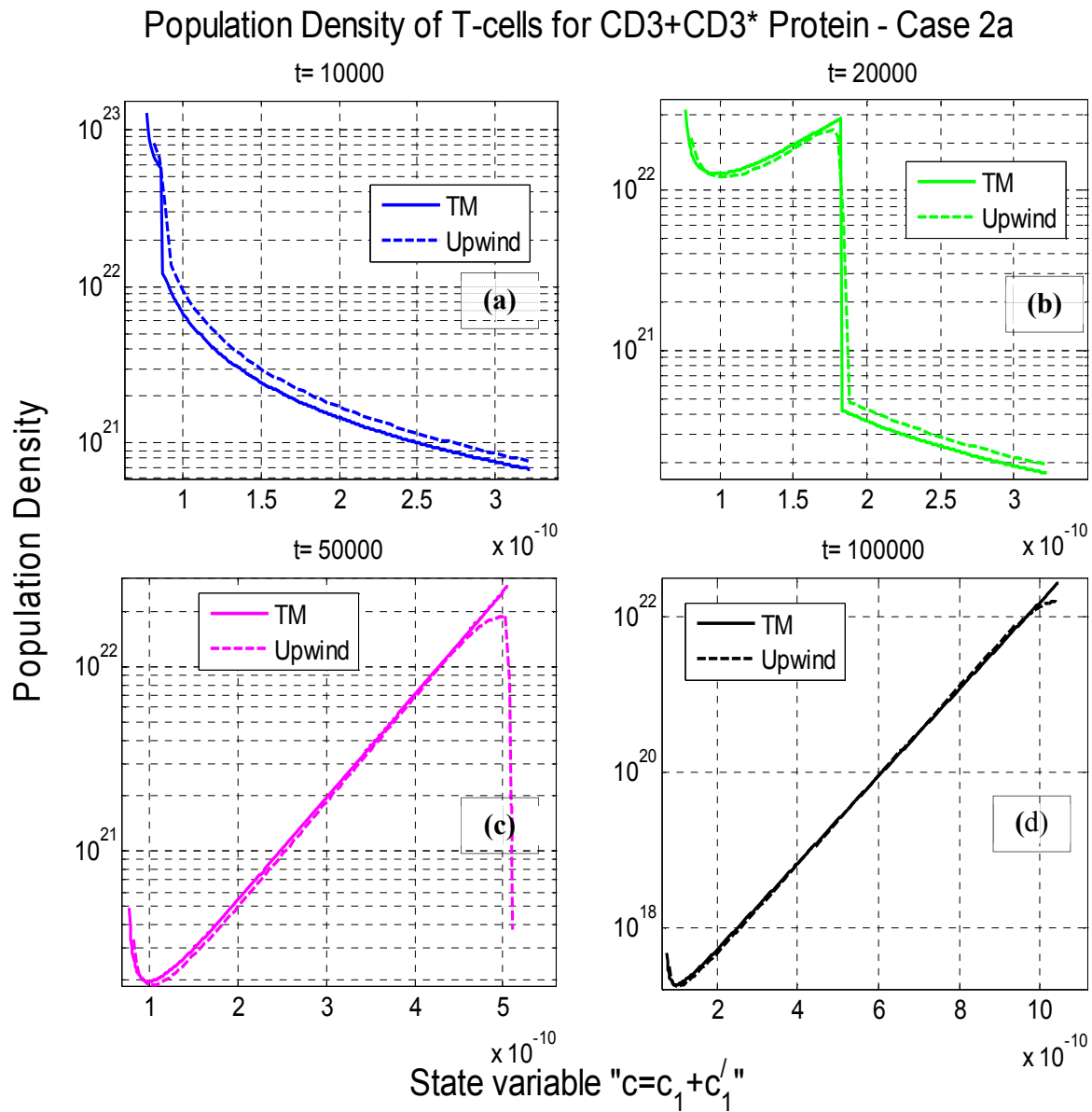


Figure 3.13: Results with finite volume scheme (Upwind as dashed line) and Transport Method (TM as line)

### 3.6 Case 2b

In the first model, the increase in the CD3 reappearance on the surface is realized without any limitation. Therefore the limited capacity of T-cell makes a contradiction and clearly shows the deficiency of that model. However, mathematically, it has shown an adequate analysis about the crossing of two curves in the linear hyperbolic PDEs. The deficiency of that model is removed, as discussed in the section 2.4.2 of Chapter 2, by introducing the half-life of internalized protein in

### 3.6 Case 2b

the Eq. 2.3a. Due to this reason, the reappearance of CD3\* on the surface of T-cell affects the population density. However, in this case, the procedure to derive the population balance equation is similar to the previous model and the solution is found for the combined surface protein of CD3 and CD3\*.

$$\left. \begin{aligned}
 \frac{\partial n(c,t)}{\partial t} + \frac{\partial}{\partial c}(G(c)n(c,t)) &= 0 \\
 n(c,0) &= 0, \\
 n(c_0,t) &= \frac{B(t)}{|G(c_0)|} \\
 \text{where } B(t) &= ae^{-bt}, \\
 \text{and } G(c(c_1,c'_1)) &= \frac{d}{dt}c(t,\tau) \\
 &= \frac{dc_1}{dt} + \frac{dc'_1}{dt} \\
 &= -k_1c_1 + k_2 \frac{V_c}{S_c} c_i(1-c'_1)
 \end{aligned} \right\} \quad (3.39)$$

The kinetic parameters ( $k_1$  and  $k_2$ ) and the parameters for total initial population  $B(t)$  defined for this case are same as in the Case 2a while the reaction rate  $G(c)$  is defined in the Subsection Second Model of the Section Case 2 in the previous chapter. The approximate methods, TM and FVS, show a nice commitment with each other as shown in Figure 3.14.

The error observed in the graph is due to the interpolation of the solutions of reaction rates, defined in Eq. (2.8). The crossing in the curves, as shown in Figure 2.6, needs a fixed grid for c-axis in order to study the density of T-cells at the crossing points. The time step for numerical methods is chosen constant in order to satisfy the CFL condition. However, the error is reduced by applying the limitation at the end of each boundary. In contrast to the numerical schemes, TM doesn't need any interpolation before finding the population density function. Therefore, TM has better representation of the solution.

In the Figure 3.14, the discontinuity is moving towards the right with the passage of time. The discontinuity shows that the population density of the T-cells with decreasing CD3+CD3\* protein

### 3.6 Case 2b

concentration on the surface matches to the population density of T-cells with increasing the concentration of the same protein. The steep descend in the solution due to discontinuity indicates that the T-cells are no more crossing each other with respect to their protein concentration. The discontinuity moves further towards right as we can observe in Figure 3.14(b) and gets vanished in the next figures. It can also be observed that the population density is increasing more rapidly at the right with the passage of time.

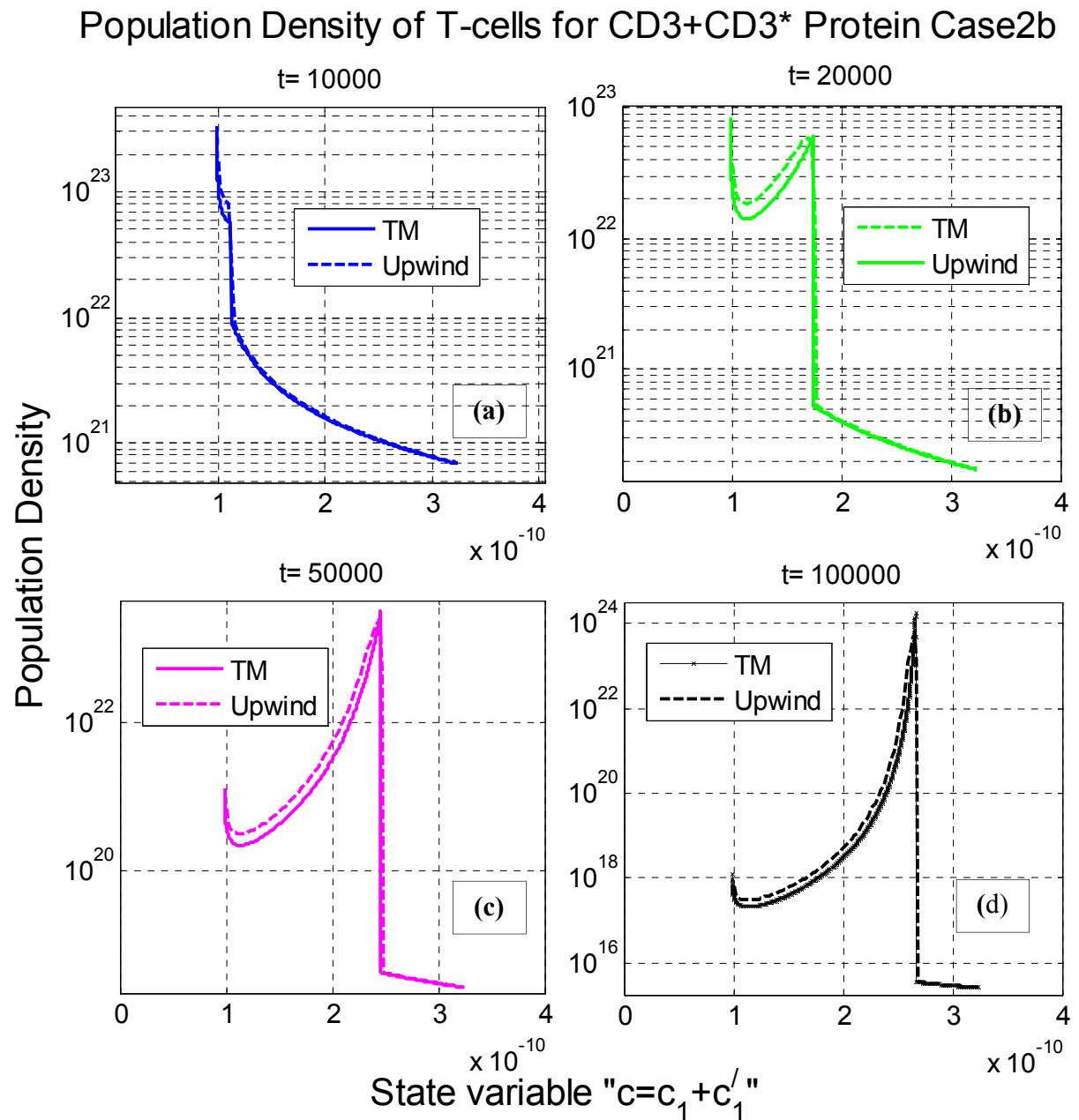


Figure 3.14: Results with finite volume scheme (Upwind – dashed line) and Transport Method (CM - line)

### 3.7 Case 3

The possible reason for the above two arguments is that the activation rate  $B(t)$  is a decreasing function of time. In contrary to the previous case, the increase in the concentration of protein does not exceed from the initial level, Figure 2.6. Therefore, the population density at the initial concentration  $c_0$  shows no discontinuity at any time  $t$  as shown in Figure 3.14.

### 3.7 Case 3

The case 3 is established in order to study the evolutionary process of population densities of T-cells based on six proteins which are remarkably changing during the activation process. The process starts from the CD3 protein internalization that results as CD3i protein. Due to its internalization, many proteins produce and come on the surface of T-cell.

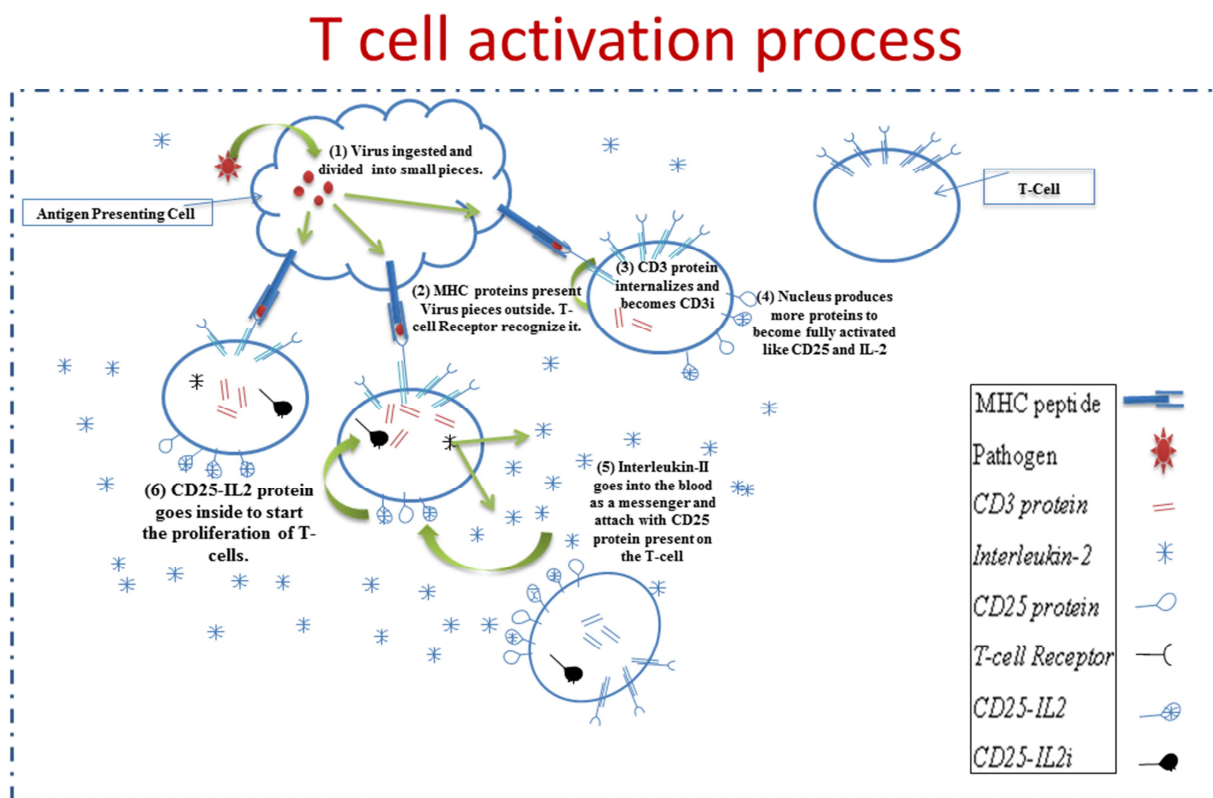


Figure 3.15: Dynamical changes in T-cells with respect to proteins and the population dynamics of the activation T-cells

In this case, we are not going to deal with CD3 reappearance. The surface proteins are CD3, CD25 and CD25-IL2 proteins. The CD25-IL2 is a binding of CD25 and IL2 proteins whereas IL2 protein is shared by the other T-cells. It goes into the blood and bind to the CD25 protein that lies

### 3.7 Case 3

---

on the surface of any activated T-cell. The internalization of this binding is considered as the sixth protein, denoted by CD25-IL2i. It has a vital role in the proliferation of T-cell as it is considered as the last signal in the cytoplasm of T-cell before the division process starts. The concept of protein dynamics is well described in chapter 2, Case 3 while the population dynamics can be observed from the Figure 3.15.

Notwithstanding the proteins are depending on each other, we only discuss here the population density of the surface proteins. Let us recall the PBE so that we can define it for the other surface proteins like CD25 and CD25-IL2. We considered the population balance modeling concept where each T-cell is considered individually as part of the population diversity [27] according to its concentration of protein, e.g. CD3 ( $c_1$ ). Therefore, the cell number (per volume unit)  $dN_1$  in each interval of CD3 concentration  $[c_1, c_1 + dc_1]$  is defined as,

$$dN_1 = n_1(t, c_1) dc_1 \quad (3.40)$$

where  $c_1$  is the abbreviation of the membrane CD3 concentration and  $n_1(c_1, t)$  is the population density for the activated T-cells with respect to the variable  $c_1$ . Population densities for CD25 and CD25-IL2 can also be defined in a similar way:

$$\left. \begin{aligned} dN_3 &= n_3(t, c_3) dc_3 \\ dN_5 &= n_5(t, c_5) dc_5 \end{aligned} \right\} \quad (3.41)$$

The CD25 and CD25-IL2 concentrations on a given cell were respectively named  $c_3$  and  $c_5$ . The three population densities change with time due to the internalization of CD3. It obeys a PBE as described in the model [25], [27]:

$$\frac{\partial n_i}{\partial t} + \frac{\partial(G_i n_i)}{\partial c_i} = B(t) \delta(c_i - c_{i,0}), \quad i = 1, 3 \text{ and } 5 \quad (3.42)$$

1.  $n_i$  representing the cell density relative to the protein  $i$  of interest (i.e.:  $i = 1$  for CD3 protein).  $n_i$  is a function of  $c_i$  and time  $t$ .
2.  $\frac{\partial n_i}{\partial t}$  representing an accumulation term

### 3.7 Case 3

---

3.  $\frac{\partial(G_i n_i)}{\partial c_i}$  being a convection or reaction term including the rate of the protein internalization or production ( $G_i$ ) at the single lymphocyte level.
4.  $B(t)\delta(c_i - c_{i,0})$  being a term of source that in that case represented the production rate of activated T cells (TL\*) according to its initial concentration ( $c_{i,0}$  before activation).

In order to simplify the handling of Dirac function ( $\delta$ ), Eq. (3.42) is transformed into

$$\frac{\partial n_i}{\partial t} + \frac{\partial(G_i n_i)}{\partial c_i} = 0 \quad (3.43)$$

with the boundary condition,

$$n_i(t, c_{i,0}) = \frac{B(t)}{|G_i(c_{i,0})|}. \quad (3.44)$$

The modulus is used in order to abstain from the piecewise function. This insures us that the population density cannot be negative. Unlike CD3 internalization, the CD25 and CD25–IL2 production rates are showing the both behaviors (increasing and decreasing) as their expression have the rise and fall during the activation process. Therefore,  $G_1 < 0$  while  $G_i$  is a non-monotonic function for  $i = 3, 5$ . The initial conditions are

$$\left. \begin{array}{l} n_i(0, c_i) = 0 \quad \text{for } c_i \neq c_{i,0} \\ \text{and } c_{1,0} > 0, \\ \text{whereas } c_{3,0} = c_{5,0} = 0 \end{array} \right\} \quad (3.45)$$

The initial concentrations of CD25 and IL2 in CD8+ T-cells were considered as null. The small minority of  $T_{\text{regs}}$  (Regulatory T cells) that spontaneously expressed CD25 was automatically not considered as they belong to the CD4+ and not CD8+ T cell population.

#### 3.7.1 Coupling of CD3 internalization and production of CD25 and CD25–IL2

The coupling of internalization of CD3, production of CD25 and CD25–IL2 dynamics raised new difficulties. Indeed, unlike CD3 down regulation, CD25 and CD25–IL2 up regulation are not

### 3.7 Case 3

---

only depended on their proper initial concentrations ( $c_{i,0}; 1 \leq i \leq 6$ ) but also on the external factors such as the dependency of proteins on each other. It means that there is an ODE system that represents the kinetics of the activation process in a given cell, as given in Eqs. (2.9) – (2.16). In order to calculate the duration of the T cell activation process at the single cell level, these ODEs need to be solved as followed,

$$\left. \begin{aligned} G_1 &= dc_1 / dt = f_1(c_1) \\ G_2 &= dc_2 / dt = f_2(c_1, c_2) \\ G_3 &= dc_3 / dt = f_2(c_2, c_3, c_4) \\ G_5 &= dc_5 / dt = f_5(c_3, c_4, c_5) \\ G_6 &= dc_6 / dt = f_6(c_5) \end{aligned} \right\} \quad (3.46)$$

with

$$\begin{aligned} t = t_0, \quad c_1 = c_{1,0} \quad c_2 = c_{2,0} = 0 \quad c_3 = c_{3,0} = 0 \\ c_4 = c_{4,0} \quad c_5 = c_{5,0} = 0 \quad c_6 = c_{6,0} = 0 \end{aligned}$$

This required the resolution of the ODE at initial conditions ( $c_{1,0}, t_0$ ) during the time scale  $[0, t_j]$ .

For that purpose, we have chosen the kinetic constants at a single cell level for describing the activation process. Then we have calculated the rate of change of time for the above six proteins while for CD3, CD25 and CD25–IL2 membrane expression, we find their population densities:

$$n_1(t_j, c_1), n_3(t_j, c_3), n_5(t_j, c_5)$$

#### 3.7.2 Solution of Density functions

The population density of T-cells is studied with the reaction rates defined above. Several numerical methods are applied to validate the results. Since the characteristic curves, Figure 2.9, are not same (as it can be seen in CD25 and CD25-IL2 plots), interpolation of the reaction rates is mandatory to find the numerical solution of PBE. The reaction rates found by the Eqs (2.9) – (2.16) are interpolated on the constant grid for the concentration. As the function is smooth, it is possible to use any interpolation technique. In this manuscript, a defined Matlab function for interpolation is used to do so. For the Transport Method, the interpolation is applied after finding the density function because the solution found by TM is not based on the reaction rates defined by the Eqs. (2.9) – (2.16).

### 3.7 Case 3

#### 1) CD3 Protein

The population density of T-cells for CD3 protein concentration is analyzed by using four methods based on analytical and numerical analysis. The exact solution is found by the MOC while the approximate solution is found by the other three methods, namely, Upwind, LWF and TM. The exact solution for the linear hyperbolic PDE is given by

$$n(c_1, t) = \begin{cases} 0 & c_1 < c_{10} \times e^{-k_1 t} \\ \frac{B(t)}{k_1 c_1} e^{\frac{b}{k_1}(\ln(c_{10}) - \ln(c_1))} & c_1 \geq c_{10} \times e^{-k_1 t} \end{cases} \quad (3.47)$$

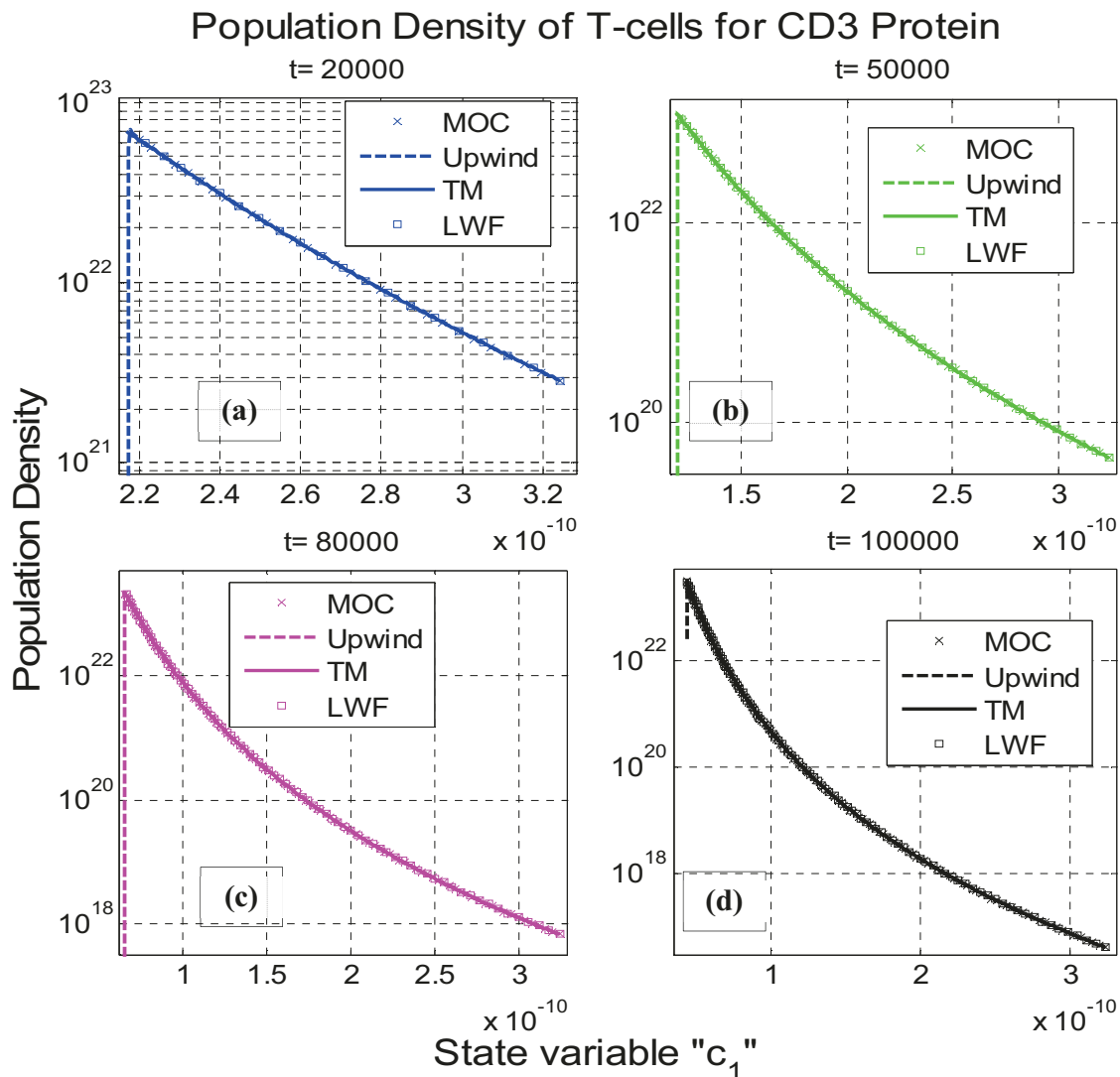


Figure 3.16: Population density of CD3 protein with respect to concentration at different times in seconds. The kinetic parameter for CD3 protein concentration is  $k_1 = 1/5 \times 10^{-4} s^{-1}$

## 3.7 Case 3

---

The initial population of activated T-cells is given by  $B(t) = ae^{-bt}$ ,  $a = 3 \times 10^8$ ,  $b = 1/7200$ . The solution can be shaped by using simple algebra. Four different times (in seconds) are presented in the Figure 3.16 for the population density function. In this figure, log-log plot is preferred because the values are at the extreme ends and it is convenient to follow in the defined way. The population density of the activated T-cells has the same maxima with a shift in the distribution of proteins for each time.

The CD3 protein has shown a very obvious behavior that was expectable due to independent linear reaction rate from the other proteins. On the other hand, it has given a good commitment between the different methods which has validated our newly developed method. Although the kinetic constant for the reaction rate was smaller than the previous cases, yet it has adequately affected the production of the other proteins by the activated T-cells. This is observed in the next population density functions for the other surface proteins due to their dependency on CD3 protein.

### II) *CD25 Protein*

The concentration of CD25 protein is depending upon the dynamical changes occurring in the other proteins and it has shown an eccentric behavior as shown in the Figure 2.8. First of all the population density for such behaviors has not been studied in the literature. In the previous studies, the population density is studied either for constant growth (reaction) rates (concentration increases at a constant rate) or for the linear reaction rates. In this study, the decrease in the concentration of CD25 protein is followed by an increase. Secondly, each characteristic curve is following a path with different reaction rate that makes the problem to find the population density of T-cells more complex.

By solving the integro-differential system numerically, given in the section 2.5, the grid points are not same for each characteristic line. It means the variation rate of one curve is not same as the others. Therefore, we need a fixed grid in order to find a numerical solution for the population density function. For this purpose, we used an interpolation technique to find the fixed grid points so that we can solve the linear hyperbolic PDEs numerically. On the other hand, the Transport Method is not dependent of the grid points; it can give better approximation. Due to interpolation,

### 3.7 Case 3

the error has increased in the numerical methods but the solutions are still following the solution found by Transport Method. The Lax-Wendroff method is used without flux limiter because there was no oscillation found during the whole simulation of the population density function.

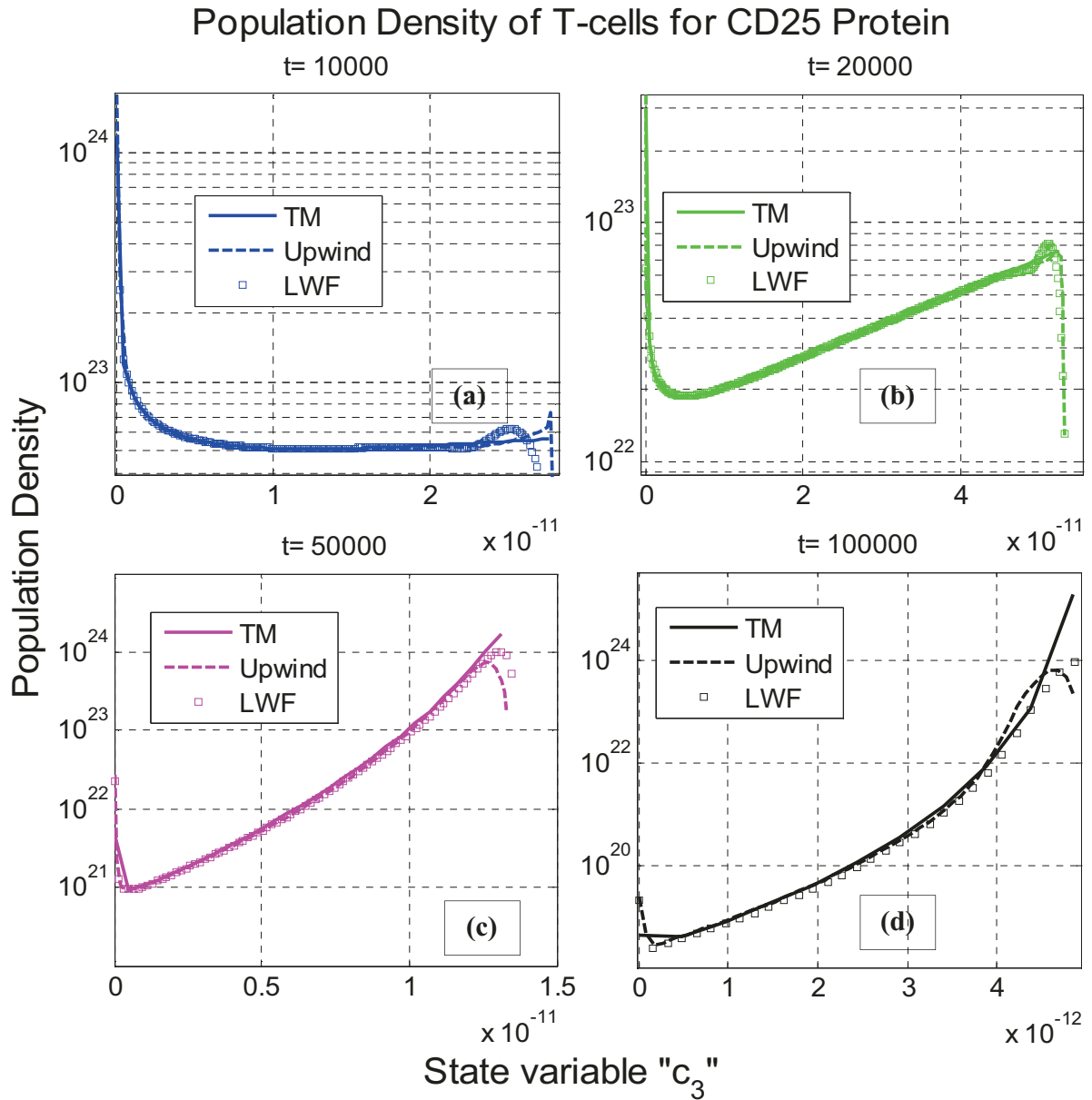


Figure 3.17: Population density of CD25 protein with respect to concentration at different times in seconds

$$k_1 = 1/5 \times 10^{-4} s^{-1}, k_2 = 1/5 \times 10^{-5} s^{-1}, k_3 = 10^{-4} s^{-1}, k_4 = 10^{-9} ms^{-1}, k_5 = 10^3 m^3 mole^{-1} s^{-1}, k_6 = 10^{-3}$$

The Figure 3.17 shows the population density of activated T-cells with respect to CD25 protein concentration at four different times. The comparison between the Figure 2.9 and Figure 3.17 can

### 3.7 Case 3

---

give us a better analysis for the population density. At time  $t = 10,000s$ , Figure 2.9 shows that the concentration is increased at a high rate. Moreover, in Figure 3.17(a), the population density shows that there is a range of concentration of CD25 protein present on the surface of activated T-cells. It is probably because, initially, the binding rate between CD25 and IL-2 is not so high due to low concentration of IL-2 in the blood. The increase in the concentration of CD25 starts decreasing afterwards due to the high level of binding of CD25 and IL2 protein. The most important phenomenon is that the characteristic curves are not crossing each other but they are converging to the specific level of the concentration as shown in the Figure 2.9. Therefore, the population density of the activated T-cells is increasing rapidly in the Figure 3.17 (c), (d)

In contrary to the CD3 protein, the CD25 and IL-2 proteins dynamics were dependent on each other. Therefore it was impossible to find the analytical solution for their population densities. The population density of T-cells was diversified rapidly in a range of CD25 protein concentration and afterwards it confined to a smaller range. But, in this confined range, the density of T-cells was very high as we can observe from the discontinuity front in the Figure 3.17. Due to the change in the kinetic parameters, the reaction rate was not so high. Similar behavior has been observed for CD25-IL2 protein but the reaction rate is not as complex as in the case of CD25 due to the monotone behavior of the solution curves.

#### III) *CD25-IL2 Protein*

The binding of IL-2 on CD25 protein starts early, after their productions. The concentration of CD25-IL2 binding increases gradually, Figure 2.9 that can be observed by the diversity of the population density of activated T-cells in the Figure 3.18. One can also observe that more and more cells are gathering with high concentration of this CD25-IL2 complex although this cluster is going inside the cell afterwards. The increase in the binding process of the protein present on the surface of the activated T-cells can subsequently affect the internalization speed that is necessary for the T-cells proliferation.

The results obtained by analytical and numerical methods have shown a nice agreement with each other and follows the natural phenomena. We use the same technique as we have used above to solve for the population density of T-cells for CD25 protein. The flux limiter is used to solve

### 3.7 Case 3

this problem due to high level of diffusion observed in the LWF method. The analytical method based on the characteristic lines and the upwind finite volume scheme has shown a good commitment with the Lax-Wendroff method.

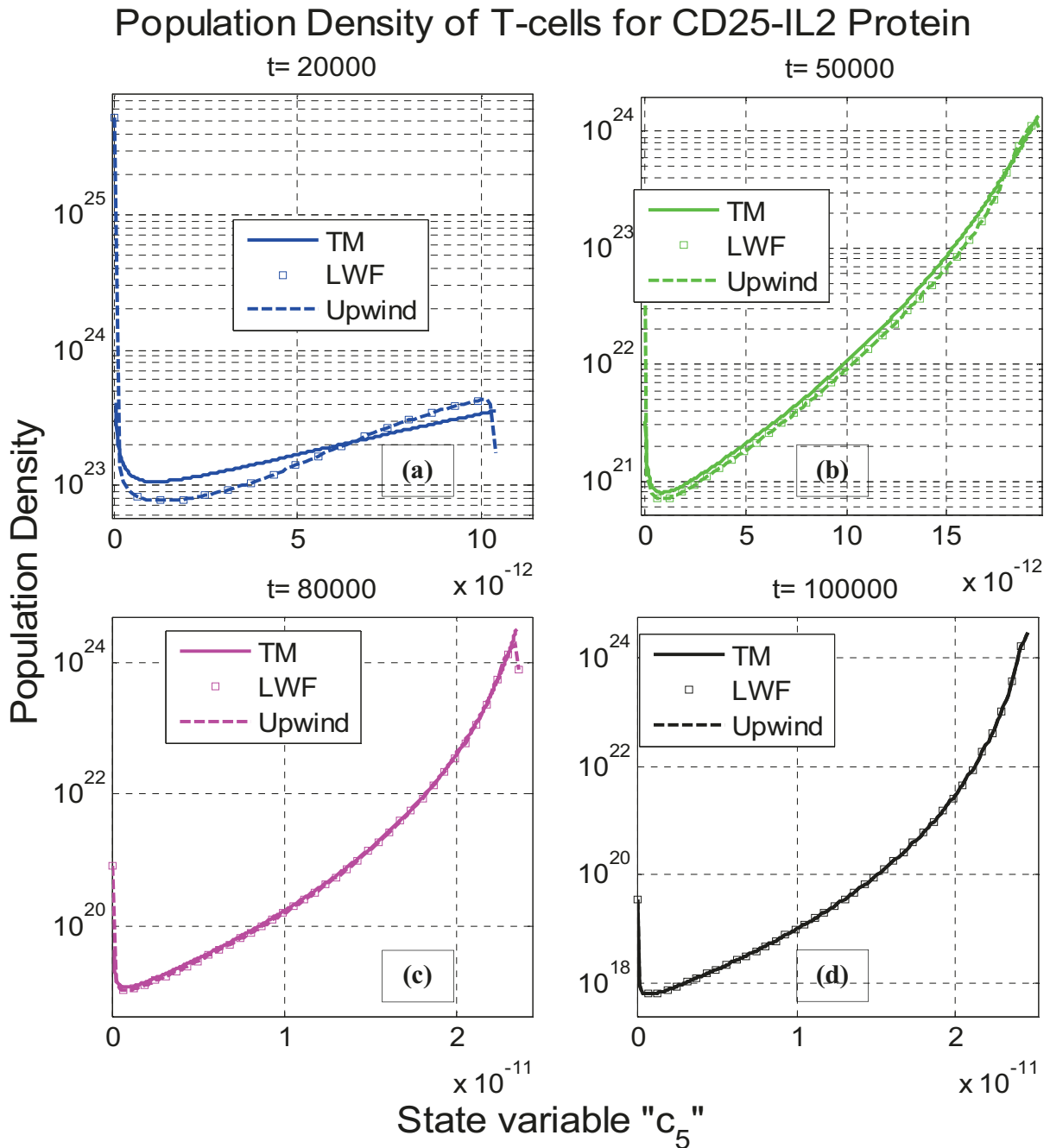


Figure 3.18: Population density of CD25-IL2 protein with respect to concentration at different times in seconds

$$k_1 = 1/5 \times 10^{-4} s^{-1}, k_2 = 1/5 \times 10^{-5} s^{-1}, k_3 = 10^{-4} s^{-1}, k_4 = 10^{-9} ms^{-1}, k_5 = 10^3 m^3 mole^{-1} s^{-1}$$

## 3.8 Case 4

---

The population density has been diversified with the passage of time. As the concentration of IL-2 rose in the blood stream, the binding of CD25 and IL-2 has increased gradually. Probably the stability at the discontinuity front in the Figure 3.18 (b), (c) and (d) is due to the degradation of the binding into the cell. This phenomenon has been observed by perceiving the range of protein concentrations on the surface of activated T-cells. At the same time, the T-cells were continuously activating and expressing their CD25 protein on the surface as well as diffusing the IL-2 signals in the blood stream which continued the process of binding and degradation until the threshold level would be reached to start the proliferation.

In the next case, the reaction rates for CD3, CD3i and IL-2 proteins are chosen higher. Therefore we observe the intersection between the concentration curves of CD25 and CD25-IL2 respectively as shown in Figure 2.10. At these intersection points, a drastic change is observed in the population density of CD25 and CD25-IL2 T-cells and the conservation laws are no more applicable by a classical way. Not only this, but also, it is not possible to apply the classical numerical techniques near such intersections. Therefore, Case 3 was obligatory in order to find the solution of the crossing problem by following TM.

## 3.8 Case 4

In case 4, we will focus on the same proteins as discussed before but here we have more general phenomena with regards to the population density of the T-cells with variation of proteins on their surfaces. If we consider that the characteristic line increases or decreases more rapidly as compared to the above case, we can observe the curves crossings each other as shown in Figure 2.10. This can make trouble to write the conservation laws for linear hyperbolic equation because the population density at crossing point has multiple origins. Moreover, we need further analysis of the Transport Method in order to find the solution.

### 3.8.1 Modified Transport Method

The characteristic lines are showing non-monotonic behavior and crossing each other at different points. The natural grid defined for this case by solving the system of ODEs in chapter 2 is

### 3.8 Case 4

irregular. It means that each curve is following a different grid for c-axis (concentration axis). The repetition of points in each curve is discussed in the above case. In this case, instead of a smooth curvy behavior of population density of T-cells, the curves intersect at some point that drastically changes the density function as shown in Figure 3.19. Basically it is a genuine behavior regarding the protein dynamics that can happen many times when the two types of T-cells are varying their concentrations of proteins at different rates during the simulation time. But, in this study, we consider that the two type of T-cells (started their activation process at different activation times) can coincide at-most one time as shown in Figure 3.19. A brief description about this phenomenon is explained in the Chapter 2 (Case 4) that can give a better understanding about such protein dynamics.

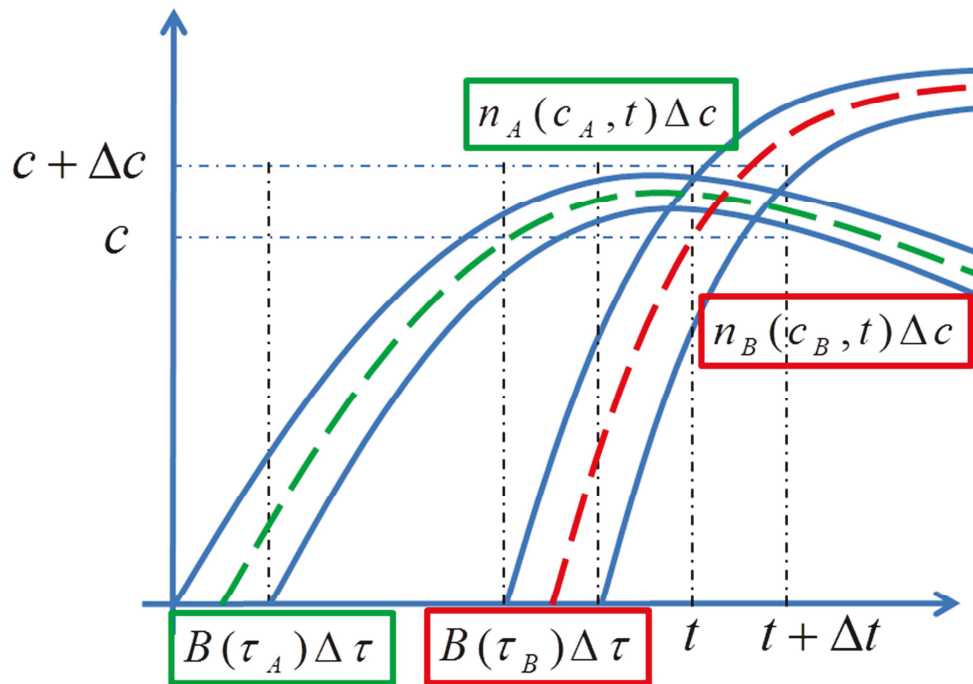


Figure 3.19: Population dynamics between of types of T-cells meeting at the crossing point lies in the interval  $[t, t+\Delta t]$ .

Consider the two (populations of) T-cells having their respective initial concentration of membrane proteins and follow their respective rate of change. The protein concentration on one T-cell that activates at time  $t = \tau_A$  varies less rapidly than the other T-cell that activates at  $t = \tau_B$  as shown in Figure 3.19. Due to this reason, the variation would not be same for each characteristic curve. For computational purpose, we define a constant grid with c-step  $\Delta c$

## 3.8 Case 4

---

between the minimum and maximum concentrations. Therefore, without any loss of generality, we can assume that the concentrations between  $c$  to  $c+\Delta c$  can coincide each other at a particular time from  $t$  to  $t+\Delta t$ . The population traveling along the characteristic curves certainly increases at this point due to same value of the protein concentrations of two T-cells and, therefore, we observe a severe change in the T-cells population density.

In this method, firstly, we will find the solution for each curve by using the Transport Method defined above. We have a little difference from case 2 where we find the density function directly. Here we will sum up the densities at the crossing points afterwards. Let us consider that  $c_A = c(\tau_A, t)$  and  $c_B = c(\tau_B, t)$  are the characteristic curves to be followed by the population densities  $n_A(c_A, t)$  and  $n_B(c_B, t)$  with initial activation time  $\tau_A$  and  $\tau_B$  respectively. Note that  $\tau_A$  and  $\tau_B$  are the average points and approximates the definite integral in the defined time intervals  $[\tau_A - \Delta\tau/2, \tau_A + \Delta\tau/2]$  and  $[\tau_B - \Delta\tau/2, \tau_B + \Delta\tau/2]$  respectively. If the curves come across each other at time  $[t, t+\Delta t]$  with concentration  $[c, c+\Delta c]$  (defined on constant grid) then the total population at the control volume will be  $n(c, t) = n_A(c_A, t) + n_B(c_B, t)$ .

### 3.8.2 Solution of Density functions

The population density of T-cells is found for the surface proteins, namely CD3, CD25 and CD25-IL2. In this case the kinetic parameter used for CD3 protein is same as in the 1<sup>st</sup> case, i.e.  $k_1 = 1/3000$ . Therefore we can refer to Figure 2.3 to analyze the population density of T-cells for CD3 membrane concentration. The CD25 and CD25-IL2 proteins are described in the previous case where the kinetic constant for CD25 protein production is quite small that made the problem simpler than this case. For the case 4, the kinetic parameters were defined in Chapter 2, section Case 4 while the rate of activation  $B(\tau)$  remains same as defined in Eq. (3.32).

The population density of CD25 protein is found in Figure 3.20 at four different simulation times, i.e.  $t = 20000, 50000, 80000, 100000$  by using the Modified Transport Method (MTM). In the start, the protein CD25 shows a rapid increase in the activated T-cells and the protein

### 3.8 Case 4

concentration is well distributed among these activated T-cells. In the Figure 3.20 , we observe that a high protein concentration is present in most of the activated T-cells while very less T-cells have low concentration of CD25. The low concentration is possibly due to two reasons: firstly, those cells that are newly activated and increase their concentration and, secondly, those cells that are binding with IL2 proteins and losing their CD25 protein on the surface.

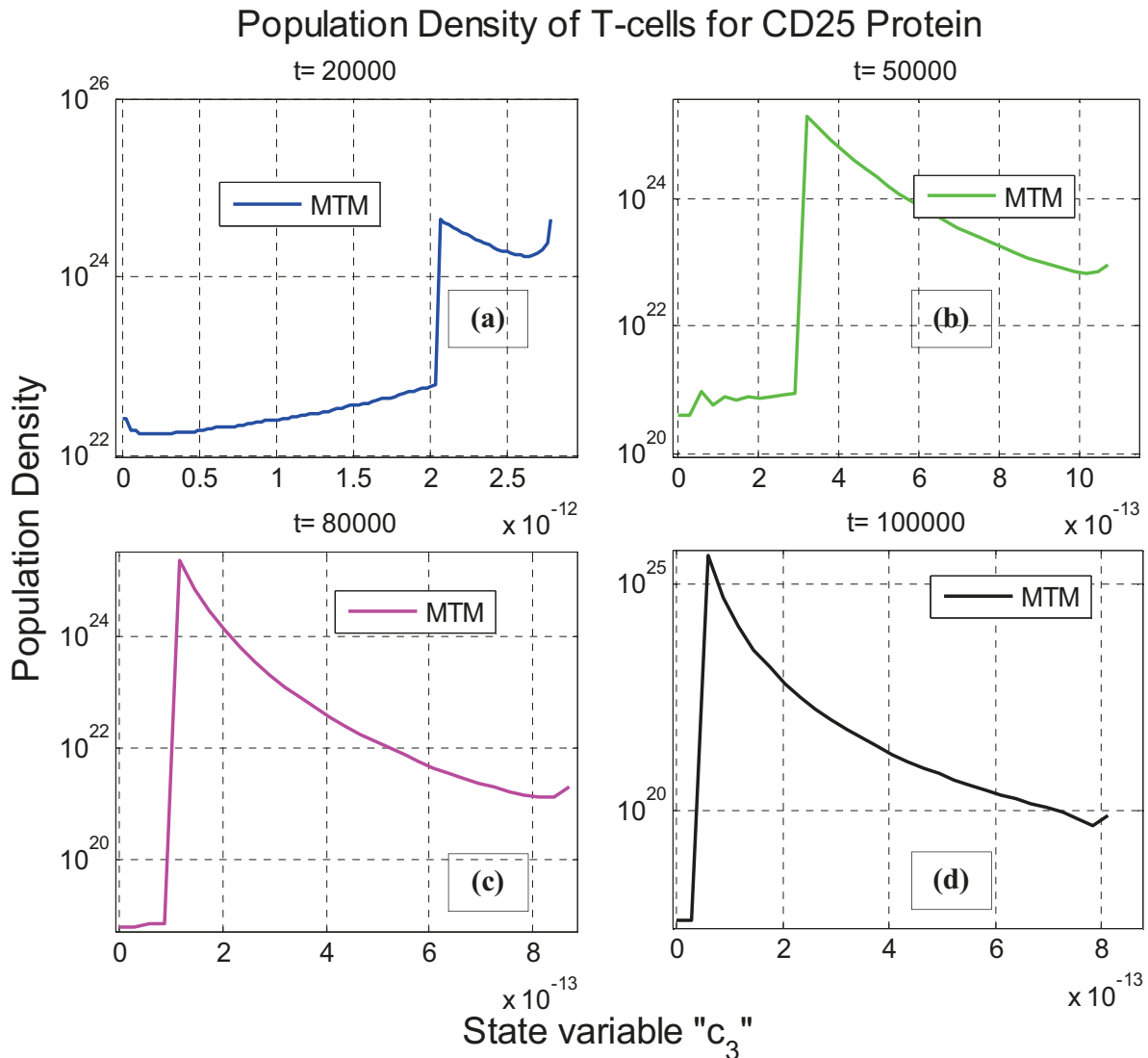


Figure 3.20: Population density of CD25 protein with respect to concentration at different times in seconds

The Figure 3.20 has shown a rapid decrease in the CD25 protein concentration due to binding with IL2 signals that are produced by all T-cells. The activated T-cells at any time  $t = \tau$  can coincide with other T-cells activated at some other time  $t \neq \tau$  with respect to their protein

### 3.8 Case 4

concentrations. This phenomenon produces the discontinuity in the T-cells population density as we can observe from the above Figure 3.20(a). The other plots show that, after time  $t$ , the protein concentration is getting low on most of the activated T-cells that can be observed by the shift in the discontinuities.

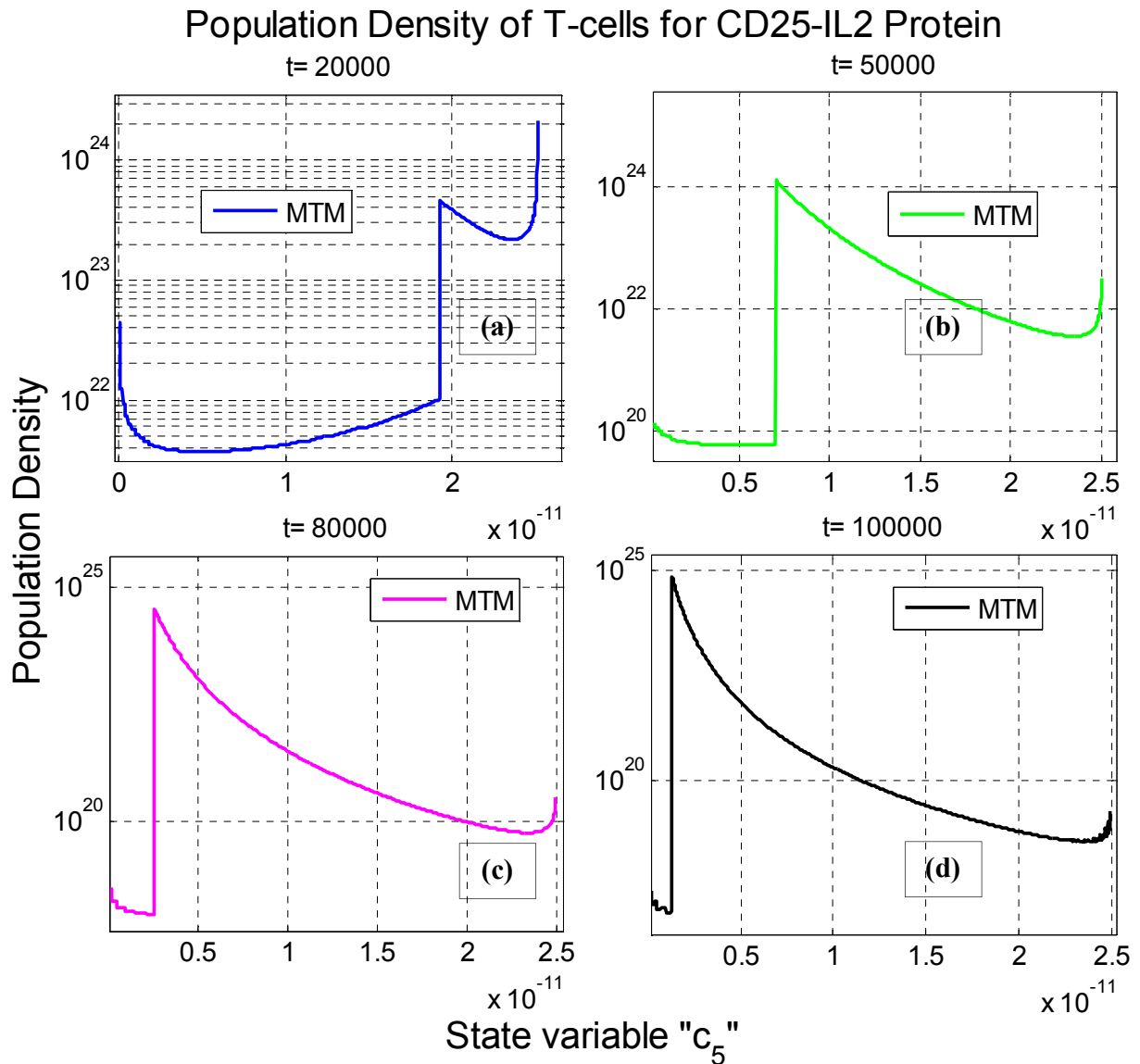


Figure 3.21: Population density of CD25-IL2 protein with respect to concentration at different times in seconds

The CD25-IL2 binding on the surface of T-cell rapidly increases after the production of CD25 and IL-2 proteins during T-cell activation. Due to the internalization of the binding, T-cells show

## 3.9 Conclusion

---

a gradual decrease of CD25-IL2 on the surface at different rates. The non-monotonic behavior of different types of T-cells coincides after a certain time and shows discontinuous behavior similar to CD25 T-cells. The discontinuity moves gradually towards left as shown in the Figure 3.21. This shows that the internalization rate is not so high because a wide range of protein concentration still remains on the activated T-cells.

The internalization of CD25-IL2 plays an important role in the proliferation of T-cells and that was one of the main reasons to study this model. Now we consider this situation as the T-cell is fully activated and now ready to divide and therefore, we can turn towards the division process by analyzing the proliferation of T-cells in the next chapter.

## 3.9 Conclusion

The process of activation of T-cells has shown diversified behaviors in the dynamics of population density. The dynamical changes at individual scales were dependent upon the proteins concentration at the initial time not only inside the cell or on the surface of the T-cells but also the outside (in the fluid). The population densities of T-cells were studied according to the surface proteins concentration.

The TM has shown a good commitment with the classical FVM and LWF. For the CD3 protein, the exact solution by MOC overlapped not only the classical methods but also TM. In the further cases, the error, observed between the numerical methods, compelled us to use the constant grid for the  $c$ -axis. This need was inevitable due to dissimilar behavior of characteristic curves. One can imagine it just by observing that the global maximum of each concentration curve is not same as shown in Figure 2.9 and Figure 2.10. Similarly, the range of concentration was also different for each curve which has made problem for the CFL condition that is mandatory to find the population density by using numerical methods.

The TM was modified according to the need in section 3.8. Since each solution curve found by solving the reaction rate in the section 2.6 has followed its own path particularly in CD25 and CD25-IL2 plots. Due to such variation in the behavior of the solution curves, conservation laws

### 3.9 Conclusion

---

didn't hold and the representation of model by using the classical way of population balance modeling became questionable. The Modified Transport Method (MTM) has made it possible to study the population density in this case but it left a question: whether is it possible to solve such conundrums by writing their (conservative) hyperbolic equations or it will remain a stunning dream?

In the above discussed cases, the population of activated T-cells is studied with respect to the concentration of CD3, CD25 and CD25-IL2 proteins present on the surface. Previously, experiments had been performed by [4] and a model has been presented in order to better understand the experimental results. The model by [4] has been studied at the hypothesis level that has provided us the chance to extend it to the values that are approaching the experimental data [8]. We followed some of the mechanism formed by [4] for finding the population density. The initial population density and the initial protein concentrations were considered with altered kinetic parameters from [8]. The results have shown a similar behavior as observed in the experiments and models. Unfortunately, there are no experimental results for CD25-IL2 protein. Although the mathematical modeling has played its part to investigate an innovative approach for population density of T-cells but it has ignored a lot of difficulties that are needed to understand the dynamics of T-cells. This dynamics was followed by all T-cells activated with same initial concentration at any activation time  $\tau$ .

The internalization of CD25-IL2 was considered as the final step to start proliferation. This process is complex as the proteins are asymmetrically dividing into two daughter cells and this process repeats itself for several times. Some simple cases will be studied in the next chapter in order to set a hypothesis for this portion.



# **Chapter 4**

## **T-cell Proliferation**

## 4.1 Introduction

---

### 4.1 Introduction

Proliferation is a division process that results with an increase in the number of several types of T-cells. This is the most important process to kill the virus as well as to produce memory T-cells that are long lasting and act more quickly and firmly against the specific viral infection. The T-cells repeat the evolutionary process of activation after the division process. The division of T-cells needs a threshold level of internalized protein CD25-IL2i that is considered in this work as the final step before T-cell division. The proliferation is followed by all the T-cells but probably at different level of CD25-IL2i protein. Also the concentrations of all the other surface proteins, including CD3, CD25 and CD25-IL2, do not have the same concentration. Instead of considering the surface proteins concentration, we consider that the T-cells start proliferation at a certain concentration of CD25-IL2i protein. The divided T-cells then follow the same process of activation. In short, in this chapter, we study the reaction rate of six proteins and the activation rate of T-cells before and after proliferation. The population densities of T-cells with and without proliferation are compared.

#### 4.1.1 Biological Structures

The division of T-cells needs a threshold level of internalized binding CD25-IL2i. It is considered here as the last signal inside an activated T-cell before the commencement of division process. The previous studies reveal that the T-cells start the process of division after 2 days and lasts this process of division for the next two to three days. Normally, the immune system do not take more than a week to get rid of the acute viral infection. It is important to review the proliferation process of T-cells with respect to their two major types, the helper CD4+ and cytotoxic CD8+ T-cells. It is observed experimentally that the activation process of CD4+ T-cells is slower than the CD8+ T-cells and therefore CD4+ T-cells takes more time to start their proliferation [45]. Also, no cell division has been observed during the first day ( $= 86400s$ ) by both in-vivo and in-vitro [45]. Normally, the CD8+ T-cells start dividing in the next couple of hours and takes 6-8 hours per division. On the other hand, CD4+ T-cells take more 12-24 hours to start the proliferation and each division needs approximately 10 hours [60], [61], [62]. The CD8+ T-cells divide 7-10 times during the process while very less CD4+ T-cells are showing their division seven or more times, [45], [63], [64].

## 4.1 Introduction

During the proliferation, many intrinsic differences between the CD4+ and CD8+ T-cells have been noted at the population level. But there are still some holes that need to be filled up in order to model the activation process after proliferation. For example, at single T-cell level, the division of T-cells is asymmetric, [65], [66]. It means that the asymmetric division distributes the proteins unequally (CD3, CD25 and CD25-IL2) between the two daughter cells after division. It is possible that the proteins are randomly distributed between the daughter cells.

Another ambiguity is that how many number of T-cells going to repeat the process of activation after proliferation? In order to analyze the proliferation according to the experimental observation and hypothetical slants, we make some hypotheses which may help us to model the problem in a better way. This would help us to understand the subsequent stimulation and proliferation effects on the magnitude of the response. Furthermore, it can help us to choose a better model which can be validated against experimental data.

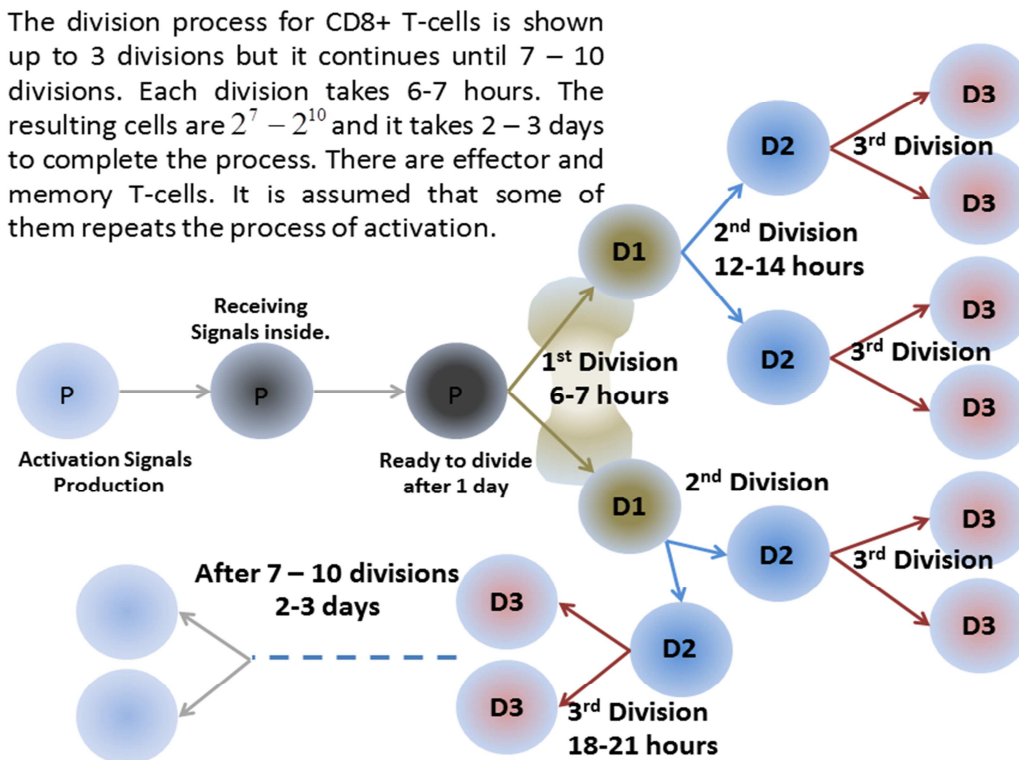


Figure 4.1: Division of a single parent T-cell after the getting fully activated.

## 4.1 Introduction

---

In this dissertation, we follow sequence of possibilities to study the protein dynamics and population density of T-cells before and after proliferation. Before proliferation, the protein dynamics and population dynamics of activated T-cells are same as described in the Chapter 2 and Chapter 3. Since the proliferation requires a sufficient amount of internalized CD25-IL2i protein, a concentration  $c_6^{thres}(\tau)$  is defined as a threshold to begin the T-cell division process. The minimum division time is considered as the transition period  $T$  during which the parent cell divides number of times into daughter cells. During the division time, no daughter cell is considered to be a part of activation process. After the transition period, some of the daughter T-cells having different concentration of proteins start their process of activation.

### 4.1.2 Simplified Model

In this study, we consider that the population beginning the activation process at time  $t = \tau$  starts proliferation at time  $t = \tilde{\tau}$ . This process takes a transition time  $T$  in which it divides the parent T-cell into  $\alpha(t)$  daughter cells. The  $\alpha(t)$  is chosen as either a constant or a uniform distribution over time  $t \geq \tilde{\tau} + T$  as shown in the Figure 4.2. For the protein dynamics, there are two possibilities due to asymmetric (unequal sharing of proteins between the daughter cells) behavior of T-cells during proliferation.

First possibility is that the population of daughter T-cells starts their activation process with the same concentration of surface and internalized proteins as the parent T-cell had at their activation time  $t = \tau$ . We can write it in the following way,

$$\begin{aligned} c_1 &= c_{10}, \\ c_i &= 0, \quad i \neq 1, 4 \end{aligned} \tag{4.1}$$

It is important to mention here that  $c_4$  (IL-2) is a global protein (i.e. shared by all T-cells). Therefore, the proliferation of T-cells does not affect the concentration of IL-2 directly.

The second possible way is the asymmetrical sharing of the protein concentration during the proliferation of T-cells. This can be defined by a uniform distribution  $D(c)$  over the total range of concentration. Again the IL-2 protein is not included in the distribution of proteins to the

## 4.2 Modeling Hypotheses

daughter T-cells. In the Figure 4.2, the concentration of CD25-IL2i protein of the daughter T-cells starts from same initial level at the activation time  $t = \tilde{\tau} + T$  as for parent cell at  $t = \tau$ .

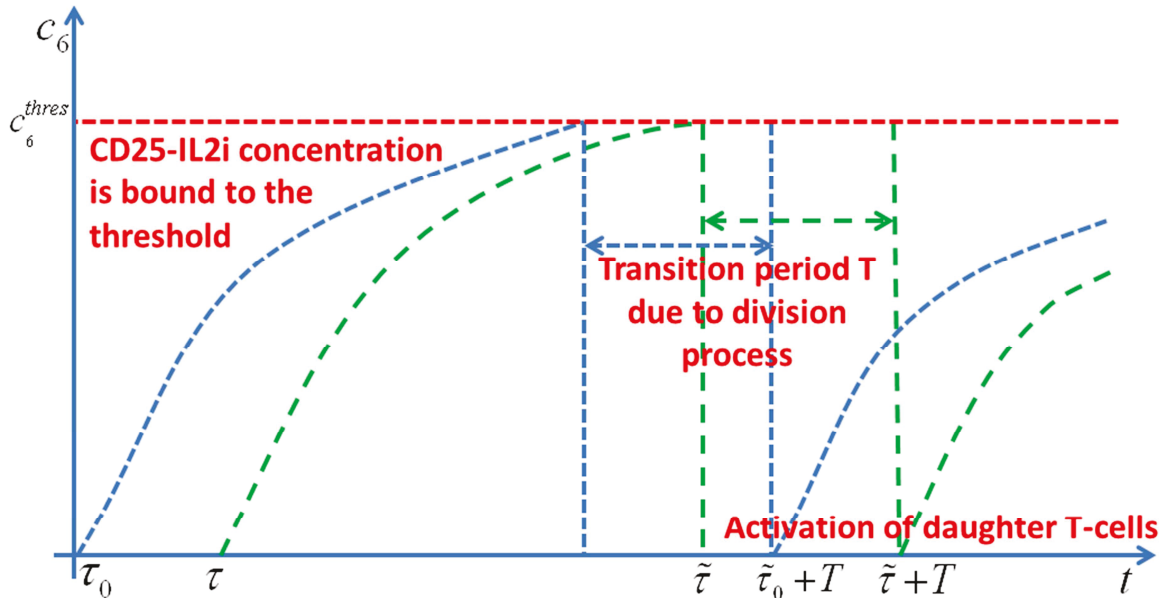


Figure 4.2: Protein dynamics at a single T-cell level. Part of the daughter T-cells start their activation process after a transition period of division.

The division of a T-cell is due to the sufficient internalization of CD25-IL2i protein concentration and not due to the change in the concentrations of surface proteins CD3, CD25 and CD25-IL2, therefore, we have mentioned the threshold of CD25-IL2i protein. The surface proteins concentrations are followed relative to the time  $t = \tilde{\tau}$  at which CD25-IL2i protein reached at its threshold level. In the next section we define the hypotheses under the conditions given above in this section.

## 4.2 Modeling Hypotheses

The initial population undergoes the activation process of T-cells after proliferation can be modeled in several ways. Suppose that the initial population of the activated T-cells at any activation time  $t = \tau$  propagates on a concentration curve  $c = c(t - \tau, \tau)$ ,  $t - \tau \geq 0$ , starts the proliferation at time  $t = \tilde{\tau}$  as shown in Figure 4.2. If  $T$  is the transition period for its division process then we can define the modeling hypotheses under the possibilities given in section 4.1.2.

## 4.2 Modeling Hypotheses

### 4.2.1 Hypothesis 1

We assume that the new cells (daughters) are activated in this hypothesis. The initial population of the activated T-cells at time  $t = \tilde{\tau} + T$  (the time after proliferation) is the sum of the initial population at time  $t = \tau$  and  $t = \tilde{\tau} + T$  as shown in the Figure 4.3. Recall the activation rate  $B(t)$ , one can write it for before and after proliferation as,

$$B(t) = \begin{cases} -\frac{dN_{NAC}(t)}{dt} & t < \tilde{\tau} + T \\ -\frac{dN_{NAC}(t)}{dt} + \alpha \left[ \frac{dN_{AC}(t)}{dt} \right]_{t=\tau(t)} & t \geq \tilde{\tau} + T \end{cases} \quad (4.2)$$

where  $\frac{dN_{NAC}(t)}{dt} = -k N_{APC} N_{NAC}$ . The parameter  $\alpha = \text{constant}$  is the number of divisions per T-cell which undergo the process of activation.  $N_{AC} (m^{-3})$  and  $N_{NAC} (m^{-3})$  are the concentrations in the activated and non-activated T-cells respectively, as defined in Eq. (3.1).

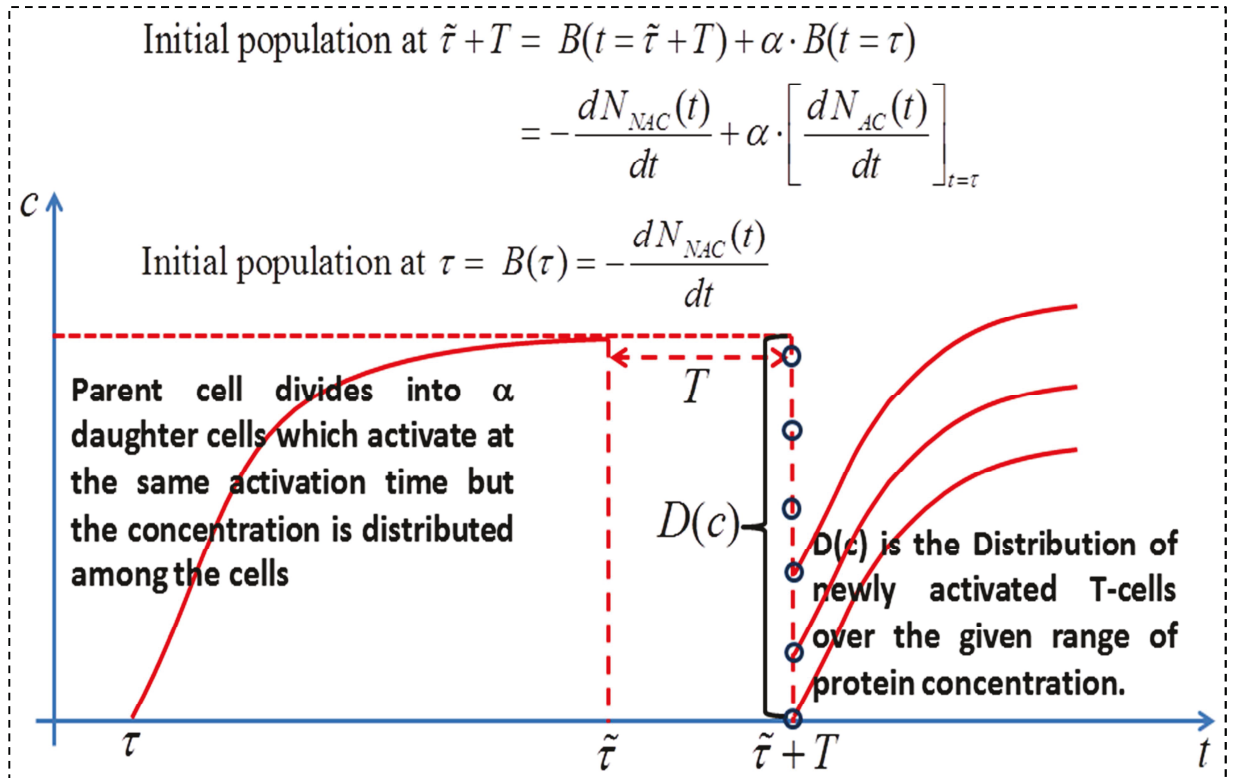


Figure 4.3: Creation of activated T-cells as virgin. Cells are activated according to Eq. (4.2) and distributed at  $t = \tilde{\tau} + T$  according to the distribution defined in the Eqs. (4.3) and (4.4).

## 4.2 Modeling Hypotheses

---

For the distribution of population of T-cells at time  $t = \tilde{\tau} + T$  with respect to their protein concentration CD25-IL2i after proliferation as shown in Figure 4.3, we can follow the concept of distribution  $D(c)$  defined in Eq. (3.3). Therefore, by using this distribution, the hypothesis can be divided into two categories:

1. In each daughter cell, the protein concentration at the time  $t = \tilde{\tau} + T$  equals to its initial concentration i.e. the concentration of protein at  $t = \tau$  as shown in the Figure 4.3.

$$D(c)|_{t=\tilde{\tau}+T} = D(c)|_{t=\tau} = \delta(c - c(\tau)). \quad (4.3)$$

2. If the protein concentration  $c$  is asymmetrically divided among  $\alpha$  daughter cells during the transition period  $\tilde{\tau} \leq t \leq \tilde{\tau} + T$  then the initial population of daughter cells at the time  $t = \tilde{\tau} + T$  could be described by the following distribution:

$$D(c) = p_1 e^{-p_2 c}. \quad (4.4)$$

Here  $p_1$  and  $p_2$  are the two parameters. The dashed line (—) at  $t = \tilde{\tau} + T$  in the Figure 4.3 corresponds to the distribution defined in Eq. (4.4).

### 4.2.2 Hypothesis 2

In this hypothesis, we assume that the daughter cells are activated. The activated parent T-cell at time  $t = \tilde{\tau}$  divides into  $\alpha$  daughter T-cells during the proliferation. The daughter T-cells are distributed over concentration among the initial population of activated T-cells after the transition period  $T$ , i.e.  $t \geq \tilde{\tau} + T$  as shown in Figure 4.4. In this way  $T$  will be considered as the minimum transition period for daughter T-cells which undergo the activation process. A part of the daughter T-cells of the same parent T-cell will start their activation process at time  $t = \tilde{\tau} + T$  while the others subsequently follow the activation process at time  $t > \tilde{\tau} + T$ . In this way, the daughter T-cells will be distributed over the time  $t \geq \tilde{\tau} + T$  and the time distribution density can be denoted by  $\alpha(t)$ . The activation rate can be followed by the following piecewise function:

$$B(t) = \begin{cases} -\frac{dN_{MAC}(t)}{dt} & t < \tilde{\tau} + T \\ -\frac{dN_{MAC}(t)}{dt} + \int_0^{\infty} \alpha(t') \left[ \frac{dN_{AC}(t)}{dt} \right]_{t=\tau(t')} dt' & t \geq \tilde{\tau} + T, \end{cases} \quad (4.5)$$

## 4.2 Modeling Hypotheses

where  $t' = t - \tilde{\tau} + T$ . The  $\alpha(t)$  distribute the population of daughter T-cells as the initial population activated at time  $t \geq \tilde{\tau} + T$ . An exponential distribution is chosen which gives a decrease with the increase in time. Therefore, the population density daughter T-cells will be distributed as monotonically decreasing function. We can define the distribution  $\alpha(t)$  as,

$$\alpha(t) = q_1 e^{-q_2(t - (\tilde{\tau} + T))}. \quad (4.6)$$

$q_1$  and  $q_2$  are the distribution parameters. Therefore  $\alpha(t)\Delta t$  are the total number of daughter T-cells in time  $t \in [t, t + \Delta t]$  and it obeys the following distribution property:

$$\int_{\tilde{\tau} + T}^{\infty} \alpha(t) dt = \text{Total number of activated daughter T-cells set to be activated}$$

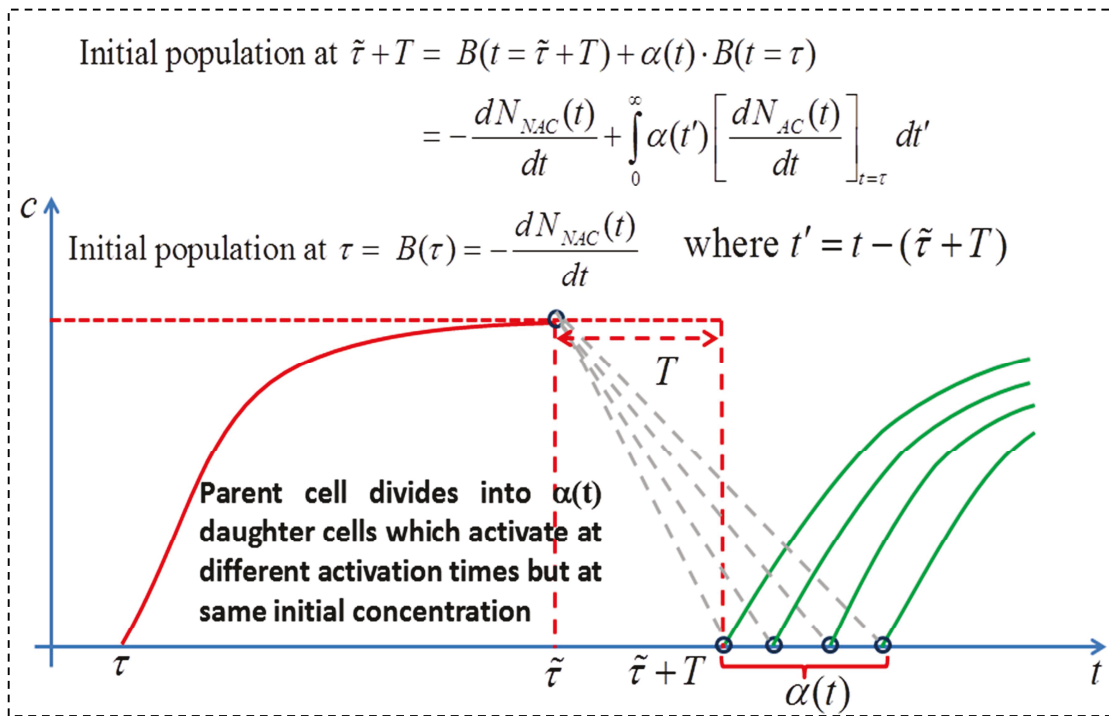


Figure 4.4: Distribution of daughter T-cells after proliferation

Now we categorize our hypothesis into two parts relative to the distribution of T-cells having the concentration  $c$ :

## 4.2 Modeling Hypotheses

1. The proliferated T-cells at time  $t = \tilde{\tau}$  are distributed after the transition period over the initial population of activated T-cells at time  $t \geq \tilde{\tau} + T$  with the initial protein concentration of Cd25-IL2i at  $t = \tau$ , as shown in Figure 4.4, is given by Eq. (4.3).
2. If the population of daughter T-cells is distributed over the initial population of activated T-cells at time  $t \geq \tilde{\tau} + T$ , then the initial population of daughter cells can be distributed as given in Eq. (4.4). This is represented in Figure 4.5.

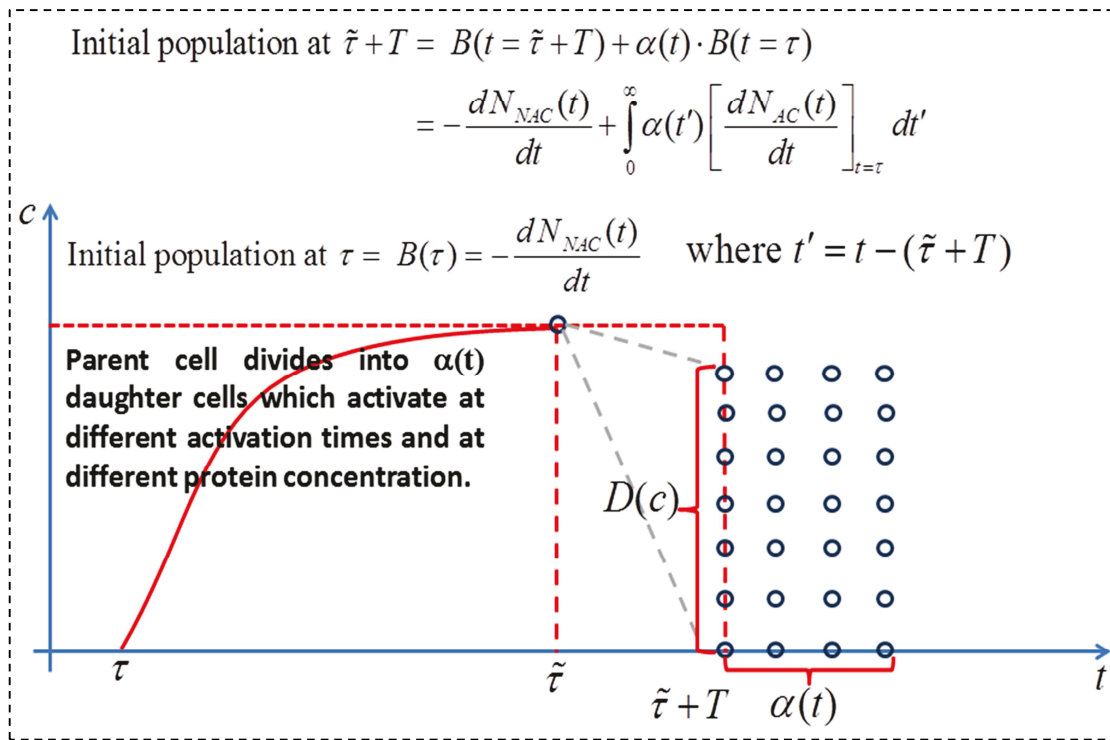


Figure 4.5: Distribution of daughter T-cells over the population of activated T-cells at  $t \geq \tilde{\tau} + T$

### 4.2.3 Hypothesis 3

We assume that the new cells (daughters) are not activated in this hypothesis. This hypothesis deals with the activation of T-cells after proliferation by following the flow of the parent T-cells at the threshold level. Furthermore, the daughter T-cells (T-cells after division but now they are non-activated) are  $\alpha = \text{constant}$  times the population of the parent T-cells and start their activation process at time  $t = \tilde{\tau} + T$  by interacting with APCs. By our previous assumption defined in Eq. (3.1), the activation rate can be written as,

## 4.3 Results

---

$$B(t) = bN_{NAC}(t), \quad \text{where } b = k \times N_{APC}. \quad (4.7)$$

It is assumed that the population of APCs remains constant during the whole simulation time. The rate of change in the non-activated T-cells remains same for  $t < \tilde{\tau} + T$  as discussed in the Eq. (3.1). After the proliferation,  $t \geq \tilde{\tau} + T$ , the population of activated T-cells increases depending upon the flux of the parent T-cells at the time of division and it is followed by an additional term after proliferation,

$$\begin{aligned} \frac{dN_{NAC}(t)}{dt} &= \begin{cases} -bN_{NAC}(t) & t < \tilde{\tau} + T \\ -bN_{NAC}(t) + \alpha \left[ \frac{dN_{AC}(t)}{dt} \right]_{t=\tau} & t \geq \tilde{\tau} + T \end{cases} \\ &= \begin{cases} -bN_{NAC}(t) & t < \tilde{\tau} + T \\ -bN_{NAC}(t) + \alpha [G_6(c_6)n_6(c_6, t - \tau)]_{c_6=c_6^{threshold}} & t \geq \tilde{\tau} + T. \end{cases} \end{aligned} \quad (4.8)$$

By solving the above ordinary differential equation, we get the following activation rate  $B(t)$ ,

$$\begin{aligned} B(t) &= \begin{cases} ae^{-bt} & t < \tilde{\tau} + T \\ a\alpha e^{-bt} I(t) & t \geq \tilde{\tau} + T \end{cases} \\ \text{where } I(t) &= \int \frac{e^{bt}}{a} G_6^{th} n_6^{th} dt + I_C \end{aligned} \quad (4.9)$$

where  $a$  is the constant of integration. The distribution  $D(c)$  is defined in Eqs. (4.3) and (4.4) in which the population of daughter T-cells is distributed over the range of concentration.

## 4.3 Results

The hypotheses considered above are based on distinct assumptions depending upon their generality and their complexity. Three hypotheses are proposed to explain the situation after the proliferation when daughter cells are ready to activate their selves. First two hypotheses are divided into two subgroups each while the third hypothesis explicates the evolution by following the flow of activated T-cells at time  $t = \tilde{\tau}$ . Since we are following the Dirac-delta function for the initial distribution of activated parent T-cells before proliferation, therefore, we discuss those

### 4.3 Results

subgroups of the hypotheses which follow the Dirac-delta function for initial distribution of activated daughter T-cells after proliferation as given in Eq. (4.3).

Since we need the threshold level of CD25-IL2i protein concentration therefore two cases (the Case 3 and Case 4) of the Chapter 2 and Chapter 3 are studied here that are based upon the protein dynamics at single T-cell level as well as at the population level. Both cases deal with the protein dynamics of all the six proteins as discussed in previous chapters. The population dynamics of T-cells is simulated for their surface proteins concentrations before and after proliferation while for the internalized CD25-IL2i protein concentration, the population dynamics is studied only before proliferation, until the threshold level.

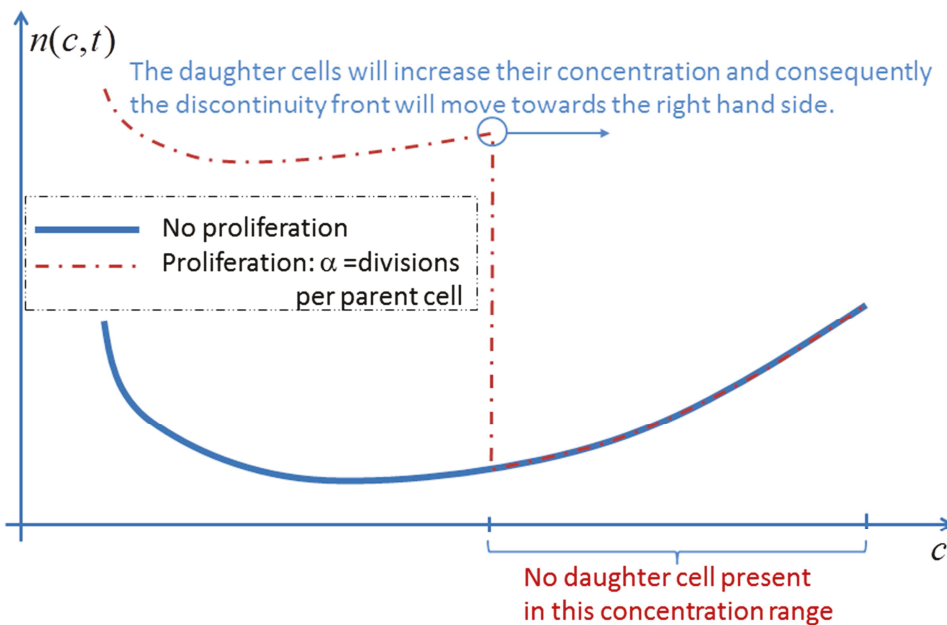


Figure 4.6: Population density of activated T-cells with and without proliferation

For the sake of simplification, each figure is divided into two categories to investigate the population density of activated T-cells: first one is the evolution of T-cells without proliferation (no proliferation) in which the daughter cells are not included. The second category involves those curves which includes the evolution process of T-cells with proliferation (proliferation with  $\alpha$  daughter cells) in which the daughter cells are included during the investigation of the population density function. The Figure 4.6 represents these two categories by describing the

## 4.3 Results

flow of population density  $n(c,t)$  in terms of the associated surface protein concentration  $c$ . In this figure, the associated proteins can be CD25 or CD25-IL2 as they increase their concentration with the passage of time on the surface of T-cell. For the CD3 protein concentration, the discontinuity of the dashed line will move towards the left hand side, instead of right hand side, because the concentration is decreasing.

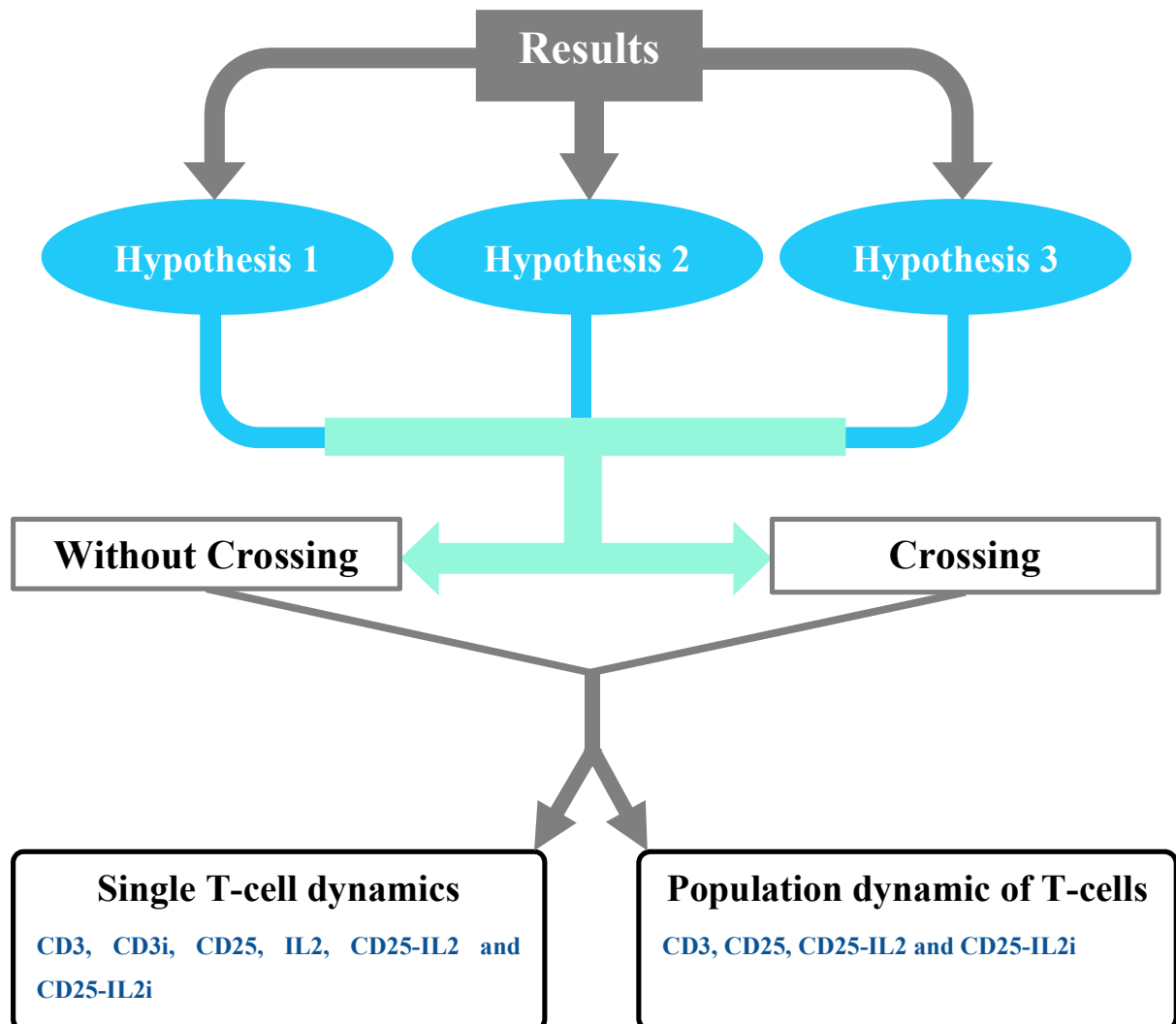


Figure 4.7: Results for the activation of T-cells after proliferation.

In Figure 4.6, the first category of 'no proliferation' is same as discussed in the Chapter 3 with prolongation of time. The second category is the combination of the population density for daughter T-cells and the population density of those activated T-cells which continued the first

## 4.3 Results

---

category. The discontinuity in the middle of the curve in Figure 4.6 arises due to the reason that there is no daughter T-cell which has the concentration higher than the concentration at the discontinuity point. As time passes, the concentration increases in the activated T-cells (particularly in cases of CD25 and CD25-IL2). Due to this reason, the discontinuity moves toward right hand side and show the distribution of concentration over the activated T-cells.

The simulations for the hypothesis 1, 2 and 3 are performed by using the methods TM and MTM. A flow chart, as shown in Figure 4.7, has been drawn to make a clear idea about the result section.

### 4.3.1 Hypothesis 1

This hypothesis proposes the distribution of the activated T-cells immediately after the proliferation (at time  $t = \tilde{\tau} + T$ ). We follow the activation rate from Eq. (4.3) and Eq. (4.2) to find the solution of the considered problem. Since the division of T-cell depends upon the threshold of CD25-IL2i protein concentration, therefore, we can follow those cases which includes the protein dynamics of CD25-IL2i. Two examples are studied here, with crossing and without crossing, in order to understand the evolution of population density of T-cells after proliferation. The parameters used for the reaction rates can be followed from the Case 3 (without crossing) and Case 4 (with crossing) of Chapter 2.

#### I) *Without Crossing*

The protein dynamics, as shown in Figure 4.8, follows the same pattern presented in Figure 2.9. The dashed line (– –) in red color shows the variation of the protein concentration in a single daughter T-cell. At the threshold of the protein concentration CD25-IL2i, i.e.  $c_6 = 0.001$ , the proliferation starts that is approximately  $t = 100,000$ s. For the simulation purpose, the transition time period for the proliferation of T-cells is considered  $t = 50,000$ s. Therefore, the daughter T-cells starts their process of activation after time  $t \approx 150,000$ s. Since the daughter cells are identical in the behavior to the other cells undergoing the activation process, the reaction rate will remain same for all of them as shown in Figure 4.8.

## 4.3 Results

The simulation is done for the next 100,000s. Afterwards, the daughter cells can repeat the process of activation since the CD25-IL2i protein concentration reaches the threshold again. IL-2 protein continues to increase as it is a global protein that is shared by all T-cells. But its concentration does also affect due to those T-cells that are in the process of division and they are not producing IL-2 protein.

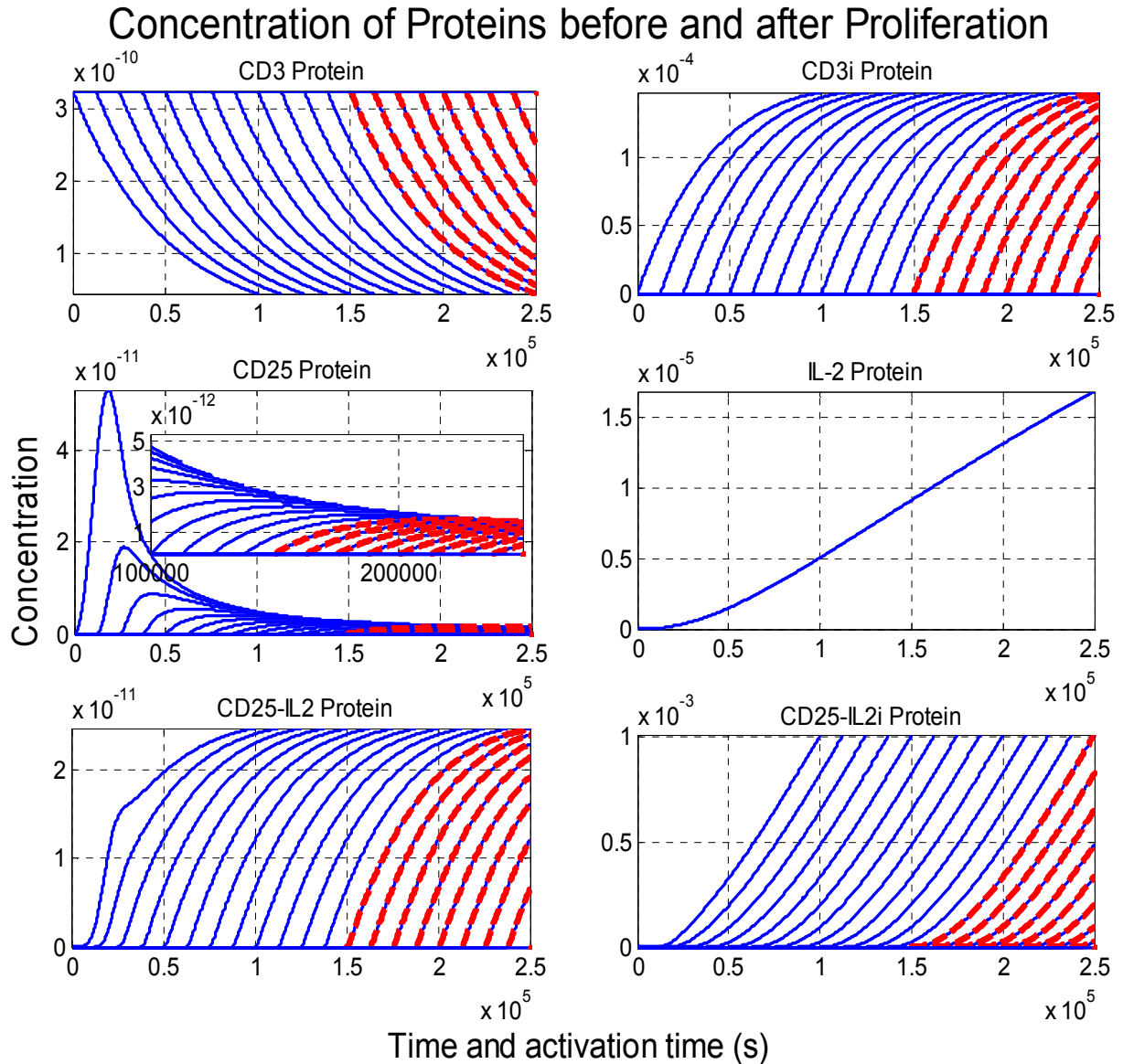


Figure 4.8: Graphical representation of protein dynamics at single T-cell level that are activating at succeeding activation times. The threshold level at which the division start is  $t = \tilde{t} + T$  that is almost  $t=100,000$  s. The daughter cells start activating after  $t=150,000$  s. The kinetic constants are given the following values:

$$k_1 = 1/5 \cdot 10^{-4} s^{-1}, k_2 = 1/5 \cdot 10^{-5} s^{-1}, k_3 = 10^{-4} s^{-1}, k_4 = 10^{-9} ms^{-1}, k_5 = 10^3 m^3 mole^{-1} s^{-1}, k_6 = 10^{-3} s^{-1}$$

## 4.3 Results

Now we discuss the population densities of T-cells for CD3, CD25, CD25-IL2 and CD25-IL2i protein concentrations. TM method is used to find the solution that is described previously in the section 3.3.2.

### Population Dynamics

Since the threshold to start the proliferation of T-cells depends upon the CD25-IL2i, we start by investigating its density function at four different times with the maximum at  $t=150,000$ s as shown in Figure 4.9. Afterwards, the population density for CD3, CD25 and CD25-IL2 proteins are studied before and after proliferation at  $\alpha=1, 4, 8$ . Their solutions are compared with the solution of no proliferation.

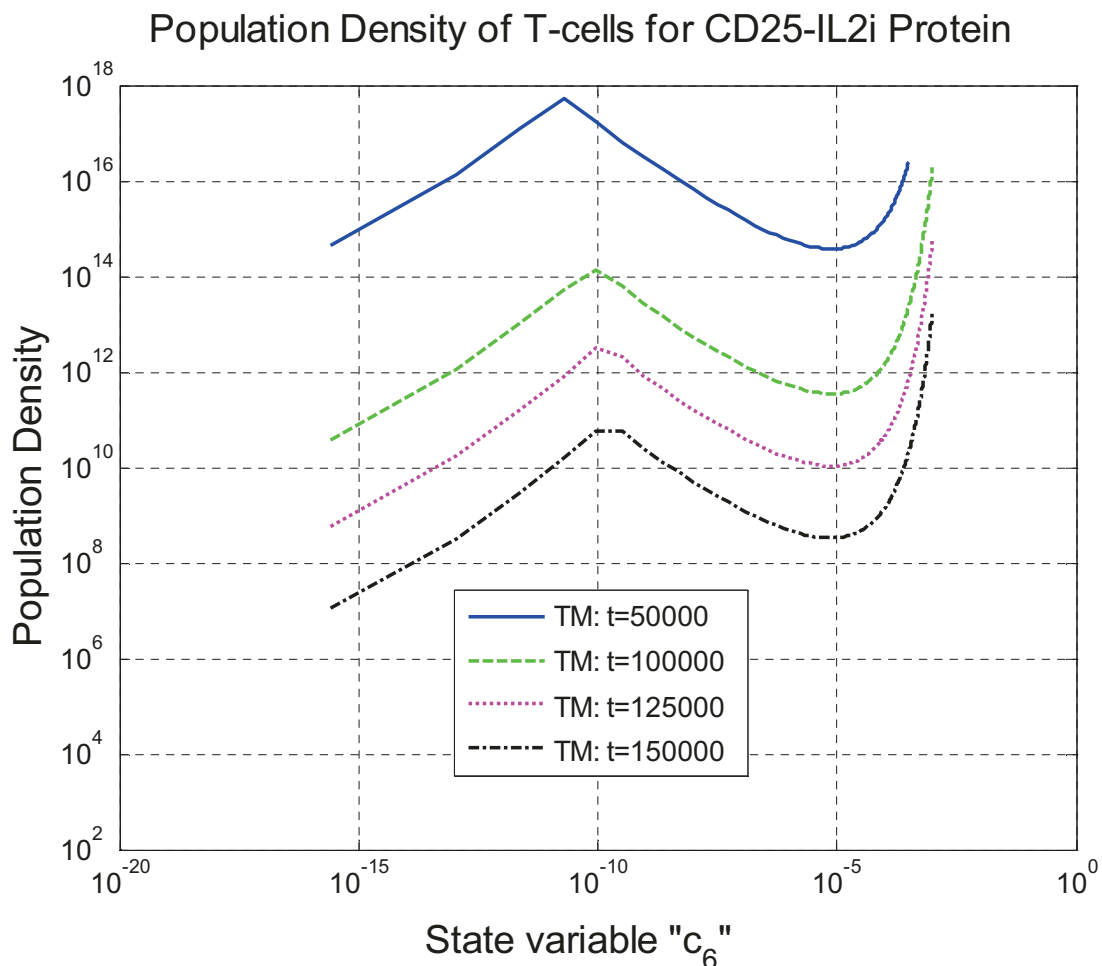


Figure 4.9: Population density of T-cells with internalized CD25-IL2i protein. The threshold level at which the division starts is  $c_6 = 10^{-3} \text{ mol.m}^{-3}$  and the time is after almost a day ( $t=100,000$  s). The daughter cells start activating after time  $t=150,000$  s.

## 4.3 Results

One can observe the drastic change between no proliferation and proliferation with  $\alpha=1$  (number of daughter cells are equal to the number of parent cells) in the Figures below, namely Figure 4.10, Figure 4.11 and Figure 4.12. The main reason is that the parent cells undergo the process of division at time  $\tilde{\tau}$  had started the process of activation at time  $\tau$ . At that time  $\tau$ , huge population of T-cells was starting their process of activation.

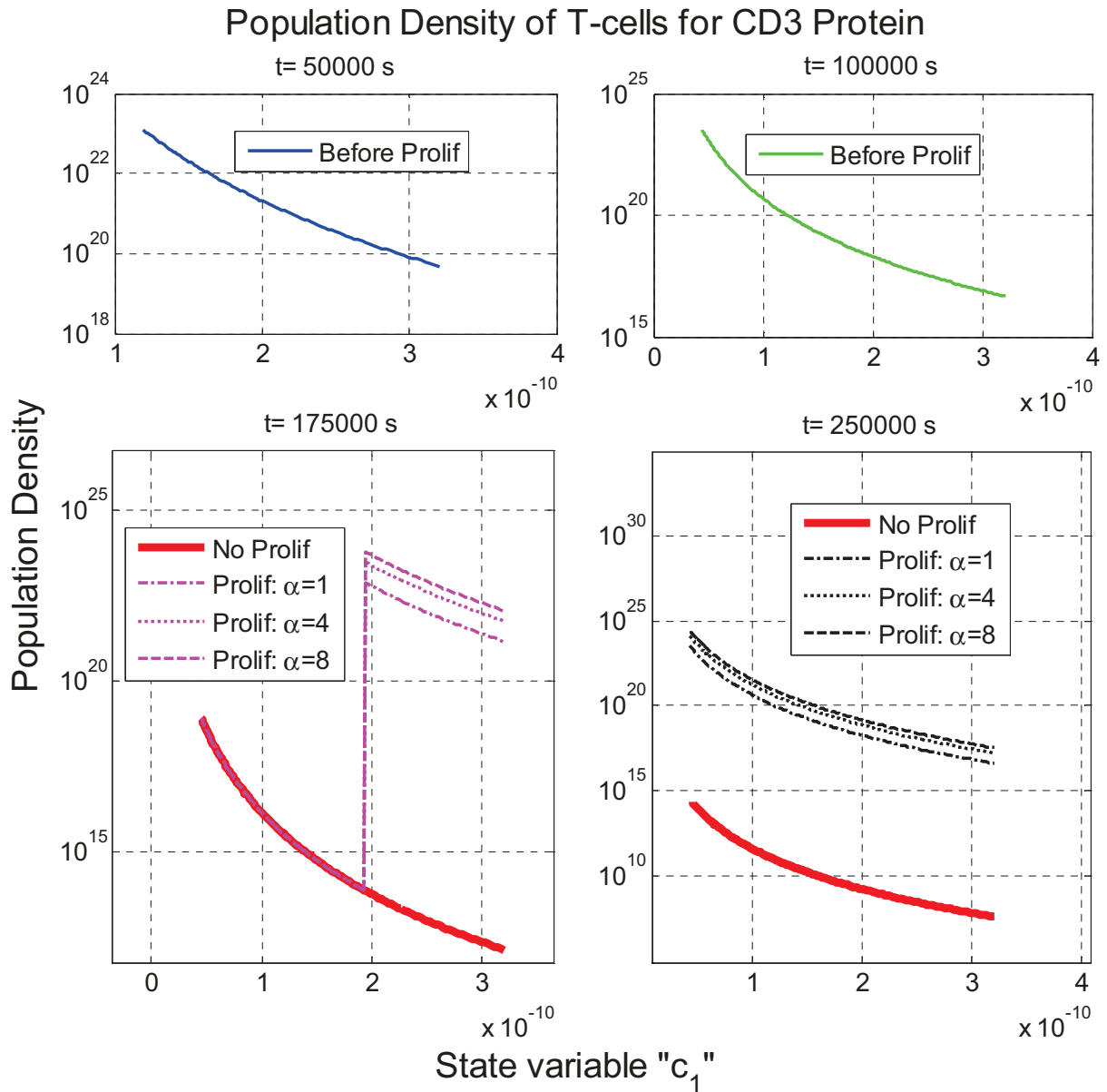


Figure 4.10: Population density of T-cells for CD3 protein. The threshold level at which the division starts is  $c_6 = 10^{-3} \text{ mol.m}^{-3}$  and the time is after almost a day ( $t=100,000$  s). The daughter cells start activating after  $t=150,000$  s. 'No Prolif' is the 'No Proliferation' curve showing the population density of T-cells without including daughter cells.

## 4.3 Results

Furthermore, for  $\alpha=4,8$  does not seem to be so far away from the curve with  $\alpha=1$  (the figures are plotted with logarithmic vertical axis). Otherwise, for  $\alpha=4,8$ , the daughter cells which undergo the process of activation are 4 and 8 times more than the parent T-cells.

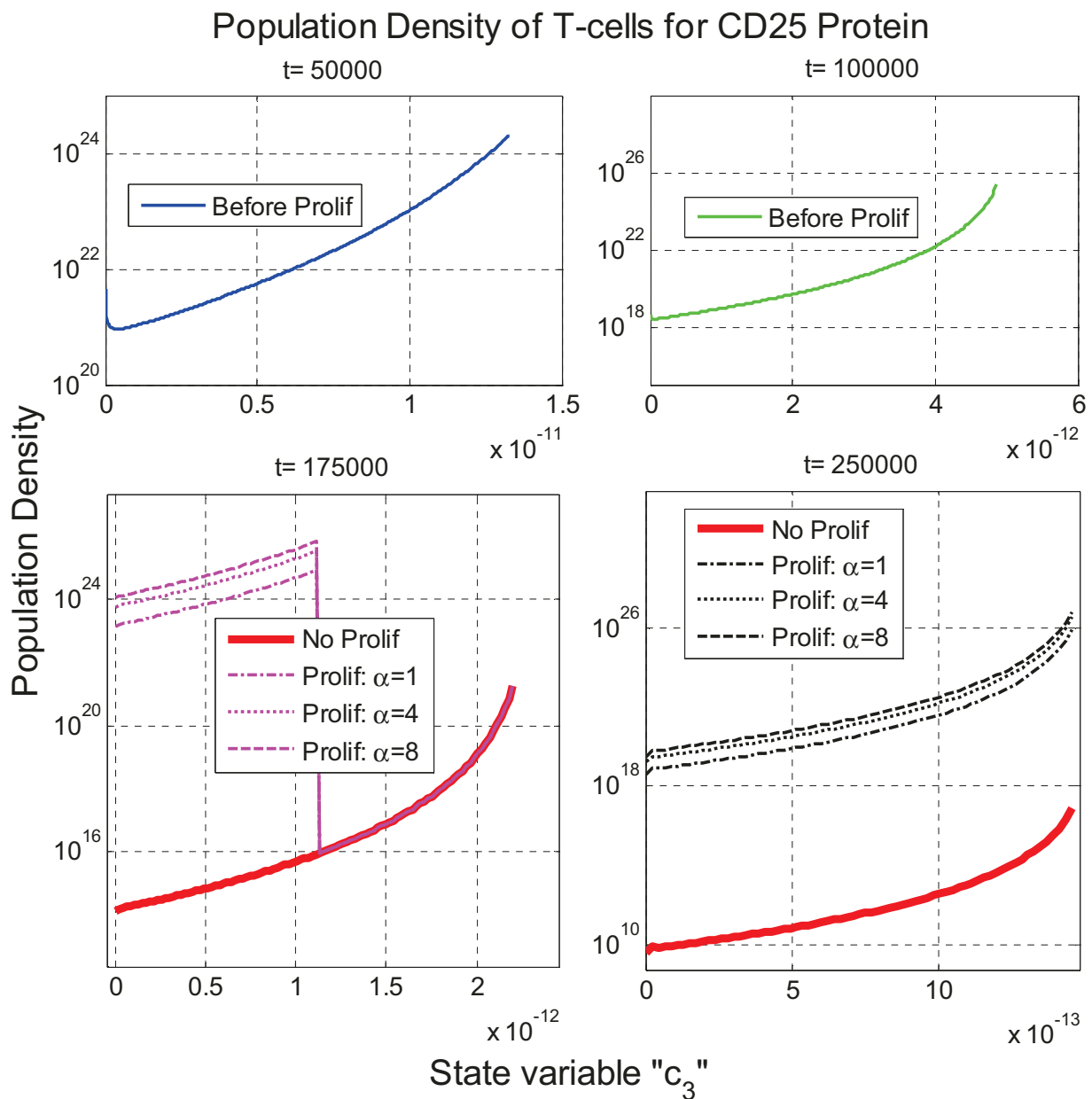


Figure 4.11: Population density of T-cells with surface protein CD25. The threshold level at which the division starts is  $c_6 = 10^{-3} \text{ mol.m}^{-3}$  and the time is after almost a day ( $t=100,000 \text{ s}$ ). The daughter cells start activating after  $t=150,000 \text{ s}$ . 'No Prolif' is the 'No Proliferation' curve showing the population density of T-cells without including daughter cells.

## 4.3 Results

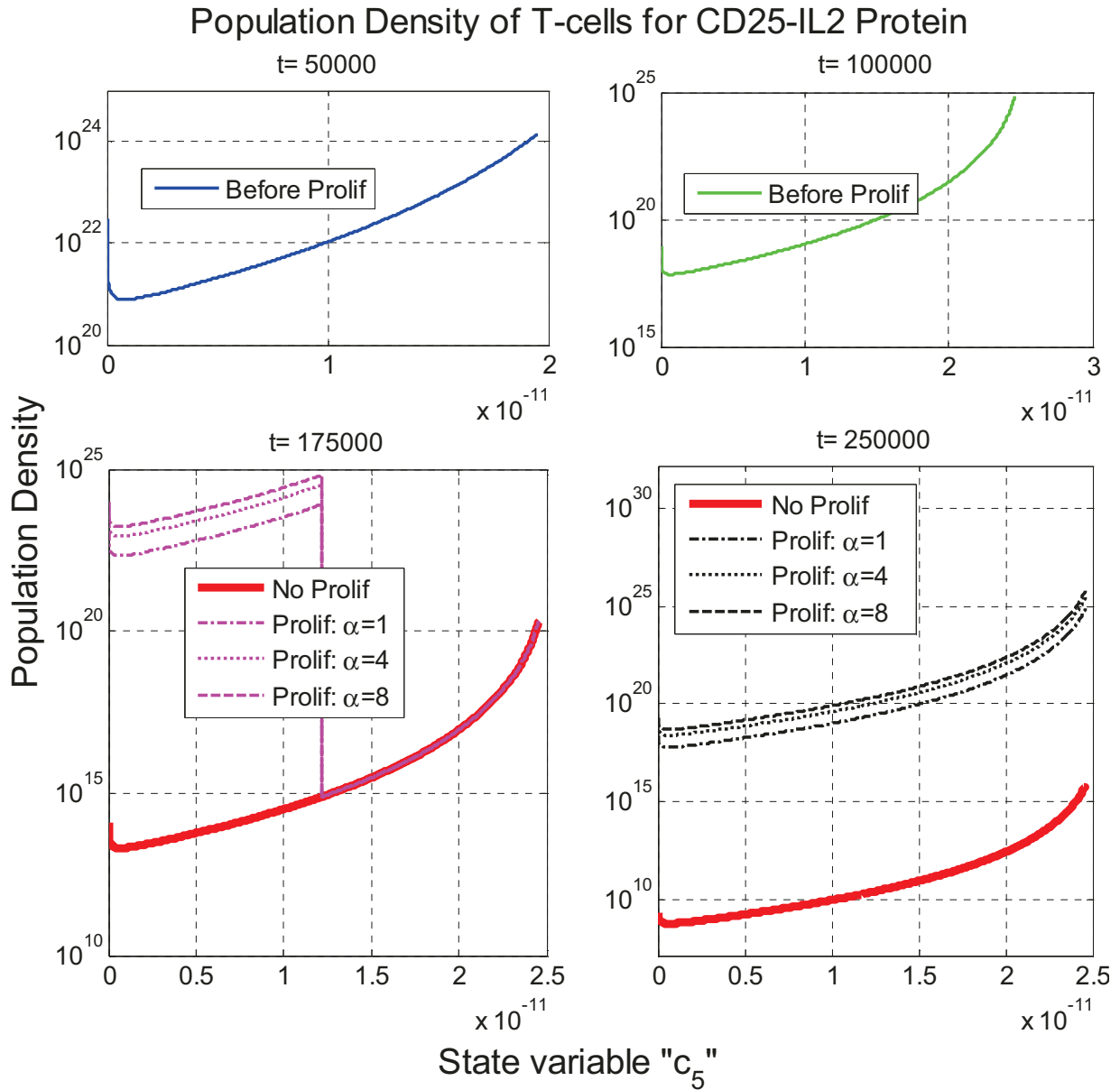


Figure 4.12: Population density of T-cells with surface binding CD25-IL2. The threshold level at which the division starts is  $c_6 = 10^{-3} \text{ mol.m}^{-3}$  and the time is after almost a day ( $t=100000 \text{ s}$ ). The daughter cells start activating after  $t=150,000 \text{ s}$ . 'No Prolif' is the 'No Proliferation' curve showing the population density of T-cells without including daughter cells.

### II) Crossing

The protein dynamics in the crossing problem has the same phenomena as discussed in the section 2.6. The only difference is the studied time period that is increased up to  $t = 250,000 \text{ s}$ . The threshold of CD25-IL2i protein concentration in order to start the division process is considered as  $c_6 = 5.6 \times 10^{-4}$ . The division starts at time  $t \approx 100,000 \text{ s}$  for the first T-cell which

## 4.3 Results

started its activation at time  $t=0$  and continues with the transition period of  $t=50,000$ s and, afterwards, the daughter cells starts their activation process as shown in the Figure 4.13. Similarly other T-cells activating at time  $t>0$  follows the same phenomena. The other proteins concentration, particularly the concentration of CD25 and CD25-IL2, are subject to the threshold time and varies relative to threshold of CD25-IL2i protein concentration.

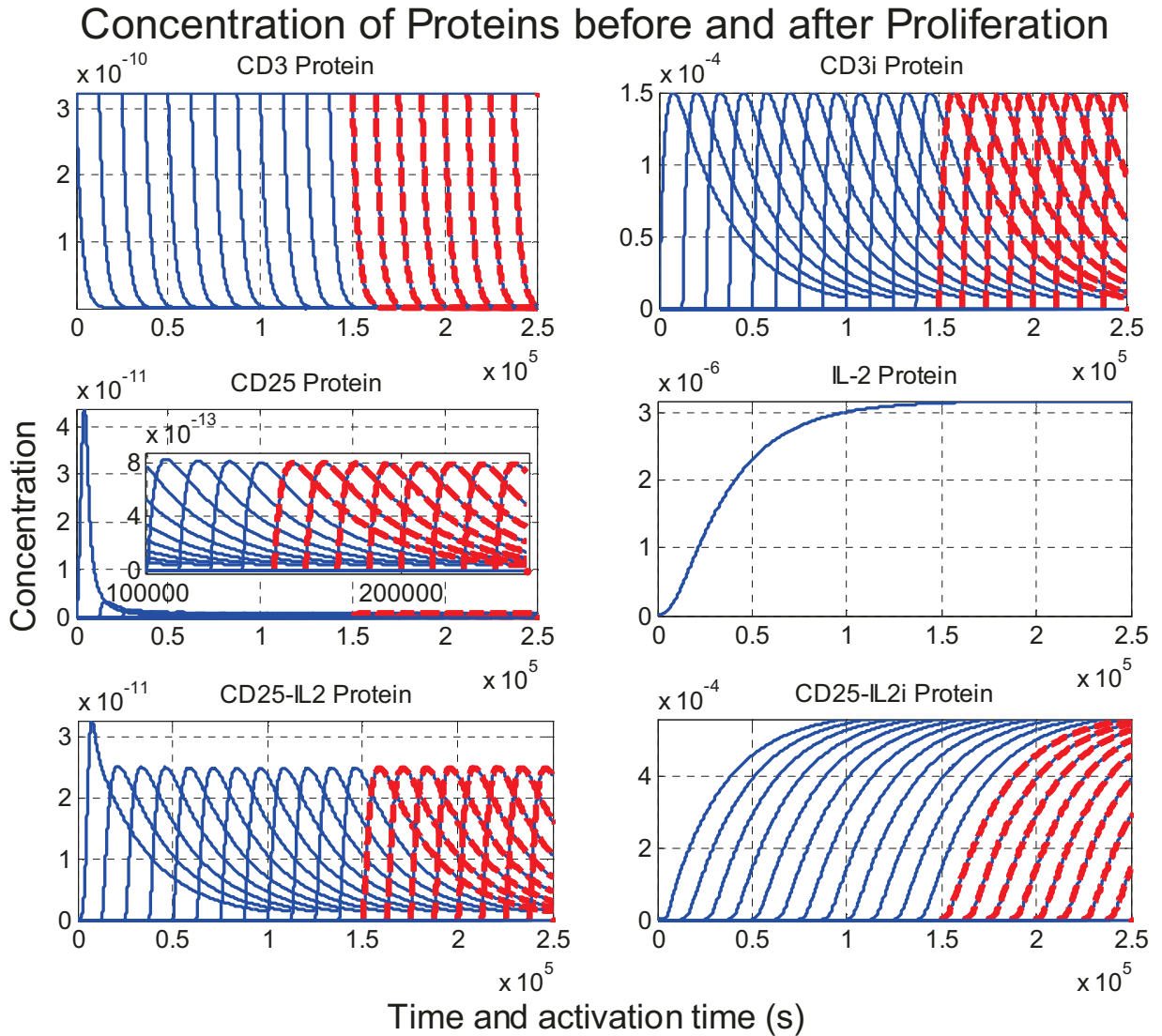


Figure 4.13: Protein dynamics at single T-cell level that are activating at succeeding activation times and crossing each other. The threshold level at which the division start is  $c_6 = 5.6 \times 10^{-4} \text{ mol.m}^{-3}$  that is almost  $t=100,000$  s. The daughter cells start activating after  $t=150,000$  s. The kinetic constants are given the following values:

$$k_1 = 1/3 \cdot 10^{-3} \text{ s}^{-1}, \quad k_2 = 1/5 \cdot 10^{-4} \text{ s}^{-1}, \quad k_3 = 10^{-4} \text{ s}^{-1}, \quad k_4 = 10^{-9} \text{ ms}^{-1}, \quad k_5 = 10^6 \text{ m}^3 \text{ mole}^{-1} \text{ s}^{-1}, \quad k_6 = 10^{-3} \text{ s}^{-1}$$

## 4.3 Results

### Population Dynamics

The population dynamics for the surface proteins concentration and the internalized protein concentration CD25-IL2i are investigated subject to their reaction rates and activation rates. All the results have been found by using our methods TM and MTM that are compared with the solutions found by without proliferation.

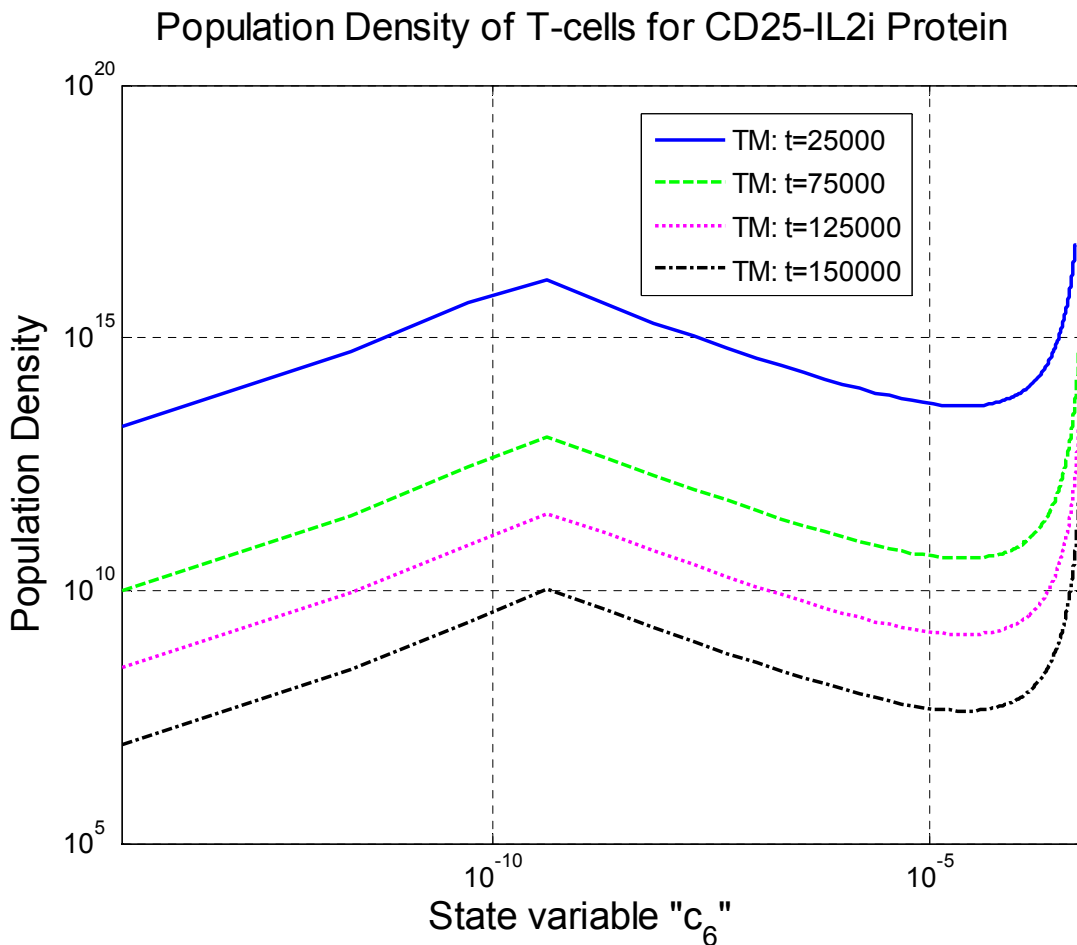


Figure 4.14: Population density of T-cells with CD25-IL2i internalized protein. The threshold level at which the division starts is  $c_6 = 5.6 \times 10^{-4} \text{ mol.m}^{-3}$  and the time is after almost a day ( $t = 100,000 \text{ s}$ ). The daughter cells start activating after  $t = 150,000 \text{ s}$ .

The population density of T-cells for the CD3, CD25 and CD25-IL2 proteins are found in the Figure 4.15, Figure 4.16 and Figure 4.17. We observe the similar difference among the population densities of T-cells without and with proliferation as we observed in the previous section, i.e. Without Crossing.

## 4.3 Results

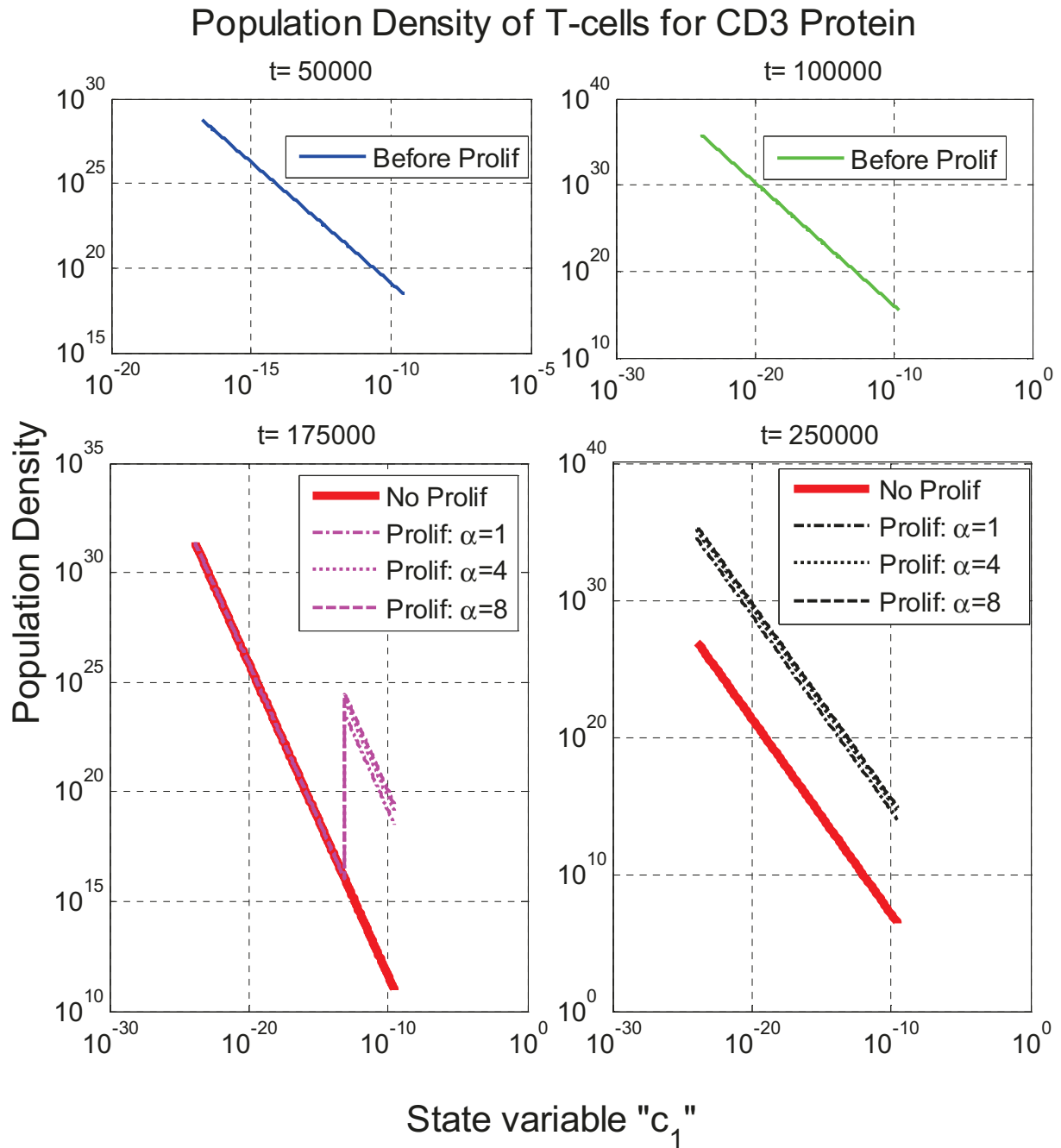


Figure 4.15: Population density of T-cells with CD3 surface protein. The threshold level at which the division starts is  $c_6 = 5.6 \times 10^{-4} \text{ mol.m}^{-3}$  and the time is after almost a day ( $t=100,000 \text{ s}$ ). The daughter cells start activating after  $t=150,000 \text{ s}$ . 'No Prolif' is the 'No Proliferation' curve showing the population density of T-cells without including daughter cells.

The overlapping of the curves in the Figures shown for the population densities of CD3, CD25 and CD25-IL2 proteins with and without proliferation shows that there is no daughter T-cell containing the concentration of the protein at the given time  $t$ . At the final time  $t=250,000$ , we

### 4.3 Results

can observe that there is no overlapping and it shows that the daughter T-cells have produced all the possible variety of protein concentration as the other virgin T-cells have.

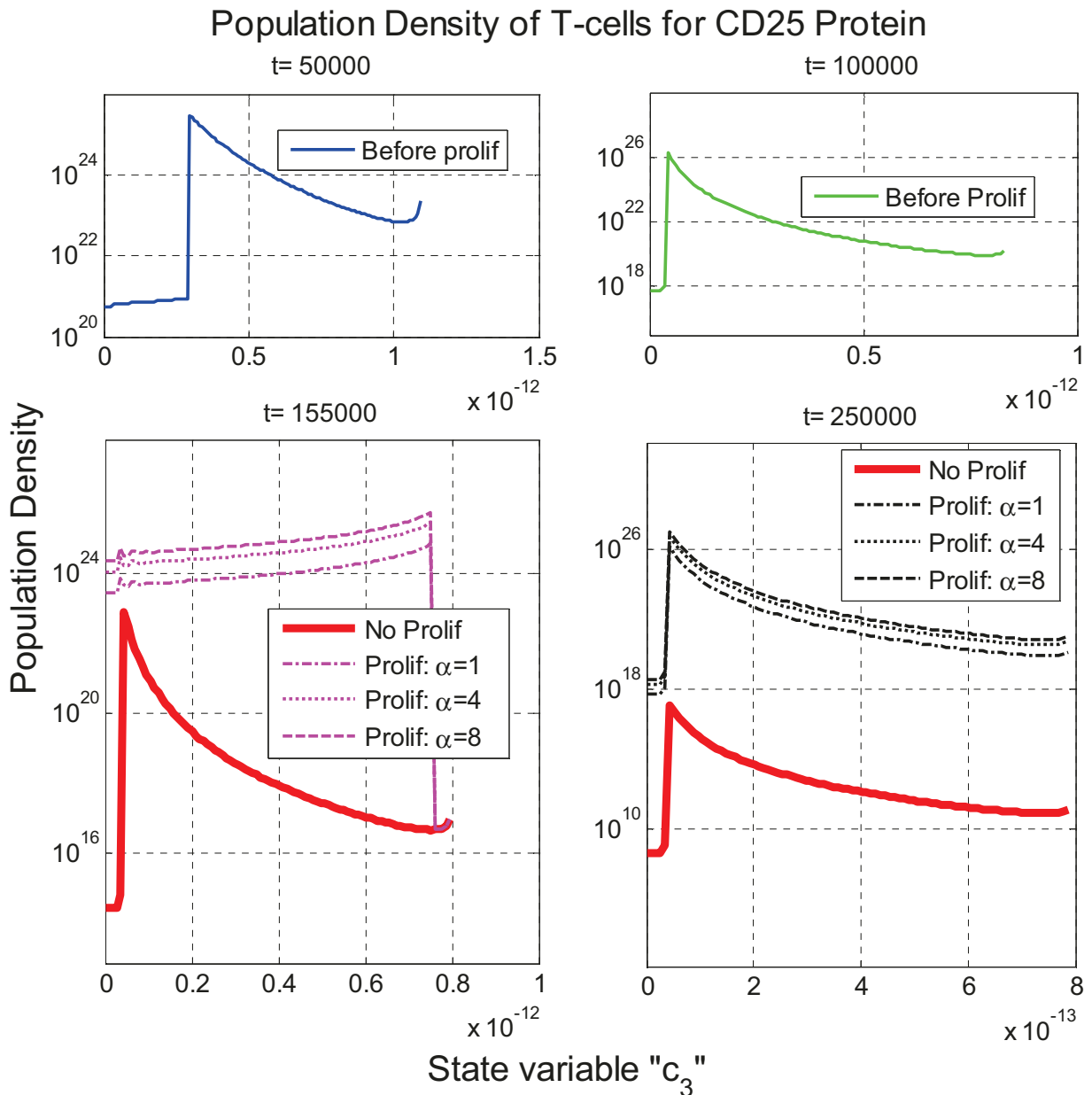


Figure 4.16: Population density of T-cells with CD25 surface protein. The threshold level at which the division starts is  $c_6 = 5.6 \times 10^{-4} \text{ mol.m}^{-3}$  and the time is after almost a day ( $t = 100,000 \text{ s}$ ). The daughter cells start activating after  $t = 150,000 \text{ s}$ . 'No Prolif' is the 'No Proliferation' curve showing the population density of T-cells without including daughter cells.

## 4.3 Results

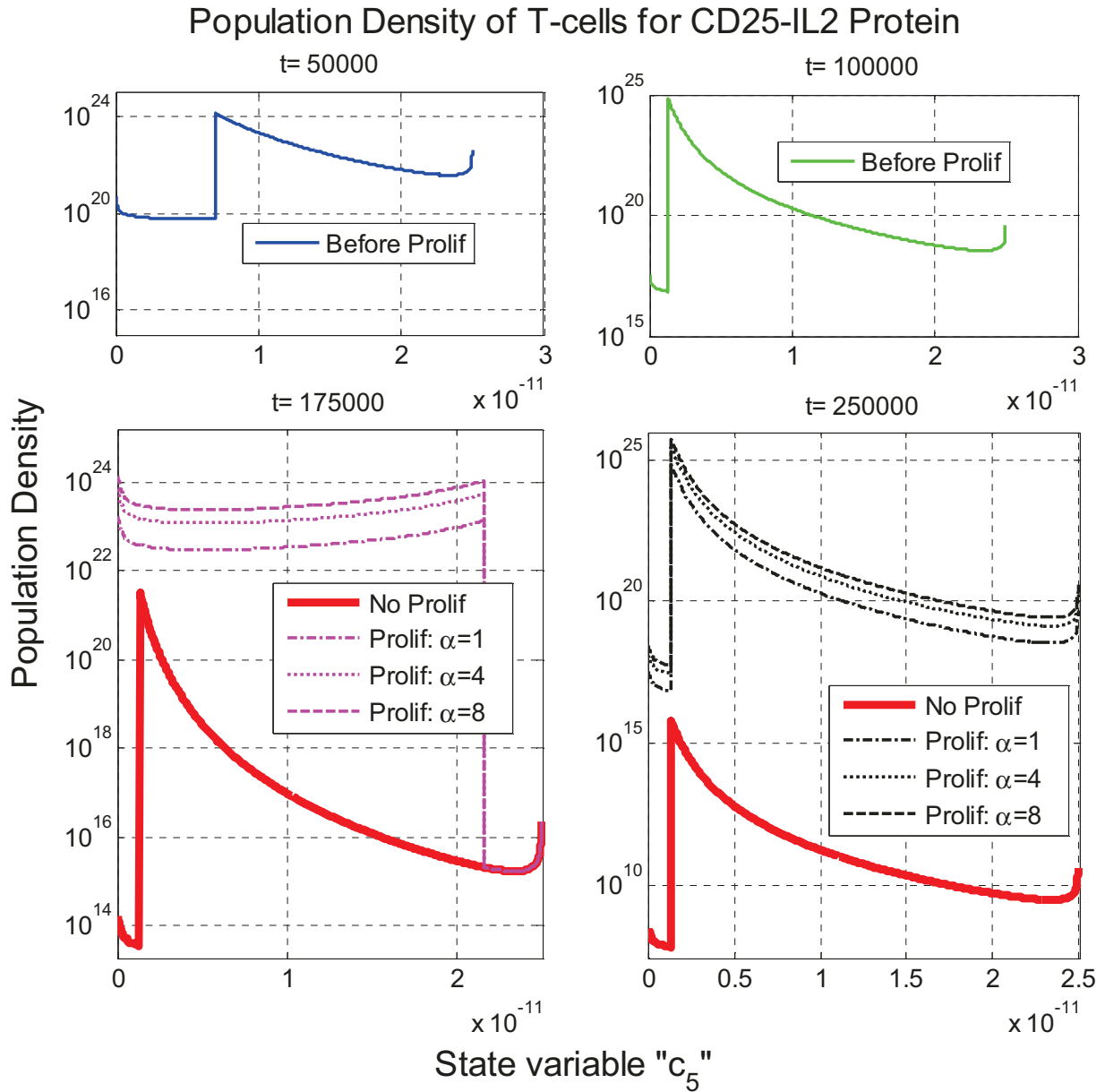


Figure 4.17: Population density of T-cells with surface binding CD25-IL2. The threshold level at which the division starts is  $c_6 = 5.6 \times 10^{-4} \text{ mol.m}^{-3}$  and the time is after almost a day ( $t=100,000 \text{ s}$ ). The daughter cells start activating after  $t=150,000 \text{ s}$ . 'No Prolif' is the 'No Proliferation' curve showing the population density of T-cells without including daughter cells.

### 4.3.2 Hypothesis 2

The hypothesis 2 is proposed to investigate the behavior of T-cells at population level after the proliferation when the daughter cells are distributed over the activation times. This hypothesis does not affect the reaction rates of the protein concentrations. Therefore, the protein dynamics at a single T-cell remains same as described in the Hypothesis 1. Here, again, we have two cases

## 4.3 Results

---

depending upon their level of complexity. Each case investigate the proposed hypothesis on the three surface proteins CD3, CD25 and CD25-IL2. The population dynamics of T-cells for CD25-IL2i protein can be followed from the Hypothesis 1 since it is discussed only before proliferation of T-cells.

### 1) *Without Crossing*

The population densities for the surface proteins are examined before and after proliferation. The population density of daughter T-cells is distributed over time ( $\alpha(t)$ ) among the initial population density after proliferation. Four distinct values of  $\alpha(t)$  are chosen by making combinations of the values for the parameters  $q_1$  and  $q_2$ . The solutions of the density functions are compared graphically between the ‘no proliferation’ and ‘proliferation’ as shown in the Figure 4.18, Figure 4.19 and Figure 4.20.

Each pair of parameters,  $q_1$  and  $q_2$ , has shown a drastic change in the population density of T-cells. It is observed that the increase in the parameter value  $q_1$  increases the number of activated T-cells while the increase in the value of the parameter  $q_2$  decreases the population density of T-cells. In the Figures, although the density of T-cells seems to be overlapped each other for the parametric pairs  $q_1, q_2 = 1 \times 10^{-3}$  and  $q_1, q_2 = 4 \times 10^{-3}$  but actually the curves are near to each other due to small variation in the parametric values. We can observe the distance between the curves for the parametric pairs  $q_1, q_2 = 1 \times 10^{-3}$  and  $q_1, q_2 = 4 \times 10^{-3}$  in the zoomed plots in the Figure 4.19 and Figure 4.20.

The population density is studied at two distinct times where a discontinuity is coming in the middle of the curve for time  $t=175,000$  in the Figure 4.18 and for time  $t=155,000$  in the Figure 4.19 and Figure 4.20. The discontinuity in the population density of T-cells for CD3 protein in the Figure 4.18 at  $t=175000$  moves towards the left hand side that can be observed at time  $t=250,000$ . On the other hand the discontinuities in CD25 and CD25-IL2 proteins move towards the right hand side as shown in the Figure 4.19 and Figure 4.20. These behaviors show that the daughters T-cells are mounting their protein concentrations with the passage of time.

### 4.3 Results

#### Population Density of T-cells for CD3 Protein

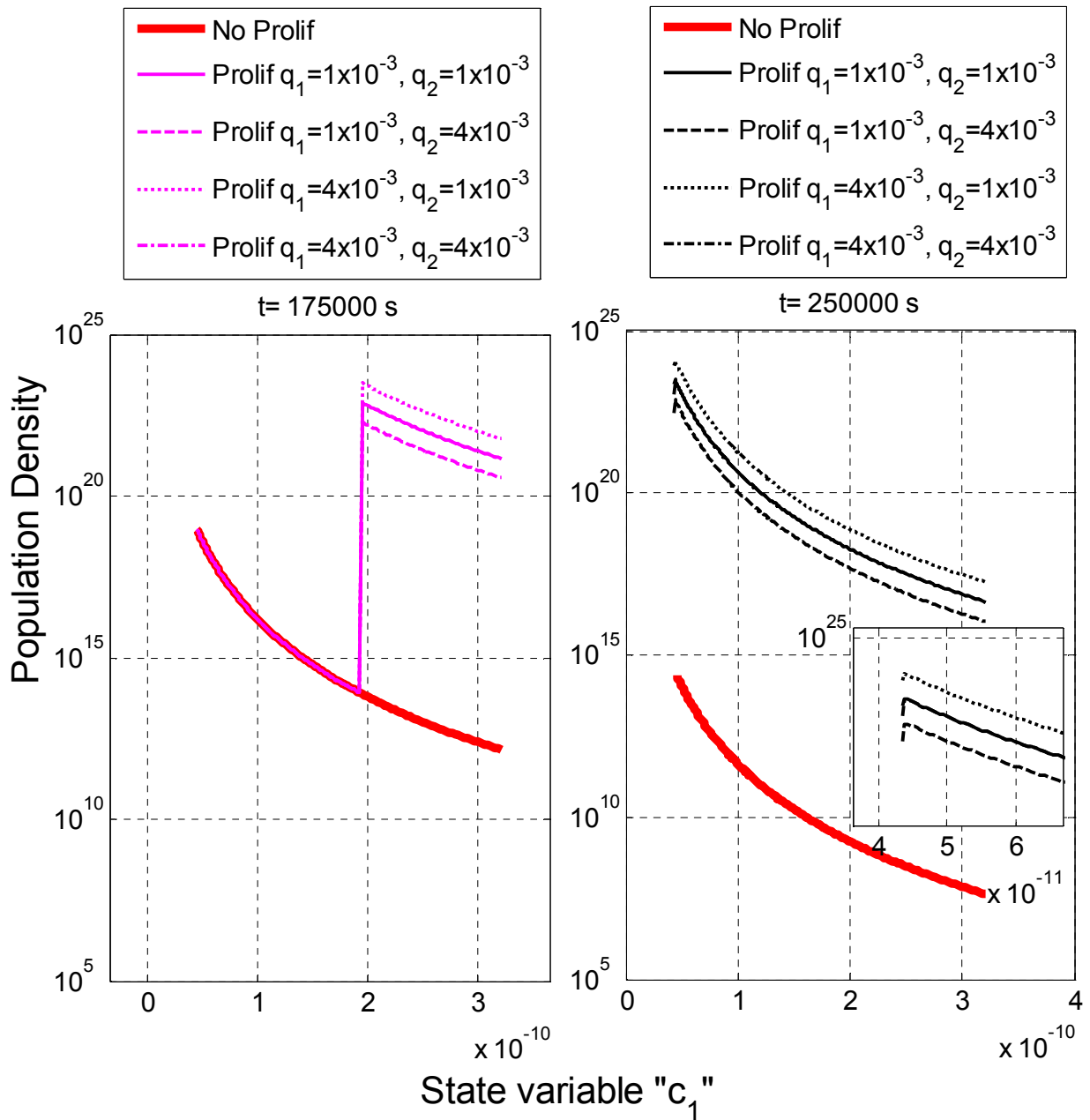


Figure 4.18: Population density of T-cells for CD3 protein. The threshold level at which the division starts is  $c_6 = 10^{-3} \text{ mol.m}^{-3}$  and the time is almost a day ( $t=100,000 \text{ s}$ ). The daughter cells start activating after  $t=150,000 \text{ s}$ .

## 4.3 Results

### Population Density of T-cells for CD25 Protein

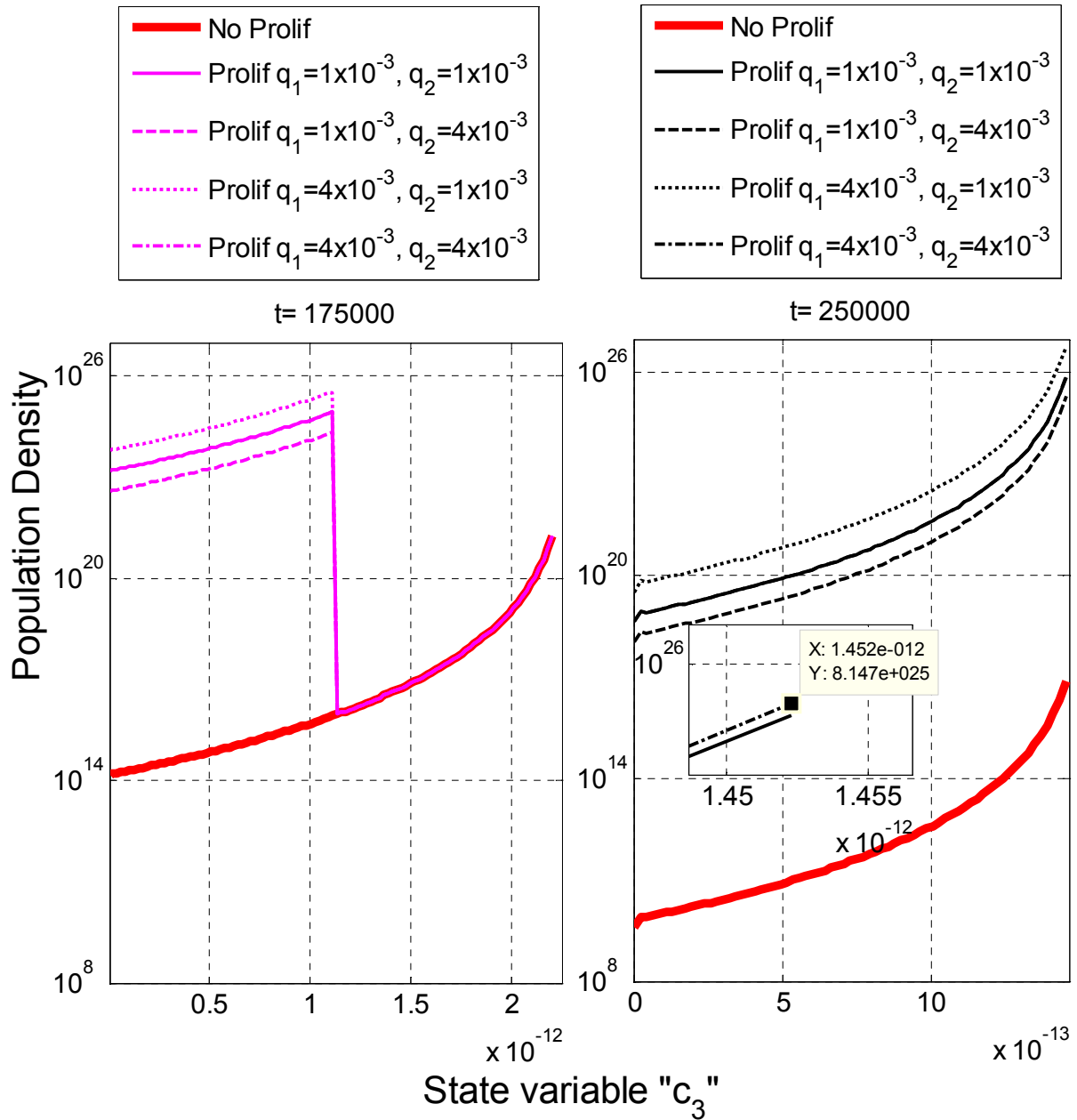


Figure 4.19: Population density of T-cells for CD25 protein. The threshold level at which the division starts is  $c_6 = 10^{-3} \text{ mol.l}^{-3}$  and the time is almost a day ( $t=100,000 \text{ s}$ ). The daughter cells start activating after  $t=150,000 \text{ s}$ .

## 4.3 Results

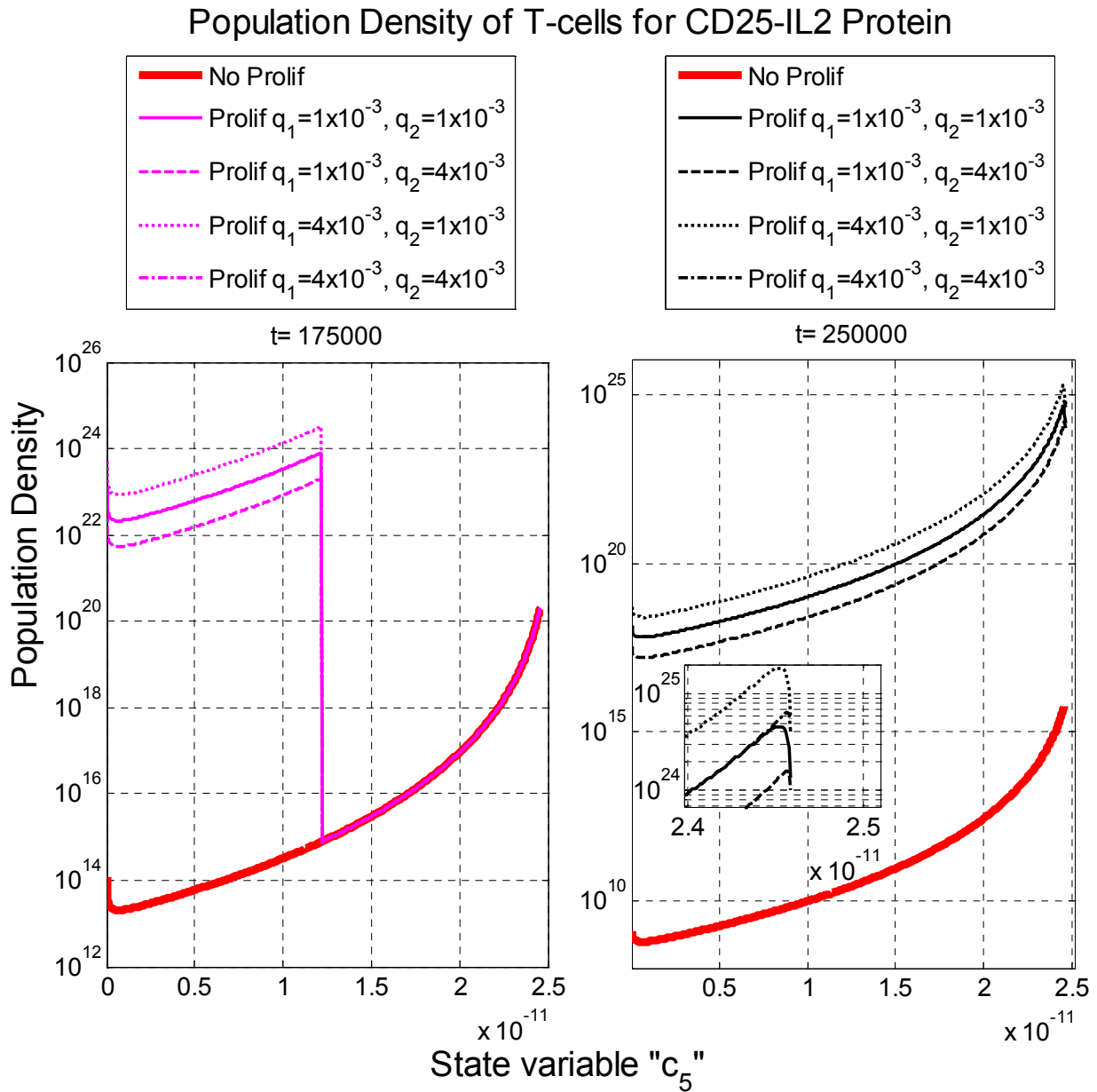


Figure 4.20: Population density of T-cells for CD25-IL2 protein. The threshold level at which the division starts is  $c_6 = 10^{-3} \text{ mol.m}^{-3}$  and the time is almost a day ( $t=100,000 \text{ s}$ ). The daughter cells start activating after  $t=150,000 \text{ s}$ .

### II) Crossing

The protein dynamics for this section can be followed from the Figure 4.13. Also the population dynamics of T-cells for the internalized protein (CD25-IL2i) concentration can be viewed by the Figure 4.14. The population densities for the surface proteins are investigated with and without

## 4.3 Results

proliferation. The solution is analyzed at four distinct parametric pairs for distribution of daughter T-cells over time as shown in the Figure 4.21, Figure 4.22 and Figure 4.23.

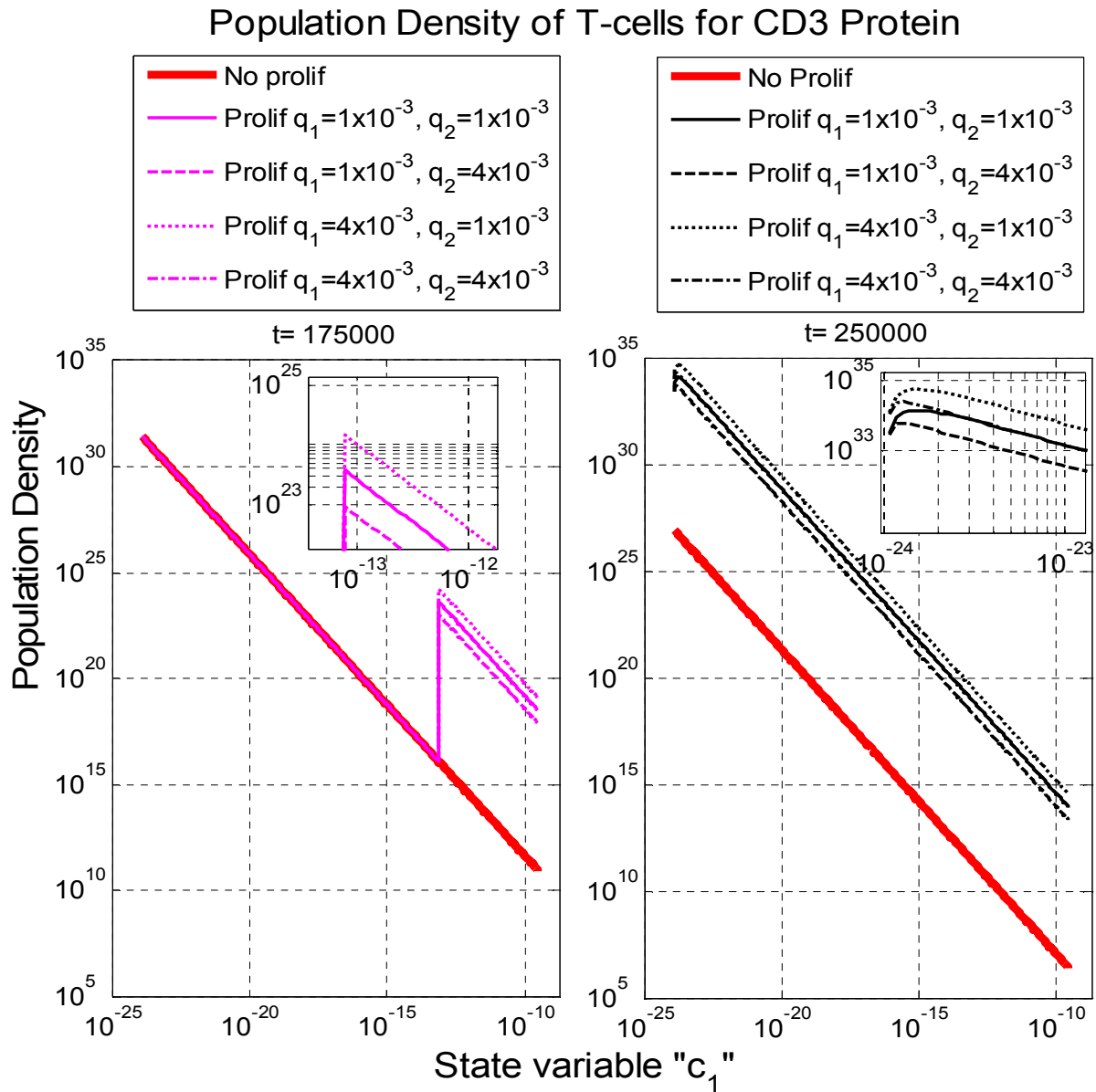


Figure 4.21: Population density of T-cells for CD3 protein. The threshold level at which the division starts is  $c_6 = 5.6 \times 10^{-4} \text{ mol.m}^{-3}$  and the time is almost a day ( $t=100,000 \text{ s}$ ). The daughter cells start activating after  $t=150,000 \text{ s}$ .

We observe the similar phenomena as defined in the above section of Without Crossing but now the reaction rate is fast and therefore we have crossing in the solution curves as we discussed in

## 4.3 Results

the Figure 4.13. The discontinuity rear in CD3 and discontinuity front in CD25 and CD25-IL2 move in the directions described in the Figure 4.6.

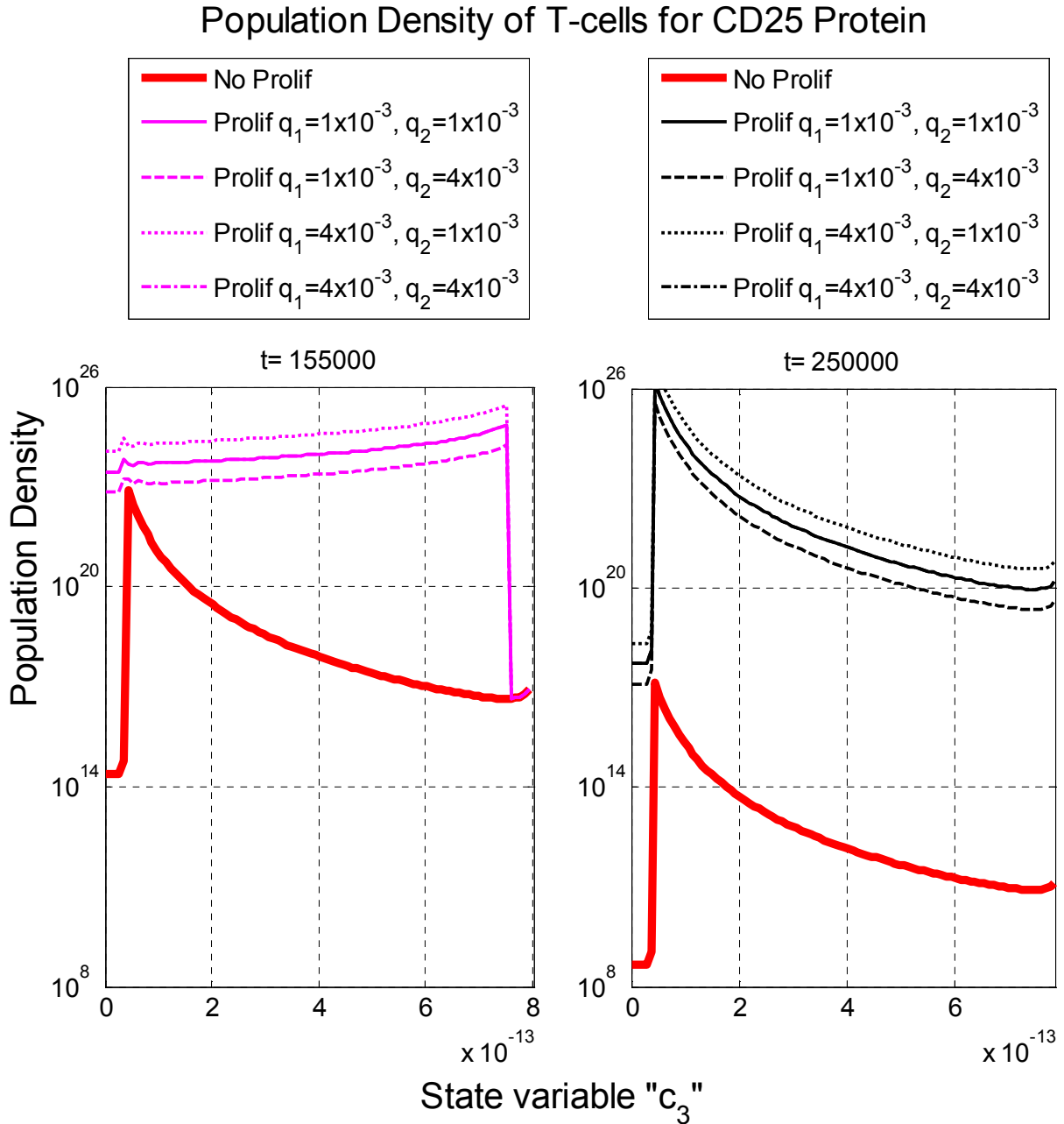


Figure 4.22: Population density of T-cells for CD25 protein. The threshold level at which the division starts is  $c_6 = 5.6 \times 10^{-4} \text{ mol.m}^{-3}$  and the time is almost a day ( $t=100,000 \text{ s}$ ). The daughter cells start activating after  $t=150,000 \text{ s}$ .

One can observe in the Figure 4.21, the simulation time taken is  $t=175,000\text{s}$  while in the Figure 4.22 and Figure 4.23 the simulation time taken is  $t=155,000\text{s}$  in order to observe a discontinuity

### 4.3 Results

front and the overlapping between 'no-proliferation' and 'proliferation'. The time variation is due to the parametric change in the reaction rate.

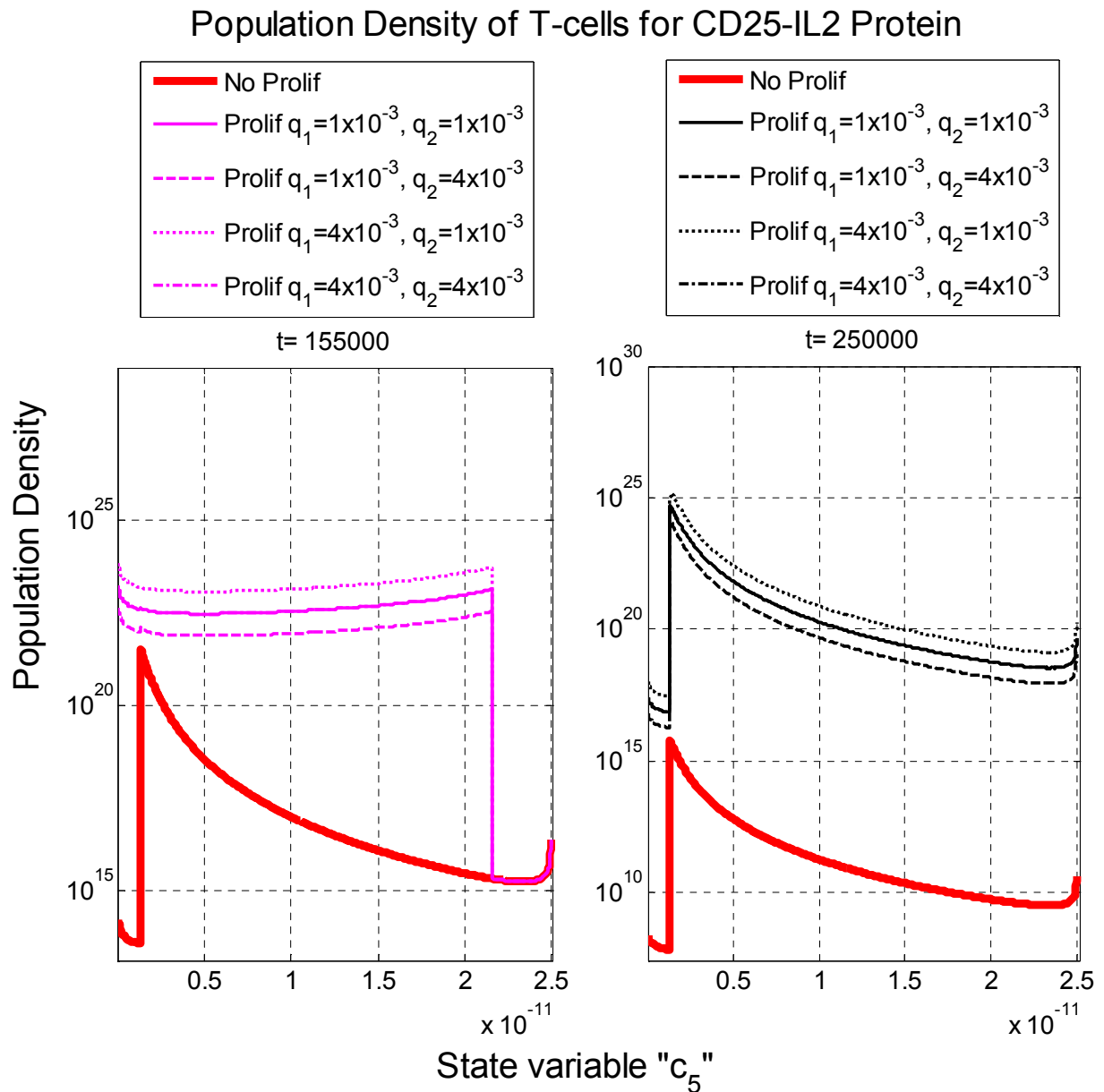


Figure 4.23: Population density of T-cells for CD25-IL2 protein. The threshold level at which the division starts is  $c_5 = 5.6 \times 10^{-4} \text{ mol.m}^{-3}$  and the time is almost a day ( $t = 100,000 \text{ s}$ ). The daughter cells start activating after  $t = 150,000 \text{ s}$ .

## 4.3 Results

### 4.3.3 Relation between Hypothesis 1 and Hypothesis 2

The results in the Sections 4.3.1 and 4.3.2 have shown very similar behavior between the hypotheses 1 and 2 for the population density of T-cells as shown in the Figures 4.10 – 4.23. This is because of the parameters  $q_1$  and  $q_2$  that are chosen for the daughters cells distribution over time  $\alpha(t)$ . However, the difference can be increased by varying the value of  $q_2$  as shown in the Figure 4.24. We can observe that the decrease in the value of the parameter  $q_2$  not only increase the population density but also it varies the slope of the curve for population density.

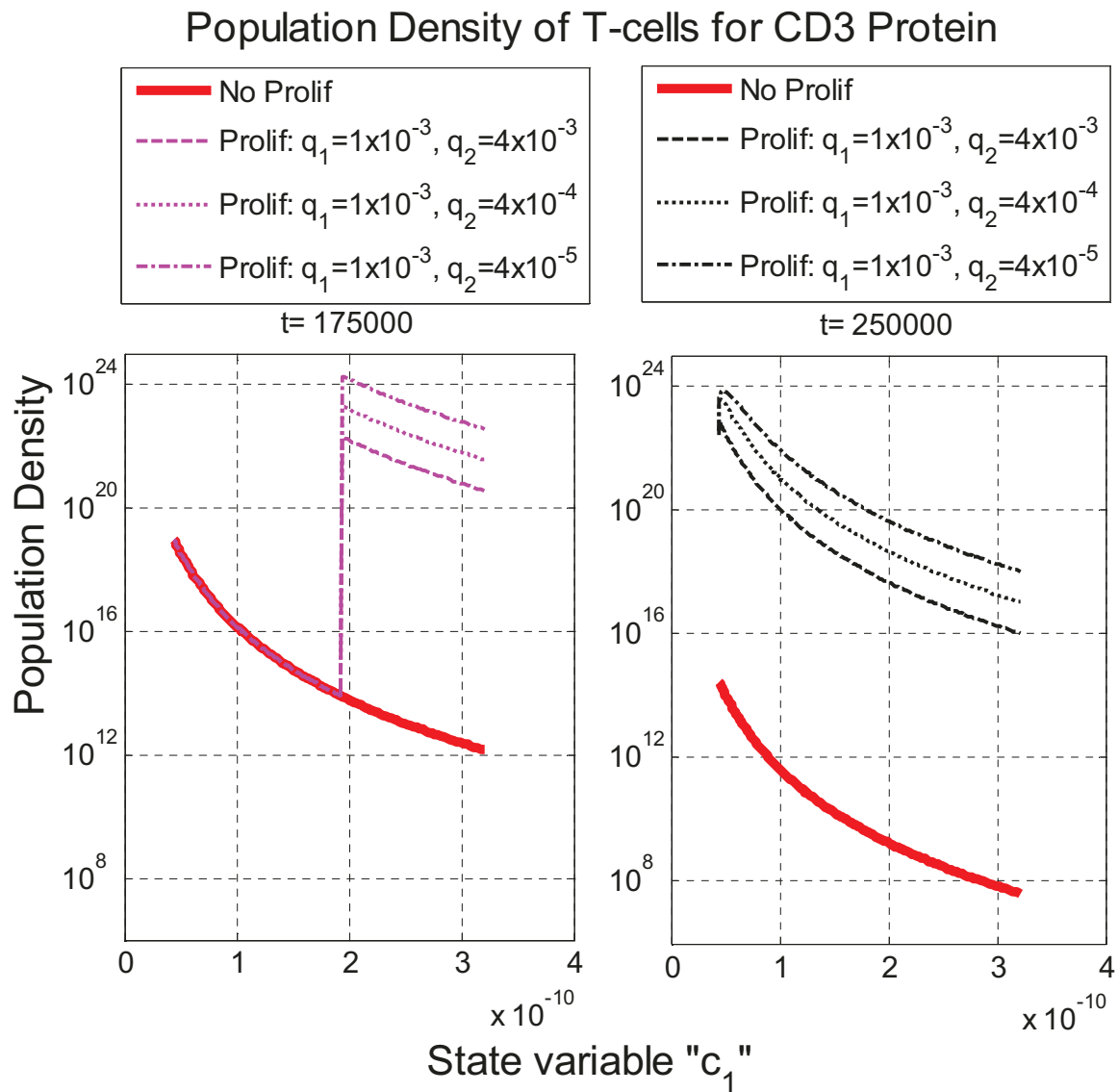


Figure 4.24: Effect of the variation in the value of  $q_2$  on the population density of CD3 T-cells.

## 4.3 Results

---

The similar behaviors can be observed for the population density of T-cells with CD25 and CD25-IL2 proteins.

Let us consider that the daughters T-cells lie at the beginning, i.e. just after the proliferation. Therefore the distribution of daughter T-cells over time 't' will approach a constant value  $\alpha$ . It makes a relation between the hypotheses 1 and 2 by the following equation:

$$\begin{aligned}\alpha &= \int_0^{\infty} \alpha(t) dt \\ &= \lim_{t_{\max} \rightarrow \infty} \int_0^{t_{\max}} q_1 e^{-q_2 t} dt = \frac{q_1}{q_2}\end{aligned}\tag{4.10}$$

In other words, by following the above equality, the daughter distribution over time defined by the hypothesis 2 will approach the number of daughter T-cells undergoing the process of activation after proliferation in the hypothesis 1.

Let us choose  $q_1 = q_2 = 10^{-3}$  then the constant  $\alpha = 1$ . In the Figure 4.25, a comparison has been done by choosing the same parameters as defined before for case of Without Crossing of curves. The reaction rate for CD3 protein concentration is same as shown in the Figure 4.8.

For the hypothesis 2, the distribution of T-cells over time is calculated by using Eq. (4.6). The solutions have shown an overlapping behavior. A small variation in the curves has been observed at time  $t=250,000$ , however, if we vary the parameter  $q_1$  or  $q_2$  we can have more differences between the two curves as we have observed in the Figure 4.24.

The relation between hypothesis 1 and 2 can be observed for the other proteins, i.e. CD25 and CD25-IL2. Moreover, the crossing case defined in the Sections 4.3.1 and 4.3.2 can also give us the similar remarks. Now we move towards the hypothesis 3 that is proposed in a different way.

## 4.3 Results

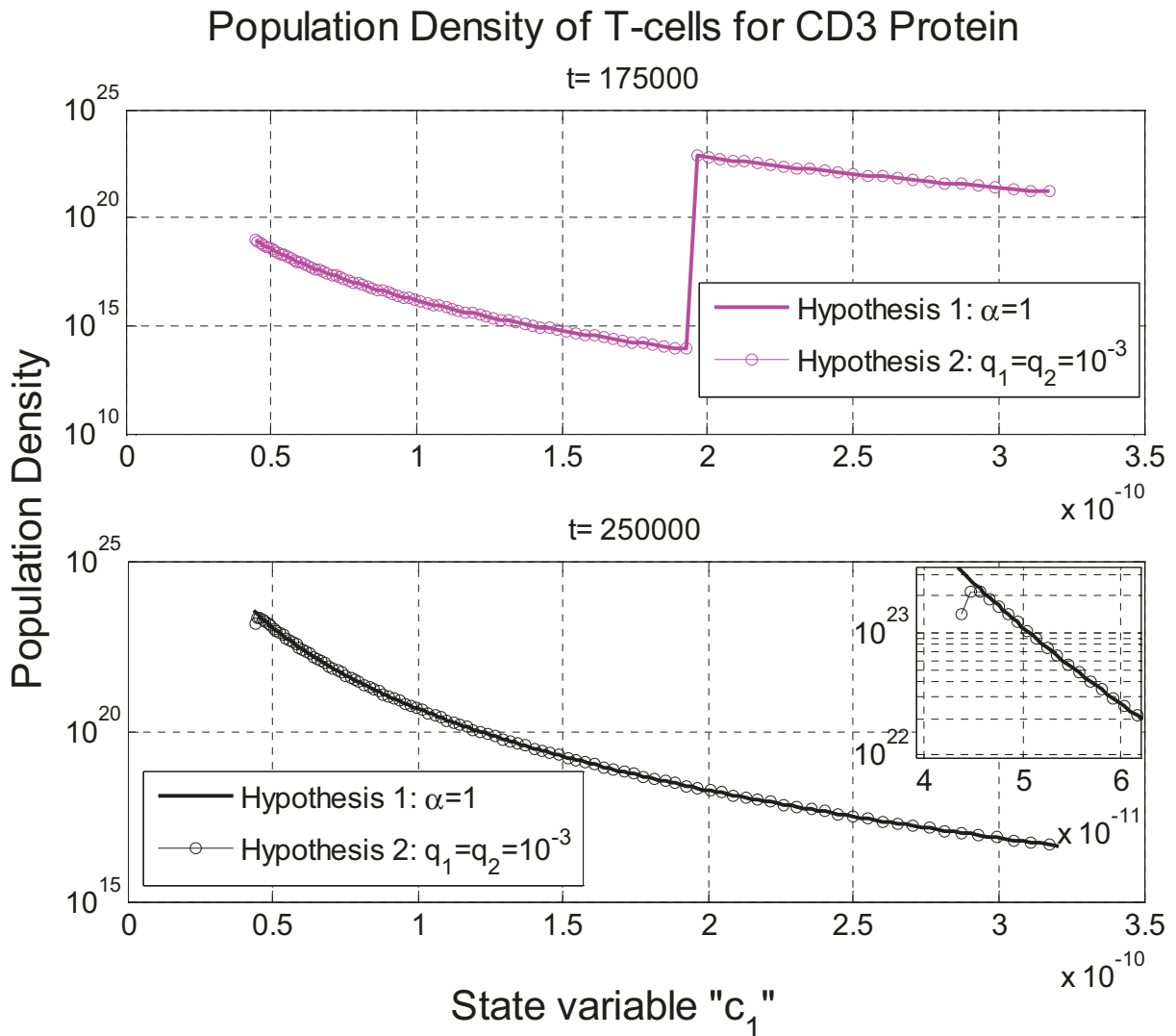


Figure 4.25: For CD3 protein, the population density of T-cells by using hypothesis 2 approaches the population density of T-cells by using hypothesis 1 if the Eq (4.10) holds.

### 4.3.4 Hypothesis 3

The proposition of hypothesis 3 originates the idea of considering daughter cells as non-activated T-cells. All the daughter T-cells which start their activation process after proliferation (at time  $t = \tilde{t} + T$ ) are according to the flow of parent T-cells at their threshold ( $t = \tilde{t}$ ). The threshold and the reaction rate are same as discussed in previous hypotheses under the subsections Without Crossing and Crossing respectively.

## 4.3 Results

---

In this section, the results have been found for the surface proteins before and after proliferations. After proliferation, the number of daughter T-cells (per parent T-cell) which undergo the process of activation are chosen  $\alpha = 1, 4$  and  $8$ . The dynamical changes in the population density of T-cells are also observed before proliferation. At the time  $t \geq \tilde{\tau} + T$ , the population density is compared between with and without daughter T-cells (proliferation and no proliferation) in order to validate the simulation after proliferation.

### 1) *Without Crossing*

The protein dynamics at a single T-cell is shown in Figure 4.8. We choose the same kinetic parameters as discussed in the previous hypotheses. The population density of T-cells for internalized protein CD25-IL2i protein is presented in Figure 4.9. For the surface proteins, the T-cell dynamics at the population level is proposed by the activation rate given by the Eq. (4.9). In the figures, “No Prolif” is the ‘No Proliferation’ curve showing the population density of T-cells without including daughter cells.

The population density is observed before and after proliferation at four distinct times for the surface proteins as shown in Figure 4.26, Figure 4.27 and Figure 4.28. We observe the same phenomenon for the population density of T-cells before proliferation. After proliferation, the population density varies according to the concentration of proteins as huge population of daughter T-cells starts activation which are considered as non-activated in the hypothesis 1 and 2.

In the Figures, we can observe that there is no discontinuity coming; instead there is a drastic increase in the population density, after proliferation, which shows a curvy behavior. This drastic increase is observed at the time  $t=175,000s$  in Figure 4.26 that is moving towards left hand side (LHS) and at  $t=250,000s$ , the figure shows that the daughter T-cells are distributed over all the given range of concentration. On the other hand, Figure 4.27 and Figure 4.28 also shows a drastic change but this drastic change moves from left to right hand side (RHS), in contrary to Figure 4.26. The drastic change covers the whole concentration axis that is shown in the figures, Figure 4.27 and Figure 4.28, at time  $t=250,000s$  as the daughter T-cells get distributed over the same range of the concentration of protein as the T-cells with no proliferation.

## 4.3 Results

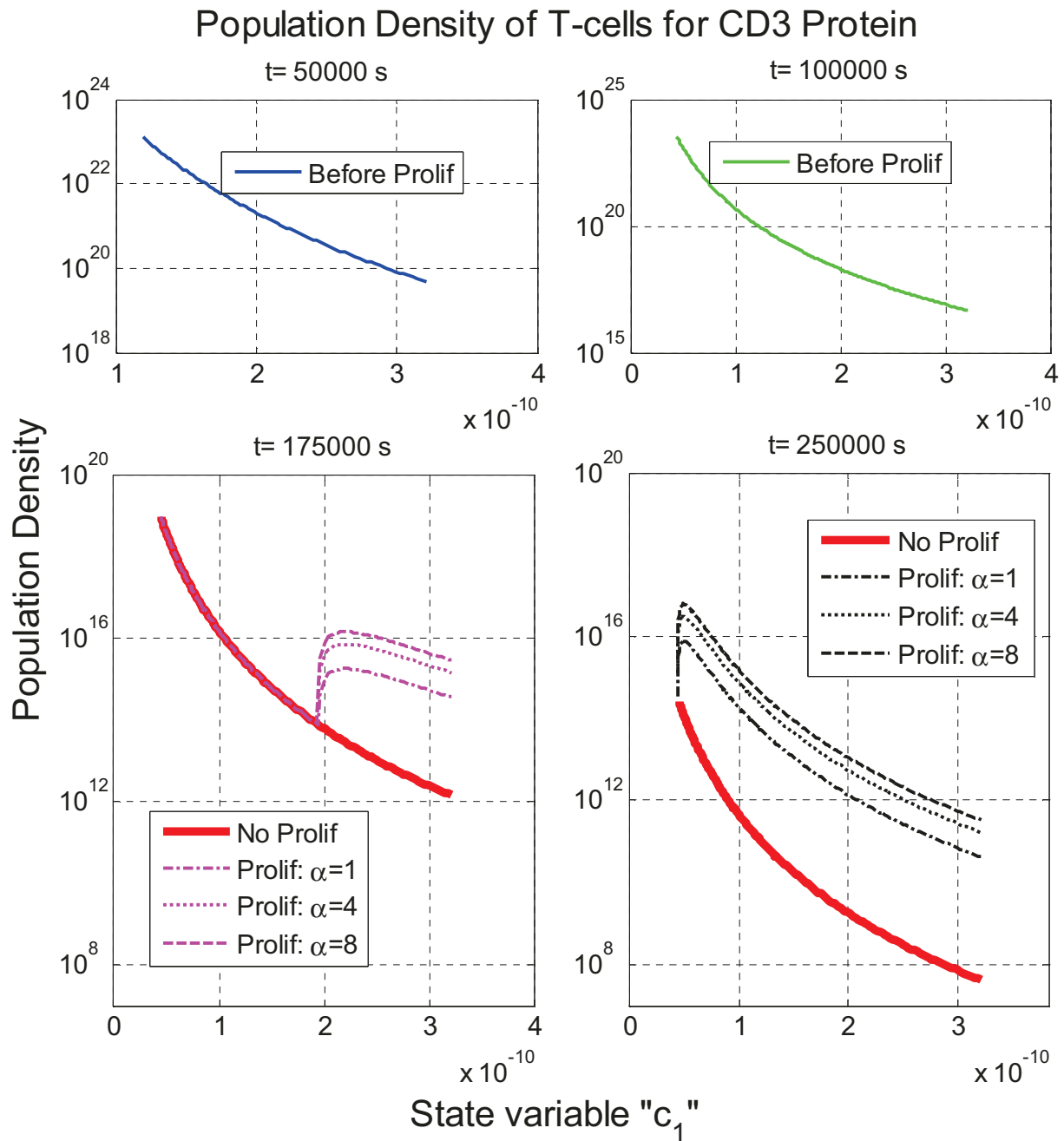


Figure 4.26: Population density of T-cells for CD3 protein. The threshold level at which the division starts is  $c_6 = 10^{-3} \text{ mol.m}^{-3}$  and the time is almost a day ( $t = 100,000$  s). The daughter cells start activating after  $t = 150,000$  s.  $\alpha$  is the number of daughter cells undergo in the process of activation. The time  $t = 50,000$  s and the time  $t = 100,000$  s are before proliferation while the time  $t = 175,000$  s and  $t = 250,000$  s are after proliferation.

## 4.3 Results

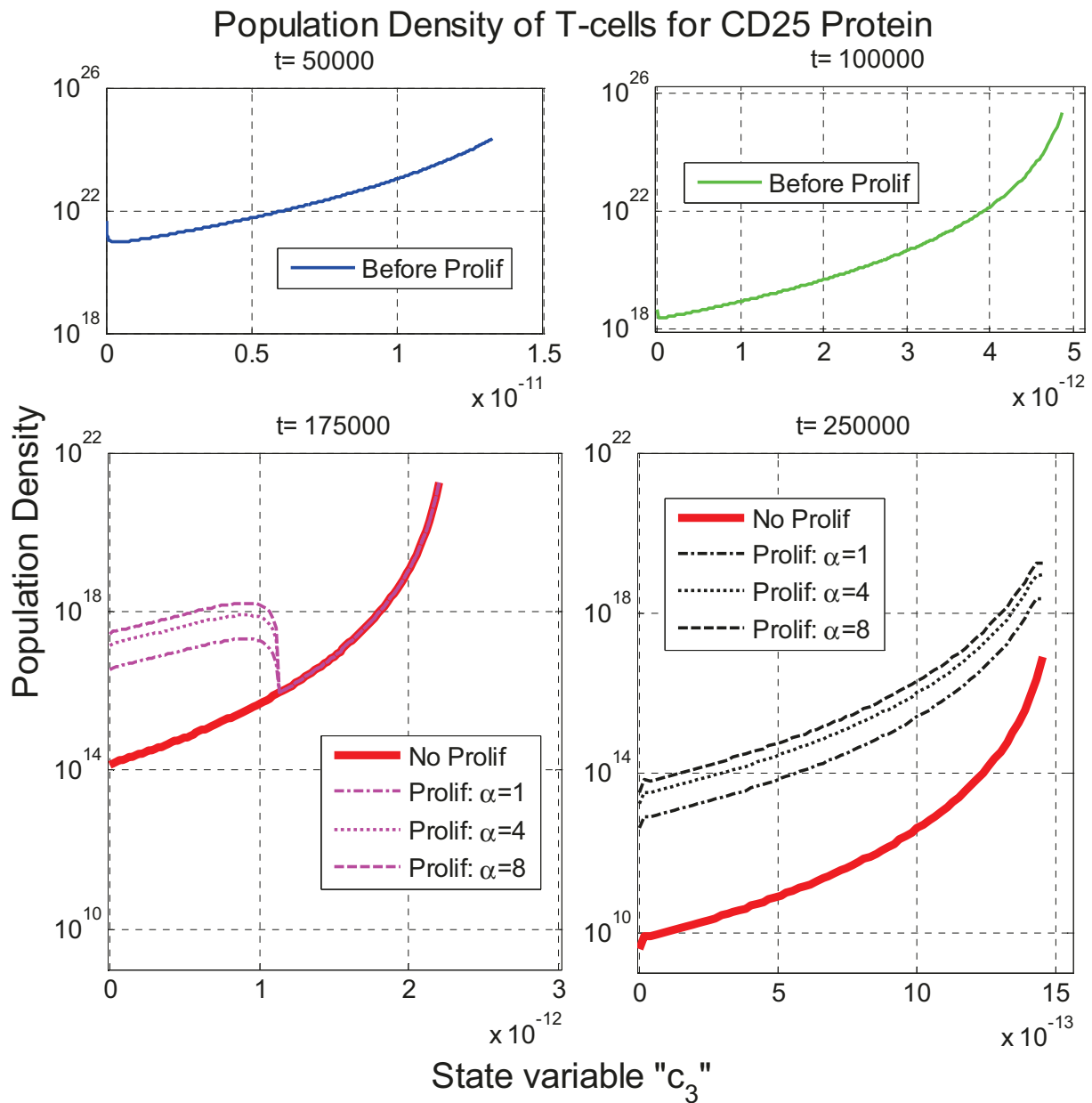


Figure 4.27: Population density of T-cells for CD25 protein. The threshold level at which the division starts is  $c_6 = 10^{-3} \text{ mol.m}^{-3}$  and the time is almost a day ( $t = 100,000 \text{ s}$ ). The daughter cells start activating after  $t = 150,000 \text{ s}$ .  $\alpha$  is the number of daughter cells undergo in the process of activation. The time  $t = 50,000 \text{ s}$  and the time  $t = 100,000 \text{ s}$  are before proliferation while the time  $t = 175,000 \text{ s}$  and  $t = 250,000 \text{ s}$  are after proliferation.

## 4.3 Results

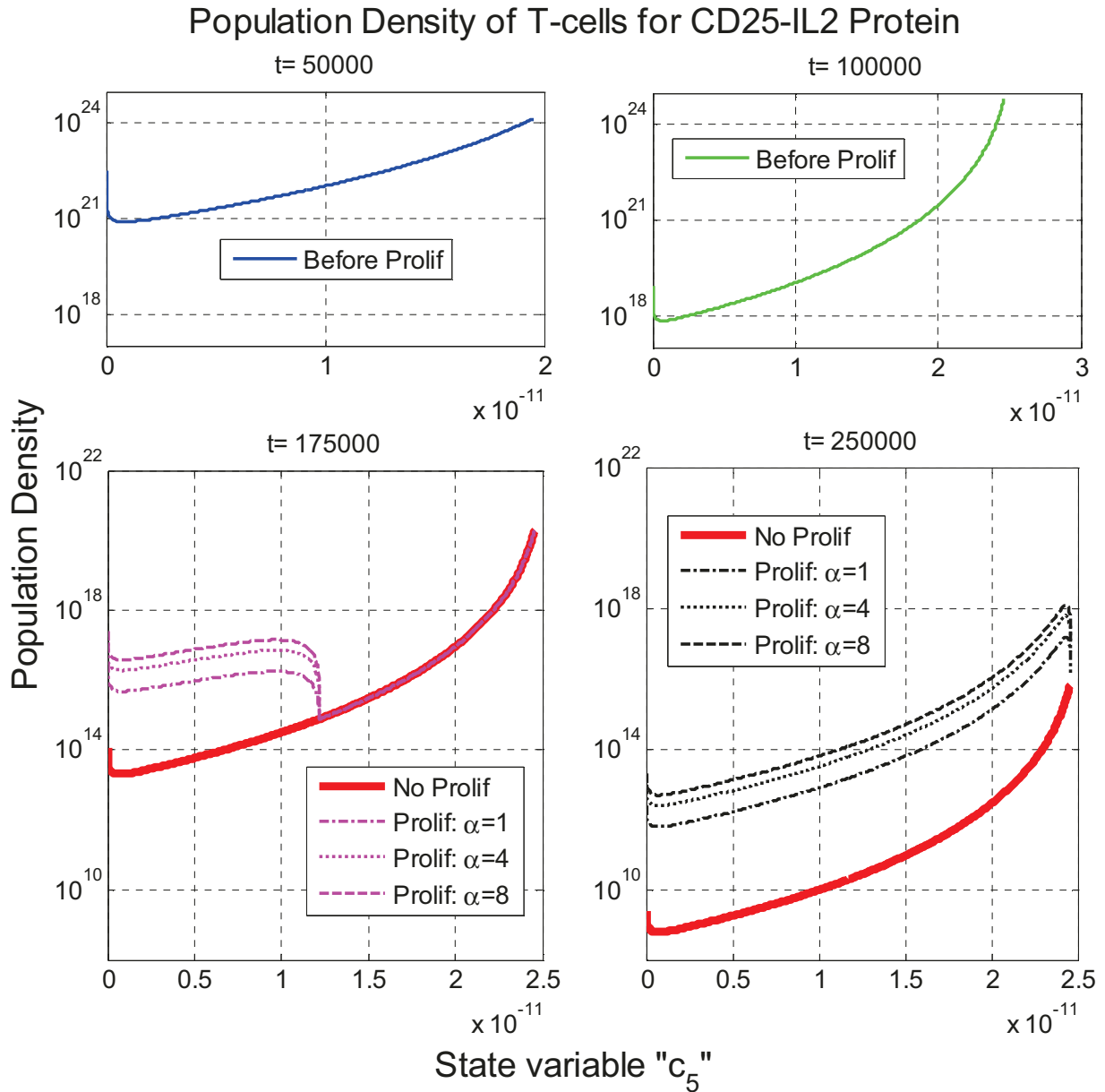


Figure 4.28: Population density of T-cells for CD25-IL2 protein. The threshold level at which the division starts is  $c_6 = 10^{-3} \text{ mol.m}^{-3}$  and the time is almost a day ( $t=100,000 \text{ s}$ ). The daughter cells start activating after  $t=150,000 \text{ s}$ .  $\alpha$  is the number of daughter cells undergo in the process of activation. The time  $t=50,000 \text{ s}$  and the time  $t=100,000 \text{ s}$  are before proliferation while the time  $t=175,000 \text{ s}$  and  $t=250,000 \text{ s}$  are after proliferation.

### II) Crossing

The crossing of curves for the surface protein concentrations CD25 and CD25-IL2 is due to the fast reaction rates as shown in the Figure 4.13. The population density of CD25-IL2i protein is investigated before in the Figure 4.14.

## 4.3 Results

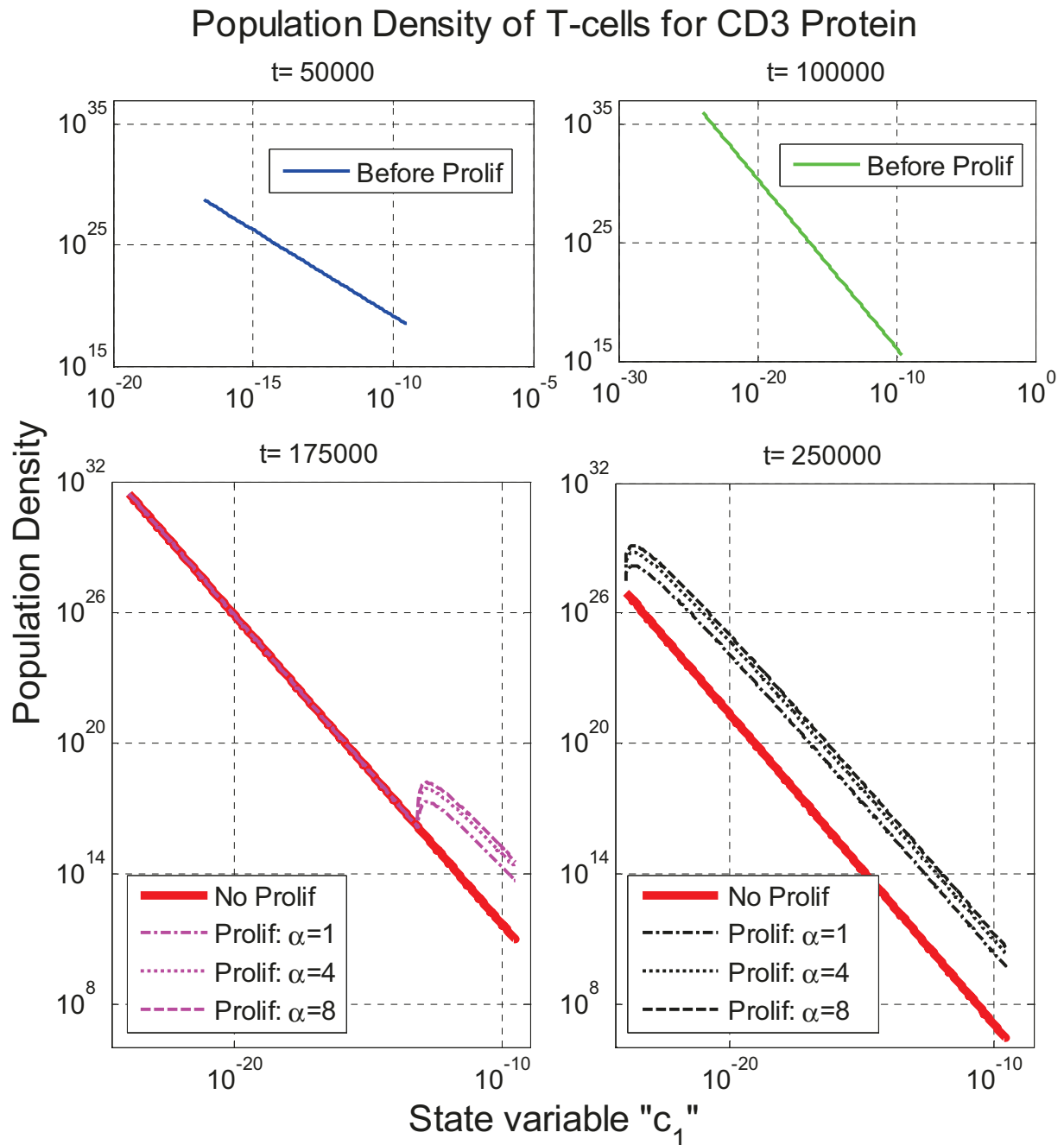


Figure 4.29: Population density of T-cells for CD3 protein. The threshold level at which the division starts is  $c_6 = 5.6 \times 10^{-4} \text{ mol.m}^{-3}$  and the time is almost a day ( $t = 100,000 \text{ s}$ ). The daughter cells start activating after  $t = 150,000 \text{ s}$ .  $\alpha$  is the number of daughter cells undergo in the process of activation. The time  $t = 50,000 \text{ s}$  and the time  $t = 100,000 \text{ s}$  are before proliferation while the time  $t = 175,000 \text{ s}$  and  $t = 250,000 \text{ s}$  are after proliferation.

The population densities for CD3, CD25 and CD25-IL2 proteins are studied to investigate the dynamical variation of concentrations on the surface of T-cells as shown in Figure 4.29, Figure

## 4.3 Results

4.30 and Figure 4.31. The initial population densities of T-cells after proliferation for surface proteins have shown a drastic increase as we observed in the previous case of Without Crossing. The time taken for CD3 protein is same as in the previous cases while for other surface proteins, the time after proliferation is  $t=155,000s$  in order to observe the drastic change at the front.

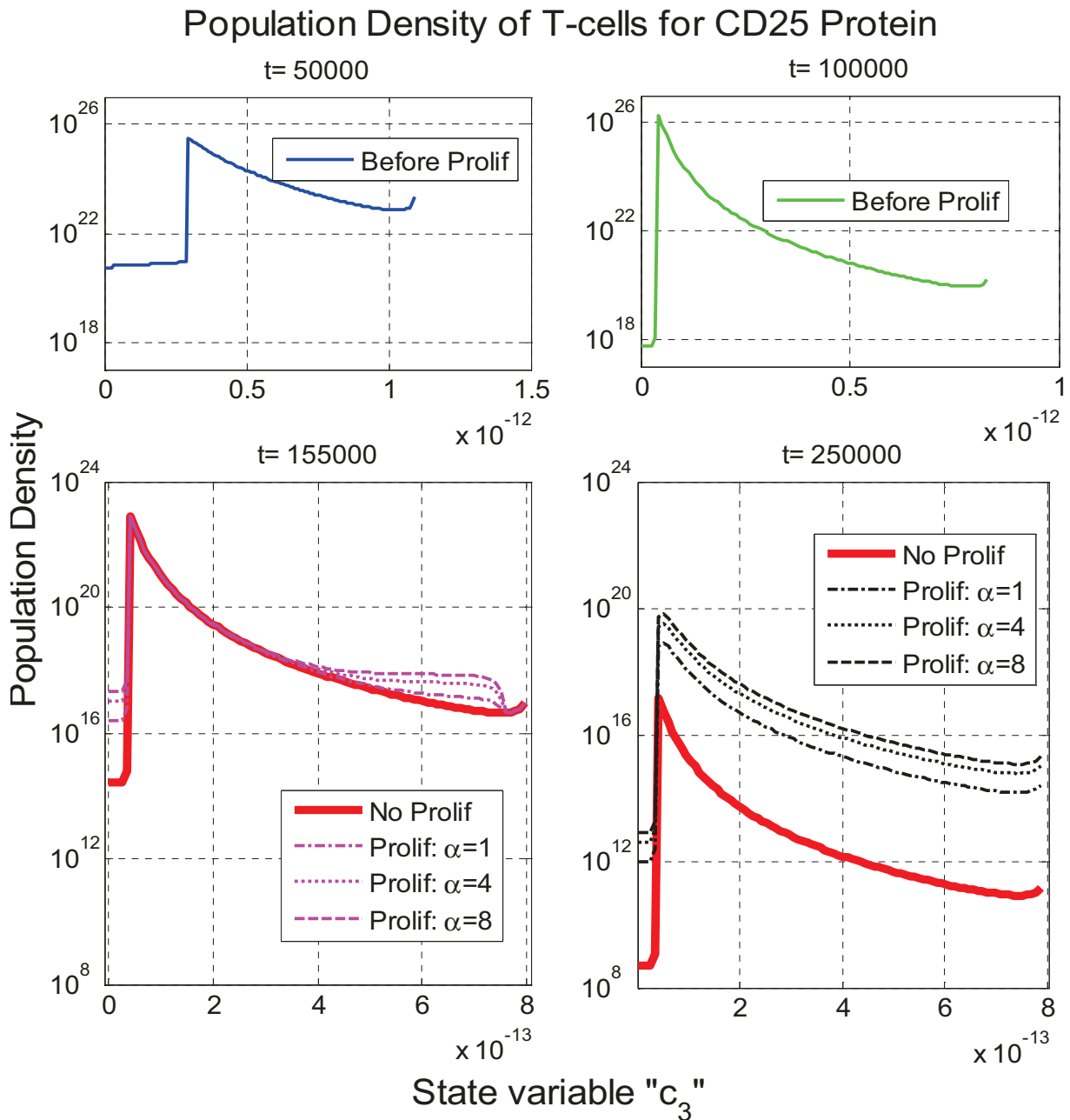


Figure 4.30: Population density of T-cells for CD25 protein. The threshold level at which the division starts is  $c_6 = 5.6 \times 10^{-4} \text{ mol.m}^{-3}$  and the time is almost a day ( $t=100,000 \text{ s}$ ). The daughter cells start activating after  $t=150,000 \text{ s}$ .  $\alpha$  is the number of daughter cells undergo in the process of activation. The time  $t=50,000 \text{ s}$  and the time  $t=100,000 \text{ s}$  are before proliferation while the time  $t=155,000 \text{ s}$  and  $t=250,000 \text{ s}$  are after proliferation.

## 4.3 Results

In contrast to the subsection Without Crossing of the section 4.3.4, the population density for the concentrations of CD25 and CD25-IL2 proteins moves the drastic change from the front (RHS) to the back (LHS). This is due to the crossing of curves in the reaction rate: Figure 4.13. This phenomenon is same as in the previous hypotheses for these proteins.

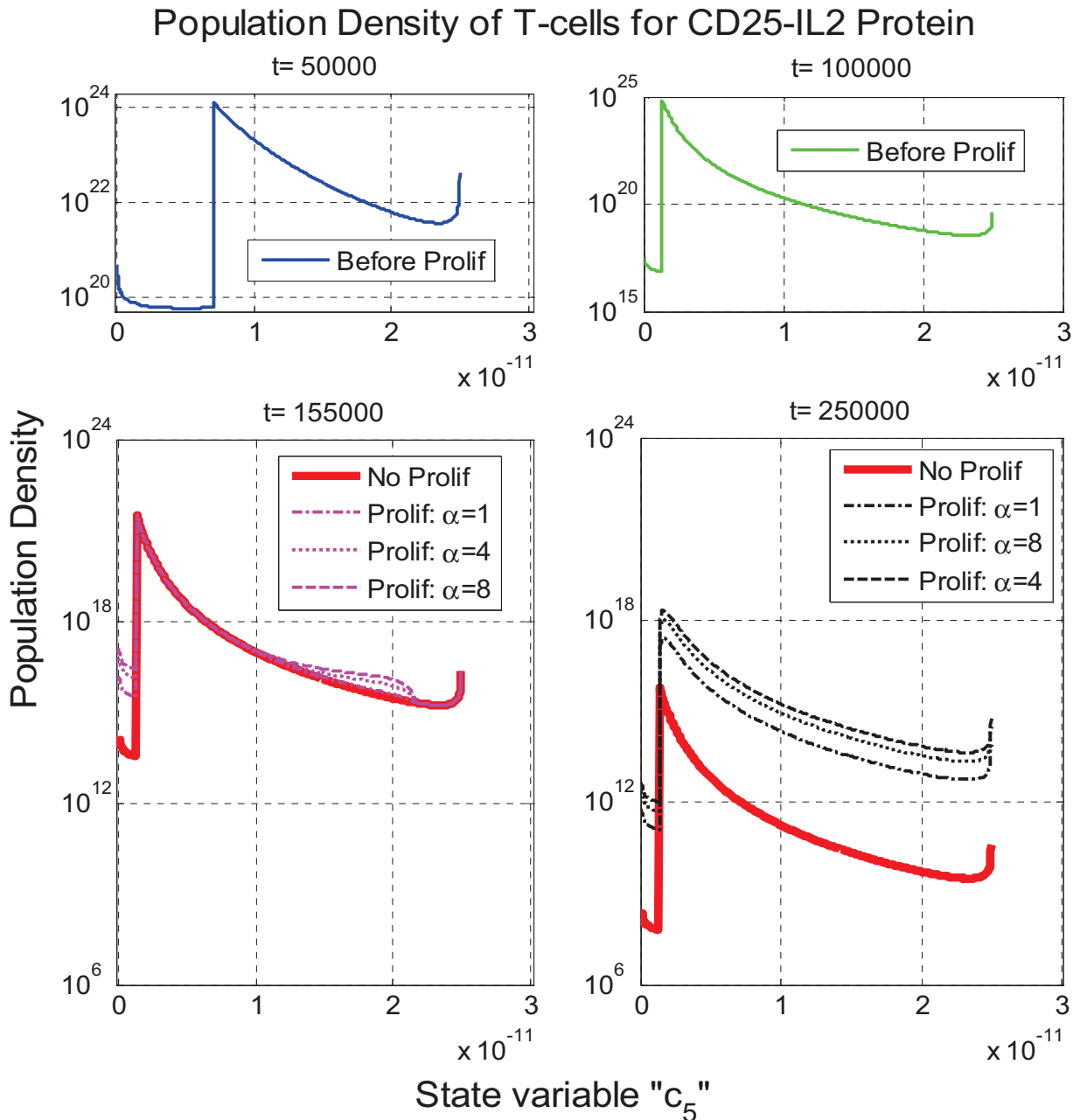


Figure 4.31: Population density of T-cells for CD25-IL2 protein. The threshold level at which the division starts is  $c_6 = 5.6 \times 10^{-4} \text{ mol.m}^{-3}$  and the time is almost a day ( $t=100,000 \text{ s}$ ). The daughter cells start activating after  $t=150,000 \text{ s}$ .  $\alpha$  is the number of daughter cells undergo in the process of activation. The time  $t=50,000 \text{ s}$  and the time  $t=100,000 \text{ s}$  are before proliferation while the time  $t=155,000 \text{ s}$  and  $t=250,000 \text{ s}$  are after proliferation.

## 4.4 Conclusion

### 4.4 Conclusion

The proposed hypotheses for the activation of T-cells after proliferation have covered all the major directions which can be followed by the T-cells during the course of action. The distribution of T-cells after proliferation were defined in first and second hypotheses for time 't' while the distribution of T-cells after proliferation for concentration 'c' is defined in all the three hypotheses. The distribution defined in Eq. (4.4) can give a better analysis for the T-cell population dynamics after proliferation. However, in this study, we investigated the concentration distribution  $D(c)$  defined in Eq. (4.3) as we followed the same distribution of concentration in the Chapter 3. Furthermore, the time distribution  $\alpha(t)$  used in this study has been defined as constant in the Eq. (4.2) and in terms of time in Eq. (4.6).

In the experimental study, particularly by flow cytometry, the mechanism is instructed to display the activated T-cells as well as non-activated T-cells. At the beginning, after proliferation, the population of non-activated T-cells is high that decreases due to their interaction with APC. This gives us an increase in the activated T-cells. This concept makes a

difference with our mathematical findings because we have investigated the T-cells which undergo the process of activation. The non-activated T-cells were defined for the distribution to get the initial population density for activated T-cells but the dynamics of non-activated T-cells is not followed in this study. A graphical relation between the experimental results and the mathematical simulation is shown in the Figure 4.32.

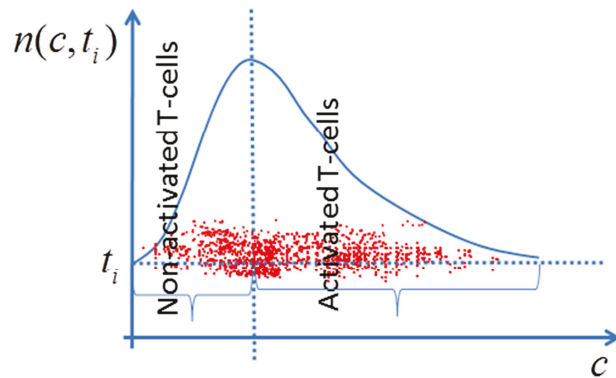


Figure 4.32: Graphical comparison between Biological and Mathematical results..

The hypotheses were defined at different level of complexity. The methodology used to study the division process by means of thresh old of the internalized protein CD25-IL2i is absolutely convincing. The first hypothesis was the simplest one and it was proposed to take the first step

## 4.4 Conclusion

---

towards the daughter T-cell activation. However, the distribution for the initial population density of T-cells over concentration 'c', defined in Eq. (4.4), can be closer to the lifelike phenomenon.

In the second hypothesis, the distribution of daughter T-cells over the time after proliferation has been discussed while the distribution over concentration 'c' is modeled and can be operated in future. The T-cell activation before proliferation is based upon the distribution defined in Eq. (4.3); therefore, the same distribution is followed after proliferation. However the distribution over time as well as over concentration shown in Figure 4.5 can give us the most general behavior among the defined hypotheses.

The third hypothesis dealt with the daughter T-cells as non-activated and has shown another way to the evolutionary process after proliferation. The discontinuity in the previous cases was the deficiency that is overcome in this hypothesis by a continuous but drastic change. Moreover the drastic change in the population density of T-cells is not as huge as in the previous hypotheses. Nevertheless the distribution over time, in this hypothesis, can give a better insight about the activation process of T-cells after proliferation and we can give a similar remark for the distribution of daughter T-cells over concentration.

The population density of daughter T-cells was followed from their parent T-cells and the density of parent cells was very high before proliferation. Therefore, the daughter cells after proliferation showed a drastic change in the population density of T-cells. Nevertheless, the drastic increase is smoother in the hypothesis 3 as compared to others. The hypothesis 1 and hypothesis 2 has shown similar phenomenon but hypothesis 2 has the capacity to vary the slope of the population density curve. The value of  $\alpha$  did not seem to be so effective because the density function values are very high (greater than  $10^{20}$ ) and the log plots have been drawn in order to visualize the results better. But, actually, it has a significant effect on the population because  $\alpha$  is the controlling parameter for the population density of T-cells in the process of activation.

# Conclusion

## Conclusion

---

This dissertation has addressed the mathematical modeling and simulation of the activation process of T-cells by using the population balance models and the concepts of differential geometry. This work has two primary focuses: the Single T-cell dynamics and the population dynamics of T-cells. Each of the subjects was focused on the activation process before and after the proliferation of T-cells. In this chapter, we briefly state these primary focuses and outline the extension of this work in the near future.

The single T-cell dynamics was discussed in Chapter 2 under four levels of complexities (four cases). Each case has dealt with the set of concentration of proteins which were depending upon each other and the variation in the concentration was represented by the set of ODEs. The simulation initiated when the T-cell started the process of activation and after each time step, a new type of T-cell followed the same phenomena. The exact solutions were found whenever possible while two numerical schemes, the Euler method and the Runge-Kutta Method of order 4, were also used to find the solutions of the system of ODEs. Moreover, the solutions were also presented in three dimensions in which activation time was introduced as the third dimension. The activation time was considered as the initial time of each type of T-cell at which the T-cell triggers its process of activation. The three-dimensional presentation has simplified the phenomena of intracellular dynamics of T-cells particularly the crossing problem in Section 2.6.

First case was based upon one protein analysis and examined the phenomena of the internalization of CD3 protein. This was the simplest model that made the basis for the next cases by investigating the 3D plots and its projection on the 2D plots. The CD3 protein dynamics has shown us the same behavior as observed in the literature [3] , [13], [15]. It has also given us an idea to extend our work towards new horizons like the reappearance of CD3 protein, Section 2.4, and the production of other proteins during the T-cells activation before proliferation.

In the second case, we discussed two models where 2<sup>nd</sup> model is the refinement of the 1<sup>st</sup> model. In both cases, the phenomenon of internalization of CD3 protein was followed from the first case which has given us a decrease on the surface concentration. Consequently it increased the concentration of CD3<sub>i</sub> protein inside the T-cell. The main reason of investigating this case was to model and analyze the concept of reappearance of the CD3 protein on the surface of T-cells

## Conclusion

---

outside CD3 synapse. This made an increase in the concentration of CD3 protein on the surface and the reappeared protein is represented by CD3\* protein. The commonality between these two models was the crossing of the curves due to the decrease in the concentration followed by an increase. However the first model didn't address the surface bound of T-cells while the second model was specifically introduced in order to overcome the deficiency of the first model, i.e. the concentration of CD3\* protein (reappeared protein) was bounded by the limited capacity of the surface area.

The next two cases, i.e. Case 3 and Case 4, have investigated the multi-protein dynamics. There are hundreds of proteins involved in the real activation process. However it was possible to reduce the number of proteins and focus on only those proteins that were interlinked to each other. This has made the problem less difficult and more understandable. The Case 3 and Case 4 have sufficiently exposed the complexity of a single T-cell dynamics by presenting the dependency of proteins on each other. Moreover the 3D visualization of the conspicuous surface proteins concentration, CD25 and CD25-IL2, has given their geometrical interpretation that is helpful to anticipate their distribution on the total population of T-cells.

The exact solution of this system of ODEs was not possible; therefore, Runge-Kutta method of order 4 method has been used to find out their numerical results. For both cases, the chosen parameters are taken from the literature. They have made the only difference of slowing and fastening the reaction rate in order to have the same complex system without crossing of curves and with crossing of curves phenomena. The Case 3 and Case 4 were further studied in Chapter 4 that has followed the same behavior after division of T-cell because the division process does not affect the dynamical changes at the intracellular level.

The above discussed four cases for the single T-cell dynamics have originated the following innovative ideas:

1. The non-monotonic behaviors of intracellular components depend upon each other.
2. The crossing of curves having a shift in time but the slope is same.
3. The crossing of curves having a shift in time and follows its own trajectory.
4. The validation of Runge-Kutta method for the system of differential equations.

## Conclusion

---

Despite the study of non-monotonicity, the realistic behavior of protein dynamics can be much complex as the concentration of surface proteins can fluctuate more than once that makes the problem more complicated. However, the given algorithm of RK-Method is flexible enough to adapt itself for finding the solutions of such cases, e.g. the sinusoidal behavior of proteins. Moreover, delays in the production of proteins can be added that are produced after the internalization of CD3 protein. The reason is, realistically, the production of CD25 protein does not start unless T-cell gets the threshold of CD3 internalization. However, for long simulation times, this phenomenon could have a minimum effect on the activation process of T-cell.

Chapter 3 and Chapter 4 focused on the population dynamics of T-cells and investigated the activation process before and after proliferation. The Chapter 3 was divided into four levels of complexities, named as four cases, which were followed from the Chapter 2, respectively, whereas the Chapter 4 has investigated the activation process of T-cells before and after division for Case 3 and Case 4 only.

Several numerical techniques have been used to validate the results in Chapter 3. A new efficient approximate technique has been introduced by geometrical study of hyperbolic conservation law known as the Transport Method (TM). This technique is based on the simple concept of differential geometry. The three other methods used to compare the results include the Method of Characteristics (MOC), Upwind Finite Volume Method (Upwind) and the Lax-Wendroff Finite Difference Method (LWF).

In the Chapter 3, each case has been investigated in order to anticipate the behavior of initial population density of T-cells over the range of concentration of surface proteins. For this purpose, the population balance modeling (PBMs) was introduced as the modeling technique that was based on two dynamical processes. The model is represented by the population balance equation (PBE) which has provided us the mathematical notations for these processes. First process is termed as activation term (assimilated as nucleation in chemical engineering) while the second process is termed as reaction term (assimilated as growth term in chemical engineering). Therefore, in this study, the general PBE became the 1<sup>st</sup> order inhomogeneous hyperbolic partial differential equation with a source term.

## Conclusion

---

The conservation of hyperbolic equation was depending upon the reaction rate present in the second process, the reaction term. The reaction rates are the rate of change in the concentration of proteins and they were followed from the Chapter 2. In Cases 1 and 3, the reaction rate didn't affect the associated hyperbolic conservation laws. Therefore, the numerical solutions for the population balance equation were possible. In Case 2, the crossing of the solution curves in the reaction rates made the equation non-conservative, however the numerical solution was possible because the slope of the solution curves were same. While in the Case 4, each curve followed its own trajectory for CD25 and CD25-IL2i proteins. Therefore, the numerical solution for such non-conservative equation was not possible. Hence, at this stage, the geometrical analysis of these curves was inevitable. In order to validate our geometrical technique (the Transport Method), the developed procedure was successfully applied on all the previous cases (Case 1, 2 and 3). Afterwards, the Modified Transport Method (MTM) defined that has followed the same phenomena as TM but it followed the constant gridlines for concentration axis to sum up the population density lying inside the control volume ( $c$  to  $c + \Delta c$ ). The prominent ideas of Chapter 3 are summarized as,

1. The PBM was studied with non-monotonic reaction rates. The classical methods have shown the diffusion because of the interpolation approximation of variable grid to the constant grid for concentration of proteins.
2. The Transport Method has given better results as compared to higher order numerical methods. However, it has also been modified to define the constant gridlines when it was applied to Case 4.
3. The limitation of PBM against crossing problems (particularly Case 4) compelled us towards the geometrical analysis of the physical processes to find the population density of T-cells.

The final chapter of thesis, i.e. Chapter 4, has been dedicated to the activation process of T-cells after proliferation. The experimental study revealed that the parent T-cells divide into two daughter T-cells with unequal distribution of protein concentrations. It is still not clear that how many of the daughter T-cells repeat the process of activation. For this reason, three hypotheses have been proposed in order to study the activation process of T-cells after proliferation.

## Conclusion

---

First hypothesis addressed the simplest way to describe the population dynamics of T-cells after proliferation. The initial population of daughter T-cells after proliferation was considered as activated after proliferation. All the initial population of daughter T-cells originated from the same type of parent T-cells was assumed to start the activation process at once (at the same activation time) after proliferation. The distribution of initial population of daughter T-cells over concentration is also defined in this hypothesis as the 2<sup>nd</sup> proposition.

The second hypothesis dealt with the distribution of daughter T-cells over the activation time after proliferation. This hypothesis also talked about the distribution of initial population of daughter T-cells over concentration of proteins. Therefore, the population is distributed over time as well as over concentration which made this hypothesis more realistic. However, after proliferation, the initial population of daughter T-cells was considered activated as in the first hypothesis.

In the first and second hypotheses, the daughter T-cells are considered activated after proliferation. Due to this reason they are treated separately as the activated population of T-cells. The third hypothesis proposed another way to deal with the activation process of T-cells after proliferation. In this hypothesis, the daughter T-cells were considered as non-activated and therefore, the discrimination between the activated and non-activated initial population of T-cells was abolished.

The TM has been used to study without crossing problems in Chapter 4 while the MTM was used to find the population density of T-cells with crossing problem. However, the population balance modeling can be applied to without crossing problems. Also the PBM can be extended from dirac-delta concentration distribution to continuous concentration distribution of the activation term, as given in Eq. (3.5).

This study has given an innovative approach to PBM by introducing non-monotonic behavior of concentration curves and the interdependent of proteins on each other. However the Transport Method has shown a very nice commitment to the whole study and overcame the deficiency of PBE at certain cases. Now it is a challenge to extend the PBM to the problem of crossings.

---

## References

- [1] D. Verkoeyen, G. A. Pouw, G. M. H. Meesters, et B. Scarlett, « Population balances for particulate processes—a volume approach », *Chem. Eng. Sci.*, vol. 57, n° 12, p. 2287-2303, juin 2002.
- [2] D. Ramkrishna, *Population Balances: Theory and Applications to Particulate Systems in Engineering*. Academic Press, 2000.
- [3] C. Bidot, « Mathematical modeling of T-cell activation kinetic », *J. Comput. Biol. J. Comput. Mol. Cell Biol.*, vol. 15, n° 1, p. 105-128, févr. 2008.
- [4] F. Z. E. Hentati, « Etude expérimentale et modélisation mathématique de la réponse lymphocytaire T », Ecole Nationale Supérieure des Mines de Saint-Etienne, 2009.
- [5] M. Hjortso, *Population Balances in Biomedical Engineering*. McGraw Hill Professional, 2005.
- [6] Y. Sidorenko, J. Schulze-Horsel, A. Voigt, U. Reichl, et A. Kienle, « Stochastic population balance modeling of influenza virus replication in vaccine production processes », *Chem. Eng. Sci.*, vol. 63, n° 1, p. 157-169, janv. 2008.
- [7] Y. Sidorenko, A. Voigt, J. Schulze-Horsel, U. Reichl, et A. Kienle, « Stochastic population balance modeling of influenza virus replication in vaccine production processes. II. Detailed description of the replication mechanism », *Chem. Eng. Sci.*, vol. 63, n° 8, p. 2299-2304, avr. 2008.
- [8] C. Bidot, « Modélisation mathématique de la réponse lymphocytaire T spécifique à une infection virale », Ecole Nationale Supérieure des Mines de Saint-Etienne, 2006.
- [9] M. J. Feito, S. Ballester, R. Díez-Orejas, G. Ojeda, G. Criado, P. Portolés, et J. M. Rojo, « CD4 dependence of activation threshold and TCR signalling in mouse T lymphocytes », *Scand. J. Immunol.*, vol. 45, n° 2, p. 166-174, févr. 1997.
- [10] G. Denkberg, C. J. Cohen, et Y. Reiter, « Critical Role for CD8 in Binding of MHC Tetramers to TCR: CD8 Antibodies Block Specific Binding of Human Tumor-Specific MHC-Peptide Tetramers to TCR », *J. Immunol.*, vol. 167, n° 1, p. 270-276, janv. 2001.
- [11] D. N. Ernst et C. C. Shih, « CD3 complex », *J. Biol. Regul. Homeost. Agents*, vol. 14, n° 3, p. 226-229, sept. 2000.
- [12] C. S. Guy et D. A. A. Vignali, « Organization of proximal signal initiation at the TCR:CD3 complex », *Immunol. Rev.*, vol. 232, n° 1, p. 7-21, nov. 2009.
- [13] S. Valitutti, S. Muller, M. Salio, et A. Lanzavecchia, « Degradation of T Cell Receptor (TCR)-CD3-? Complexes after Antigenic Stimulation », *J. Exp. Med.*, vol. 185, n° 10, p. 1859-1864, mai 1997.
- [14] G. M. Lord, R. I. Lechler, et A. J. T. George, « A kinetic differentiation model for the action of altered TCR ligands », *Immunol. Today*, vol. 20, n° 1, p. 33-39, janv. 1999.
- [15] F.-Z. El Hentati, F. Gruy, C. Iobagiu, et C. Lambert, « Variability of CD3 membrane expression and T cell activation capacity », *Cytometry B Clin. Cytom.*, vol. 78, n° 2, p. 105-114, mars 2010.
- [16] J. Rachmilewitz, « Serial triggering model », *Adv. Exp. Med. Biol.*, vol. 640, p. 95-102, 2008.

- 
- [17] S. Shahabuddin, « Expression and release of IL-2 receptor and production of IL-2 by activated T lymphocyte subsets », *J. Clin. Lab. Immunol.*, vol. 36, n° 1, p. 27-32, sept. 1991.
- [18] S. Hodge, G. Hodge, R. Flower, et P. Han, « Surface and intracellular interleukin-2 receptor expression on various resting and activated populations involved in cell-mediated immunity in human peripheral blood », *Scand. J. Immunol.*, vol. 51, n° 1, p. 67-72, janv. 2000.
- [19] L. J. Carreno, S. M. Bueno, P. Bull, S. G. Nathenson, et A. M. Kalergis, « The half-life of the T-cell receptor/peptide-major histocompatibility complex interaction can modulate T-cell activation in response to bacterial challenge », *Immunology*, vol. 121, n° 2, p. 227-237, juin 2007.
- [20] J. Madrenas, « Differential signalling by variant ligands of the T cell receptor and the kinetic model of T cell activation », *Life Sci.*, vol. 64, n° 9, p. 717-731, 1999.
- [21] L. Rong, J. Guedj, H. Dahari, D. J. Coffield Jr, M. Levi, P. Smith, et A. S. Perelson, « Analysis of hepatitis C virus decline during treatment with the protease inhibitor danoprevir using a multiscale model », *PLoS Comput. Biol.*, vol. 9, n° 3, p. e1002959, mars 2013.
- [22] A. Saxena, J. Jacobson, W. Yamanashi, B. Scherlag, J. Lamberth, et B. Saxena, « A hypothetical mathematical construct explaining the mechanism of biological amplification in an experimental model utilizing picoTesla (PT) electromagnetic fields », *Med. Hypotheses*, vol. 60, n° 6, p. 821-839, juin 2003.
- [23] B. Kohler, « Mathematically modeling dynamics of T cell responses: predictions concerning the generation of memory cells », *J. Theor. Biol.*, vol. 245, n° 4, p. 669-676, avr. 2007.
- [24] D. Ramkrishna et A. W. Mahoney, « Population balance modeling. Promise for the future », *Chem. Eng. Sci.*, vol. 57, n° 4, p. 595-606, févr. 2002.
- [25] A. D. Randolph et M. A. Larson, *Theory of particulate processes: analysis and techniques of continuous crystallization*. Academic Press, 1988.
- [26] M. E. Kavousanakis, N. V. Mantzaris, et A. G. Boudouvis, « A novel free boundary algorithm for the solution of cell population balance models », *Chem. Eng. Sci.*, vol. 64, n° 20, p. 4247-4261, oct. 2009.
- [27] M. Stamatakis, « Cell population balance, ensemble and continuum modeling frameworks: Conditional equivalence and hybrid approaches », *Chem. Eng. Sci.*, vol. 65, n° 2, p. 1008-1015, janv. 2010.
- [28] V. Sivadon-Tardy, D. Orlikowski, R. Porcher, T. Sharshar, M.-C. Durand, V. Enouf, F. Rozenberg, C. Caudie, D. Annane, S. van der Werf, P. Lebon, J.-C. Raphaël, J.-L. Gaillard, et E. Gault, « Guillain-Barré syndrome and influenza virus infection », *Clin. Infect. Dis. Off. Publ. Infect. Dis. Soc. Am.*, vol. 48, n° 1, p. 48-56, janv. 2009.
- [29] H. Kropshofer et A. B. Vogt, Éd., *Antigen Presenting Cells: From Mechanisms to Drug Development*. 2006.
- [30] M.-P. Lefranc et G. Lefranc, *The T Cell Receptor FactsBook*. Gulf Professional Publishing, 2001.
- [31] R. N. Germain, « T-cell development and the CD4-CD8 lineage decision », *Nat. Rev. Immunol.*, vol. 2, n° 5, p. 309-322, mai 2002.
- [32] B. Alberts, A. Johnson, J. Lewis, M. Raff, K. Roberts, et P. Walter, « Helper T Cells and Lymphocyte Activation », 2002. [En ligne]. Disponible sur: <http://www.ncbi.nlm.nih.gov/books/NBK26827/>. [Consulté le: 15-mai-2013].

- 
- [33] M. Freeman, « Feedback control of intercellular signalling in development », *Nature*, vol. 408, n° 6810, p. 313-319, nov. 2000.
- [34] R. N. Germain, « MHC-dependent antigen processing and peptide presentation: providing ligands for T lymphocyte activation », *Cell*, vol. 76, n° 2, p. 287-299, janv. 1994.
- [35] M. P. Rout, J. D. Aitchison, A. Suprpto, K. Hjertaas, Y. Zhao, et B. T. Chait, « The yeast nuclear pore complex: composition, architecture, and transport mechanism », *J. Cell Biol.*, vol. 148, n° 4, p. 635-651, févr. 2000.
- [36] S. J. Singer et G. L. Nicolson, « The fluid mosaic model of the structure of cell membranes », *Science*, vol. 175, n° 4023, p. 720-731, févr. 1972.
- [37] B. Favier, N. J. Burroughs, L. Wedderburn, et S. Valitutti, « TCR dynamics on the surface of living T cells », *Int. Immunol.*, vol. 13, n° 12, p. 1525-1532, déc. 2001.
- [38] M. P. Keith, « Interleukin-2 Signal Transduction: A Diffusion-Kinetics Model », mai 1993.
- [39] T. K. Dasaklis, C. P. Pappis, et N. P. Rachaniotis, « Epidemics control and logistics operations: A review », *Int. J. Prod. Econ.*, vol. 139, n° 2, p. 393-410, oct. 2012.
- [40] H. Trottier, « Deterministic Modeling Of Infectious Diseases: Theory And Methods », *Internet J. Infect. Dis.*, vol. 1, n° 2, 2001.
- [41] F. Ball, « Analysis of a stochastic SIR epidemic on a random network incorporating household structure », *Math. Biosci.*, vol. 224, n° 2, p. 53-73, avr. 2010.
- [42] H. W. Hethcote, « The Mathematics of Infectious Diseases », *SIAM Rev.*, vol. 42, n° 4, p. 599-653, janv. 2000.
- [43] L. Star et S. M. Moghadas, « The Role of Mathematical Modeling in Public Health Planning and Decision Making », déc-2010.
- [44] E. Terry, J. Marvel, C. Arpin, O. Gandrillon, et F. Crauste, « Mathematical model of the primary CD8 T cell immune response: stability analysis of a nonlinear age-structured system », *J. Math. Biol.*, vol. 65, n° 2, p. 263-291, août 2012.
- [45] S. M. Kaech, E. J. Wherry, et R. Ahmed, « Effector and memory T-cell differentiation: implications for vaccine development », *Nat. Rev. Immunol.*, vol. 2, n° 4, p. 251-262, avr. 2002.
- [46] E. L. Haseltine, D. B. Patience, et J. B. Rawlings, « On the stochastic simulation of particulate systems », *Chem. Eng. Sci.*, vol. 60, n° 10, p. 2627-2641, mai 2005.
- [47] S. Qamar, M. P. Elsner, I. A. Angelov, G. Warnecke, et A. Seidel-Morgenstern, « A comparative study of high resolution schemes for solving population balances in crystallization », *Comput. Chem. Eng.*, vol. 30, n° 6-7, p. 1119-1131, mai 2006.
- [48] S. Qamar et S. M. ur Rehman, « High Resolution Finite Volume Schemes for Solving Multivariable Biological Cell Population Balance Models », *Ind. Eng. Chem. Res.*, vol. 52, n° 11, p. 4323-4341, mars 2013.
- [49] Koren B., « A robust upwind discretization method for advection, diffusion and source terms ». [En ligne]. Disponible sur: <http://www.tue.nl/en/publication/ep/p/d/ep-uid/272984/>. [Consulté le: 01-août-2013].
- [50] R. J. LeVeque, *Finite Volume Methods for Hyperbolic Problems*. 2002.
- [51] O. Dushek, « Analysis of Serial Engagement and Peptide-MHC Transport in T Cell Receptor Microclusters », *Biophys. J.*, vol. 94, n° 9, p. 3447-3460, mai 2008.

- 
- [52] S. Tian, R. Maile, E. J. Collins, et J. A. Frelinger, « CD8+ T Cell Activation Is Governed by TCR-Peptide/MHC Affinity, Not Dissociation Rate », *J. Immunol.*, vol. 179, n° 5, p. 2952-2960, janv. 2007.
- [53] T. W. McKeithan, « Kinetic proofreading in T-cell receptor signal transduction », *Proc. Natl. Acad. Sci. U. S. A.*, vol. 92, n° 11, p. 5042-5046, mai 1995.
- [54] H. Liu, M. Rhodes, D. L. Wiest, et D. A. Vignali, « On the Dynamics of TCR:CD3 Complex Cell Surface Expression and Downmodulation », *Immunity*, vol. 13, n° 5, p. 665-675, nov. 2000.
- [55] Q. Ali, T. Eric, G. Frederic, et L. Claude, « Mathematical Modeling for the Activation of T-Lymphocytes: Population Balance Modeling with Non Conventional Growth Law », 2012, p. 662-670.
- [56] K. A. Smith, « The quantal theory of immunity », *Cell Res.*, vol. 16, n° 1, p. 11-19, 2006.
- [57] M. B. Abbott, *An Introduction to the Method of Characteristics*. American Elsevier, 1966.
- [58] A. D. Polyanin, *Handbook of Linear Partial Differential Equations for Engineers and Scientists*, 1<sup>re</sup> éd. Chapman and Hall/CRC, 2001.
- [59] S. A. Sarra, « Journal of Online Mathematics and its Applications | The Method of Characteristics & Conservation Laws », 2003. .
- [60] P. Wong et E. G. Pamer, « Cutting edge: antigen-independent CD8 T-cell proliferation », *J Immunol*, vol. 166, p. 5864-5868, 2001.
- [61] H. Veiga-Fernandes, U. Walter, C. Bourgeois, A. McLean, et B. Rocha, « Response of naive and memory CD8+ T cells to antigen stimulation in vivo », *Nat. Immunol*, vol. 1, p. 47-53, 2000.
- [62] S. M. Kaech et R. Ahmed, « Memory CD8+ T-cell differentiation: initial antigen encounter triggers a developmental program in naive cells », *Nat. Immunol*, vol. 2, p. 415-422, 2001.
- [63] R. Mercado, « Early programming of T-cell populations responding to bacterial infection », *J Immunol*, vol. 165, p. 6833-6839, 2000.
- [64] K. E. Foulds, L. A. Zenewicz, D. J. Shedlock, J. Jiang, A. E. Troy, et H. Shen, « Cutting Edge: CD4 and CD8 T Cells Are Intrinsically Different in Their Proliferative Responses », *J. Immunol.*, vol. 168, n° 4, p. 1528-1532, févr. 2002.
- [65] J. T. Chang, « Asymmetric T lymphocyte division in the initiation of adaptive immune responses », *Science*, vol. 315, n° 5819, p. 1687-1691, mars 2007.
- [66] C. G. King, S. Koehli, B. Hausmann, M. Schmalzer, D. Zehn, et E. Palmer, « T Cell Affinity Regulates Asymmetric Division, Effector Cell Differentiation, and Tissue Pathology », *Immunity*, vol. 37, n° 4, p. 709-720, oct. 2012.